The Nottingham Trent University
Library & Information Services

SHORT LOAN COLLECTION

Date	Time	Date	Time

Please return this item to the Issuing Library.
Fines are payable for late return.

THIS ITEM MAY NOT BE RENEWED

Short Loan Coll May 1996

40 0681795 X

ProQuest Number: 10290350

All rights reserved

INFORMATION TO ALL USERS
The quality of this reproduction is dependent upon the quality of the copy submitted.

In the unlikely event that the author did not send a complete manuscript
and there are missing pages, these will be noted. Also, if material had to be removed,
a note will indicate the deletion.



ProQuest 10290350

Published by ProQuest LLC (2017). Copyright of the Dissertation is held by the Author.

All rights reserved.
This work is protected against unauthorized copying under Title 17, United States Code
Microform Edition © ProQuest LLC.

ProQuest LLC.
789 East Eisenhower Parkway
P.O. Box 1346
Ann Arbor, MI 48106 – 1346

SOME EFFECTS OF SUBSURFACE STRESS ON WEAR BEHAVIOUR

by

DAVID ANTHONY HILLS

Thesis submitted in partial fulfilment of the requirements for the degree of Doctor of Philosophy to the Council for National Academic Awards

This work was carried out in the Department of Mechanical and Production Engineering of Trent Polytechnic, Burton Street, Nottingham.

1979

MPHD 3

Contents

	Pages
Abstract	1
Nomenclature	2-3
1.Introduction	
1.1 Wear and its Classification	4-8
1.2 Parameters involved in Wear	9-11
1.3 Delamination and Dislocations	12-17
1.4 The Continuum and Wear	17-22
1.5 Fracture Mechanics and Wear	22-27
2.Surface Treatments and Residual Stresses	
2.1 Surface Treatments	28-32
2.2 Properties of Electrodeposits	32-41
2.3 Wear tests	41-61
2.4 Contact and Residual Stresses-their Interdependence	61-72
3.Fracture Mechanics and Wear	
3.1 Justifying the use of Fracture Mechanics	73-78
3.2 The Determination of Stress Intensification Factors	78-84
3.3 Deriving S.I.F.'s for the Wear Problem	84-102
4.Extensions of the Fracture Problem	
4.1 Cracks under Compression	103-119
4.2 The application of Fracture Mechanics to Pure Rolling	119-126
4.3 The Initiation of Cracks	126-139
4.4 Non-linear Aspects of Crack Propagation	139-144
5.An Estimation of Crack Growth Rates	
5.1 Difficulties unique to Wear	145-150
5.2 Estimating Stage and Rate of Crack Growth	150-160
5.3 Applying the Results found to Wear	160-162

5.4 Further aspects of Crack Growth 162-165

6.Shakedown

6.1 Concept of Shakedown 166-180

6.2 Shakedown of a Rolling Ball in a Groove 180-199

6.3 Vertical Shakedown of two Cylinders 199-206

6.4 Vertical Shakedown of a Ball 206-213

7.Conclusions 214-216

References 217-234

Technical Papers bound in after references;

"An Automated Plating Stress Monitor" Ref.76

"The Physical Influence of Surface Treatments on Wear" Ref.95

"On the Application of Fracture Mechanics to Wear" Ref.135

"A Fracture Mechanics approach to Rolling Contact Fatigue" Ref.186

Acknowledgements

I hope that the customariness of an acknowledgement to one's supervisor will not detract from my genuine thanks. Dr David Ashelby, my Director of Studies and a metallurgist, has shown great patience with the mindless number-crunching of a would-be elastician, and has provided the starting point for many topics of investigation. His efforts are even more noteworthy in view of the excessive teaching load he has carried during much of the work. The assistance of Dr Waterhouse of Nottingham University, another tolerant metallurgist, and Professor Stanley of Manchester University, who has helped with the applied mechanics, is also gratefully recorded.

The interest and advice given by Professor Johnson of Cambridge University was particularly welcome and valuable, providing as it did the starting point for new investigations. Also, Dr Pook of the National Engineering Laboratories provided useful data for fracture mechanics work.

Lastly, I should like to thank Dr Alan Austin, sometime fellow research student and wizzard mountaineer, for discussions on miscellaneous topics in elasticity during highly compliant tea-breaks.

The papers bound in at the end of this thesis were written by the author, who gratefully acknowledges the many helpful suggestions and criticisms given by Dr.Ashelby and Dr.Waterhouse. The work they embody is described more fully in the main text.

Abstract

Wear is studied from applied mechanics aspects only. It is postulated that both sliding and rolling pairs wear by the propagation of cracks a short distance beneath the surface, causing the loss of surface layers in the form of thin sheets. This has been called 'delamination'. Fracture mechanics has been assumed to be valid under contact load conditions, and the stress intensification factors for mode II (and where appropriate, mode I) growth are determined. Using a development of the work of others on the use of crack tip plastic zones to find propagation rates, the growth rate of wear cracks is predicted to be consistent with wear rates observed: much more work is needed before a true positive correlation can be established. It is pointed out that wear cracks grow in what is apparently a vacuum, and that, even under the exactly antisymmetrical shear stress distribution of rolling contact, they do not experience equal and opposite periods of mode II growth. Therefore, if only contact stresses were present, it might be expected that wear crack growth parallel to the surface would be unstable, so that wear particles would be equi-axed. This is not observed experimentally, and the creation of tensile sub-surface residual stresses is cited as a possible stabilising influence. It is found that such stresses are a likely outcome of shakedown for several configurations, and new shakedown limits are found for three dimensional contacts. The effect of residual stresses on wear is studied experimentally by deliberately building in a static stress system, and the optimum stress to apply is found for several geometries.

Nomenclature

With the exception of a few sundry equations which appear once only, the parameters used are defined below;

A	Constant in Paris' fatigue equation
E	Young's modulus
F_i	Image force
G	Rigidity modulus
I_1	First invariant, complete stress tensor
J_2	Second invariant, deviatoric stress tensor
K_i	Stress Intensification Factor, mode i
K_{IC}	Fracture toughness
L	Bearing life
N	Number of fatigue cycles, or passes
P	Applied load, line load.
Q	Applied shear load, line load
R	Roller radius
R_G	Groove radius(relaxed)
R_G^o	Groove radius(stressed by residual stresses)
a_o	Contact radius
a'	Interplanar spacing
a	Lattice parameter, semi-width of contact in x-direction
b	Burger's vector, semi-width of contact in y-direction
b_o	Contact half-width
c	Crack half-length
d	Depth to datum level
h	Thickness of low dislocation density zone, contact
k	$\frac{b}{a}$ oblateness of ellipse unit on crack face
k_i	$\frac{1-\nu_i^2}{\pi E_i}$
m	Paris exponent
n	Wear rate exponent, ratio K_{II}/K_I

p Normal 'pressure', fraction of force to relax

p_o Peak contact pressure

q Shear 'pressure'

r Distance from crack tip

r_o Atomic radius

r_p On-axis ($\theta=0$) monotonic plastic radius at crack tip

r'_p On-axis reversed plastic radius

s_{ij} Deviatoric stress component

t Thickness of electrodeposit

u Displacement near crack tip

w Dislocation width, contact patch width under uniform load

x,y,z Cartesian coordinates

x^*,y^*,z^* Normalized Cartesian coordinates (to characteristic contact dimension)

α Friction angle

β Coffin-Manson exponent

δ Influence coefficient

ϵ_{ij} Strain

θ Angle of polar set, particularly for crack-tip coords.,

$\bar{\sigma}$ Spherical stress where centreline is reference

σ_{ij} Stress component (complete)

σ_o Yield stress in simple tension

σ_{ra} Average residual stress

σ_{ri} Instantaneous residual stress

ϵ_o Yield strain

τ_o Yield in pure shear

μ Coefficient of friction

ν Poisson's ratio

ω Depth of groove

ω_o Depth of groove at centreline

Tensor notation is not used in this thesis and no summation is implied by the use of subscripts i,j,k.

1. Introduction

1.1 Wear and its classification

Wear is the degradation and loss of the original surface of a material due to rolling or sliding contact with another body, usually over an extended period of time. It is rarely catastrophic in itself, though it may well lead to catastrophic failure. For instance, the wear of piston rings in an internal combustion engine may only have the immediate effect of permitting the escape of working fluid, and therefore reducing efficiency. However, to maintain the same power may now necessitate higher speeds, and hot gasses escaping down the bore will result in higher running temperatures, so that any wear debris is likely to be welded onto the bore or piston, causing interference. Eventually, the engine may seize. The replacement of worn parts is often expensive, because, besides the cost of components and labour, the lost production of a machine may need to be considered, eg. in 1976 a rolling mill undergoing repair was estimated by Eyre (1) to represent production losses of £4000 per hour. Because of these expenses the study of wear has become increasingly important, and the word 'tribology' was coined to describe the study of wear, friction and lubrication. Tribological studies should lead not only to new treatments and configurations providing improved wear resistance, but to reductions in the energy expended by non-conservative motion. Also, solutions are being provided for bearings working in severe environments such as a vacuum, at high temperatures, or with extremely high relative velocities

between the wearing pair.

Since Bowden and Tabor's treatise(2), several texts have been published with different emphases. An energy balance approach to wear, including the use of free surface energies to speculate on the degree of cold welding is the theme of books by Rabinowicz(3) and Moore(4), whilst the latter also examines the wear of plastics. Design aspects, lubrication and metallographic features are described in the handbook by Neale(5), and mechanical topics are treated, inter alia, in Sarkar(6) and in Halling(7). This thesis builds largely upon work presented in the last two books, and, following their authors, will begin by broadly classifying wear. These divisions are the classical ones, and the proportion of failures for which each is responsible is shown as estimated by Eyre(1);

A. Adhesive Wear. 15%

Adhesive wear does not require mechanical interference of surface imperfections, but occurs when the local contact pressure is sufficient to cause the surface to yield, resulting in sufficiently intimate contact for welding to occur. Subsequent motion causes the junction to break either side the weld, because the weld material itself is stronger owing to work hardening.

B. Abrasive Wear. 50%

This occurs when hard particles, either embedded within a surface or existing separately, gouge elongated chips or slivers from a component. The wear resistance of a metal to such action is usually proportional to its hardness. See, eg. Sakamoto and Tsukizoe(8).

C. Erosive Wear 8%

Erosion is normally associated with the action of minerals on metal surfaces, rather than a metal-metal phenomenon. It is similar to abrasion, though purely normal impacts may be important.

D. Fretting 8%

Fretting is a specialised type of wear which occurs when mating surfaces are undergoing small amplitude($\sim$100μm) oscillatory motion. Debris is usually a powder.

E. Chemical 5%

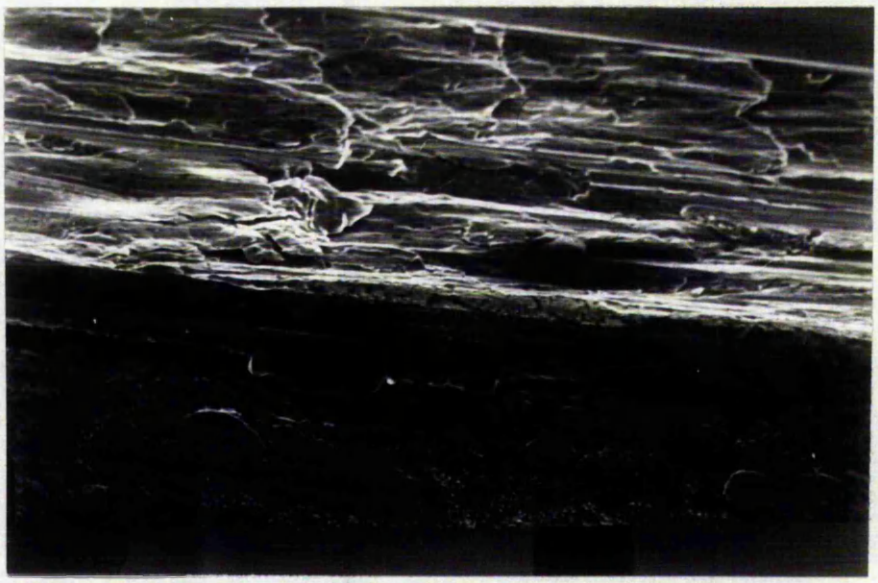
Corrosion accelerates the degradation of wearing sufaces, and produces abrasive debris.

Eyre does not mention the other 14% of failures, but a large proportion must be realised as rolling wear.

F. Rolling Wear

Rolling wear is different from the other wear mechanisms mentioned because it does not require a component of relative motion tangential to the mating sufaces. Also, there may be no apparent deterioration of the surface until the wear particle detaches itself.

Recent theories classify wear differently, according to the morphology of the worn surfaces. In particular, Suh(9) has described some surfaces as having undergone 'delamination'. A delaminating surface has many platelets of material, typically about 10μm long and 1μm thick removed, leaving several more potential plates still attached to the surface, fig.1. Detached plates do not retain their form, but are quickly rolled into approximately spherical debris. Many, but not all worn surfaces show this type of



A typical Delaminating Surface-nickel being worn under Sliding conditions. Fig.1

The worn part of the surface is towards the top of the photograph. A slight burred over edge to the wear track may be seen, and, in the foreground, the unworn surface.

morphology,and examples of delamination have been found under adhesive conditions by Suh (9), under normal impact loading by Rice(10) and upon ground surfaces, which might be looked upon as a type of controlled abrasive wear, by Doyle and Turley(11).

The Delamination theory does not really contradict the long-established Archard theory of adhesive wear (12), but rather complements it: from a straightforward acceptance of Archard's theory one might expect approximately equi-axed wear particles to result, whereas they are frequently elongated, as suggested by delamination, and the worn surface is rarely pitted. However, Archard's hypothesis explains adequately the transference of material from one wearing component to the other, which is often observed, and also points out why it is not always the interfacial bonds which fail.

The mechanism by which delamination occurs is still to be explained. It is suggested that delamination proceeds by the propagation of a crack, approximately parallel to and very near to the surface, which eventually turns upwards, creating a wear particle. On a rather larger scale, the same process is thought to be responsible for the generation of spalls under pure rolling conditions, and for this reason a unified approach to the two processes is thought feasible. A detailed model covering the two configurations is presented in chapter 3.

1.2 Parameters involved in Wear

It is clear that the rate of wear of a rolling or sliding pair will depend on many parameters. These may be split into (a) those which might be expected to have an influence if 'model' materials were being worn and (b)those which complicate the picture when using real materials. Since lubricated contacts will not be treated, the possible parameters in class (a) are:

1. Type of relative motion,ie. rolling, sliding or impact.
2. Applied load, and constitutive relation of wearing materials
3. Relative velocity & its type: single direction or oscillatory
4. Coefficient of friction.
5. Geometry of contacting surfaces, plus a measure of the surface roughness.

In principle, the data mentioned should be sufficient to analyze the mechanical processes of wear under any conditions, provided the material were isotropic, homogeneous, and unaffected by any heat generated.Variables belonging to category (b) are:

6. Microstructure and crystallography; size and distribution of grains, lattice orientation within surface grains
7. Presence of inclusions & second-phase particles
8. Thermal stability and possibility of a phase transformation
9. Oxidation of surface. This is a particularly important variable, since the presence of a stable, well-adhered oxide may provide lubrication and reduce wear, whilst a poorly adhering abrasive oxide will certainly accelerate wear. The importance of oxidation was demonstrated by Welsh(13).

With the exception of a short consideration of the behaviour of dislocations near a free surface, reported in

(1.3), this work has considered the wear problem only from the continuum viewpoint. The restrictions of such an approach are well appreciated, but it is felt that considerable insight into wear problems may nevertheless be gained, and, providing systems are chosen where the influence of variables 6-9 is small (eg. relatively inert pure f.c.c. metals), the results should be valuable. A further parameter which will virtually be ignored is surface roughness. Normally, providing the contacting surfaces are not smooth to the point where large areas of adhesion are present, wear is independent of initial roughness, since a steady state is quickly achieved. This has been found in sliding (14) and rolling-with-traction configurations (15). though under pure rolling a higher roughness normally leads to a reduction in fatigue life. Greenwood and Tripp(16) showed that the contact pressure distribution of a roughened sphere approached that of a perfectly smooth sphere as the load was increased, and so for the majority of contact applications the surface topography does not influence the overall stress field. This might be expected from an application of St. Venant's principle, though the assumption is invalid very near the surface, where the influence of discrete asperities will be apparent. Also. the presence of distinct flaws will affect the bulk stress field as shown by Gerlach and Lokhamp(17).

The simplification of a continuum stress approach means that all the classical methods of elasticity, and in particular the contact stress solutions of Boussinesq, Flamant and Hertz are available. There are difficulties encountered in contact work which are not found in other applications of stress analysis. For example, under Hertzian

contacts the yield point is initially reached well below the surface, so that for loads only slightly in excess of the elastic limit a plastic zone is formed which is surrounded by elastic material, and is unable to flow. Therefore the Prandtl-Reuss rules are difficult to apply, and, strictly, deformation plasticity may not be used because the loading is not proportional. All three principal stresses are negative over a large proportion of the contact field, and this gives difficulties in assessing fatigue failure, because classical fatigue relations characterise the tensile stresses tending to open the crack root in, say, a rotating bending test. Except very near the surface, where one principal stress is always positive, it is clear that shear loading on cracks, inclusions and flaws plays a key role in causing wear. The influence of shear loading on these features under more easily controlled conditions is not well documented, because the application of pure shear is not easy to apply stably, using a loading frame. Also, when at least one of the principal stresses is positive, as it usually is, this tends to dominate any brittle behaviour.

Lastly, the relatively small value of the deviatoric stress in comparison with the absolute value of the spherical stress component means that finite element solutions are often inaccurate unless fine nets are used. Correspondingly powerful computers are therefore required, and yet more capacity is needed to handle the effects of cracks or plasticity.

1.3 Delamination and Dislocations

As has been mentioned, the delamination theory of wear began by Suh (9) examining the nature of worn surfaces and noting their similarity with a delaminated composite. At the time Suh advanced the idea that the thickness of the plates which detached was governed by the dynamics of dislocations in the surface grains. Specifically, he suggested that a zone with a low density of dislocations existed for a short distance down form the surface. This layer, being free of defects, would flow freely with respect to the interior without the formation of voids, thereby reducing the possibility of crack initiation. Suh also suggested that this layer would be much softer than the bulk material, though it is difficult to see how the absence of dislocations which provide a material with the ability to flow at moderate stresses, could show such a phenomenon. All that would seem possible is a lack of work-hardening, since no dislocation locking could occur. A paper by Kirk and Swanson(18) claimed to have found a soft surface layer: micro-hardness tests were performed on a vertical section through a wear track in copper, and did indeed show a fall-off in hardness near the surface. However, the authors reported the interior hardness of the material too, and this was similar to that found at the very surface, so that the intervening hardened zone might be better interpreted as work hardening near the severest Hertzian stresses. More recent work by Ruff(19,20) using the SACP technique failed to recognise any change in the surface properties in worn iron. In spite of the current scepticism towards a dislocation explanation a short exposition of the estimation

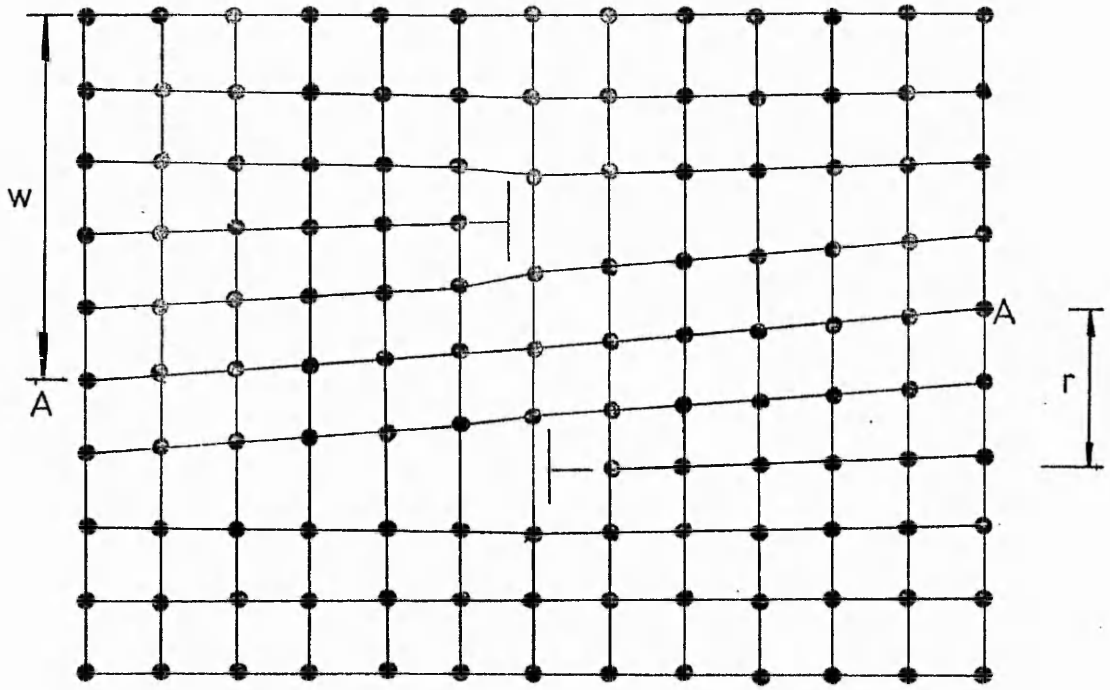
of zone thicknesses may prove useful, particularly for comparison with other results presented later.

If a dislocation is found near the surface of a metal it is acted upon by an 'image force'. For a simple cubic lattice the principle is illustrated by considering two line dislocations of opposite sign near to each other within the crystal, fig.2. Each dislocation has a unit Burger's vector, considered separately, but the sum of the two is zero and the corresponding long-range elastic energy of distortion is also zero. If the lattice above the line A-A is removed, giving a free surface, the forces on the dislocation in the lower half of the crystal remain unaltered. Since the force attracting a dislocation to the surface is found by the method of images it is called an image force:

$$F_i = \frac{d}{dr}(E) \qquad (1)$$

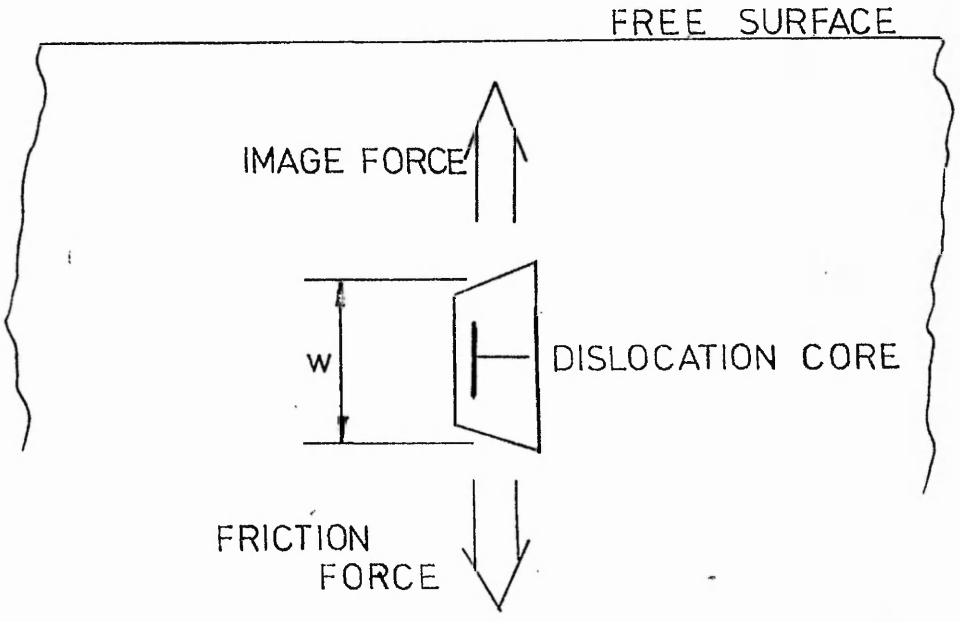
where E is the elastic energy of the dislocation.
There is a frictional force resisting the motion of a dislocation through a lattice, and the edge of the low dislocation density zone is assumed to be where this force is just balancing the image force. Unfortunately, it is rather difficult to determine the friction force for a single phase metal. In his original paper, Suh(9) gives several estimates for two-phase and precipitation-hardening alloys, but no hint on evolving a value for an elemental metal. The best estimate is probably provided by the Peierls-Nabarro force, ie. the force needed to move a single dislocation through an otherwise perfect crystal:

$$\sigma = \frac{2G}{1-\nu} \exp\left(\frac{-2\pi w}{b}\right) \qquad (2)$$



THE CONCEPT OF AN IMAGE FORCE

FORCES ON A DISLOCATION NEAR A SURFACE



Dislocation dynamics. Fig.2.

A further difficulty arises is estimating the width of the dislocation, but a rough value given by Cotterell is:

$$w = \frac{a'}{1-\nu} \qquad (3)$$

where a' is the interplanar spacing. Note that equation (2) is very sensitive to dislocation width, and hence to characteristic stacking fault energies. Since the Peierls-Nabarro force is applicable only to glissile motion, the only dislocations of interest in an f.c.c. metal are;

$$\begin{aligned} &\text{Unit dislocation, where } |b| = \frac{a}{\sqrt{2}} \\ &\text{Shockley partial, where } |b| = \frac{a}{\sqrt{6}} \end{aligned} \qquad (4)$$

For an edge dislocation (21):

$$E = \frac{Gb^2}{4\pi(1-\nu)} \log_e\left(\frac{r}{r_o}\right) + E_{core} \qquad (5)$$

where E_{core} is the anelastic energy associated with the core. Neglecting this, and substituting equations (2) & (5) into (1) gives:

$$h = \frac{b^2}{8\pi a'}(1-\nu)\exp\left(\frac{-2\pi a'}{b(1-\nu)}\right) \qquad (6)$$

For an h.c.p. crystal the smallest (lowest energy) glissile dislocations are unit dislocations in the basal plane:

$$\text{Unit dislocation, } |b| = a \qquad (7)$$

Using these calculations the possible low dislocation density zones for a number of f.c.c. and h.c.p. metals were evaluated and the results are presented in table 1. In addition to the difficulties mentioned, the following limitations should be borne in mind;

A. The calculations assumed that the glide planes are perpendicular to the surface. Clearly, this will not generally be the case and indeed Suh(22) comments that there is some evidence to suggest that slip planes are re-oriented after wear, parallel to the surface. Further, it is assumed

Table 1. Depth of Low Dislocation Density Zones

A. Face Centred Cubic Metals

Metal	ν	h_{unit}	$h_{Shockley}$	r_o
Aluminium	0·34	22	2200	0·29
Cobalt	0·34	19	1900	0·25
Copper	0·35	22	2400	0·26
Gold	0·42	57	12300	0·29
Iridium	0·44	70	19100	0·27
Iron	0·25	12	784	0·25
Lead	0·35	91	24700	0·35
Nickel	0.31	14	1100	0·25
Platinum	0·38	33	4700	0·28
Rhodium	0·32	17	1400	0·27
Silver	0·37	31	3900	0·29

B. Hexagonal Close Packed Metals

Metal	ν	h_{ideal}	h_{real}	r_o
Cadmium	0·21	7·6	18	0·30
Magnesium	0·31	18	18	0·32
Nickel	0·37	26	27	0·25
Titanium	0·32	19	15	0·29
Zinc	0·26	7·1	22	0·27

All dimensional quantities are in units of nm.

h_{ideal} refers to a (c/a) ratio of 1·633

r_o is atomic radius or lattice constant 'a' in h.c.p.

h_{real} refers to values obtained when using actual values of 'c' and 'a'.

Data were obtained from Barrett & Massalski and the Nuffield advanced Data Book

that the slip direction is perpendicular to the surface; this is unlikely to be the most energetically favourable glide direction in the majority of crystals.

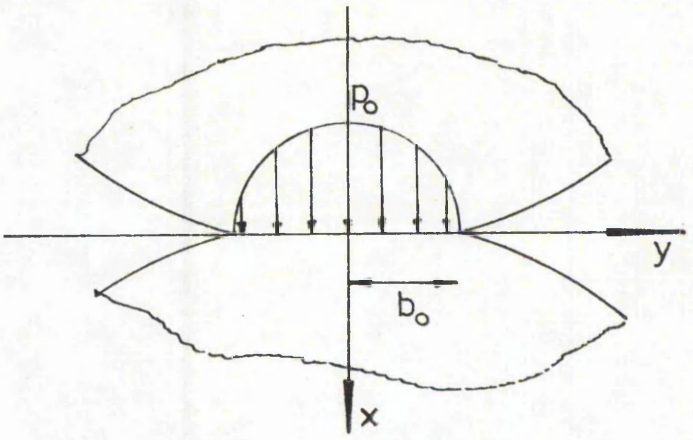
B. Since the Peierls-Nabarro force was used, the interactive forces between several dislocations contained in the same crystal were ignored.

C. Nothing has been said about sessile dislocations. They could exist in equilibrium very near the surface, and would behave as possible pile-up points for other dislocations, encouraging void formation. This is clearly at variance with Suh's hypothesis.

From these comments, the low dislocation density zone, if it exists, could be expected to have a very ill-defined boundary. The essential result of the theory is that the wear sheet thickness, which is expected to be comparable with the zone's depth, should depend only on the material (and perhaps have a weak dependece on grain size). The applied load should <u>not</u> influence the plate thickness, nor should the presence of any stress parallel to the surface alter the mode or rate of wear. Wear experiments performed inside a SEM have recently shown the first statement to be invalid(23), because the plate thickness increased with load. The second aspect is treated in chapter 2.

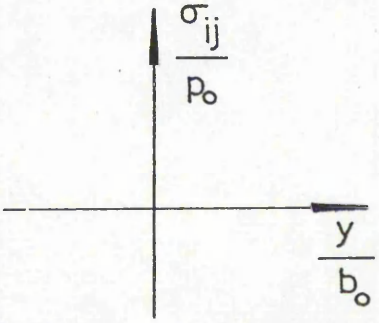
1.4 The Continuum and Wear

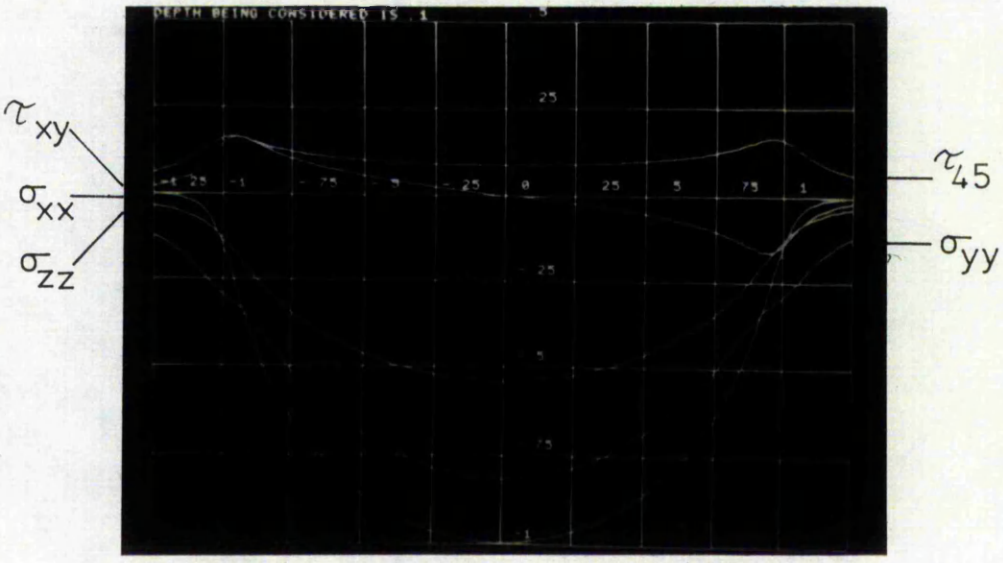
Most early explanations of rolling wear make use of solutions based on a perfect, flawless material. The object was simply to try and assess the most probable depth of failure, and correlate experimentally the wear rate with applied load. Similar techniques seem rarely to have been



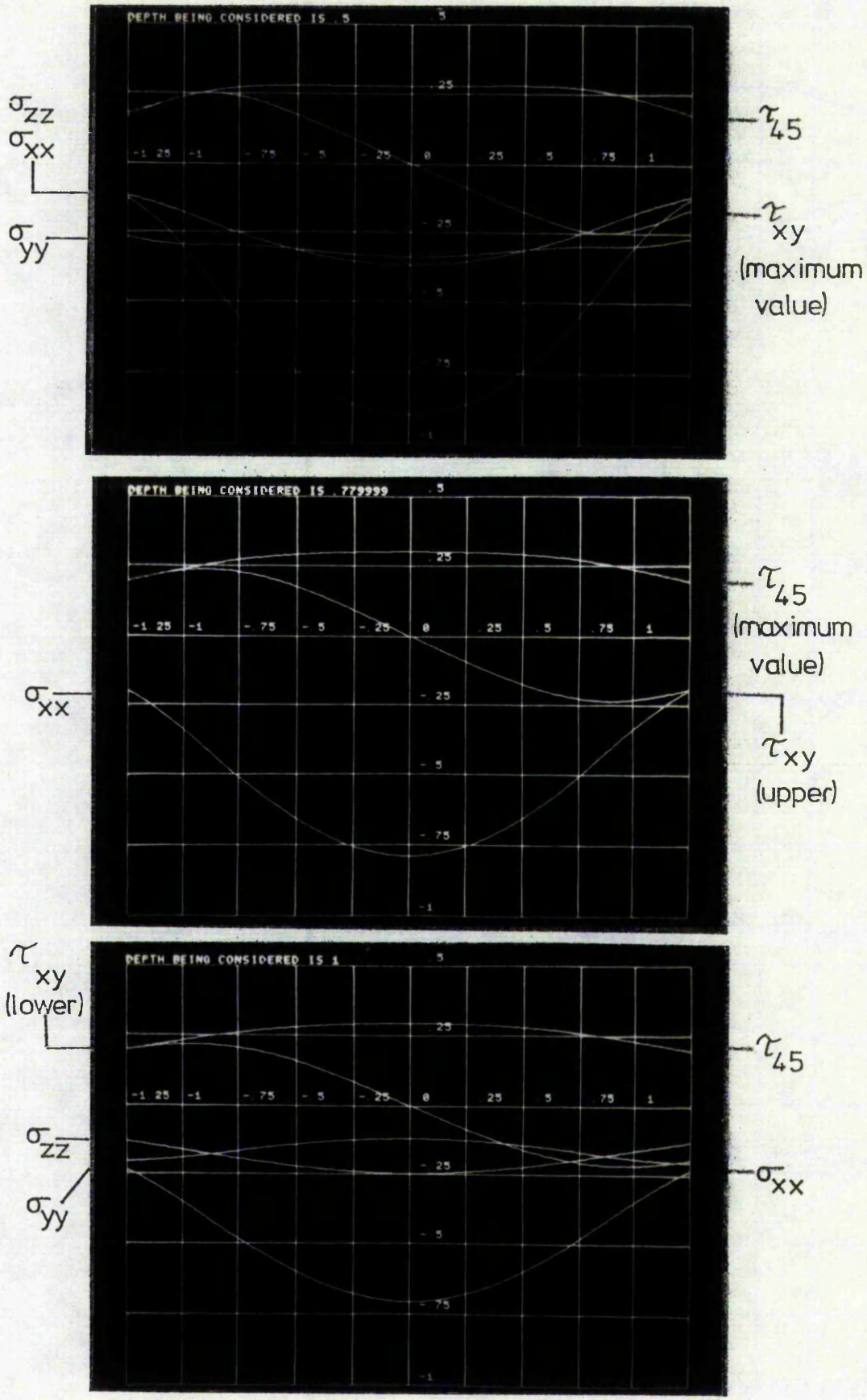
Coordinate System used in 2-D Roller Calculations Fig.3.

Key to photographs:
Depths normalized by b_o.





Variation of stresses beneath a roller .Fig. 4a.



Variation of stresses beneath a roller. Fig.4b.

applied to sliding wear, possibly because solutions to the three-dimensional Hertz problem with traction have not become available until much more recently.

Consider the case of two-dimensional rolling contact, fig.3. Many experiments have been performed to assess the life of rollers, and these were reviewed by Johnson(24). With the exception of a small area near the surface, just beyond the contact patch, all direct stresses are negative. Since the depths at which cracks are found is well below this tensile region, attention was focussed on the role of shear stresses in causing the growth of cracks. The solution to the complete stress field for this problem was found by Beliaev, and is given in English by Radzimovsky(25). The variation of stresses with distance from the contact strip is shown for various depths in fig.4. The direct stresses are all symmetrical with respect to y, whilst the only non-zero shear stress, τ_{xy}, is antisymmetrical. The stresses are given by;

$$\frac{\sigma_{xx}}{p_o} = -e^{-\alpha}\sin\beta + \Gamma\sin\beta\sinh\alpha$$

$$\frac{\sigma_{yy}}{p_o} = -e^{-\alpha}\sin\beta - \Gamma\sin\beta\sinh\alpha$$

$$\frac{\sigma_{zz}}{p_o} = -2\nu\, e^{-\alpha}\sin\beta \qquad (\epsilon_{zz}=0)$$

$$\frac{\tau_{xy}}{p_o} = -\frac{\sin\beta\,\sin2\beta\,\sinh\alpha}{\cosh2\alpha - \cos2\beta} \qquad (\tau_{xz}=\tau_{yz}=0) \qquad (8)$$

where; $\Gamma = 1 - \dfrac{\sinh2\alpha}{\cosh2\alpha - \cos2\beta}$

Letting; $x^*=x/b_o$ and $y^*=y/b_o$

$$u = 1-x^{*2}-y^{*2}$$

Then: $\sqrt{2}\sin\beta = (u+\sqrt{u^2+4x^{*2}})^{\frac{1}{2}}$ $\sqrt{2}\sinh\alpha = (-u+\sqrt{u^2+4x^{*2}})^{\frac{1}{2}}$

The other quantities required may be found by appealing to standard trigonometric identities. Two important quantities which might govern the strength condition of rollers are;

A. Largest Shearing Stress, τ_{45}

$$\tau_{45} = \tau_{xy}^2 + \tfrac{1}{4}(\sigma_{xx}-\sigma_{yy})^2 \qquad (9)$$

This quantity has a maximum value given by $\frac{\tau_{45}}{p_o} = 0{\cdot}304$ which is attained on the axis of symmetry, at $y^*=0, x^*=0{\cdot}78$ Since it represents the largest shearing stress found, τ_{45} may be used to find the elastic limit, by Tresca's criterion

$$\text{ie. } \tau_{45} \leqslant \tau_o$$

$$\text{or } \frac{p_o}{\tau_o} \leqslant 3.29 \qquad (10)$$

This gives the largest load which may be supported by the rollers without plasticity, and locates the severest state of stress found.

B. Largest Range of Shearing Stress

As τ_{xy} is an odd function of y, material beneath a rolling pair experiences a complete reversalof shear stress on any plane parallel to the surface, ie. a <u>range</u> of shear stress of $2\tau_{xy}$. The maximum value of τ_{xy} is $\left|\frac{\tau_{xy}}{p_o}\right| = 0{\cdot}256$ and is located at $x^*=0{\cdot}5$, $y^*=\pm 0.85$.It was usually accepted that the fatigue limit for a subsurface crack be based on this quantity (26).

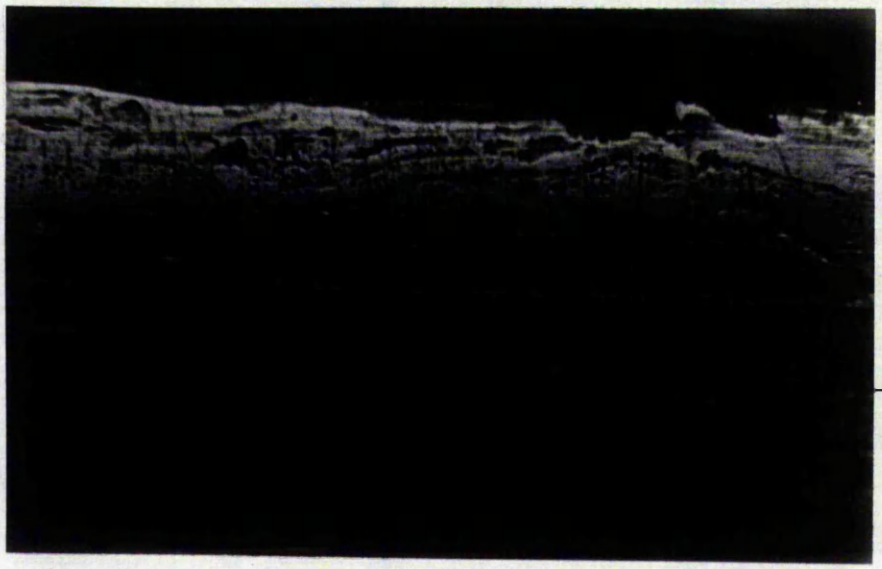
As a frictional force is applied in conjunction with the normal load the point of severest stress moves upwards and forwards. At the same time another maximum develops at the surface and at coefficients of friction greater than 0·367 the yield condition is always reached at the surface first. Wear life estimations for a sliding configuration using the continuum solution have recently been presented

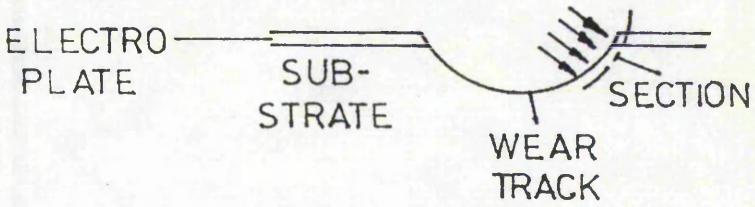
by Jain and Bahadur(27), though they consider three-dimensional contacts, and examine the tensile stresses near the surface. The other point of severe stress is of the order of half the semi-width of contact below the surface, at a depth not inconsistent with delamination, eg. A typical delaminating sheet has a thickness of about 1 μm, whilst a typical equilibrium roughness for a wearing pair which does not form a glaze is 1-3 μm C.L.A. The contact patch associated with an asperity will therefore have a diameter of about 3-5 times the thickness of the sheet, and the critical depths of worst stress and detaching sheet approximately coincide.

These propositions will be considered in greater detail in chapter 2, when the effect of residual stresses will also be taken into account. Analysis of this sort, because it does not provide for the presence of growing cracks, can only give a rough idea of the mechanisms of wear. A method will now be introduced whereby the influence of the cracks themselves may be properly allowed for.

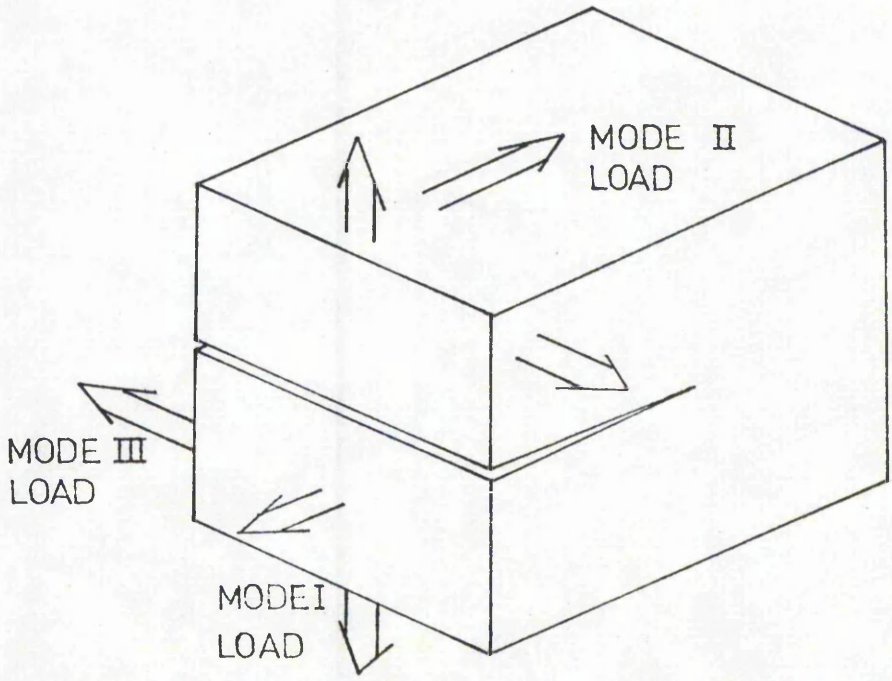
1.5 Fracture Mechanics and Wear

One of the curious features of sliding wear is the way surface layers of a body appear to flow with ease plastically, and at the same time show features of brittleness, fig.5. Nor is the phenomenon one of simple work-hardening, for enormous strains, up to 8 in copper, have been detected (28), when materials under tensile loading conditions would long since have failed. Bridgman's classic experiments of the 1950's illustrate that a large confining pressure ($\bar{\sigma} \ll 0$) can improve ductility considerably, and





Rolling Wear track showing large number of voids. Fig.5.



The three ways in which a crack may be loaded.Fig.6.

this may, to some extent, explain the large strains. Nevertheless, the entire history of spalls and the final fracture of delaminating sheets are both brittle phenomena. For this reason fracture mechanics is beginning to prove useful in studying wear.

Fracture mechanics started in 1920 when Griffith examined the failure of completely brittle glasses. He used the elastic stress concentration factor (e.s.c.f.) for an elliptical hole, recently determined by Inglis, and took the limit as it became infinitesimally wide and crack-like. From this Griffith deduced the release of local elastic energy if the crack were to grow, and postulated that this would occur spontaneously if the elastic energy released exceeded the energy needed to create new crack surfaces. It transpired that this would happen if the quantity $\sigma\sqrt{c}$ reached a critical value, and the result was confirmed experimentally. The most important advances were then made after the Second World War, following the brittle failure of several continuously welded ships. A dimensionally similar quantity to that used by Griffith was recognised as being the key parameter, providing the material yielded to only a limited extent, and this was given the symbol 'K'. The quantity 'K' is given a variety of subscripts. Consider fig.6, which shows the three ways in which a crack may be loaded. The variable which governs the rate of crack growth is called the stress intensification factor (S.I.F.) and is defined for each loading arrangement; K_I is the S.I.F. corresponding to the opening mode, K_{II} relates to the shear mode and K_{III} to the antiplane shear mode. Stress intensification factors always have dimensions of force×length$^{-3/2}$

and characterise accurately the crack tip stresses in terms of the distant loading and component geometry. Except for very simple geometries they are quite difficult to determine. Note, too, that they are always proportional to the applied load. When a critical value of S.I.F. is attained, called the fracture toughness and denoted, for mode one under plane strain conditions by K_{IC}, the crack will propagate freely. Normally, as the crack grows, so the S.I.F. increases. Thus, as soon as the crack starts to grow it will continue to do so at an ever increasing rate and brittle fracture results. One of the advantages of fracture mechanics is the unified approach to fatigue and brittle fracture which is made possible. Thus, under repeated loading, even if the fracture toughness is not reached, some crack growth will occur, and the amount of growth is often proportional to ΔK^4. Empirical laws relating the crack growth to the S.I.F. exist, so that by integrating them the life of a component can, in principle, be found. Below a critical threshold S.I.F., designated ΔK_{IC} no crack growth will occur: this corresponds to the idea of a fatigue limit in classical fatigue.

It is apparent from previous comments that under rolling wear conditions only shear mode, or mode II crack growth can occur. When a tractive force is also applied a zone of tension develops behind the contact zone and in this region mode one growth may also be possible. Polk and Rowe(29) estimated the rate of crack growth in failing rollers by sectioning, and extensive experimental work by Soda et al (30) lead them to the conclusion that

wear is a fatigue controlled process. Halling(31) in a novel theoretical paper recognised wear as being due to fatigue. None of these authors attempted to use fracture mechanics to assess wear, and it was left to Suh (32) again to provide some innovation in determining S.I.F.'s. More recently, work has been published by Hornbogen(33) stating the role of fracture toughness as the determining factor of wear rate, though his hypothesis was based on a dimensional argument, rather than mechanics. Also, McClintock(34) has examined the stresses and plasticity around a crack lying beneath a rolling contact. Even this paper avoided using the S.I.F. by using an unusual continuum-dislocation hybrid approach. Fegredo and Pritchard(35) performed sectioning on worn rollers undergoing rolling/sliding and clearly identified growing subsurface cracks. Muro et al (36) have treated the growth of surface cracks in rollers of high quality steels experimentally, and their paper is important because it introduces the key role of residual stresses. Muro found that cracks were often surface initiated and identified the initiation of cracks with a small zone of residual tensile stress. Later, it will be shown that such a residual stress has a very significant effect in many configurations. Zum Gahr(37) has recently applied fracture mechanics to abrasive wear.Wear as a fatigue process has been the subject of papers by Kolozsvary(38) and Finkin(39), the latter using the Coffin-Manson exponent to treat asperity fatigue. Finally, Roberts et al very recently published a paper (40) on the wear of dental alloys in which they cite fracture toughness as the best measure of wear resistance.

Returning to the question of whether wear cracks are

surface or subsurface initiated, it appears that three factors strongly influence the location;

A. Because of the severe state of stress introduced at the surface, and the increased amount of microslip, any shear traction applied strongly encourages surface initiation. This condition exists at gear teeth, where there is normally a small tangential motion.

B. Poor quality steels with many subsurface flaws and precipitates tend to produce subsurface initiation, because of the large number of stress-raisers and the questionable bond of second phase particles. Further, inclusions may break in a brittle manner and provide a stress concentrator.

C. Boundary lubrication often causes any surface flaws to grow more quickly than those not open to the surface, because of the hydraulic action of lubricant as it is pumped towards the crack tip.

Now that the various possible techniques of mechanics which might be used to assess wear have been specified, one particular topic will be studied, viz. the influence of pre-existing stresses on wear. Mainly continuum mechanics will be used.

2. Surface treatments and Residual Stresses

2.1 Surface treatments

In this chapter the physical influence of surface treatments on wear is considered, with particular emphasis on the residual stress often incorporated. This parameter is not normally evaluated, but is shown here to have a considerable effect on wear rate and the morphology of worn surfaces.

Surface treatments are attractive because a wear resistant coating may be produced which does not compromise the properties of the interior, so that, for example, a hard, brittle coating may be formed on a tough steel component. It is possible to classify treatments into those which require the laying down of an extra layer of material, such as electrodeposition, vapour deposition and ion implantation, and those which do not, such as shot-peening and ball burnishing. Further, the materials chosen for the coating fall into two distinct categories; those which are very much harder than the substrate, such as chromium, and those which are much softer, such as cadmium or gold (because the volume of material required is very small, material costs are low and choosing a precious metal is economically reasonable). Clearly, each class of treatments must have a different type of influence on wear rate. Reviews of surface treatments were published by James et al (41) and by Hurricks(42).

Shot-peening and ball burnishing do not influence the chemistry of a component in any way, and so must have solely a physical influence. Three main effects are;

A. The surface finish of the component is improved.

B. Plastic deformation of surface layers produces work-hardening.

C. Compressive residual stresses are introduced into surface layers.

Work hardening is suggested by Rajasekariah and Vaidyanathan (43) as being mainly responsible for improved wear resistance, as they found that wear rate decreased monotonically with burnishing load, whereas the surface finish deteriorated at high loads. Fretting experiments conducted by Waterhouse (44) using shot-peened stainless and mild steels showed considerable improvements over untreated steels. Waterhouse points out the possibility of residual stresses being modified by plastic deformation during wear, so that shake-down to a common residual stress system might occur. However, the clamping pressures used in his experiments would seem too low, and the initial stresses probably persisted.

The value of putting a thin layer of soft material on a hard substrate was recognised by Bowden and Tabor(2). They reasoned that a soft layer would flow easily under traction forces and so transmit low stresses to the substrate, whilst the strength of the interior would be better able to withstand fatigue stresses. For this to be effective, the thickness of the soft layer must clearly be less than the depth of worst Hertzian stresses. Sliding wear experiments were performed by Jahanmir et al (45,46) using cadmium plate. They found that the wear rate was initially high, but that as the coating thinned to about 0·1μm the wear rate fell significantly. The explanation put forward was that the 'equilibrium' plating thickness corresponded to

Suh's dislocation-free zone, so that the plate was free of defects. Bowden and Tabor's bulk explanation seems equally feasible, particularly as Jahanmir's experiments relied on the attainment of a quasi-equilibrium thickness by running in wear, which is always more rapid. Experiments by Takagi and Liu(47) and by Antler(48) illustrate the lubrication provided by gold. This is especially useful for wiping electrical contacts, because of the inertness and conductivity of gold, but its softness leads to difficulties in ploughing,ie. severe abrasive wear (48).

The laying down of a hard surface material seems to be equally effective in reducing wear, though the thickness needed is rather larger than that quoted by Jahanmir, and the worst Hertzian stresses occur within the treated layer. Hard electrodeposits, usually of nickel or chromium, find immediate application in the repair of worn or wrongly machined components, and Falex tests have shown that the repair has at least as good wear resistance as the original. Electrodeposited or electroformed balls are used in high speed ball bearings, where their low mass leads to lower centrifugal loading (51,52). A more rigorous examination of the parameters controlling the wear of chromium was undertaken by Eyre and his co-workers (53,54). Chromium electrodeposits frequently have a large tensile stress built in, and this produces a cracked surface. In the more severely cracked 'channel-type' chromium debris was often trapped, producing severe three body wear. Further, the poorer mechanical strength of channel chromium lead to a flaking of the surface. Briscoe et al (53) noted the brittle, though plastic, nature of chromium, and characterised the hardness

by applying a spherical indentor and noting when a complete circumferential crack had formed. This is very similar to the technique of estimating the critical flaw size of a material, by producing a Hertzian cone crack (55). Thus, the wear experiments were really related to a brittle fracture toughness parameter rather than the hardness. Also, variation of toughness and corresponding wear resistance with plating current density were reported.

There have been some publications on the influence of plating variables on wear resistance and other mechanical properties. Ledford and Dominik(56) showed that some additives to nickel plating baths produced typefaces with a better wear resistance. A comparison of the wear resistance of conventionally deposited and electroless nickel was made by Wiegand and Heinke(57) who found that electroless nickel gave poor results, owing to its brittleness, even though it was the harder of the two. They also recognised the deleterious effect of a large built in tensile stress, though this was not quantified.

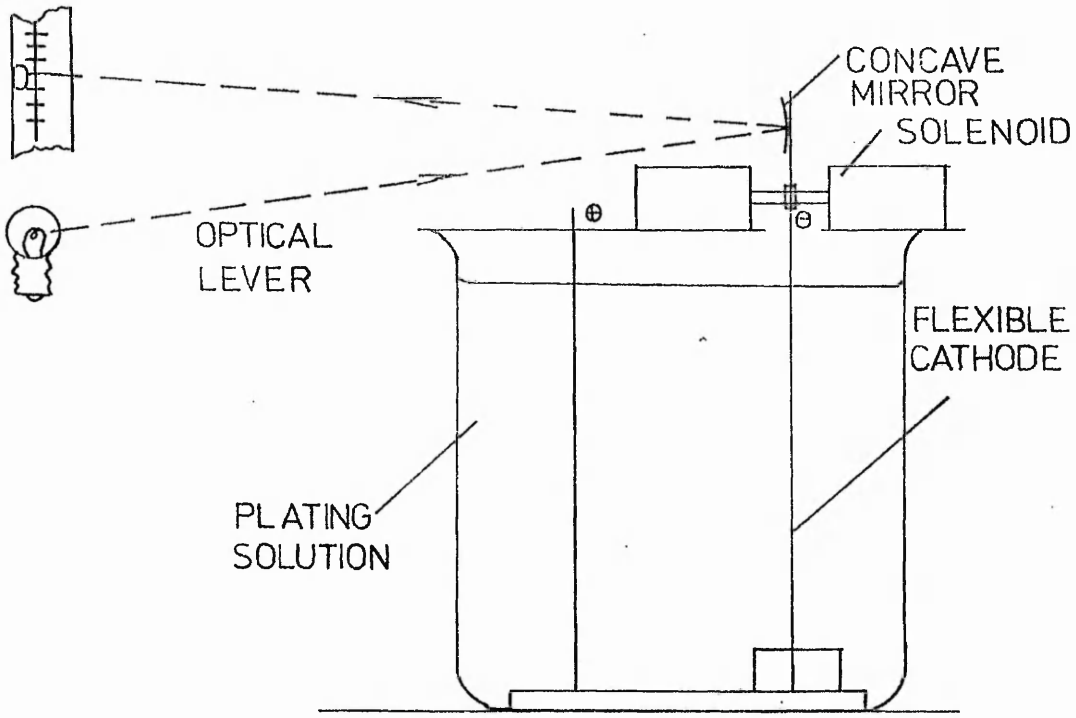
Residual stresses seem to be important in reducing wear, therefore, in peened, burnished and deposited treatments. The easiest stress to control and to measure is that found in electrodeposits. It was therefore decided to measure experimentally the wear of electrodeposits with different built in stresses. Nickel was chosen as the most suitable electroplate, since its elastic properties are nearly the same as steel, which was used as the substrate, and there would therefore be no discontinuities in the stress field at the interface. Some effort was spent in determining the stress incorporated in the deposit, and

the method developed is described in the next section.

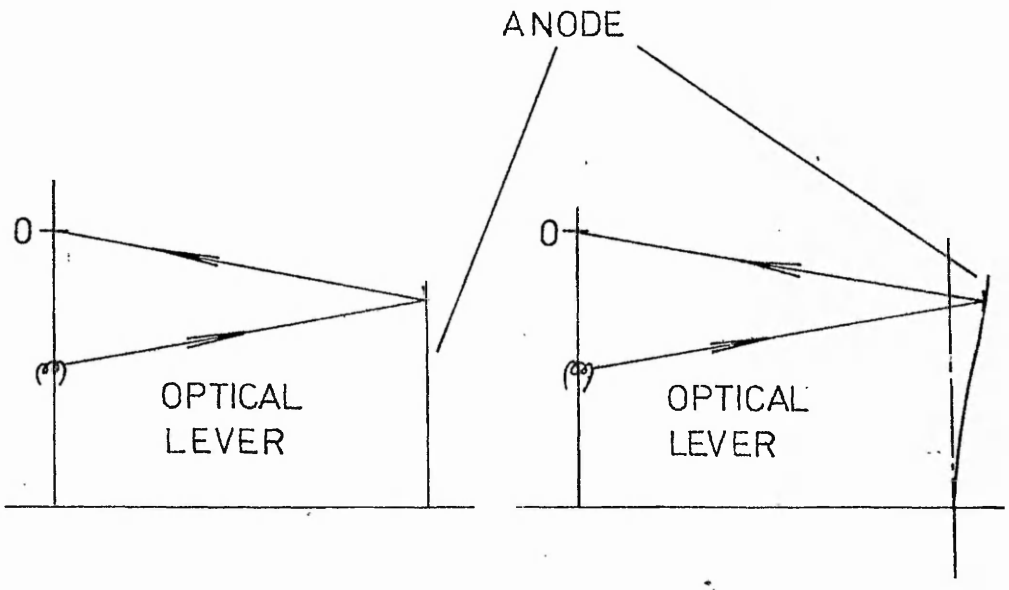
2.2 Properties of Electrodeposits

There have been many reviews of the various methods available to determine the stress in a deposit, notably by Williams(58), Walker(59) and Borchert(60). Recently, Weil(60) pointed out the distinction between long-range ordered stresses, ie. those which would contribute to the distortion of a thin component, and the short-range stresses found within individual grains and affect mainly the measured hardness of the material, rather than causing any macroscopic change of shape. An instrument to measure the second type of stress was given by Begh et al (62), whilst many papers have been published describing the assessment of macroscopic stress; methods based on the distortion of a nominally straight strip are given by Hoar and Arrowsmith(63,64), Gabe and West(65), Norris(66) and Sykes and Rothwell(67). Methods using a spiral strip are mentioned by Brenner and Senderoff(68,69) and instruments based on the dilatometer are described by Cleghorn et al (70), Gabe(71) and Kushner(72).

Of these devices, the one which seems to be the most fundamental and to introduce the smallest number of unknowns is that of Hoar and Arrowsmith, shown in fig.7. The cathode of the plating bath is a thin strip, stopped off with protecting lacquer on the side further from the anode. Affixed to the top are the armatures of a pair of solenoids, which work antagonistically, and a concave mirror. The mirror is part of an optical lever. As plate is laid down, any stress present bends the cathode and hence tilts the



The Hoar and Arrowsmith apparatus. Fig. 7.



Lack of uniqueness of null position. Fig. 8.

mirror. By applying a suitable current to each solenoid, a force is generated which maintains the strip at the null position, and a note is made of the solenoid current. Calibration is performed by putting in a fresh "cathode" and tilting the apparatus onto its side. Known weights are then added to the cathode tip, and the current needed to maintain equilibrium is noted. Hoar and Arrowsmith's method has these advantages;

a. The elastic constants of the substrate do not need to be known. Any anisotropy of the substrate does not affect the instrument.

b. Very little relaxation of the deposit is permitted, although a very slight S-shape will develop.

c. It is essentially frictionless, but the damping effect of the plating solution and surface tension may influence the result at very low forces.

d. The specimen is much simpler to make than that needed for a spiral contractometer.

e. The current distribution is nearly uniform.

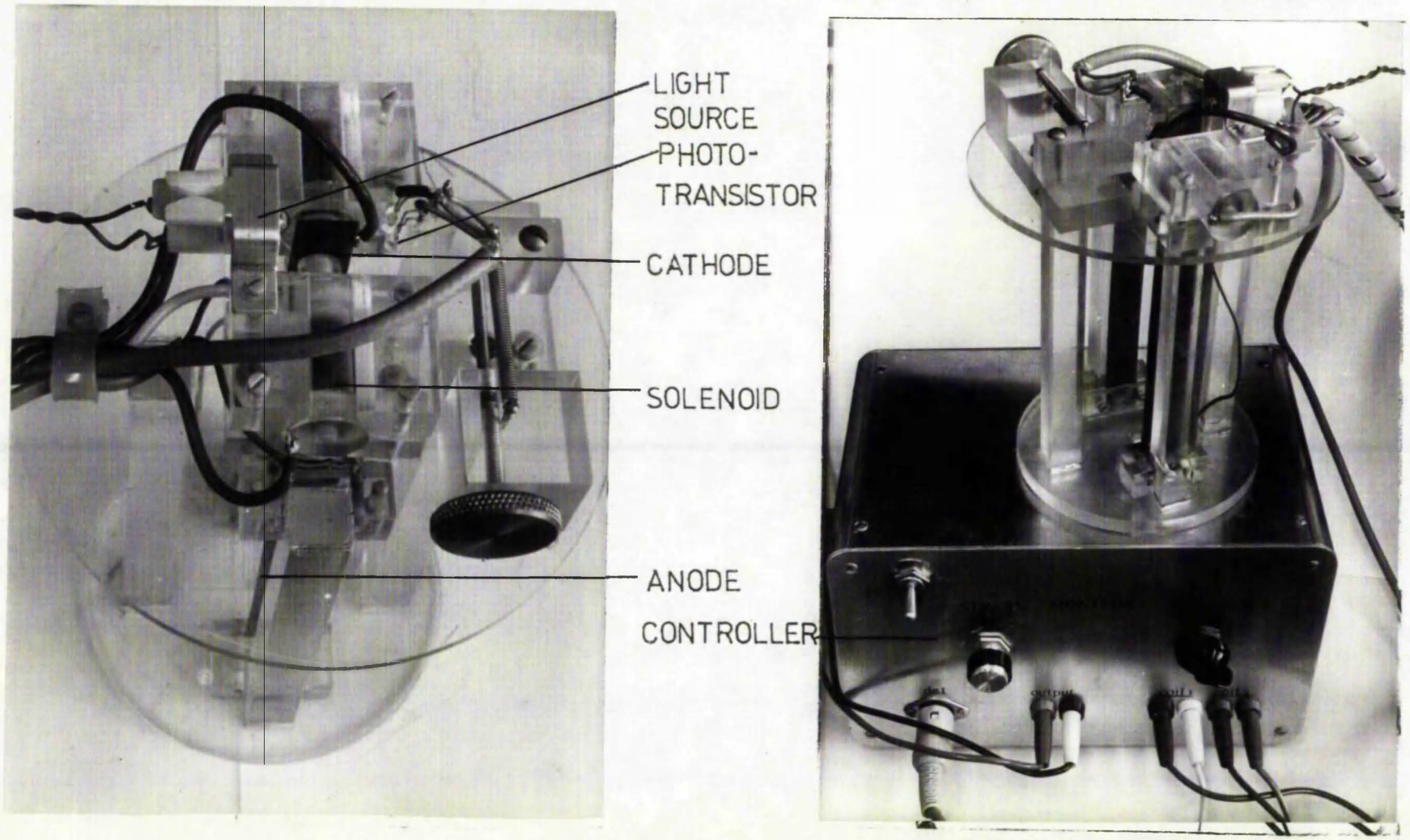
The disadvantages are;

a. The armature assembly has to be aligned and fixed before fitting into the rest of the apparatus. This has to be done for each test and is both tedious and detrimental, since cleaning activates the surface causing rapid deterioration. The final electrolytic etch may be done with the strip in place.

b. Owing to anticlastic distortion and lateral stresses within the strip, high tensile stresses can cause the strip to become a shallow dish shape, increasing its rigidity.

c. The plating solution cannot be agitated or aerated.

d. Perakh(73) pointed out that because the angle of the



Automated Hoar & Arrowsmith apparatus.

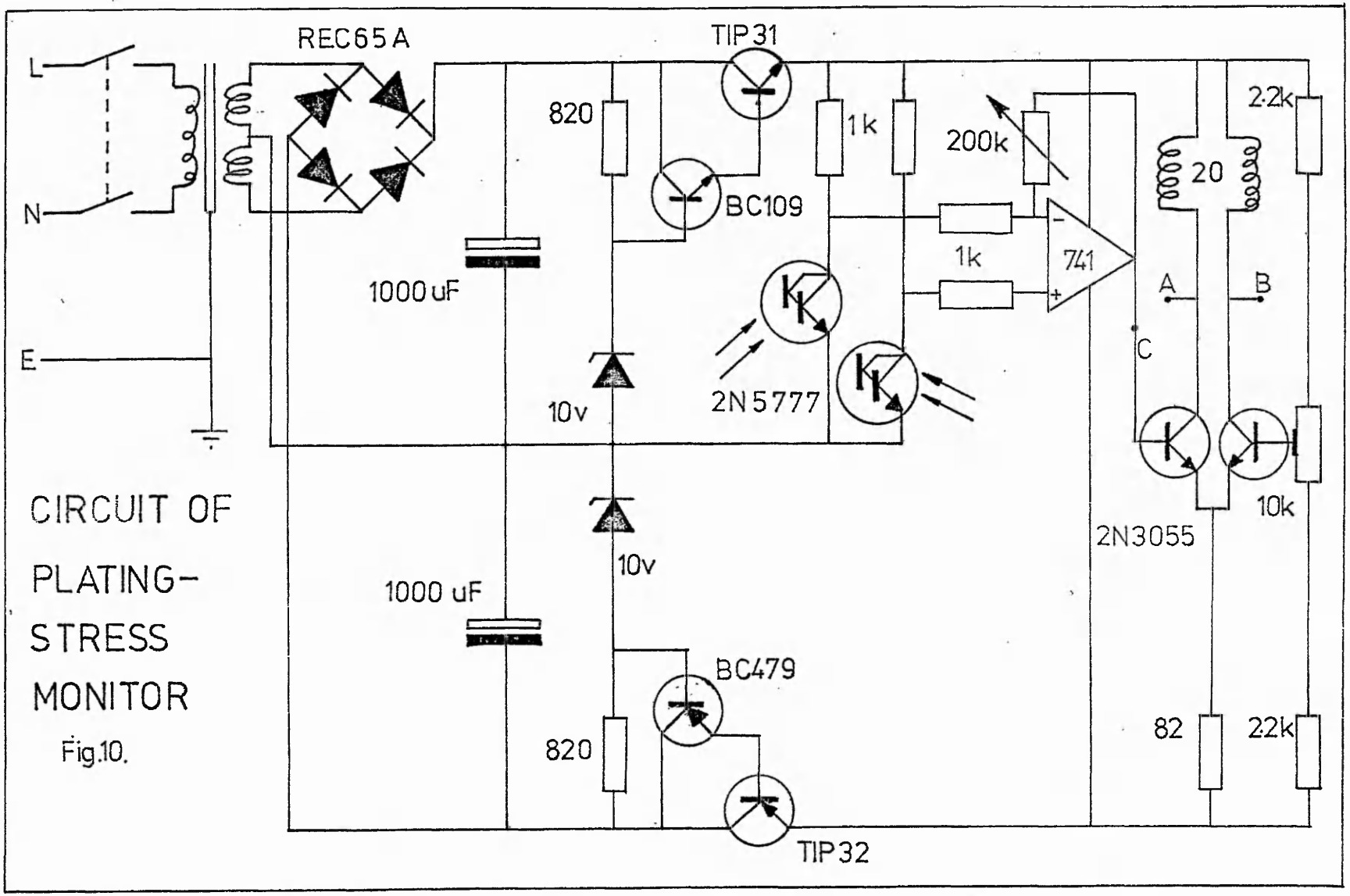
Fig. 9.

strip is not uniquely determined by its position, there may be ambiguity in the null position, as shown in fig.8.

An automatic plating stress monitor has been described by Koch et al (74) which was based on the spiral contractometer, and another by Sykes et al (75), which was based on the old technique of measuring the deflected form of a strip. These methods are convenient but lack the accuracy of Hoar and Arrowsmith's method. The apparatus to be described is an automated version of Hoar and Arrowsmith's device which records the force on the strip and removes some of the other drawbacks.

The same basic arrangement as Hoar and Arrowsmith's is used, fig.9., but the optical lever is replaced by a light beam shining across the plane of swing of the strip. Two closely-mounted photo-transistors lie in the shadow of the strip, and, in the equilibrium position, have approximately equal amounts of light falling on them. As the strip bends one photo-transistor is covered more than the other, and this difference is supplied to a controller, which adjusts the ratio of current in the two solenoids so as to centralise the strip. A signal proportional to the current ratio is fed to a chart recorder. Objection (d) is therefore removed, since the apparatus is sensitive only to the lateral position of the strip. Further, owing to the finite separation and area of the photo-transistors a small oscillation of the strip occurs (of amplitude about 1mm); this tends to agitate the plating solution and produces plates of noticeably better quality, with no porosity.

Fig.10 is a circuit diagram of the controller. There



CIRCUIT OF PLATING-STRESS MONITOR

Fig.10.

is a standard three-rail power supply and the light sensors are connected to an operational amplifier in difference amplifying mode. The gain is limited by a variable feedback resistor, though the addition of an otherwise desirable capacitive integrating term lead to instability. The output of the operational amplifier is connected to a transistor pair whose total emitter current is constant. Each transistor drives a solenoid and the null position can be adjusted by varying the nominal base potential of one transistor. All adjustments must be performed with the apparatus immersed because of the additional damping provided by the plating solution.

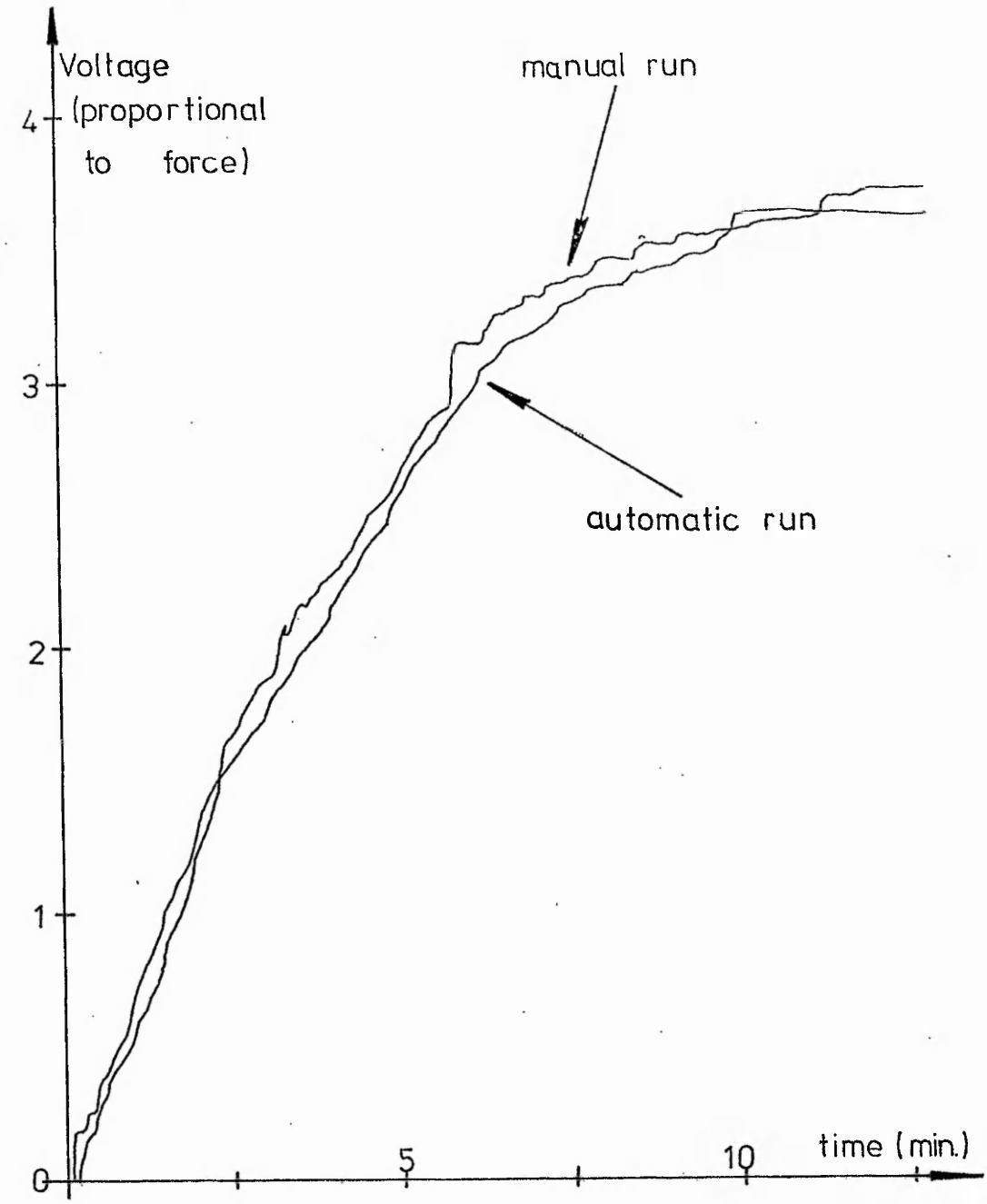
Calibration was performed in a novel way since difficulties were experienced with the method usually given in the literature, ie. adding milligramme weights to the strip. The weight of the strip and armature alone loads the device beyond the useful range. Therefore calibration was performed by gradually tilting the assembly and noting the pen-recorder reading. The equivalent load is found by considering the strip to be a cantilever with a uniformly distributed load due to self weight and a point load at the end due to the weight of the armature. The restoring force is thus given by;

$$F = g.\sin\theta(\tfrac{3}{8}m_1+m_2) \qquad (11)$$

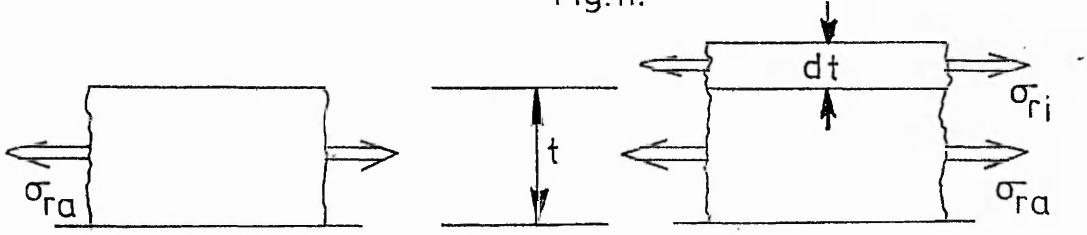
where m_1 is the mass of the strip.

m_2 is the mass of the armature.

A manual run was performed as a check by breaking the circuit at point C (fig.10), monitoring the output with a voltmeter, and adjusting the base voltage by a potentiometer. A comparison of two nominally identical runs is shown in



Typical pen-recorder traces for tensile electrodeposit.
Fig.11.



Deducing the instantaneous stress. Fig.12

fig.11. Notes on the improved apparatus were published (76).

The average stress within the deposit, in terms of the restoring force applied is;

$$\sigma_{ra} = \frac{2.l.F}{b.t.t_o} \qquad (12)$$

where l, b and t_o are the length breadth and thickness of the strip and t is the thickness of the deposit.

The variation of average stress with thickness was found to be of the same form as the law proposed by Kushner(72);

$$\sigma_{ra} = A+B.e^{-kt} \qquad (13)$$

What is required is the way the stress varies through the depth of the deposit. Consider fig.12, which shows the deposit after plating to a depth t, and after an extra thickness dt has been added. The new average stress is given by;

$$\sigma'_{ra}(t+dt) = \sigma_{ri}dt + \sigma_{ra}t$$

$$\sigma_{ri}dt = (\sigma_{ra}+d\sigma_{ra})(t+dt) - \sigma_{ra}t$$

$$= \sigma_{ra}dt + (t+dt)d\sigma_{ra}$$

$$\sigma_{ri} \doteq t.\frac{d\sigma_{ra}}{dt} + \sigma_{ra} \qquad (14)$$

Substituting equation (13) into equation (14) gives;

$$\sigma_{ri} = A + B(1-kt).e^{-kt} \qquad (15)$$

The constants A, B and k are obtained by fitting curve (13) to the pen recorder trace at three widely separated points.

To determine some other properties of nickel electroplate a strip of stainless steel was plated. The coating, of thickness 0·02 to 0·04 mm, was released by carefully filing material from around the edges. A piece of masking tape was stuck over the divorced plate and a standard tensile test specimen cut out. The specimen was peeled

off and a tensile test performed on an 'Instron'. The following results are the average of five tests performed on stress-free electroplate;

$$\sigma_o = 506 \text{ Nmm}^{-2}$$

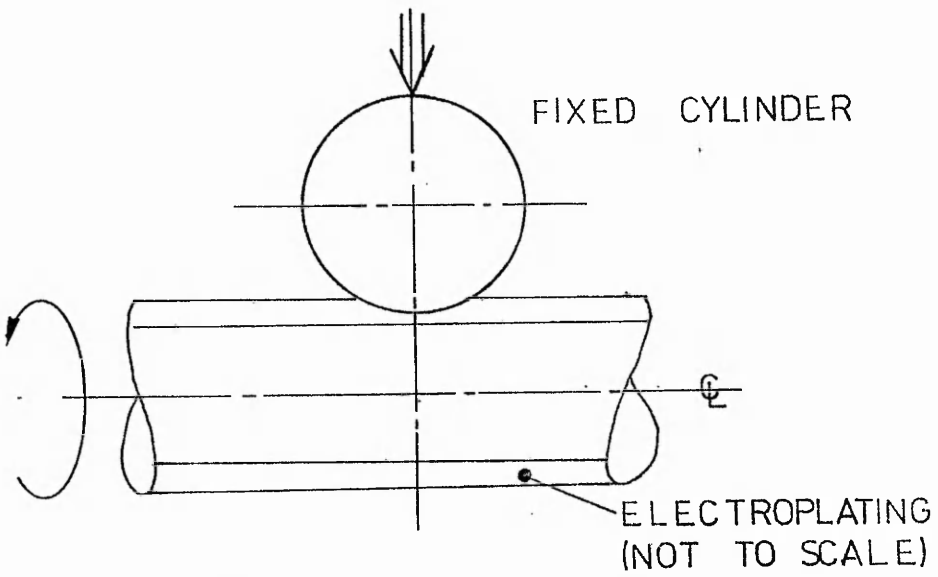
$$\epsilon_o = 1{\cdot}28\%$$

$$E = 195 \text{ Nmm}^{-2}$$

The yield stress is within 5% of that obtained from a micro-hardness test. A severe limitation of the technique is an inability to plate material containing a large tensile stress, because the stress causes splitting and peeling. Etching the surface of stainless steel prevents this but makes the plate difficult to remove without breaking up.

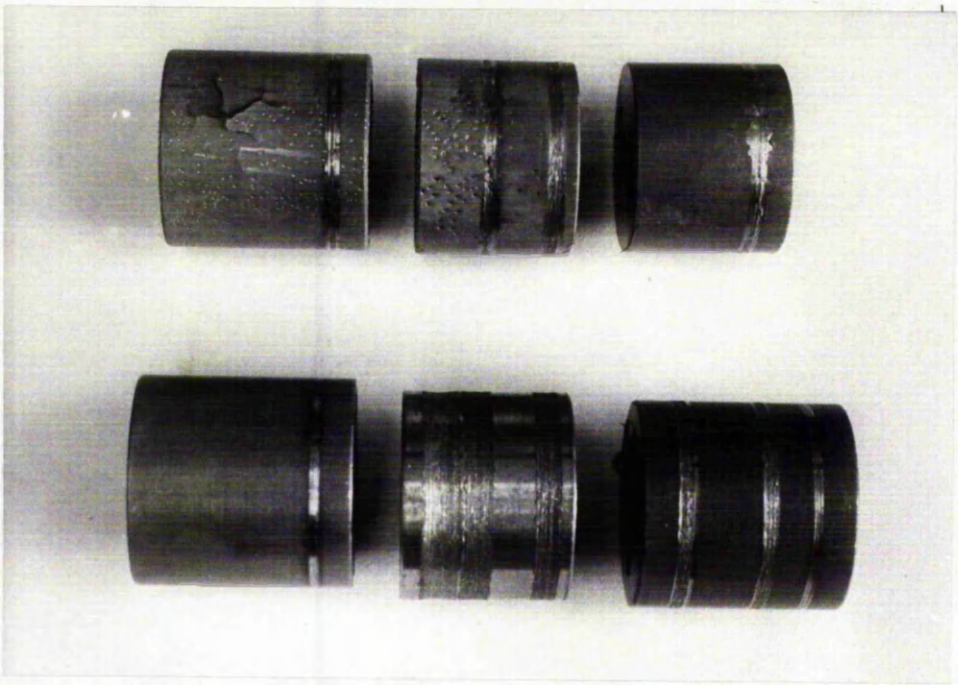
2.3 Wear tests

Wear tests were done on a small lathe originally modified as a student project (77). A crossed cylinder arrangement was used which has the advantage that no ploughing occurs; this was found to be a difficulty with pin on cylinder arrangements, but it has the disadvantage that the thickness of plate being worn is not constant, fig.13. Tests were carried out at a load of 19·4 N with a turning speed of 360 r.p.m.. The cylinders used had a diameter of 25 mm, the stationary one being hardened silver steel. The specimens were plated from an all-chloride bath, which is more tolerant of impurities, and, according to Broszeit(78), produces nickel with a greater wear resistance, at least in corrosive conditions. By plating with a cool (25 °C) bath using direct current, a tensile stress of about $+400 \text{Nmm}^{-2}$ was found to develop. By gradually warming the bath to 60 °C and at the same



Variation of electroplate thickness across contact patch . Fig.13.

time superimposing a square-wave on the plating current, an idea due to Kendrick(79), the internal stress could be reduced to negilible proportions. A square wave of 400 Hz and giving approximately 15% de-plating per cycle was most effective in annulling the stress. This was provided by using a signal generator connected to a d.c. amplifier, and the current was measured by monitoring the voltage drop across a standard one ohm resistor, using an oscilloscope. Compressive stresses were introduced by making the plating solution 0·01 M with respect to benzene sulphonic acid (80). Applying a square wave again reduced the absolute value of the stress, this time from a maximum of just over $-200 Nmm^{-2}$. The stresses quoted are average stresses, as found using the apparatus just described, and the conditions were replicated as far as possible (temperature, current density and square wave superposition) when plating a cylinder specimen.



Top left: very high tensile stress has caused cracking, even before wear. Some porosity.

Top centre: severe porosity caused by insufficient bath agitation.

Top right: this coating adhered poorly (owing to improper cleaning) and wear has cause peeling of the plate.

Bottom left: a smooth, bright wear track in good quality nickel plate.

Bottom centre: coarse, severe wear track in unplated steel.

Bottom right: the left hand wear track has worn through in the centre and shows severe wear of steel. Either side, the crossed cylinder was supported by nickel.

Some plating defects and wear tracks. Fig.14.

The hardness of each specimen was measured before performing a wear test. Owing to the thinness of the electrodeposit (about 10μm), it was not possible to use an ordinary hardness tester, because the depth of impression would be so large that the associated plasticity field would extend well into the substrate. Therefore a Leitz micro-hardness tester was used, with a Vickers pyramidal indentor. Ideally, for a hardness of about 160 V.H.N., the absolute minimum load of 25g. should have been used, but difficulty was experienced in obtaining repeatable results because of the small size of the resulting impressions. Therefore, a load of 50g. was used consistently for the tests, giving impressions about 30μm across. The estimated penetration corresponding to this load and hardness is 3·2μm, so that the bulk of the flow zone should lie within the deposit. There will inevitably be some "anvil" effect from the substrate, though the elastic behaviour of nickel and steel are very similar.

Fig.14 shows a selection of worn specimens, and defects which were found. To eliminate the porosity seen in some examples a motor was fitted to rotate the specimen during plating; this also helps to maintain an even thickness of plate. There was no obvious difference between the wear regimes of the specimens (except for the unplated steel). A summary of results is tabled below, each entry being the aggregate of five experiments. Several results had been discarded owing to plating faults- poor adhesion, porosity, cracking of tensile specimens and uneven deposits. Some results are plotted in fig.15.

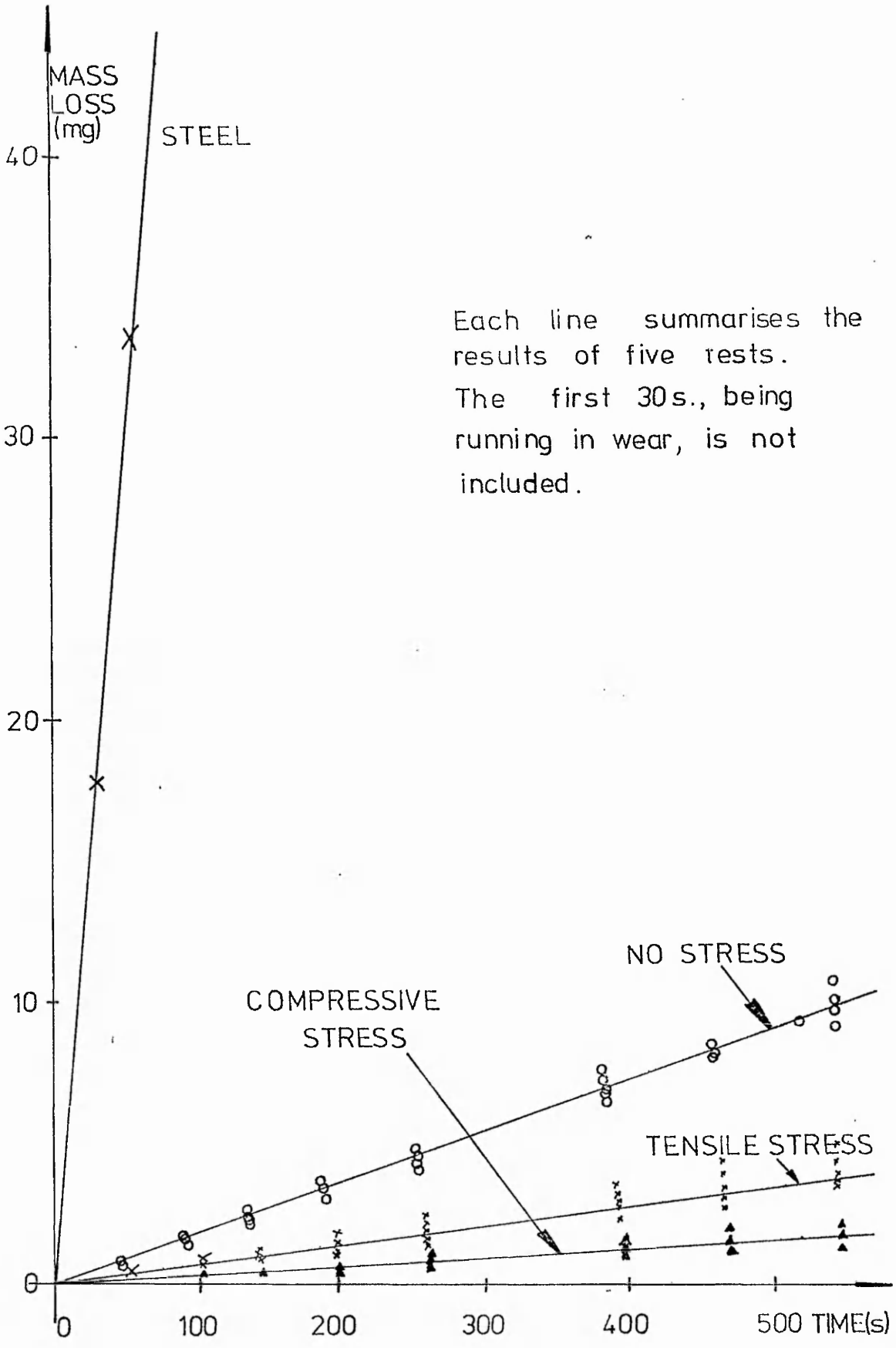
Table 2. Results of Preliminary Set of Wear Tests

Deposit thickness (μm)	Stress (Nmm^{-2})	Hardness V.H.N.	Wear (mgs^{-1})	C.L.A. (before wear) (μm)
Steel	-	200	0·805	1·0
50	+400	260	0·007	1·6
50	0	160	0·018	0·9
50	-175	220	0·003	0·4
18	0	165	0·018	1·0
130	0	153	0·018	0·9

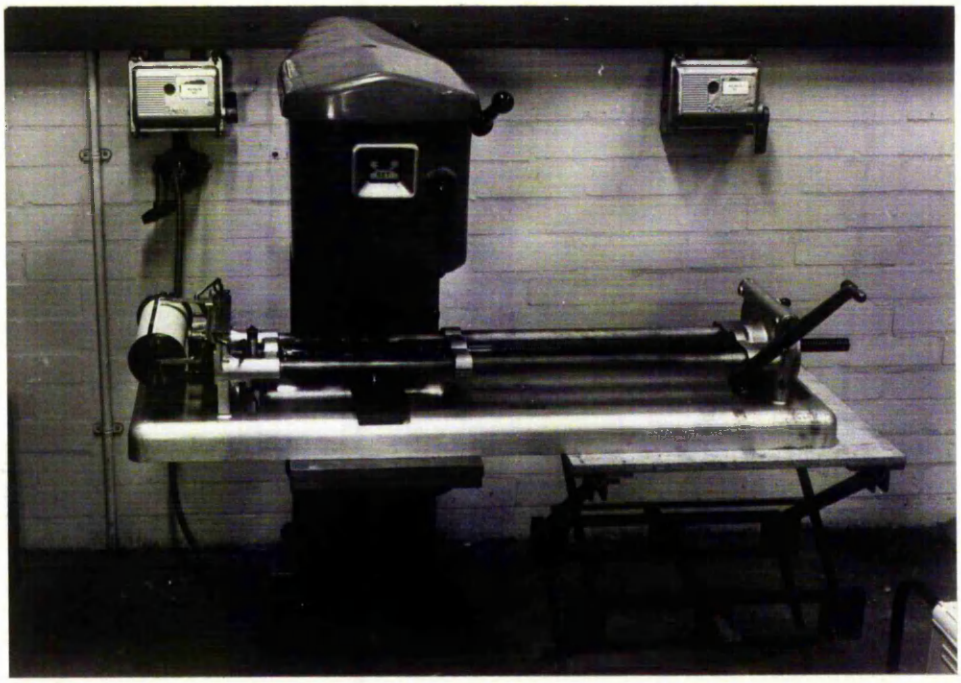
Very thin deposits (2·5μm), tried on one or two specimens, failed more less immediately, possibly because of the way the deposit depth varies across the contact patch, as mentioned earlier. The following conclusions were drawn;

1, Wear seems to be independent of thickness, above a certain critical thickness. Georges and Kabinowicz(81) arrived at the same conclustion for chromium, cobalt, rhenium and rhodium.

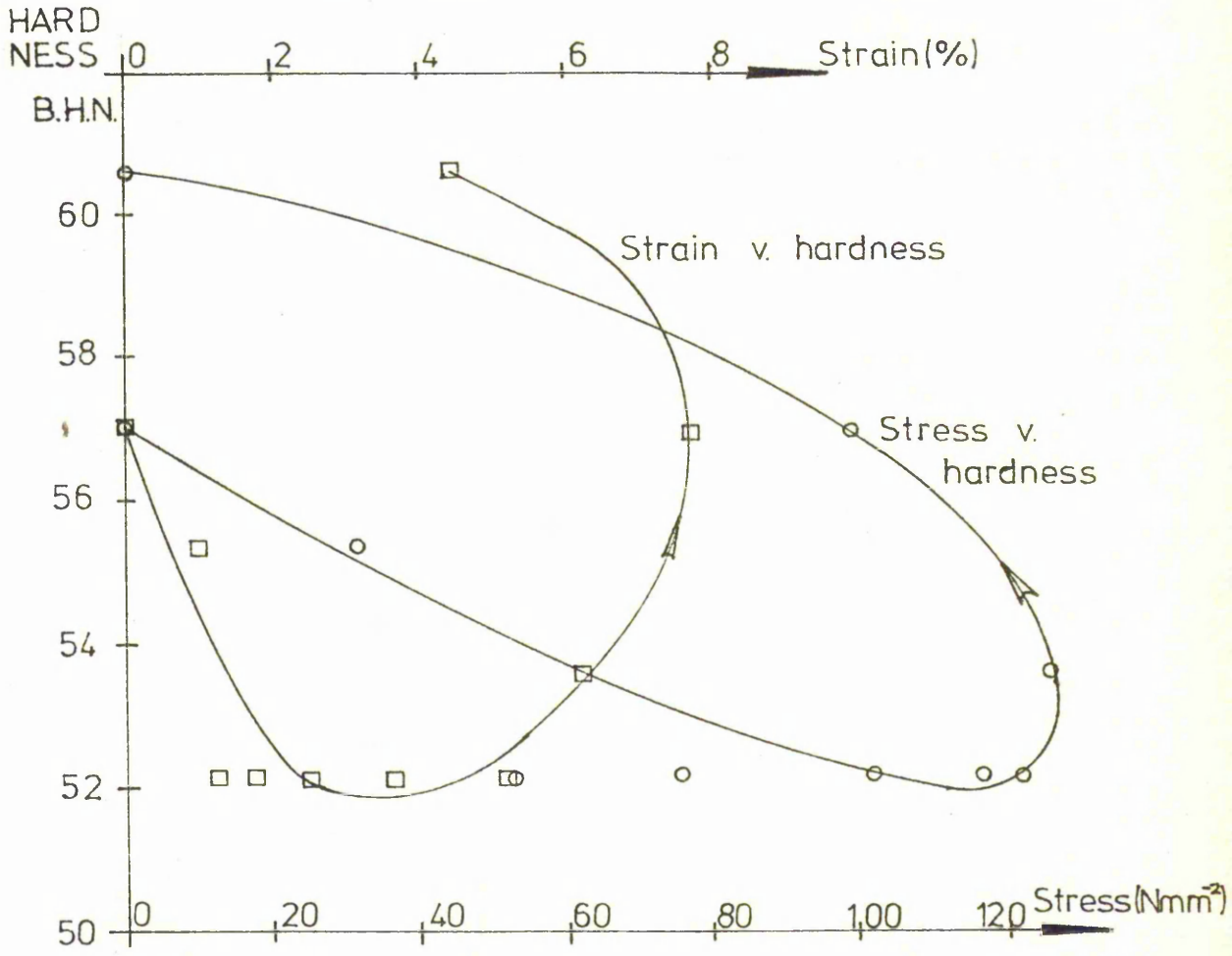
2. The rate of wear decreases with increased surface hard-



Results of preliminary set of crossed cylinder tests . Fig.15.



Hounsfield tensometer mounted on Brinell hardness tester. Fig16.

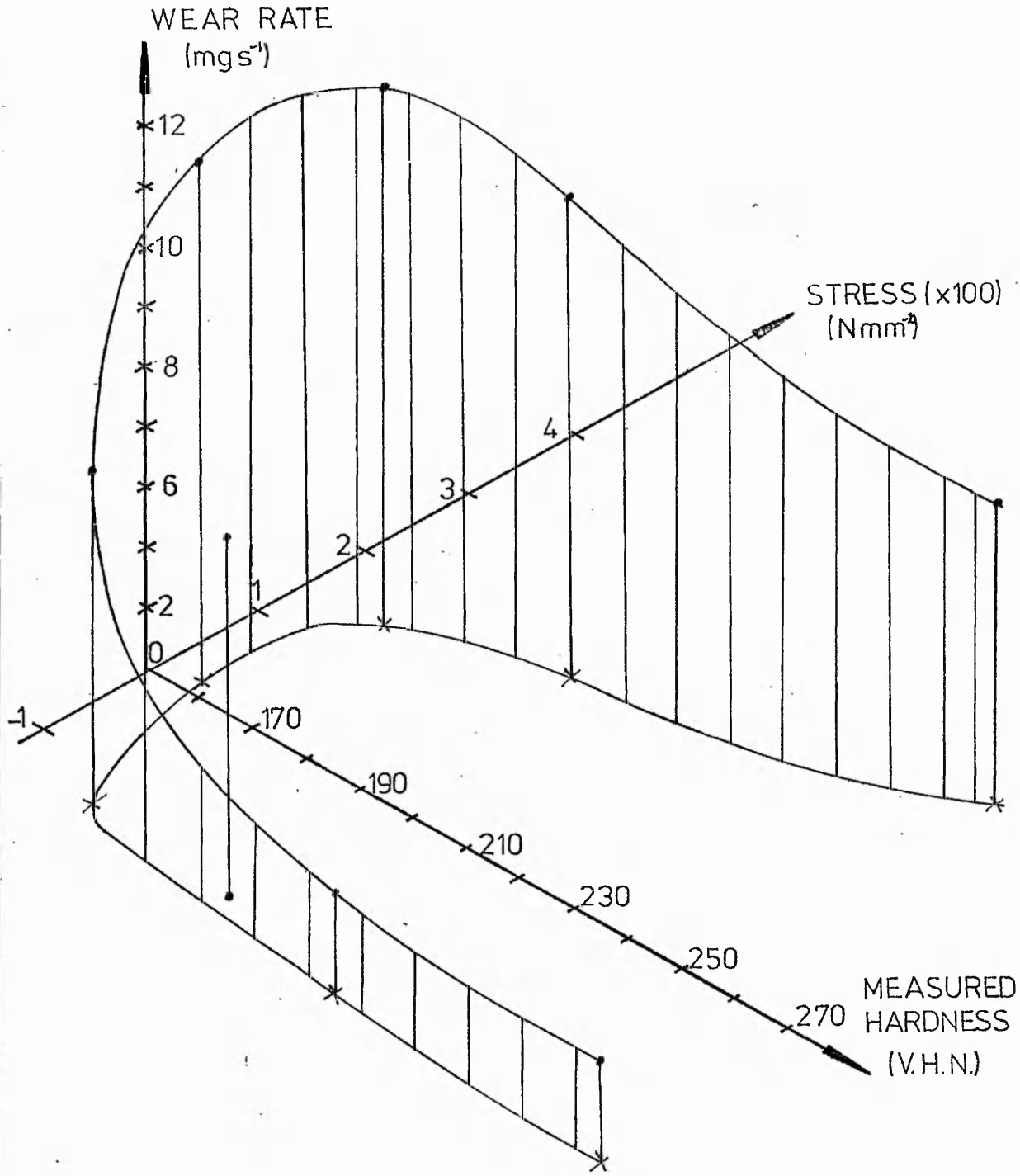


Apparent hardness v. uniaxial stress, for aluminium. Fig.17.

ness. This is to be expected from Archard's theory.
3. The surface benefits from having a compressive stress built into it.

It was observed that specimens with a high tensile stress wear quite well. This could be due to their greater hardness since it was anticipated that the tensile stress itself would be deleterious. Normally, a tensile stress would lower the apparent yield point, as in auto-frettage, so that the true hardness of these specimens could be rather higher than that measured. Also, the micro-stresses, which were not taken into account, may have contributed to a high hardness. This effect was investigated a little further by performing some hardness tests on specimens mounted in a tensometer, fig.16, so that a known uniaxial stress could be imposed (note that this varies from the test cylinders, which contain biaxial stresses). The specimens used were $\frac{1}{4}$" thick aluminium and copper strip, the latter having been rolled heavily by hand in an attempt to work harden it. When tested under an increasing tensile load, the copper showed a monotonically decreasing hardness. Results for the aluminium specimen are depicted in fig.17; initially the measured hardness fell, as with copper, but at high imposed strains work hardening occured. When 90% of the yield stress was reached the specimen was relaxed, causing its hardness to return to higher than its original value, because of the work hardening. As each indentation was made the stress dropped slightly, since local yield causes relaxation in the 'Hounsfield' tensometer.

Within a wearing pair the material experiences two reversals of shear stress per pass. The yield stress will



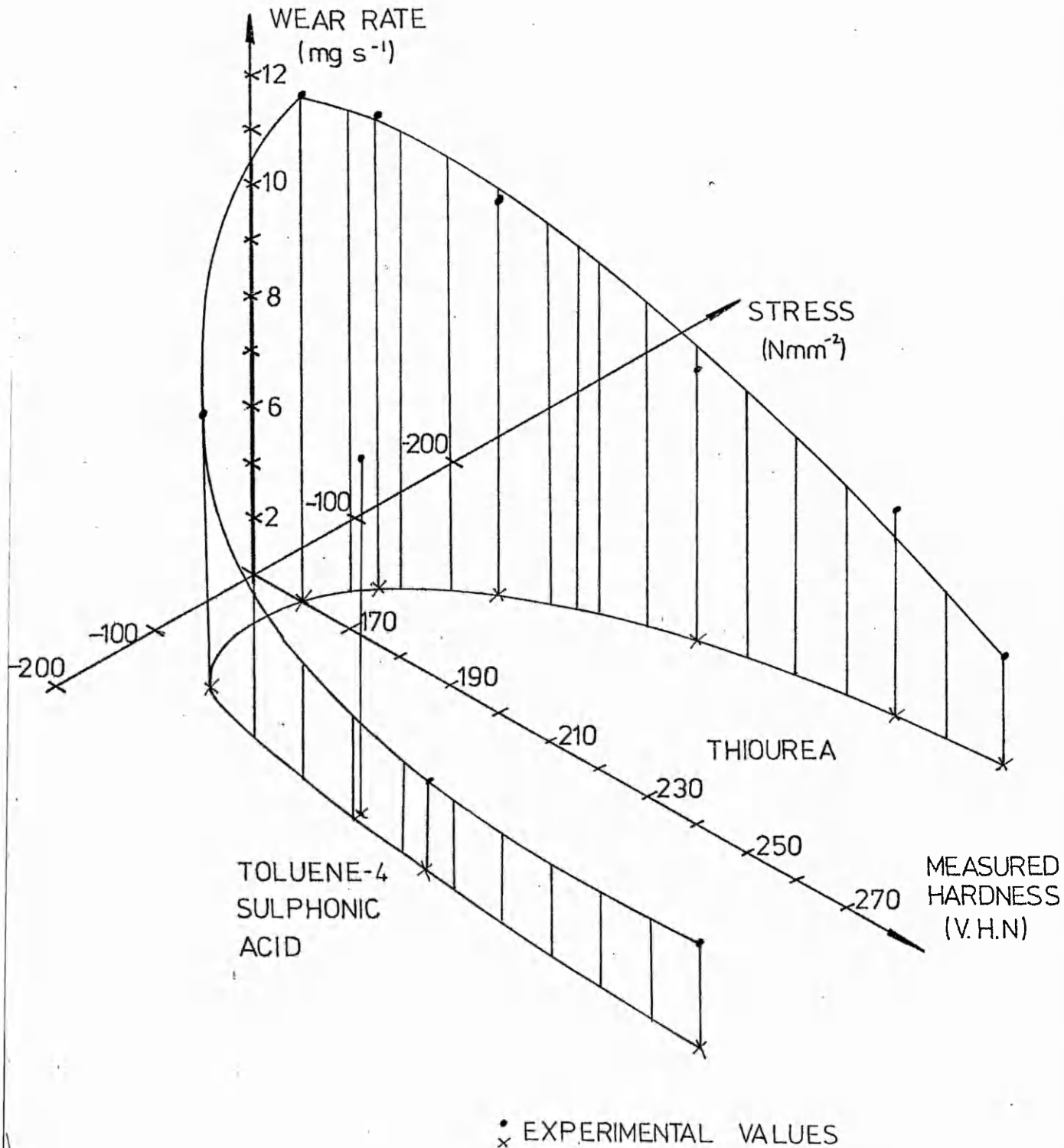
STRESS RELIEVER USED: TOLUENE-4-SULPHONIC ACID

×,• EXPERIMENTAL VALUE

Sliding wear test results-wear v. hardness v. stress. Fig.18.

vary for each application of shear, not simply because of the variation of any residual stresses which may augment or reduce, but because of the Bauschinger effect. Paul(82) notes that some 'generalized Bauschinger effect' might be expected to operate on the yield in pure shear, independently of any direct-stress phenomenon. These influences cannot be properly quantified at the moment.

Further wear tests were performed with varying locked in stresses and measured hardnesses. The results are summarised in fig.18. Points on the curve are the average of three tests, with one anomolous wear rate at V.H.N. of 195 with a built in compressive stress. This may have been caused by a poorly adhering electroplate. The highest wear rate is when the locked in stress is roughly zero, though the curve is not very sensitive to variations in stress here, particularly for small tensile stresses. A second stress-reliever was used to assess the effect of including different complexing agents in the bath. Unfortunately, all additives affecting stress used in plating baths would appear to contain sulphur, since it is a large atom, and when included in the lattice produces a local compression field. This is relieved in the direction perpendicular to the free surface since there is no material to support such a stress. The influence of sulphur as a solid lubricant was considered and so the coefficient of friction was monitored in all the tests. It was always a little over 0·3, with some stick-slip being experienced until running-in was complete. Results from experiments using two different stress-relievers are compared in fig.19. Thiourea, used in the second set of tests,has a greater



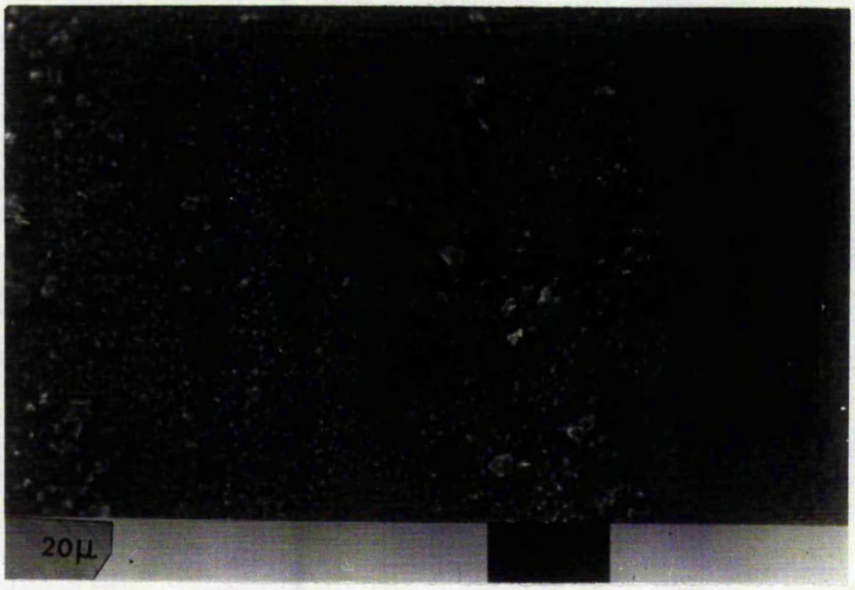
A Comparison of two stress relievers. Fig.19.

influence when only a small compressive stress is present. This may be associated with the size or nature of the ligand field which forms around thiourea, but was not investigated further.

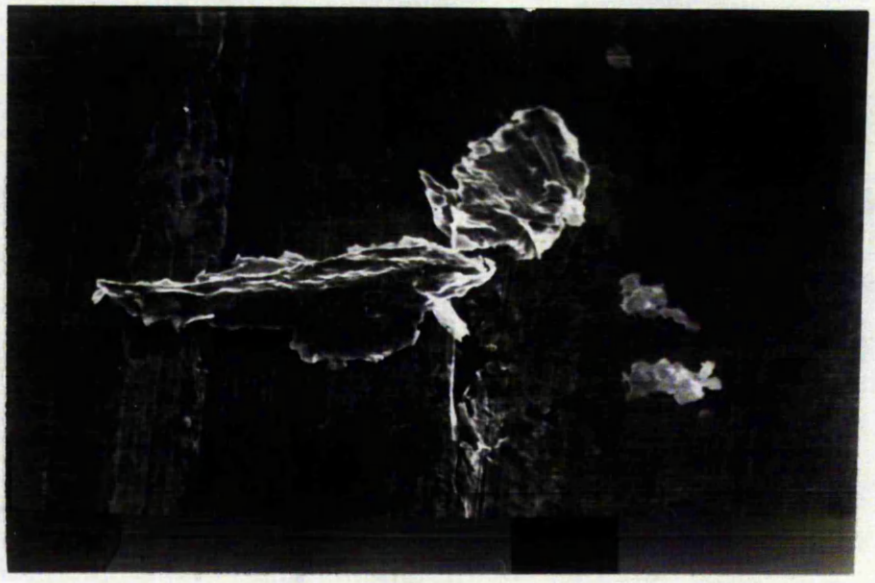
Scanning electron microscopy was performed on several wear tracks, fig.20. Fig.20a shows the unworn surface which seems to have grown in a 'wheatfield' manner, though a few nodules are visible. The surface finish of the deposit was usually slightly better than that of the substrate, and was of high brightness when the current density was large ($\sim 1 Adm^{-2}$). Also shown is a delaminated sheet which has been welded back onto the wearing surface, and is unusual in not having been rolled up. Subsequent micrographs, fig.20b-d show, respectively, the wear tracks of nickel which were compressively stressed, stress-free and stressed in tension. It is apparent that wear proceeded in each case by delamination, and there is also evidence of plastic flow in some cases. There were no stick-slip striations generated by third body wear to be seen, presumably because local contact pressures were high enough to cause adhesive action when loose bodies were generated. There was some difference in wear morphologies;

A. Compressive Stress.

If a large compressive stress is incorporated, ie. $\sigma_{xxr} = \sigma_{yyr} = -200 Nmm^{-2}$ (fig.21), c.f. $\sigma_o = 506 Nmm^{-2}$, then this will augment the large, negative spherical component of applied contact stress, and encourage ductile flow. Stresses within the surface layer of a circular contact patch (as is produced by crossed cylinders of similar radii and elasticities) were found by Hamilton and

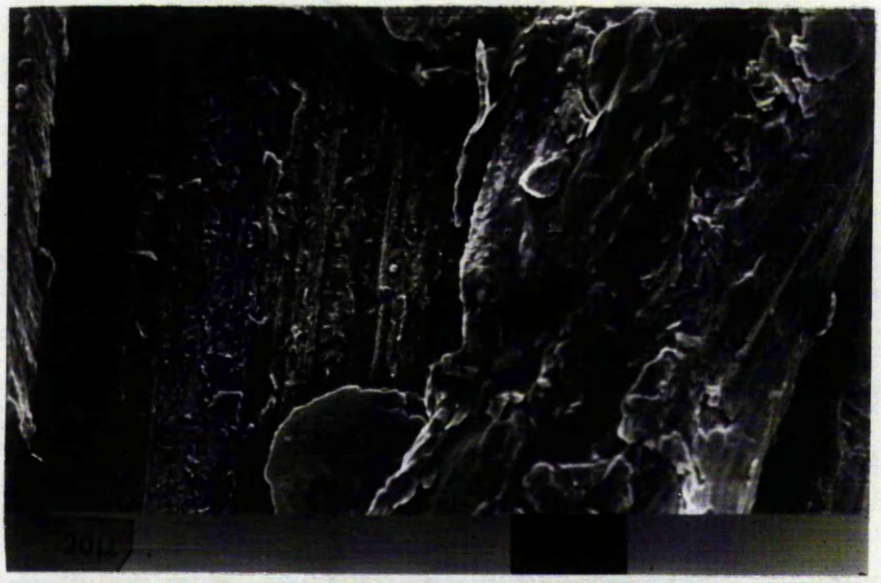


Unworn 'wheatfield' Appearance of Electroplate



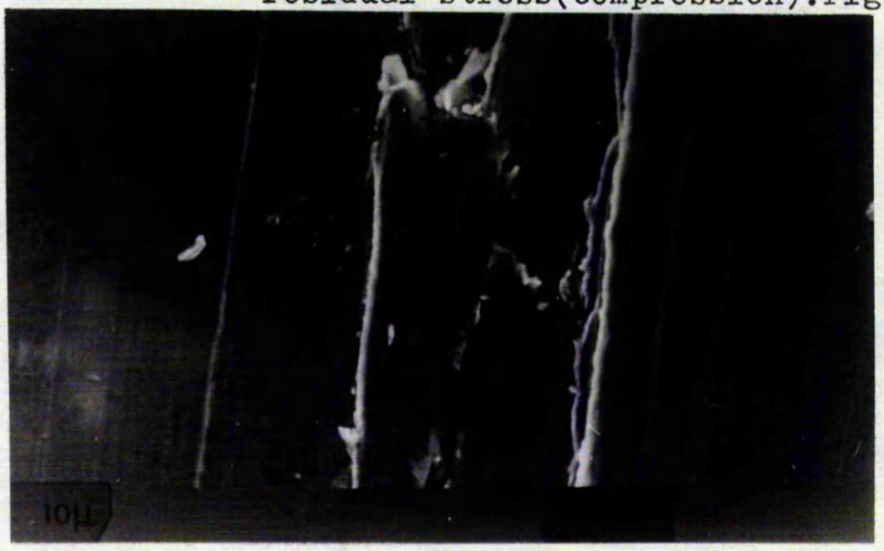
Wear fragment welded back onto a lightly worn surface

Scanning Micrographs of Electroplate.Fig.20a





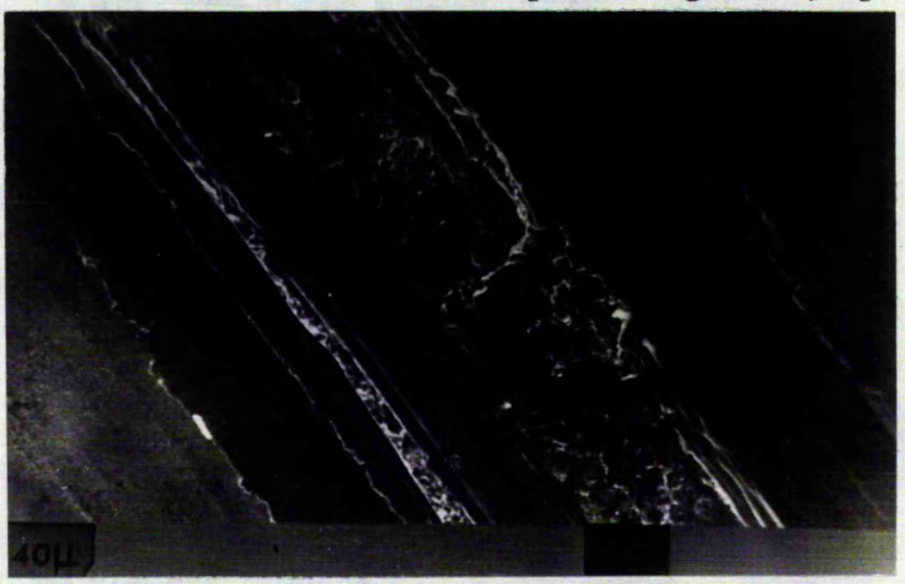
Micrographs of nickel electroplate containing a negative residual stress(compression).Fig.20b

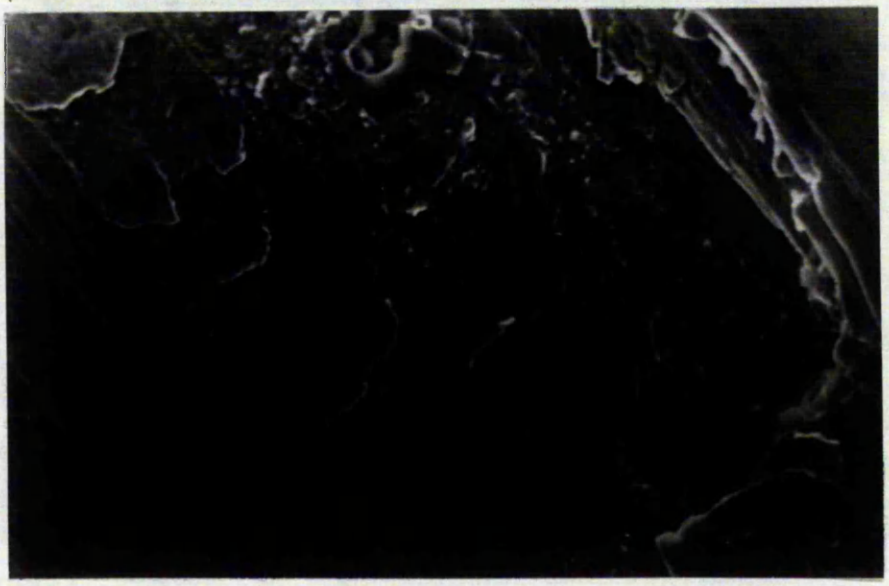


Stress-free nickel electroplate (see overleaf,too).Fig.20c



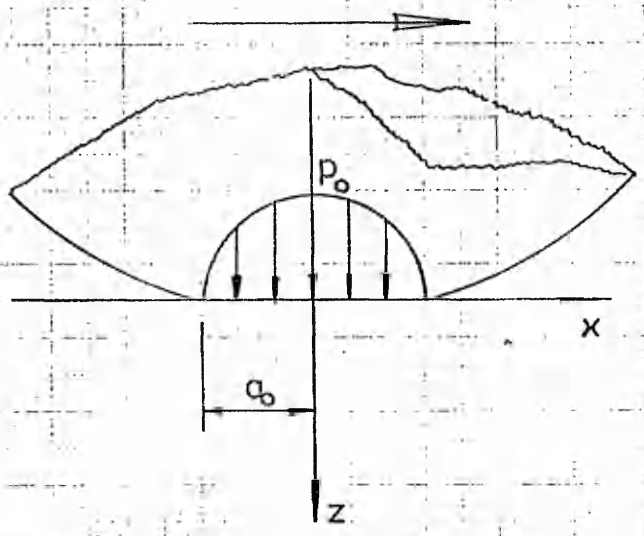
Worn, stress-free nickel electroplate.Fig.20c.(& previous page)





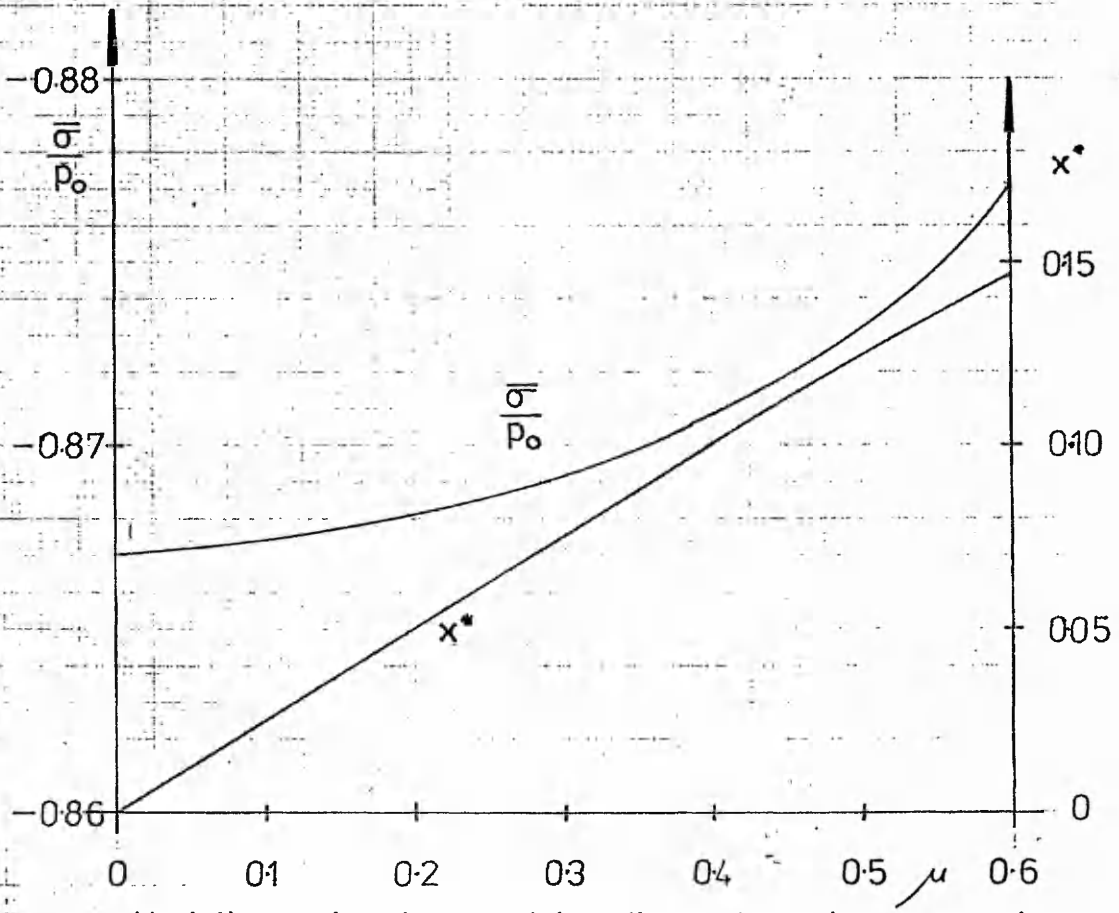
Worn nickel electroplate with large tensile stress.Fig.20d

FIG.20b-d. SPECIMENS FROM CROSSED-CYLINDER WEAR TESTS



Coordinate system used in 3-D contact problems which include friction. Fig.21

Starred quantities are normalized by a_o.



Variation of value and location of most compressive hydrostatic stress with friction. Fig.22a

Goodman(83). For y=z=0, fig.21;

$$\frac{\sigma_{zz}}{p_o} = -\sqrt{\{1-x^{*2}\}} \qquad \frac{\tau_{xz}}{p_o} = \sqrt{\{1-x^{*2}\}}$$

$$\frac{\sigma_{xx}}{p_o} = \left[\frac{1-2\nu}{3x^{*2}}\left\{1-(1-x^{*2})^{3/2}\right\} - \sqrt{1-x^{*2}}\right] - \frac{\mu}{8}x^*(4+\nu) \qquad (16)$$

$$\frac{\sigma_{yy}}{p_o} = -\left[\frac{1-2\nu}{3x^{*2}}\left\{1-(1-x^{*2})^{3/2}\right\} + 2\sqrt{1-x^{*2}}\right] - \frac{3\mu}{8}x^*\nu$$

Thus, $\bar{\sigma} = \frac{1}{3}(\sigma_{xx}+\sigma_{yy}+\sigma_{zz})$

$$\frac{\bar{\sigma}}{p_o} = \frac{1}{3}(-2(1+\nu)\sqrt{1-x^{*2}} - \tfrac{1}{2}\mu x^*(1+\nu))$$

It is easy to show that this has a maximum at $x=\frac{\mu}{\sqrt{16+\mu^2}}$

The maximum (most negative) spherical stresses are given in table 3 below and are summarised in fig.22a, for $\nu=0{\cdot}3$.

Table 3. Most negative hydrostatic stress beneath a Circular Contact Patch.

μ	x*	$\frac{\bar{\sigma}}{p_o}$
0	0	-0·867
0·1	0·025	-0·867
0·2	0·050	-0·868
0·3	0·075	-0·869
0·4	0·100	-0·871
0·5	0·124	-0·873
0·6	0·148	-0·877

For the case of two identical cylinders pressed together, the peak contact pressure p_o is given by(7); $p_o=0{\cdot}616\sqrt[3]{\frac{E^2P}{R^2}}$ (18)

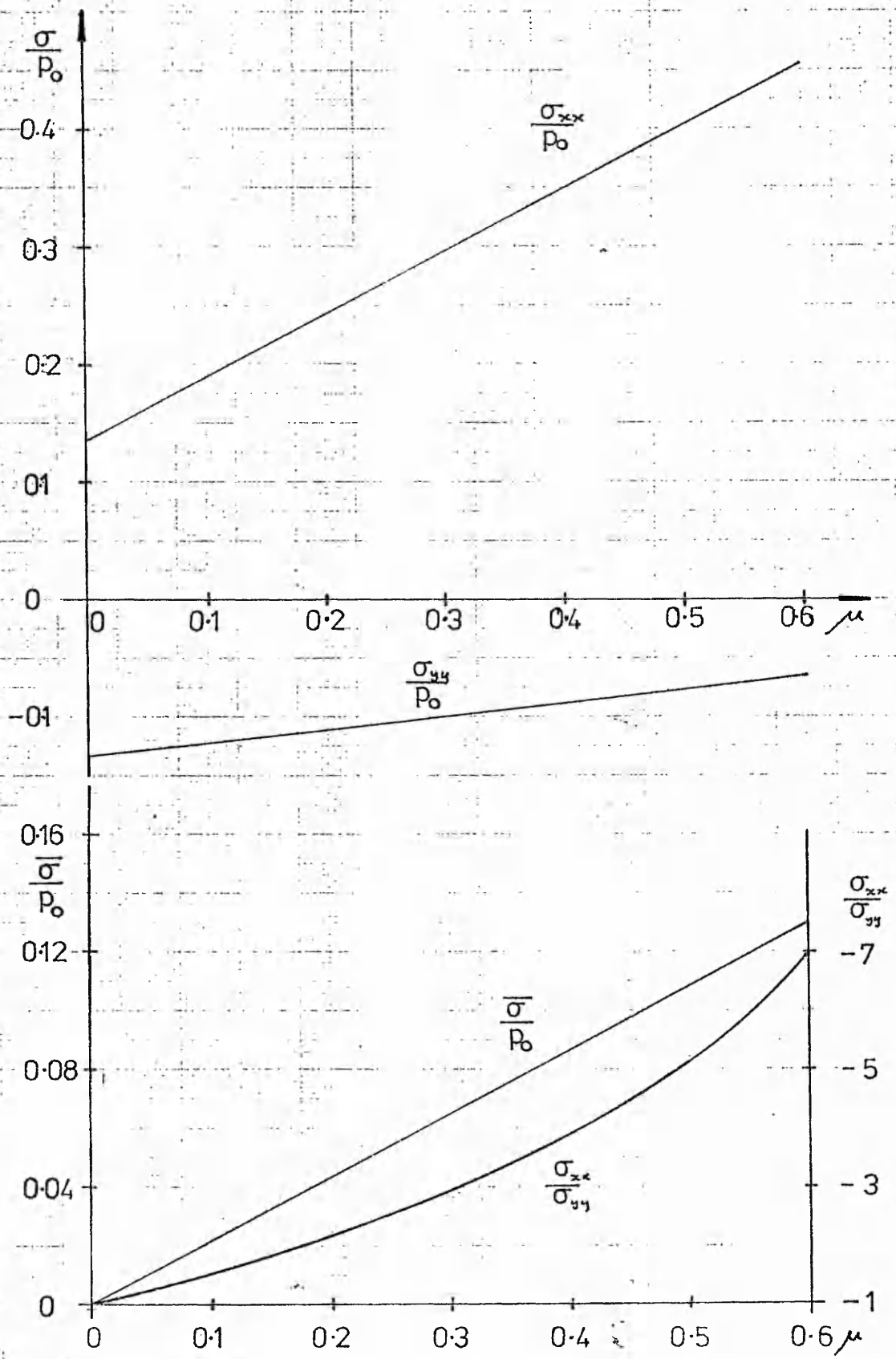
With the loading and geometry specified earlier this gives;

$p_o=1086\ \text{Nmm}^{-2}$

$\bar{\sigma}=944\ \text{Nmm}^{-2}$

$a_o=0{\cdot}092$ mm

Together with the built in stress, a total spherical stress is present of $\bar{\sigma}=-1210\text{Nmm}^{-2}$, ie. $|\bar{\sigma}|\approx 2{\cdot}4\,\sigma_o$. Thus, because such a large compressive stress is present, it might be expected that considerable ductility would result. This is supported by an examination of the micrographs (fig.20b) obtained by means of an S.E.M., where there is considerable evidence of plastic flow. Some material has flowed and built



Variation of stresses with friction at point of largest hydrostatic tension. Fig. 22b

up into lands supporting the load, whilst the unworn original appearance is visible between them.

B. No stress

It appears that there is very much less plastic flow in this case (fig.20c), and most of the cracks are parallel with the sliding direction. Some wear debris is to be seen, but the morphology represents an intermediate stage between the plasticity and flow just described and the brittleness of the third class of failure.

C. Tensile Stress

Here, a large tensile stress, ie. $\sigma_{xxr}=\sigma_{yyr}=+400 Nmm^{-2}$ had been built in, and the result is very considerable transverse cracking (fig.20d), with few signs of ductility and some longitudinal cracks.

The point of largest tensile stress is at the centre of the trailing contact edge, ie.at $x^*=-1$. If this is substituted into equations (16), the following relations are obtained;

$$\sigma_{zz}=\sigma_{xz}=0$$

$$\frac{\sigma_{xx}}{p_o}=\frac{1-2\nu}{3}+\frac{\mu}{8}(4+\nu) \qquad \frac{\sigma_{yy}}{p_o}=-\frac{1-2\nu}{3}+\frac{3\mu}{8}\nu \qquad (19)$$

At the same point, $\frac{\overline{\sigma}}{p_o}=\frac{1}{6}\mu(1+\nu)$

The stresses present at $x^*=-1$, for $\nu=0{\cdot}3$ are given in fig.22 and in table 4 below.

As can be seen, as the coefficient of friction increases the probability of transverse cracking increases, both because of the increasingly large tensile stress σ_{xx}, and because the spherical component of stress becomes more tensile. For the case of the apparatus used, and with the quoted superimposed tensile stress, at the worst point

Table 4. Tensile Stresses at the Trailing Edge of a Circular Sliding Contact

μ	$\frac{\sigma_{xx}}{p_o}$	$\frac{\sigma_{yy}}{p_o}$	$\frac{\bar{\sigma}}{p_o}$	$\frac{\sigma_{xx}}{\sigma_{yy}}$
0	0·133	-0·133	0	-1
0·1	0·187	-0·122	0·022	-1·53
0·2	0·241	-0·108	0·043	-2·23
0·3	0·295	-0·100	0·064	-2·95
0·4	0·348	-0·088	0·087	-3·95
0·5	0·402	-0·077	0·108	-5·22
0·6	0·456	-0·066	0·130	-6·91

$\bar{\sigma}$=+336Nmm^{-2},ie. $\bar{\sigma}\approx\frac{2}{3}\sigma_o$. This, of course, is of the opposite sign to the previous example, and the tensile environment will encourage cracking.

The extreme cases studied are likely to represent the regimes of wear only under very large locked in stresses. As one moves towards the zero stress condition each mechanism is likely to decay, though at zero stress enough may be present of each for particle detachment to occur simultaneously by both modes. This could explain why the wear rate was highest with little residual stress. The influence of locked in stress on apparent hardness has been mentioned as a complicating factor which is hard to quantify. Another factor is the influence of the hydrostatic stress component on the actual failure stress. Normally, for a metal, it is usual to assume that the yield stress is independent of average stress. However, for minerals, where failure is truly brittle, a measure of the average stress or 'confining pressure' is included as in the Coulomb-Navier equation (84), which is seen as

being a modified Tresca criterion;

$$|\tau| \leqslant \tau_o - \mu.\bar{\sigma} \qquad (20)$$

where μ is the coefficient of internal friction.
Thus the hardness, which is proportional to τ_o, might be related to failure in a more complicated way. Note, too, that equation (20) represents the simplest possible variation of failure stress with average stress, viz. a linear dependence; many more complicated and arguably realistic equations are given by Paul(82).

Lastly, the question of the persistence of the original locked in stresses should be considered. Since the yield condition for a circular contact patch is $\frac{p_o}{\tau_o} \leqslant 2{\cdot}77$, it is apparent that for the wearing pair used, where $\frac{p_o}{\tau_o}=3{\cdot}72$ some initial yielding would occur, if no other stresses were present. Thus, subsequent loading would experience the effect of residual stresses left by the first excursion into the plastic regime. This phenomenon is known as shakedown, and is treated more fully in chapter six. It might be expected that because of this the final equilibrium stress state would be independent of any initial residual stresses. In an ideal material this might be the case, but the different morphologies encountered here indicate that either the equilibrium stress state <u>is</u> dependent on the locked in stress or that the wear mechanism is determined by what happens during the first few cycles before shakedown is complete. Jahanmir and Suh(85) have pointed out that nucleation of wear cracks is possible during two or three wear passes, which indicates their importance. Also, experiments by Fujita and Yoshida(86) in which the

direction of rolling contact in a fatigue test was changed after many cycles, causing a reduction in fatigue life, show the clear influence of self generated stresses on wear rate.

2.4 Contact and Residual Stresses-their Interdependence

In this section, the effect of superimposing a known stress field on three types of contact loading is discussed. First, the influence of residual stresses on a rolling ball such as in a ball bearing, will be examined. The stresses on the axis of symmetry for such an arrangement are given by, inter alios, Huber(87):

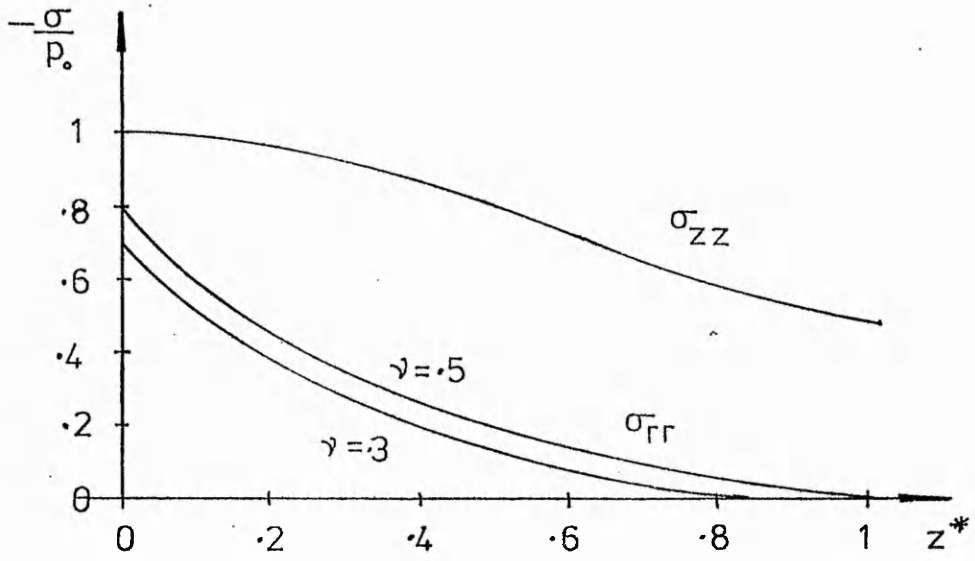
$$\frac{\sigma_{rr}}{p_o} = \frac{\sigma_{\theta\theta}}{p_o} = -(1+\nu)\left\{1 - z^*\tan^{-1}\left(\frac{1}{z^*}\right)\right\} + \frac{1}{2}\,\frac{1}{1+z^{*2}}$$

$$\frac{\sigma_{zz}}{p_o} = \frac{-1}{1+z^{*2}} \qquad (21)$$

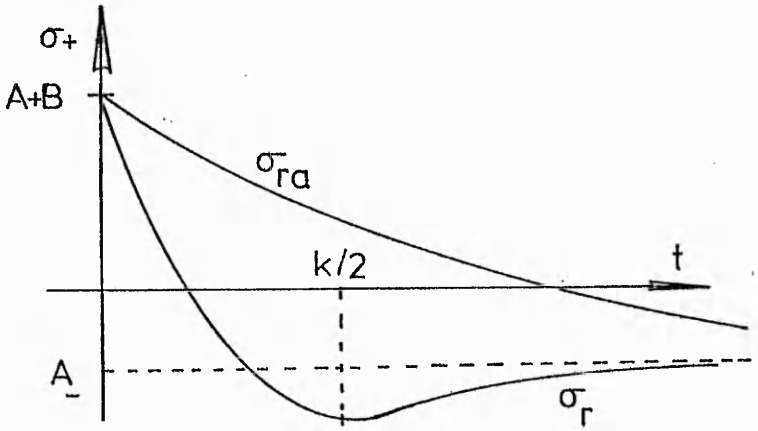
in cylindrical coordinates. These stresses are shown in fig.23; note that they are all negative, and that σ_{zz} has the largest absolute value. Since it is not possible to place a uniform residual stress in the z-direction, because equilibrium with the free surface cannot be maintained, the only way to reduce the stress difference is to place extra compressive stresses in the r-θ plane, ie. parallel to the surface. This may be most easily seen by applying von Mises' criterion (note that von Mises' criterion and Treca's criterion are equivalent under cylindrical stress conditions). From Jaeger(84);

$$J_2 = \frac{1}{6}\left\{(\sigma_{rr}-\sigma_{zz})^2+(\sigma_{zz}-\sigma_{\theta\theta})^2+(\sigma_{\theta\theta}-\sigma_{rr})^2\right\} + \tau_{\theta r}^{\,2} + \tau_{\theta z}^{\,2} + \tau_{zr}^{\,2}$$

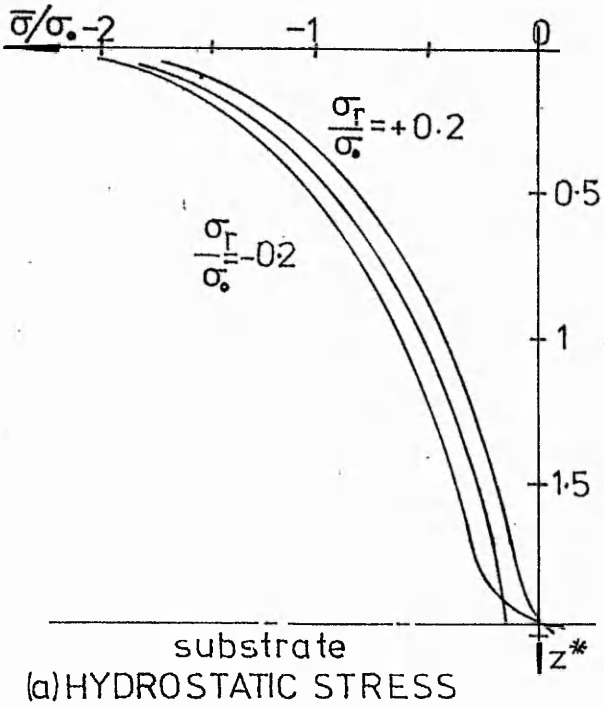
$$= \frac{1}{3}\,(\sigma_{rr}-\sigma_{zz})^2 \qquad (22)$$



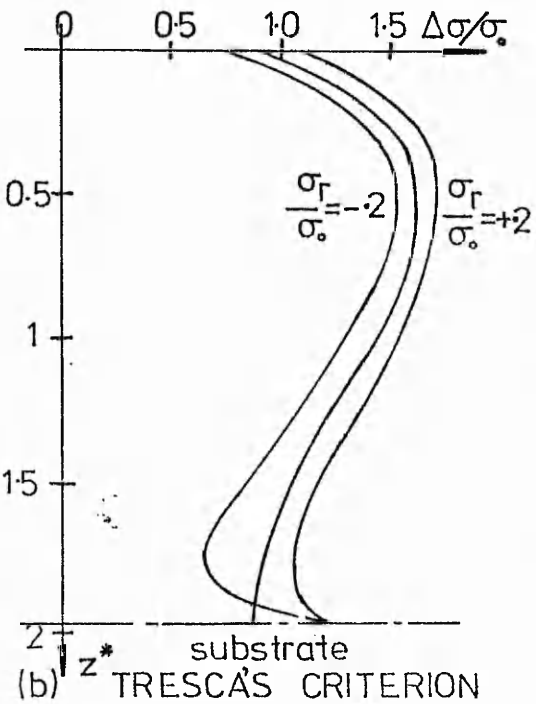
On axis stresses-Hertzian load distribution. Fig23.



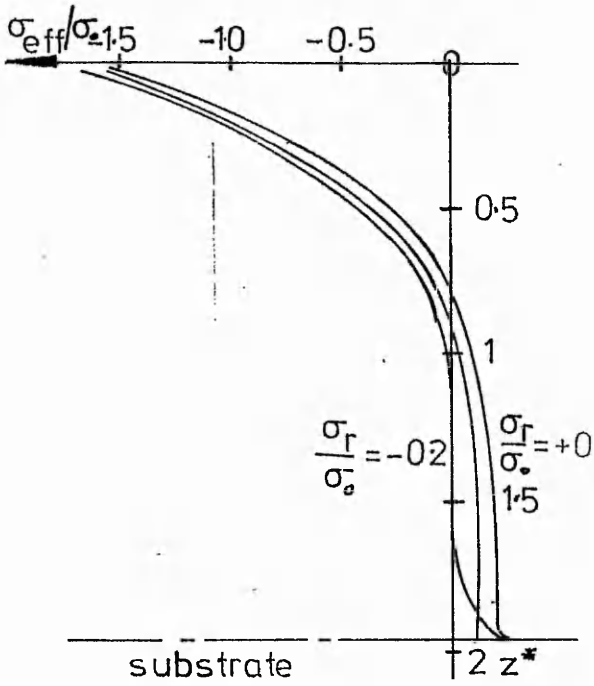
Typical variation of stress with thickness-compressive deposit Fig. 24.



(a) HYDROSTATIC STRESS



(b) TRESCA'S CRITERION

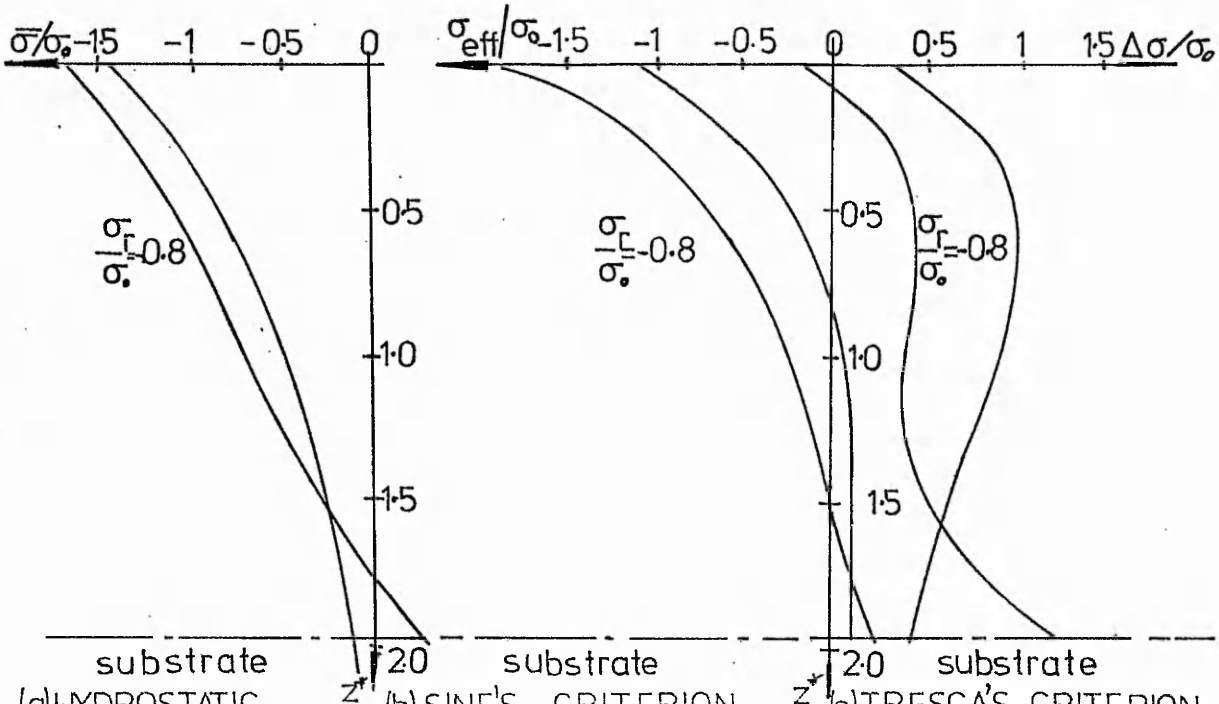


$\frac{p_o}{\sigma_o}$ = 2·34 [the shakedown limit]

$\frac{\sigma_r}{\sigma_o}$ = ± 0·2

(c). SINE'S CRITERION

Stress Parameters beneath a heavily loaded ball. Fig. 25



(a) HYDROSTATIC STRESS

(b). SINE'S CRITERION

(c) TRESCA'S CRITERION

$\frac{p_o}{\sigma_o}$ = 1·39 [the elastic limit]

$\frac{\sigma_r}{\sigma_o}$ = -0·8

Stress parameters beneath a lightly loaded ball. Fig 26

and von Mises criterion is;

$$J_2 \leqslant \tau_o^2 \qquad (23)$$

It is apparent from equation (22) that to minimise J_2 the stress difference must be minimised. Fig. 24 shows the usual variation of stresses within a deposit, for the case of a compressively stressed deposit. Note that the initial layers are tensile, but that a compressive regime is soon entered (the nomenclature is consistent with equations 13-15). To match such a stress system with that of spherical contact, it is clear that the most compressive stress, ie. at $t = \frac{2}{k}$, should coincide with the worst Hertzian stresses, which are at a depth of $z^* = 0{\cdot}481$. However, in many practical cases such an optimization would not seem to be worthwhile, for two reasons; first, the magnitude of stresses normally involved in a contact problem means that the small extra gain would be insignificant, and, secondly, the closeness of the highly deleterious interfacial tensile stress to the worst Hertzian stresses would not be desirable. Nevertheless, there are several cases of lightly loaded contacts such as relay or switch contacts where such an optimization would probably be beneficial. In figs.25,26 are shown the stress parameters on the axis for a heavy load and for a light load: details of loading are given with the figures. Also shown in these figures is 'Sine's Criterion'. This is an attempt to determine the fatigue limit for a circular contact using classical fatigue techniques. There are very few fatigue criteria which can cope with the effects of triaxial loading and non-zero average stress. Such criteria were reviewed by Toor(88) and the one chosen for this investigation is also given in Dieter(89). It is quoted in

the latter, and may easily be re-written in terms of stress invariants as;

$$\sqrt{3J_2} \leqslant \sigma_{fl} - \frac{\sigma_{fl}}{\sigma_{uts}} I_1 \qquad (24)$$

Its similarity with von Mises' criterion and the Goodman diagram is evident. Consider one of the principal directions. Its stress history is shown in fig.27. The mean stress is taken as the residual stress plus half of the contact stress, and the magnitude of the fully reversing stress is given by the contact stress alone. Thus I_1 is referred to $\sigma_r + \frac{1}{2}\sigma_{ij}$ and J_2 is referred to σ_{ij}, σ_{ij} being a typical contact stress component. The variable plotted on the graphs is;

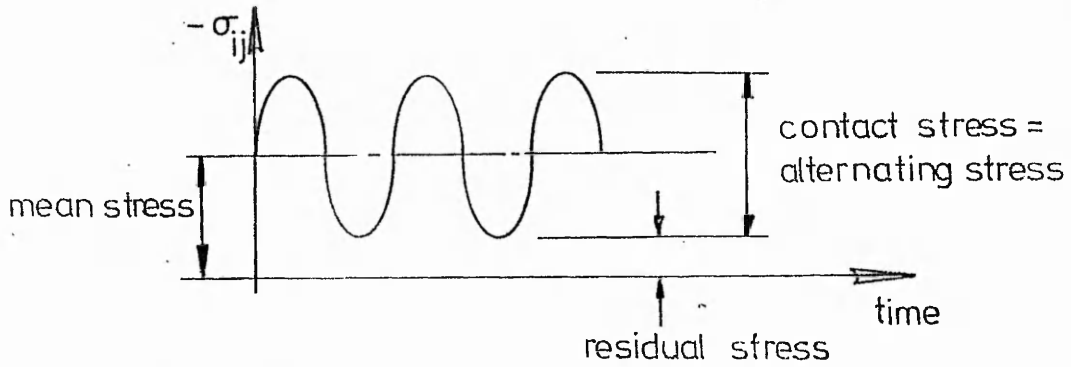
$$\sqrt{3J_2} + \frac{\sigma_{fl}}{\sigma_{uts}} I_1$$

where σ_{fl} and σ_{uts} for nickel are substituted.

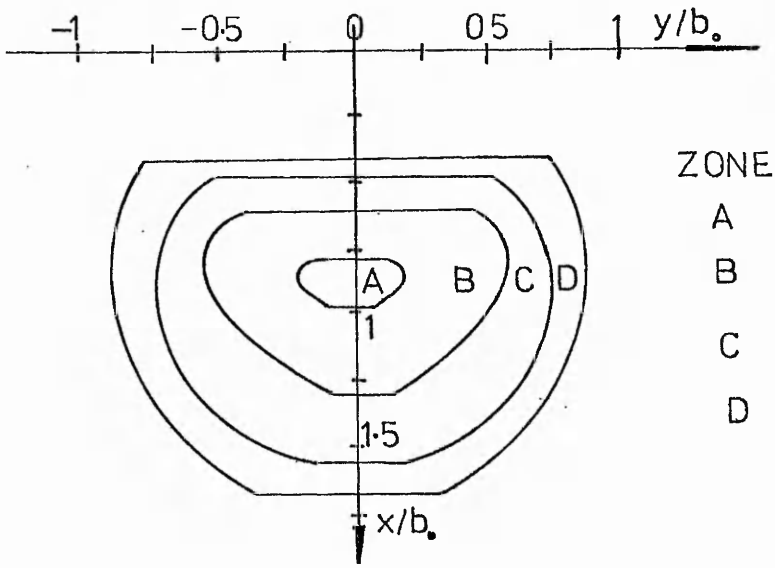
Failure is therefore predicted when this parameter reaches $+\sigma_{fl}$. From the results it is clear that no ball-bearing should ever fail! This illustrates the difficulties mentioned in chapter one, because the criterion characterises opening and not shear type crack growth.

The beneficial effect of compressive stress is obvious from the diagrams, as is the deleterious effect of the more usual tensile stress (90). Surprisingly, in spite of the large interfacial tensile stress, failure there is rare, probably because the interface is reputedly stronger than either the substrate or the electroplate, for a large range of materials (91). Some consideration will now be given to the development of the yielded zone beneath a rolling pair.

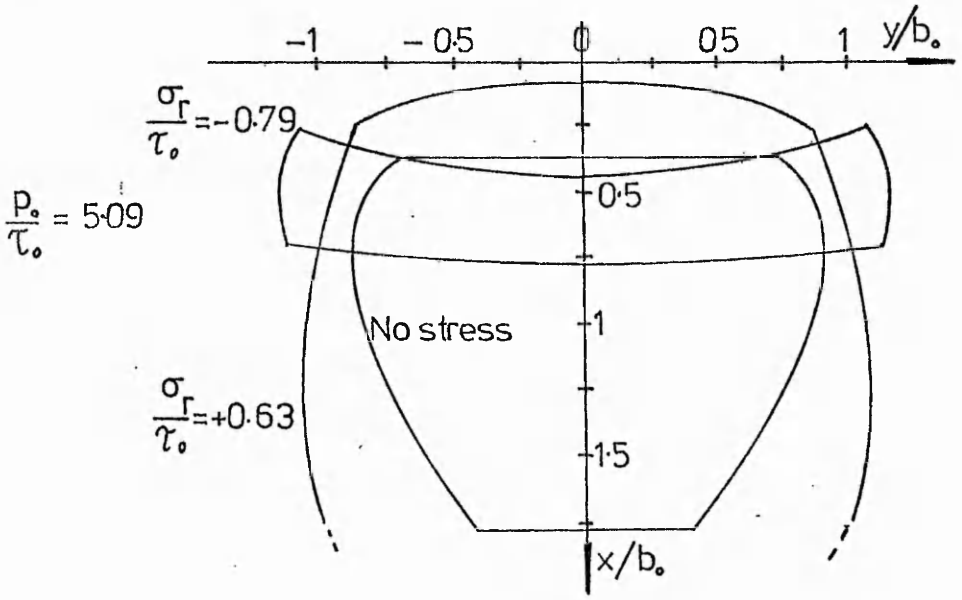
The previously quoted equations (8), due to Beliaev, describe the elastic stress field between two rollers pressed together without friction. However, providing that



Variation of stress components with time. Fig.27.

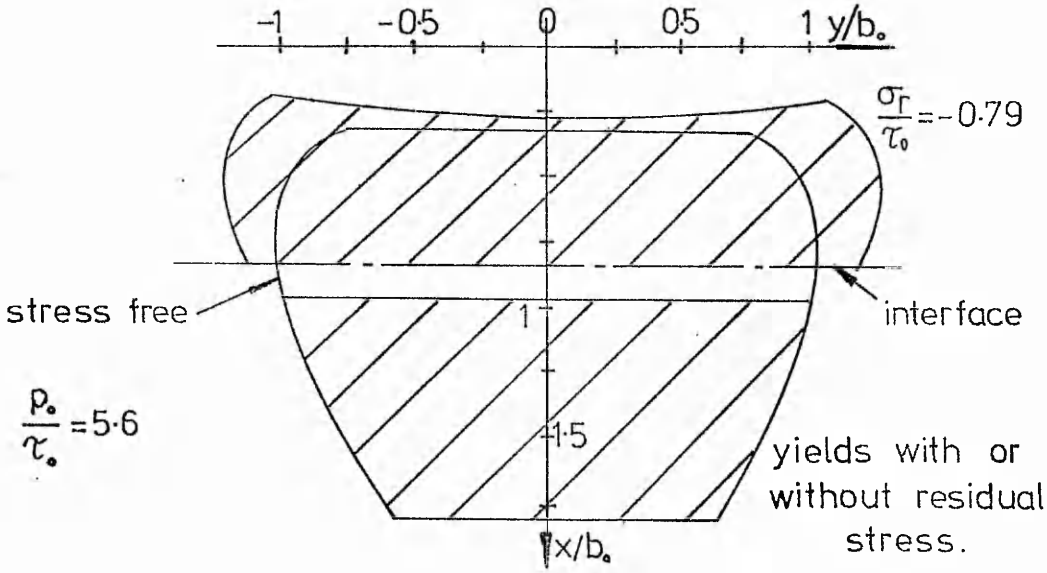


The development of the yielded zone beneath a roller. Fig 28.

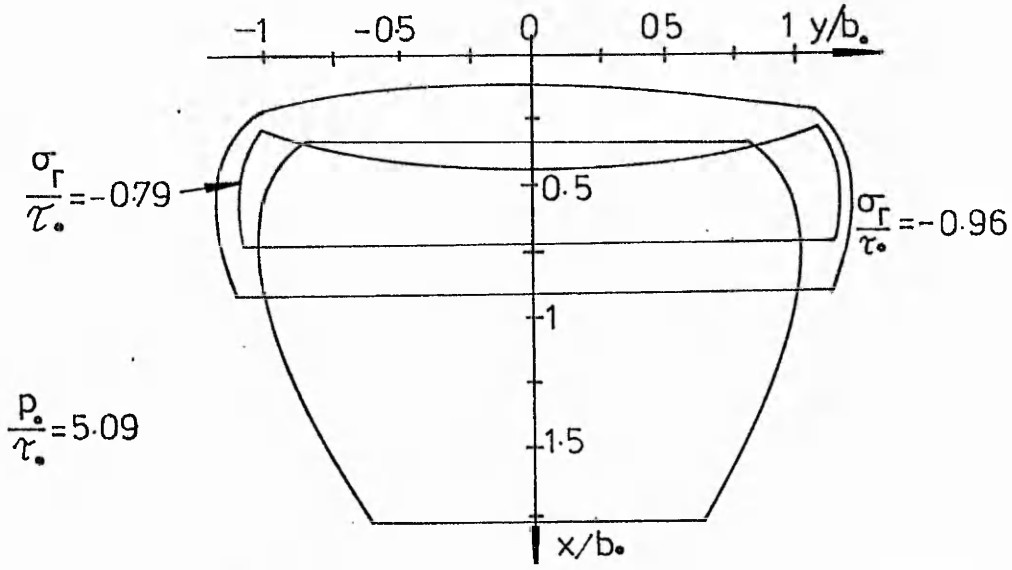


The effect of moderate residual stresses on plastic zone size Fig. 29.

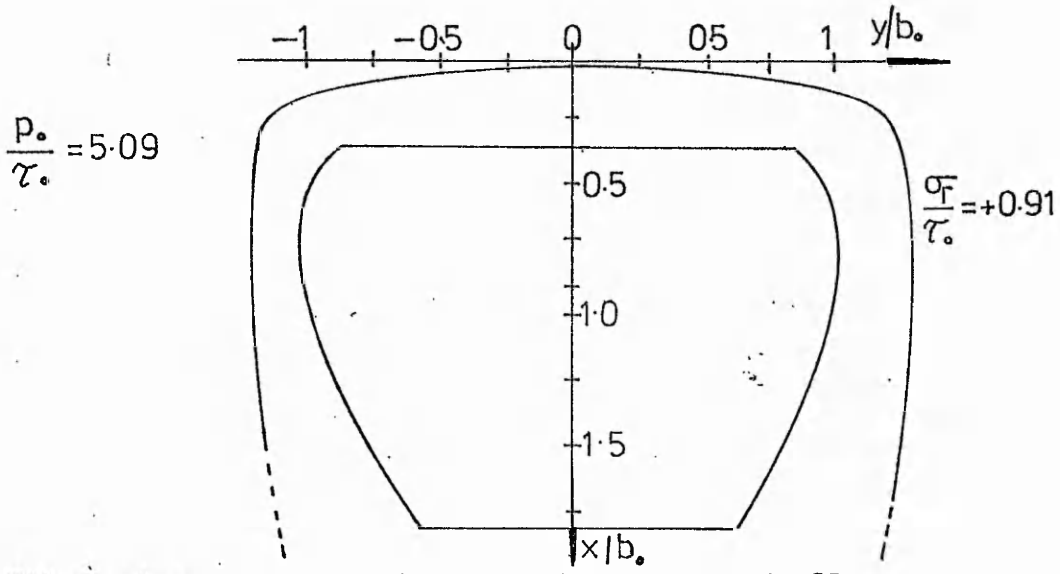
SOME YIELDED ZONES BENEATH A ROLLER



Effect of having too thin a compressive layer. Fig.30



Effect of having too great a compressive stress. Fig31.



Effect of a large residual tensile stress. Fig. 32

the elastic limit is not greatly exceeded, it is acceptable to use the same equations to describe the elasto-plastic strain field, since the elastic region confines the plastic zone, and dominates the solution. The stresses in the elastic portion are then given by Hooke's law, and the elastic-plastic boundary corresponds to von Mises criterion. Notwithstanding any shakedown which may occur, the presence of any pre-existing stresses within the surface layers should control the size of the plastic zone and hence limit the amount of damage incurred. The development of the yielded zone is shown in fig.28. The principal difference between shakedown and pre-imposed static stresses is that the first case results in a differing residual stress in the x and y directions (fig.3) whereas the second case is limited to a cylindrical residual stress system, ie. $\sigma_{xxr}=\sigma_{yyr}$. Fig.29 illustrates the beneficial effects to be gained by using a thick layer of compressively stressed material, for the reduction in size of the plastic zone is apparent. Two pitfalls to be avoided, however are;

a. If the beneficial effect of the residual stress is removed too soon, the region of plasticity actually becomes larger. The depth of pre-stressed zone must be at least equal to the depth of plasticity in its absence. A layer which is slightly too thin results in a pair of plastic zones thinly separated by an elastic layer, fig.30.

b. If a very large compressive stress is applied, fig.31, then material may actually start to yield in the opposite direction, ie. $\sigma_{xx},\sigma_{yy} \ll \sigma_{zz}$. The very large compressive stresses found in ion plated samples (92) would not seem, by themselves, to be beneficial.

As was to be expected, tensile stresses have an adverse effect, fig.32. The optimum value of compressive stress to apply depends on the load and material yield stress; its value is derived as a by-product of shakedown calculations in chapter six.

A sliding cylinder will now be briefly examined. The solution for the elastic stresses generated is due to Smith and Liu(93) and is also treated by Poritsky(94). Using the coordinate system of fig.3 with a tractive force of value $p.\mu$ acting in the positive y direction, one obtains the following;

Defining, $K_1^* = (1+x^*)^2+z^{*2}$

$$K_2^* = (1-x^*)^2+z^{*2}$$

$$\prod = K_1^* \sqrt{\frac{K_2^*}{K_1^*}} \sqrt{\left\{2\sqrt{\frac{K_2^*}{K_1^*}} + \left(\frac{K_1^* + K_2^* - 4}{K_1^*}\right)\right\}}$$

Then $$\psi = \frac{\pi}{\prod}\left(1 - \sqrt{\frac{K_2^*}{K_1^*}}\right) \qquad \Psi = \frac{\pi}{\prod}\left(1 + \sqrt{\frac{K_2^*}{K_1^*}}\right) \qquad (25)$$

And;

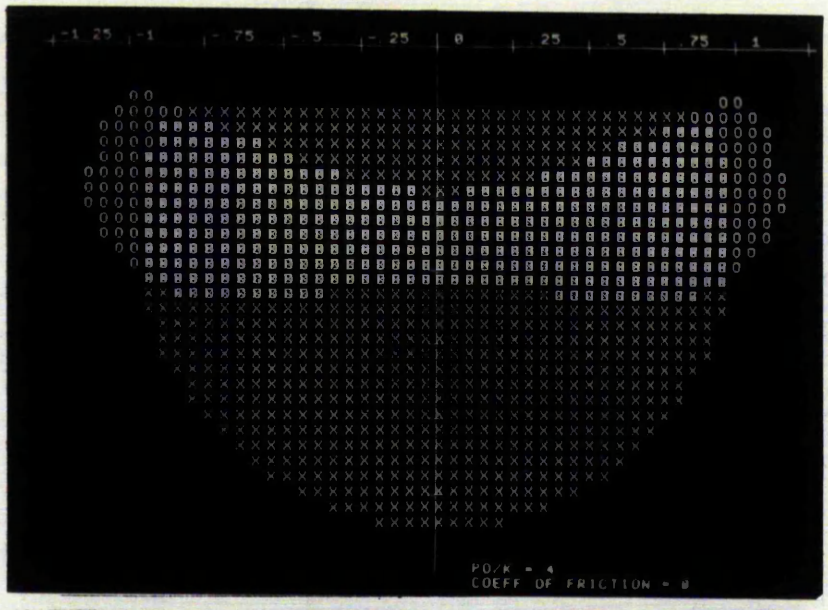
$$\frac{\sigma_{yy}}{p_o} = -\frac{1}{\pi}\left\{z^*\left[\Psi\ (1+2x^{*2}+2z^{*2}) - 2\pi - 3x^*\psi\right] + \mu\left[\Psi\ (1-x^{*2}-z^{*2})2x^* + 2\pi x^* + (2x^{*2}-2-3z^{*2})\psi\right]\right\}$$

$$\frac{\sigma_{xx}}{p_o} = -\frac{1}{\pi}\left\{z^*\left[\Psi\ -x^*\psi\right] + \mu\, z^{*2}\psi\right\}$$

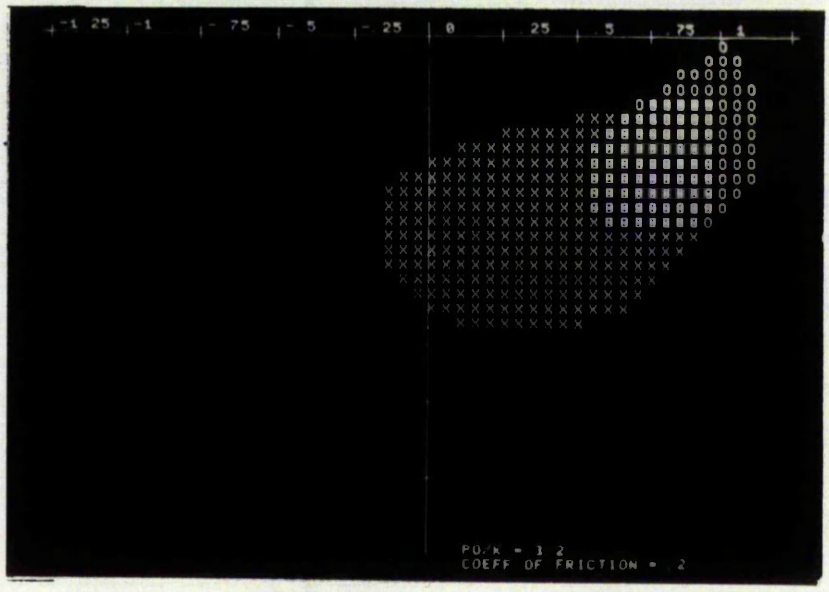
$$\frac{\tau_{xy}}{p_o} = -\frac{1}{\pi}\left\{z^{*2}\psi + \mu\left[\Psi(1+2x^{*2}+2z^{*2})z^* - 2\pi z^* - 3x^*z^*\psi\right]\right\}$$

$$\sigma_{zz} = \nu(\sigma_{xx}+\sigma_{yy}) \qquad \epsilon_{zz} = \tau_{xy} = \tau_{yz} = 0$$

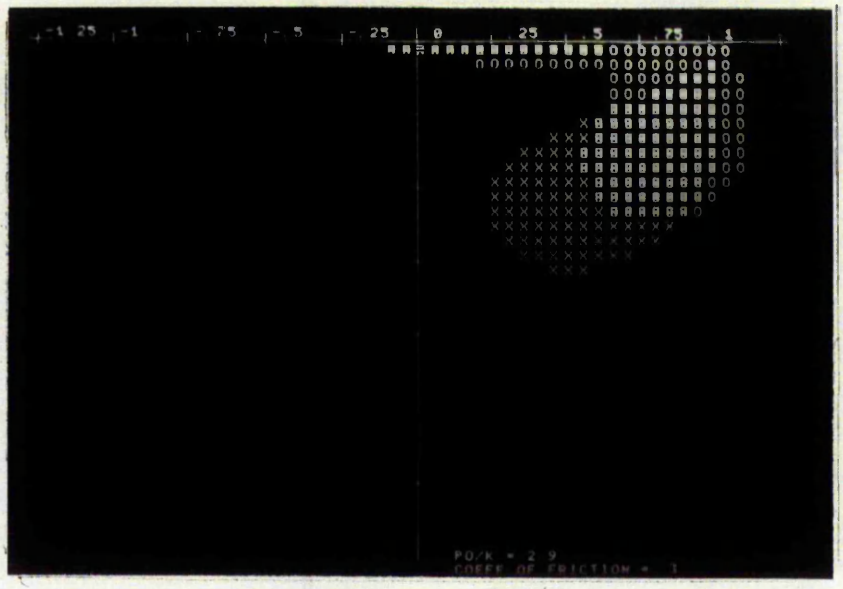
The optimum value of residual stress, to reduce plasticity to a minimum, was added, for various coefficients of friction, and the results are shown in fig.33. The loads chosen are the shakedown limits, ie. the load which would eventually just shakedown and cause the plasticity zones to condense at discrete points. As can be seen, pre-existing





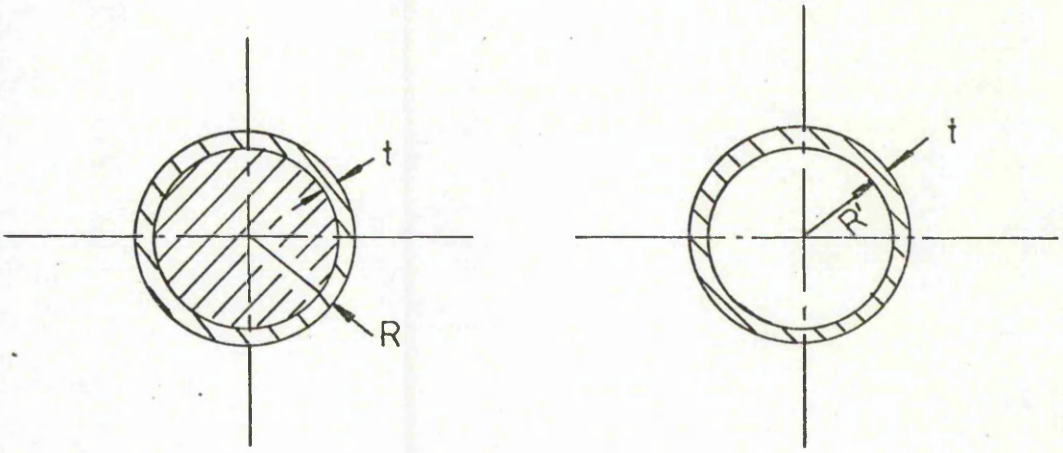


See overleaf for details, fig.33,a-c.



Plasticity zones for sliding cylinder, full slip. The tractive force is acting to the right (+ve direction), and the load applied in each case is at the shakedown limit. In the photographs k is the yield in pure shear (elsewhere τ_o), and the plasticity zones shown are those occurring on the first pass, ie. before shakedown. The zone marked with a "x" is in a stress-free material, and the zone marked "O" is in material containing the optimum cylindrical residual stress. Von Mises' criterion is used throughout.

Fig.33.



ELECTRODEPOSITED CYLINDER

DETACHED ELECTROPLATE

Evaluating stresses within the substrate. Fig.34.

"cylindrical" residual stresses can reduce significantly the amount of plasticity, though shakedown cannot be achieved according to von Mises' criterion (which would require two independently variable stresses). Note, too, the way a second region of plasticity develops at the surface for high coefficients of friction.

Finally in this chapter, the subsurface stresses found within the substrate of a plated material will be considered. Fig.34 shows the cylindrical test pieces used in the wear tests. If the deposit annulus is imagined detached from the substrate and is under plane stress conditions, providing $R \simeq R'$, $t \simeq t'$, $R \gg t$ the thin tube calculation may be employed. From symmetry, there can be no interfacial shear. Let the mean electrodeposit stress be $\tilde{\sigma} = \frac{1}{t} \int_t \sigma_{ri} . dt$

Then, for equilibrium, $2R\, \sigma_{rr} = 2t\, \tilde{\sigma}$

$$\text{ie. } \sigma_{rr} = \sigma_{\theta\theta} = \tilde{\sigma}\left(\frac{t}{R}\right) \qquad (26)$$

Thus the stress within the substrate for this configuration is negligible.

Now that a bulk interpretation of the sliding wear experiments has been presented, a detailed model of delamination using fracture mechanics will be attempted.

3. Fracture Mechanics and Wear

3.1 Justifying the use of Fracture Mechanics

A semi-quantitative argument has just been provided to explain the different surface morphologies found. However, so far no argument has been provided to explain why wear fragments are often in the form of thin, flat plates rather than, say, equi-axed lumps. The early dislocation explanations of delamination (9) have largely been retracted in recent years, for several reasons;

A. There has never been any direct evidence for the existence of a low dislocation density zone.

B. Any calculation of the thickness of such a zone shows it to be very ill-defined.

C. A dislocation explanation leads to the conclusion that the wear plate thickness is material dependent but is independent of load. This is not found in practice (96), nor is independence from locked-in stresses confirmed.

Bates et al (97) published comments supporting reason (B) and proposed deducing wear debris shapes using applied mechanics. Beagley (98) comments that the wear-sheet separation problem would be best treated by crack mechanics and initiation by examining the stress-raising effect of inclusions. He also points to difficulties in estimating a dislocation free zone when the surface is oxidised or glazed. In view of these objections Suh presented a revised explanation (99), using the physics of crack growth in a continuum as his starting point. From there, three steps are needed to establish wear estimates from basic quantities;

A. First, a means of nucleating cracks is required.

B. When a well-developed crack is present, it is propelled by the applied load. The stress intensification factor enables the crack growth rate to be estimated in terms of the loading.

C. Eventually, the crack turns upwards to appear at the surface causing a wear particle to detach. Criteria must be found to determine when a crack turns, and also how many cracks are growing at any one time, so that the wear volume can be found.

The literature illustrating the importance of fracture mechanics in wear has been reviewed in chapter one. Direct justification for using fracture mechanics is difficult to find, but several established wear relations give the same dependence on load and coefficient of friction. It is approximately true that the S.I.F. for mode II crack loading is proportional to the local shear stress in the absence of the crack. Also, the crack growth rate can be related to the S.I.F. by using Paris' fatigue equation. Whilst, strictly speaking, in its present form it relates to mode I loading, it is expected to be valid for mode II growth;

$$\frac{dc}{dN} \propto \Delta K^m \qquad (27)$$

where ΔK is the range of S.I.F. and N is the number of load cycles through which the crack has passed. The constant m lies in the range 2·5 to 4 for metals and for steel is about 3. It will be assumed that wear rate is proportional to crack growth rate. With these premises, several wear equations are reviewed;

A. Suh and Sridharan (100) and Mitchell and Osgood (101) have shown that wear rate is often proportional to the coefficient of friction. Now, the shear stress at any point

beneath a sliding contact is given by;

$$\tau^{3}_{max} \propto P(a+\mu)$$

where the proportionality 'a' is associated with normal loading. For many cases, it is true that $a \ll \mu$, giving;

$$\tau^{3}_{max} \propto \mu$$

However, as stated above

$$\tau_{max} \propto \Delta K$$

Thus $$\Delta K \propto \mu^{\frac{1}{3}}$$

and $$\frac{dc}{dN} \propto \left(\mu^{\frac{1}{3}}\right)^{m}$$

so that, for steel at any rate, wear rate is roughly proportional to friction coefficient, providing that it is not negligible.

B. The I.B.M. wear model (102) has two components-the 'Zero Wear Model', where zero wear is defined as a wear depth comparable with the surface finish, and the 'Measurable Wear Model'. The latter is rather complicated, but zero wear conditions for various durations are inversely proportional to τ^{9}_{max}. Now, under Hertzian loading, with or without friction, $\tau^{3}_{max} \propto P$, so that wear rate $\propto P^{3}$ according to the I.B.M. model, under geometrically similar conditions. Because of the imposition of geometrical similarity, no allowance should be made for the changing contact width, and hence the simplified proportionality results of $\tau_{max} \propto p_o$, and $p_o \propto P$. Sustituting into the Paris equation;

$$\text{Wear rate} \propto \frac{dc}{dN} \propto (P)^{m}$$

so that again wear rate is roughly proportional to the cube of the load.

C. Palmgren, when discussing the life of rolling elements (103), suggested that wear rate was proportional to the

cube of the load, supporting the above'law'.

More direct justification was sought by Fleming and Suh (104) who conducted crossed-cylinder wear tests using two aluminium alloys with widely differing Paris exponents. They recognised that, because other physical properties were inevitably different, the tests could not be conclusive. It was nevertheless verified that under conditions of equivalent loading (ie. when normalised by the yield stress) the alloy with the larger 'm' value wore more quickly.

This suggested a simpler experiment which would be more reliable, viz. performing crossed cylinder tests using different loads, but the same pair of wearing materials. Providing that there are no discontinuities in the wear rate graphs, indicating the formation of stable oxides, it would be reasonable to assume that only the stress intensification factor being generated would change. The S.I.F. is also some complicated function of crack length, and so would depend on the contact radius. Therefore, the contact radius was kept constant, by changing the radius of the cylinder. The following proportionalities exist;

$$p_o \propto \sqrt[3]{\frac{P}{R^2}} \qquad a_o \propto \sqrt[3]{PR}$$

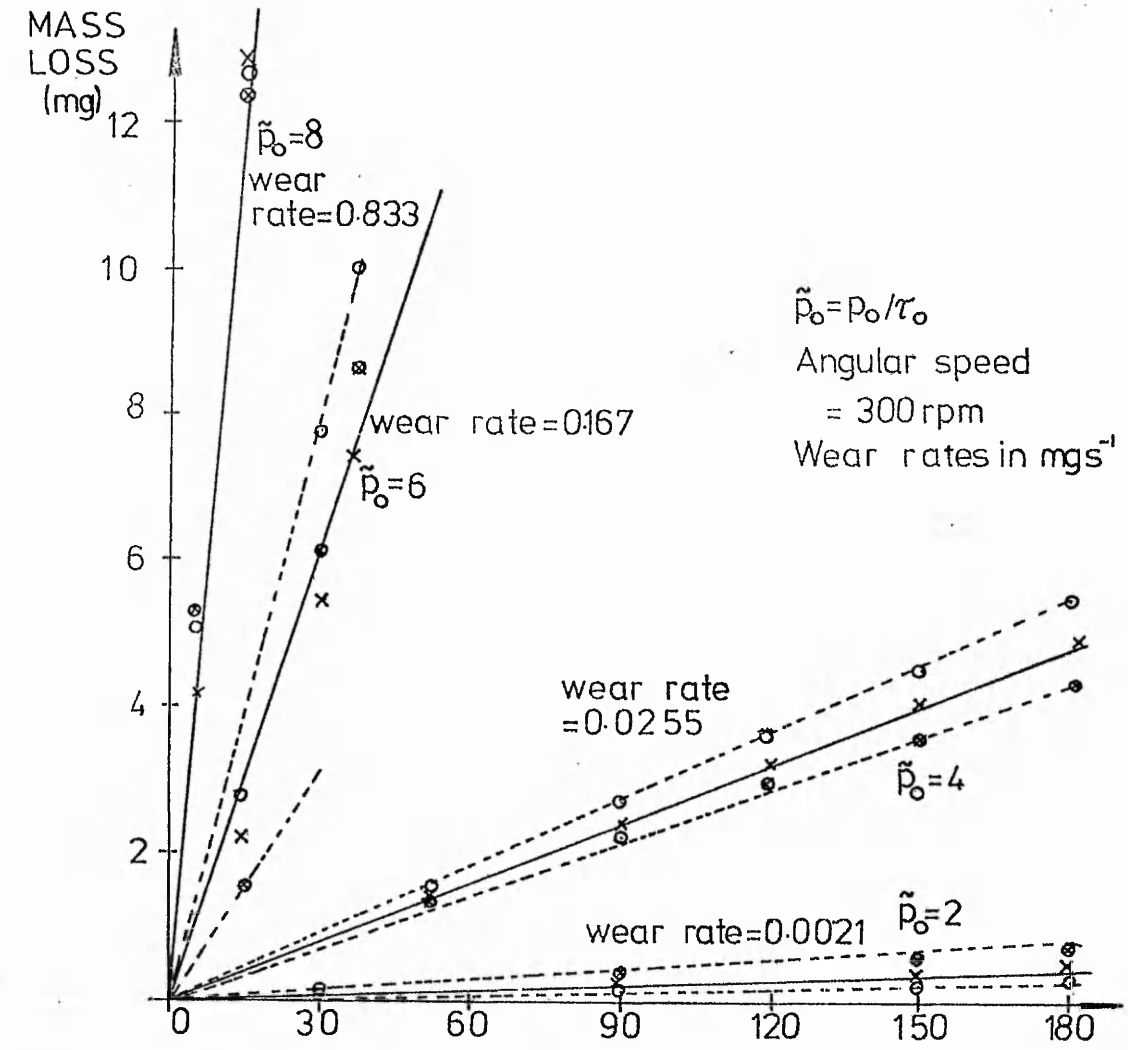
Thus, for the tests, the product P.R was kept constant.

Therefore: $p_o \propto P \qquad p_o \propto \tau_{max} \qquad \frac{dc}{dN} \propto P^m$

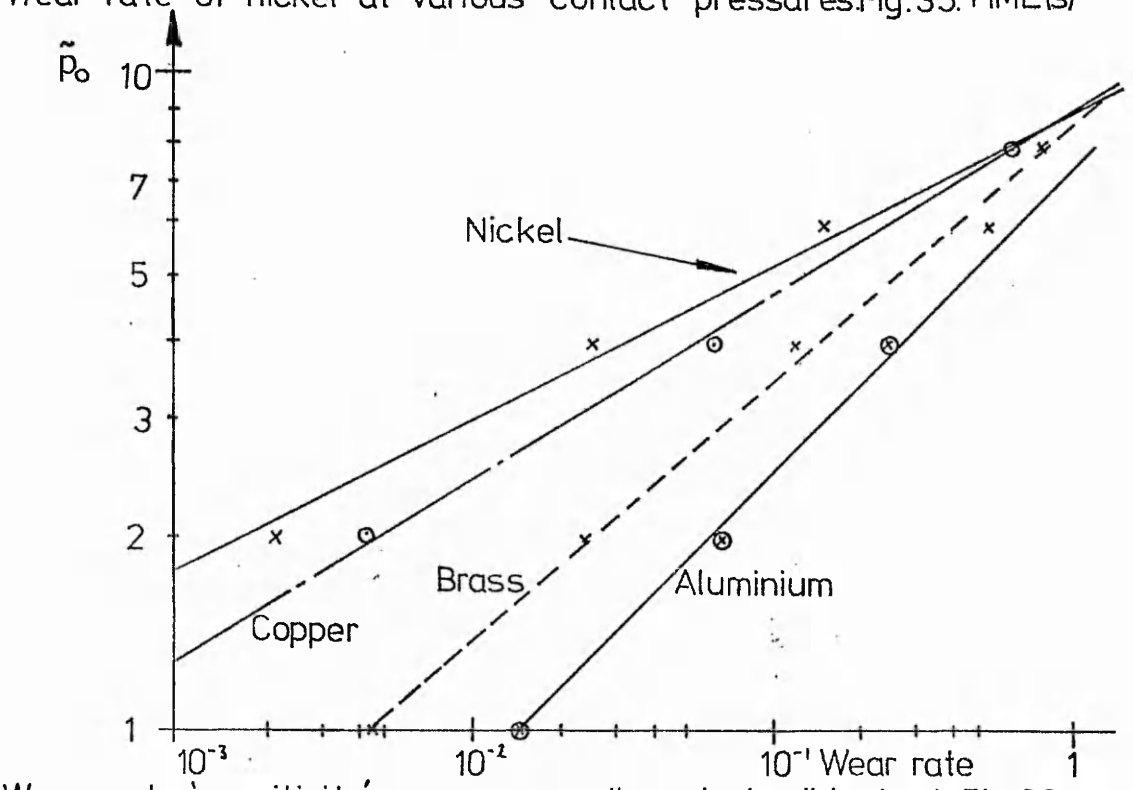
If wear were a propagation controlled fracture problem it would be expected that, with the constant contact patch provided;

$$\text{wear rate} \propto P^n \quad \text{and} \quad n=m$$

The results of one set of tests for nickel electroplate are shown in fig.35, and the results of these and other tests using different materials are summarised in fig.36.



Wear rate of nickel at various contact pressures. Fig. 35.



Wear rate 'sensitivity' summary – all against mild steel. Fig. 36.

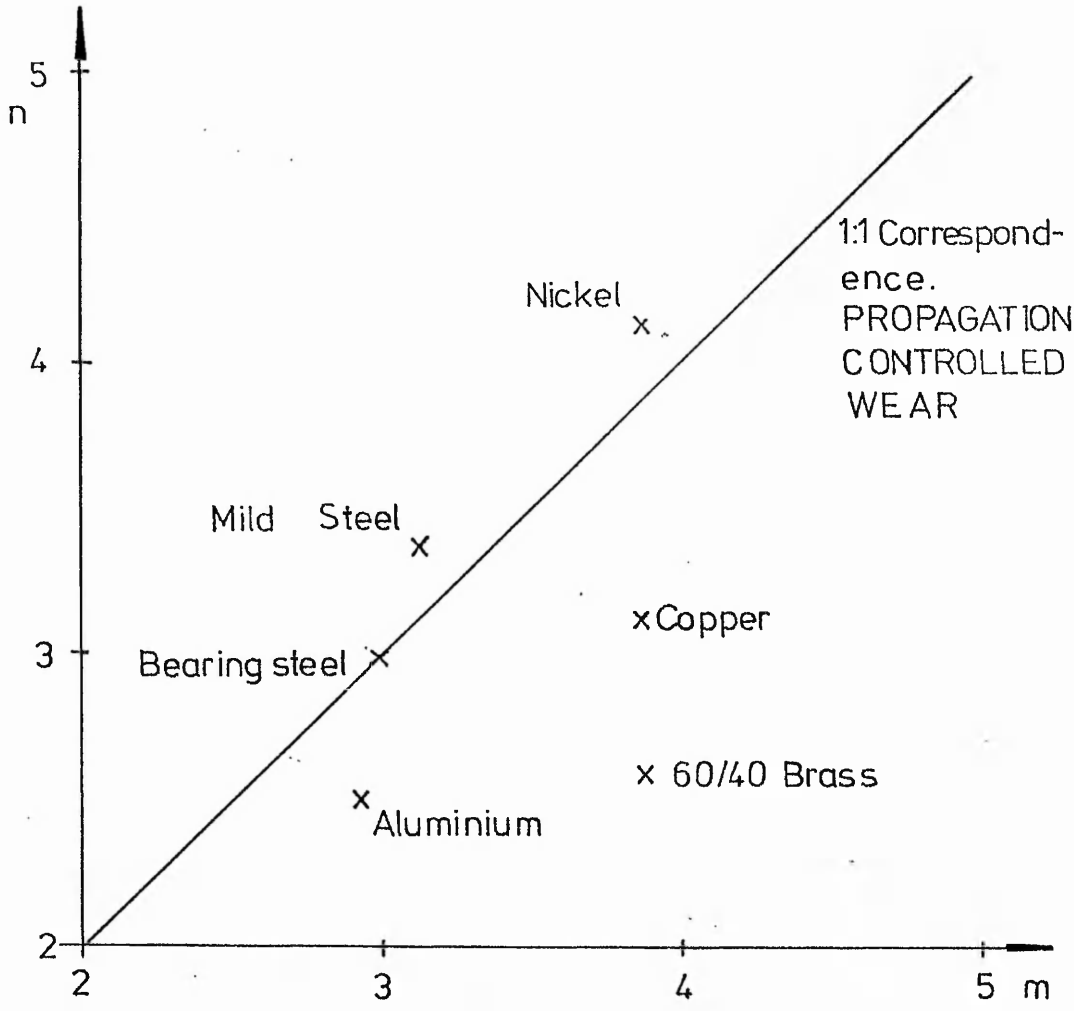
It was encouraging to find that the wear results did obey a power law approximately, but transferring the values onto a plot of m versus n (fig.37) was less conclusive. The lower than expected value of n suggests a lower wear rate than anticipated at high loads, which might be attributed to greater oxidation due to frictional heating. All experiments were in the mild regime, including steel on steel.

In spite of the lack of a really positive result from the last mentioned experiment, it was decided to proceed with a fracture mechanics analysis. An introduction to the problem of determining S.I.F.'s is now given.

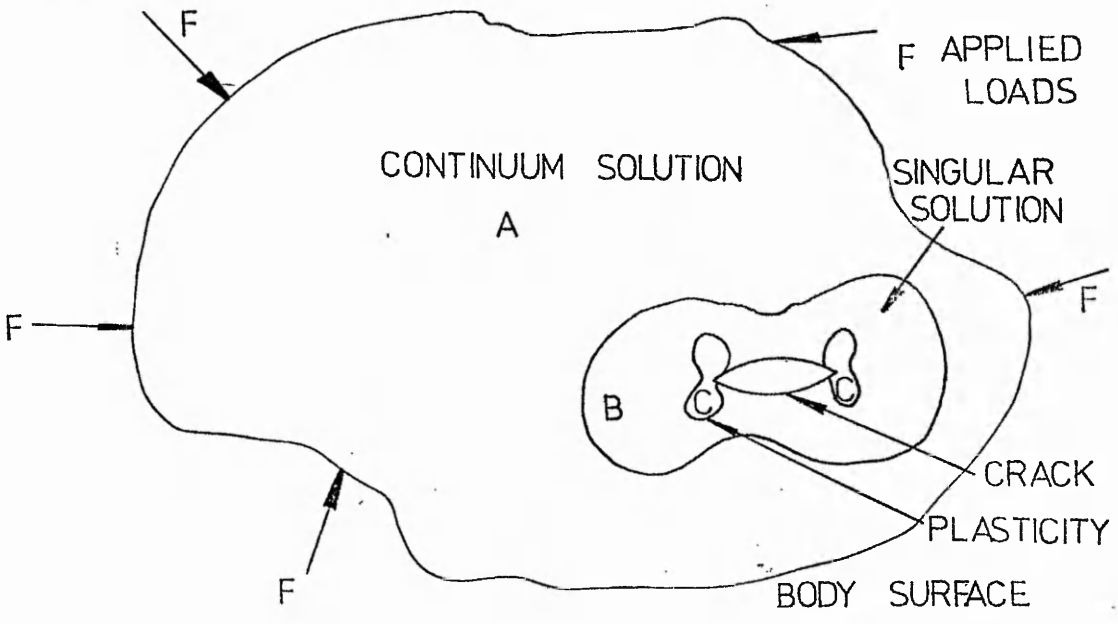
3.2. The Determination of Stress Intensification Factors

Some of the basic notions of fracture mechanics have been presented in section 1.4, and these will now be discussed more rigorously. Texts on fracture mechanics include Hertzberg, which deals with all aspects of the subject including metallography(105). Knott(106) treats post yield aspects fully as well as providing an introduction, whilst Broek(107) looks at fracture mainly fom the mechanics viewpoint. Lawn and Wilshaw(108) deal with truly brittle materials, and therefore treats fracture mainly from an energy consideration, but it seems unique in attempting also a discussion of crack initiation. Introductory papers have been published by, inter alios, Knott(109), Rolfe(110) and Hayes(111,112).

The complete inadequacy of classical failure criteria to determine the brittle failure stress of a material (maximum principal tensile stress or strain, maximum distortion energy &c.) necessitated the development of a new technique. It was well known that the stress-raising



A Comparison of Paris and wear exponents. Fig.37.



Zones of validity of various equations in cracked body. Fig.38.

effect of notches and holes often leads to the growth of cracks, but it was not possible, using the elastic stress concentration factor, to predict what would happen when a defect became infinitely sharp, because the apparent stress concentration factor was always infinite. A different quantity which overcame this difficulty was the stress intensification factor, which characterised the stress field at the crack tip: it is known from analysis that the product of stress and strain at a perfectly sharp crack undergoes a singularity of the type;

$$\sigma_{ij} \cdot \epsilon_{ij} \propto \frac{1}{r} \qquad (28)$$

where r is the distance from the crack tip. This equation is true whatever the constitutive relation of the material. For an elastic material, where $\sigma_{ij} \propto \epsilon_{ij}$. equation (28) may be re-written as;

$$\sigma_{ij} = \frac{K}{\sqrt{2\pi r}} f(\theta/?) \qquad (29)$$

where K is the S.I.F. and θ is polar coordinate measured from the crack centreline away from the crack. Note that there is an angular dependence experienced by the stresses and that the singularity predicted by the e.s.c.f. is preserved. The stress field within a cracked body may be separated into three regions. each with a different governing equation. fig. 38;

A. Far away from the crack, its effect is negligible, and the stresses present are those which would have been found within an uncracked body. This is to be expected from St. Venants's theorem.

B. A small distance from the crack ($0{\cdot}1c < r < 5c$, say) the variation of the stresses is completely independent of the rest of the component, in as much as they vary

according to equation (29). Thus, it is only the magnitude of stresses which is governed by the boundary conditions, within this region.

C. Because of the predicted singularity, there is a critical radius, r_p, where the yield criterion is exceeded. The exact nature of stresses and strains for $r < r_p$ is still unknown, as in most elasto-plastic problems, but there is certainly some blunting of the crack tip.

Providing that the plastic radius, r_p, remains much less than the crack half-length ($r_p < 0{\cdot}05c$, say), even at fracture, then the material behaviour at the crack tip will be governed entirely by zone 'B', ie. the singular elastic stress field will dominate, and the S.I.F. controls fracture. This is the key stipulation of linear elastic fracture mechanics (l.e.f.m.) and no account need be taken of the tiny zone of plasticity. If the plastic zone is significant in size compared with the crack, various approximations and adjustments need to be made, to allow for the yielding. The greater the yielding the greater the problems encountered, until finally with very tough materials yielding precedes fracture. Post yield fracture mechanics is needed to treat such problems (113), and for the time being this difficult subject will be avoided.

For simple configurations, the stress intensification factor can often be written in the form;

$$K_I = m\sigma\sqrt{\pi c} \qquad (30)$$

where σ is the nominal distant stress and m is some modifying constant, to allow the exact configuration to be taken into account, eg. edge-cracked plate, centre-cracked plate of finite width &c.. A compendium of these and more

difficult results was published by Rooke and Cartwright (114). However, in the case of a wearing half-space the configuration is too awkward for any of the standard results to be adopted, and so the following methods, as reviewed by Cartwright and Rooke(115), were considered;

A. Stress Functions

Westergaard(116) derived a real (Airy) stress function which shows the correct singularity and may be matched to some simple boundary conditions. Muskhelishvili(117) uses a complex stress function and a complex stress intensification factor $K_I - iK_{II}$. Conformal mapping may be used to map the crack into a circular hole, and the method has the advantage that under combined mode loading both S.I.F's may be determined at once. An extension to the modes I and III plane is possible.

B. Boundary collocation

By expressing the stress function of (A) as a finite series a set of simultaneous equations may be established relating the terms of the series to the boundary conditions known. Since the number of terms commonly used is limited, a perfect fit of the boundary conditions is often not possible and so a least squares fit may be needed, giving rise to the term 'collocation'. A common series from which to begin collocation is that expressed by Williamsin polar coordinates (118).

C. Stress Concentrations

By taking the limit of the stress concentration factor carefully it is sometimes possible to derive the corresponding S.I.F.

D. Green's Functions

Certain Green's functions,or weighting functions, are known exactly for point loads applied to the faces of cracks. For instance, a pair of self-equilibrating point loads, Q, applied a distance x from the centre of a crack in an infinite body give rise to an S.I.F. at the tip x=c of;

$$K_I = \frac{Q}{\sqrt{\pi c}} \left\{ \frac{c+x}{c-x} \right\}^{\frac{1}{2}} \qquad (31)$$

Hence a distributed pressure, p(x), across the crack face would give rise to an S.I.F. of;

$$K_I = \frac{1}{\sqrt{\pi c}} \int_{-c}^{c} \left\{ \frac{c+x}{c-x} \right\}^{\frac{1}{2}} p(x).dx \qquad (32)$$

This technique has been the topic of a recent paper by Cartwright and Rooke(119).

E. Dislocation Models

These take the form of arrays of dislocations, arranged so that the sum of the Burger's vectors matches the displacement at the crack tip. Also, the elastic stress field is in equilibrium with the stress field which would exist in the cracks absence, so that overall equilibrium is maintained. There is no general method available to apply this method.

F. Finite Elements

A large net of elements may be used to model the component including the crack, and the S.I.F. deduced by examining the local stress or strain gradient, or using an energy method, base on Rice's J-integral(120). These techniques were evaluated by Shaw(121) who also developed a special crack tip element which shows the correct singularity.

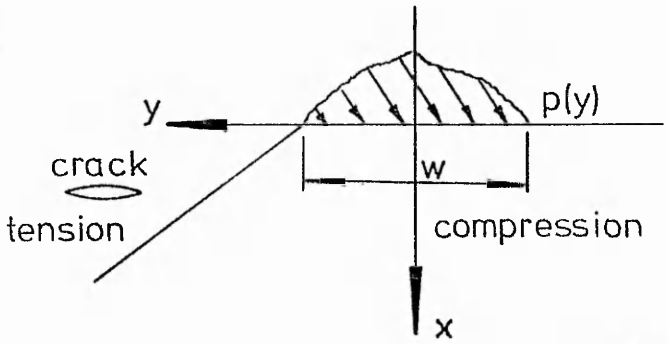
G. Photoelasticity

Plastic models made from an optically active material may be used in a polariscope to find the S.I.F., again by examining the local stress gradient. This has the advantage that under combined mode loading K_I and K_{II} may be separated.

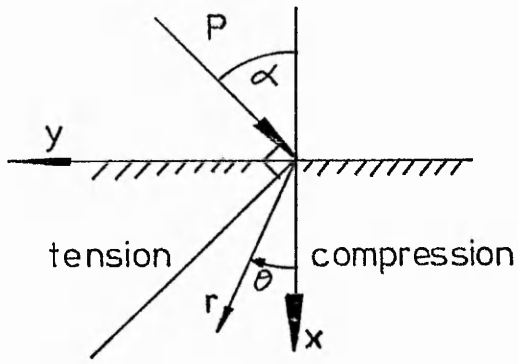
Returning to the case of a subsurface crack beneath a wearing half-space, methods A and B are inappropriate owing to the mathematical complexity of the solutions. Methods C and E were thought to be out of the question because of the extraordinary loading conditions where these techniques behave badly. At the time, a sufficiently large computer was not available for F nor was a polariscope for method G (photoelastic methods may also have presented some problems in making the crack). A technique was therefore developed based on Green's functions. Although the method is suitable in detail only for the wear problem, the general technique adopted could be used to determine S.I.F.'s under many awkward load conditions. The accuracy achieved is believed to be disproportionately high to the computing power needed, compared with, say, the finite element method.

3.3 Deriving S.I.F.'s for the Wear Problem

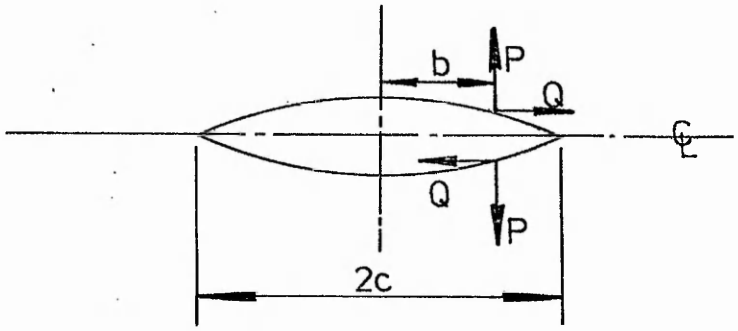
Fig.39 shows the wearing half-space with some arbitary loading applied to it by the second, sliding body. Whether the shear tractions are applied by an adhesive or abrasive mechanism is unimportant, as, for the time being, is the scale of the diagram. The width of applied load,w, could be the entire apparent contact patch or it could be on the scale of a single asperity.



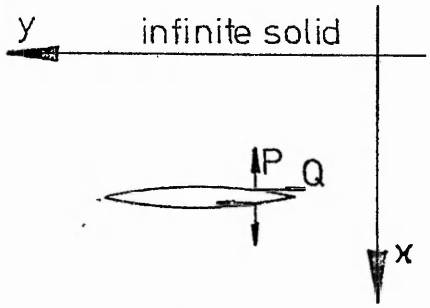
Wearing half-space subjected to arbitrary inclined load.Fig.39.



Nomenclature for line loaded half-space(Flamant problem).Fig.40.



Forces applied to crack faces. Fig.41.



The Green's function used assumes an infinite space.Fig.42.

Initially, the assumption will be made that for the crack to grow at all it must be open. Consider fig.40 which shows an inclined line load applied to a half-space. The resulting stresses were found by Flamant and are(122);

$$\sigma_{rr} = -\frac{2P}{\pi r}\cos(\alpha+\theta) \qquad \sigma_{\theta\theta}=0$$

so that;

$$\begin{aligned}
\sigma_{xx}&=\sigma_{rr}\cos^2\theta = -\frac{2P}{\pi x}\cos^3\theta\cos(\theta+\alpha)\\
\sigma_{yy}&=\sigma_{rr}\sin^2\theta = -\frac{2P}{\pi x}\sin^2\theta\cos\theta\cos(\theta+\alpha)\\
\tau_{xy}&=\sigma_{rr}\sin\theta\cos\theta = -\frac{2P}{\pi x}\sin\theta\cos^2\theta\cos(\theta+\alpha)
\end{aligned} \qquad (33)$$

Thus, for the crack to grow it must be located so that $\sigma_{xx}>0$, ie. $\cos(\theta+\alpha)<0$ or $\theta>\frac{\pi}{2}-\alpha$. For the simple line load configuration the crack must therefore lie in the wake of the load, behind a line perpendicular to its line of action. Returning to the more general load arrangement, (fig.39), an exact evaluation of the tension/compression interface depends on the surface pressue distribution, but it is approximately perpendicular to the inclination of the load. Therefore a crack passing beneath the load experiences compression for most of the time, and a brief period of opening when the load has passed over. Note that as the coefficient of friction tends to zero so the tension zone vanishes. Hence a crack beneath a rolling load will never open.

The method to be used to find the stress intensification factors is the 'pseudo-stress' method. First, the stresses within the wearing half-space are found due to the applied surface loads, in the absence of the crack. A crack is then inserted at the desired location, so that boundary conditions at the crack face are no longer satisfied. A set of forces is applied to the crack faces to

restore equilibrium,ie. to clear the crack faces of all stresses. These same loads applied to the crack face may also be used to determine the S.I.F.'s, using the appropriate Green's functions. For a crack within an infinite body, and having normal and shear loads applied, these are (123);

$$K_I' = \frac{1}{2\sqrt{\pi c}} \left\{ P\left(\frac{c+b}{c-b}\right)^{\frac{1}{2}} + \frac{Q}{2}\left(\frac{1-2\nu}{1-\nu}\right)\right\}$$

$$K_{II}' = \frac{1}{2\sqrt{\pi c}} \left\{ Q\left(\frac{c+b}{c-b}\right)^{\frac{1}{2}} - \frac{P}{2}\left(\frac{1-2\nu}{1-\nu}\right)\right\} \qquad (34)$$

under plane strain conditions.See fig.41.

So that, if $P = \sigma_{xx}.dy$ and $Q = \tau_{xy}.dy$

$$K_I = \int_{-b}^{b} K_I' \, dy$$

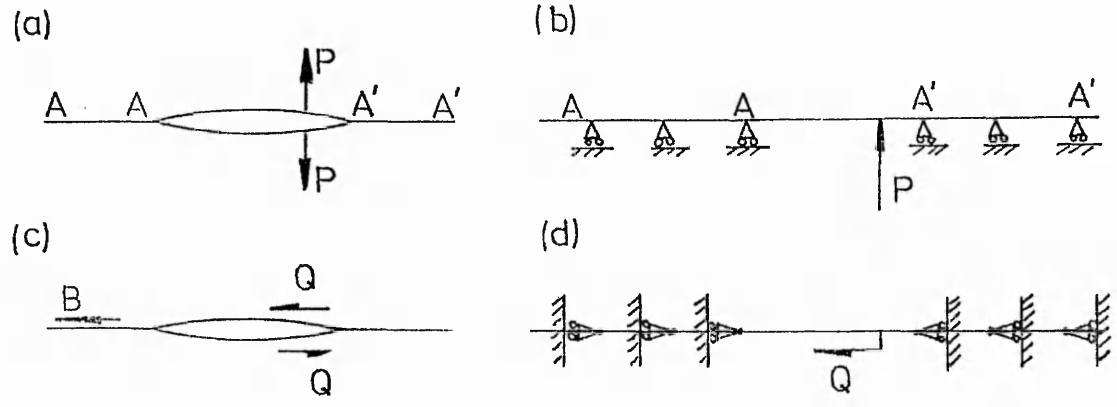
$$K_{II} = \int_{-b}^{b} K_{II}' dy \qquad (35)$$

Note, though, that the exact solution has not been found. This is because the Green's functions are for an infinite solid, and so the application of forces to the crack faces will give rise to non-zero stresses on the surface of the half-space. Such stresses are clearly not in equilibrium with the free surface, though Suh(32) accepted the solution just described without modification. Far below the surface this is valid, since the applied pairs of forces on the crack faces are self-equilibrating, and thus their long-range effect is negligible.

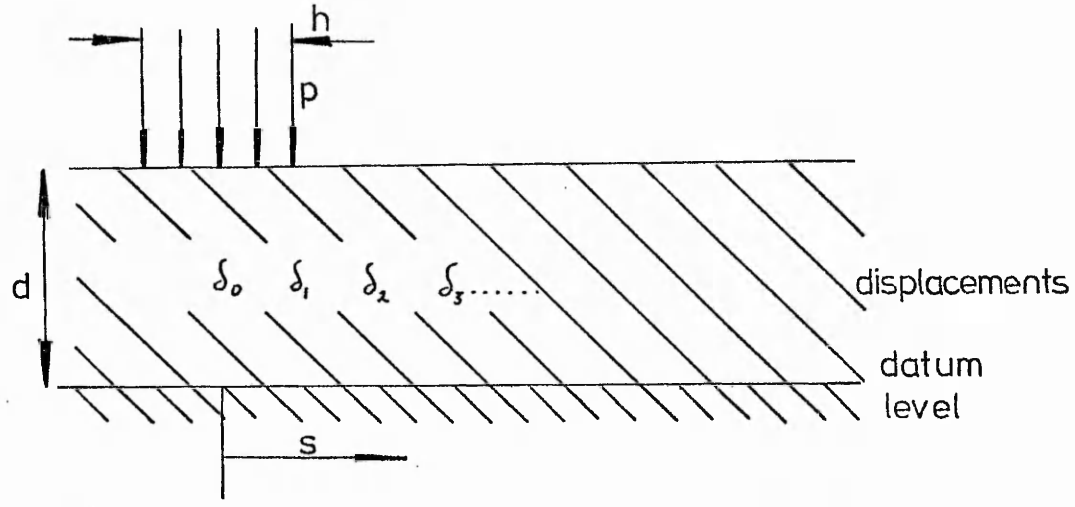
Since the purpose of the study is to investigate cracks near the surface, a better approximation is desirable. Fig.42 shows the crack within the wearing half-space, and under the action of the loads applied to the crack faces. What are required are the stresses $\sigma_{xx}(0,y)$, $\sigma_{yy}(0,y)$, $\tau_{xy}(0,y)$ which would exist if the crack lay in an infinite

body. Then, by applying new 'pressures' $-\sigma_{xx}(0,y)$ and $-\tau_{xy}(0,y)$ equilibrium would be restored. A new pseudo-stress field within the half space ($x \leqslant 0$) would be generated, and this would give rise to further unequilibrated stresses on the crack faces. New forces would need to be applied to the crack giving an extra contribution to the S.I.F.'s and further out of balance forces on the surface x=0. By repeating the method several times a converging solution would be obtained.

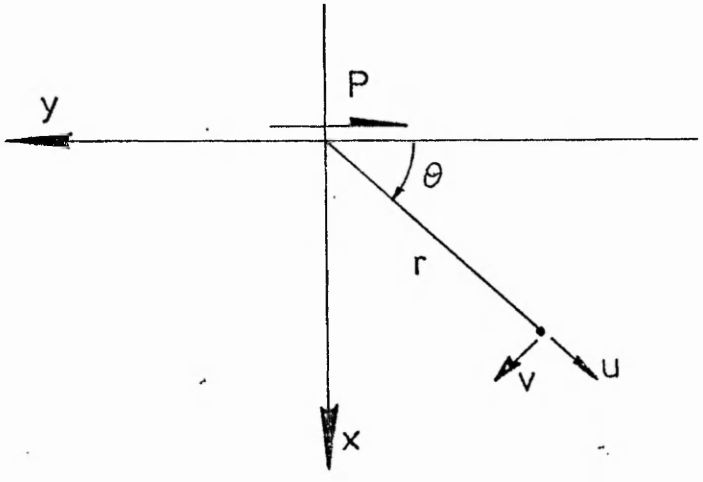
Solving the problem posed in fig.42 was not easy, and no solutions were found in the literature. Consider first a pair of normal forces, P, fig.43a. Since equal and opposite forces are applied, there can be no lateral displacement along the lines A-A and A'-A', from symmetry. Thus the cracked space could be replaced with the upper half-space of fig.43b with roller constraints along the boundary outside the limits of the crack. Further reduction is not possible because in general the distribution of the forces P along the crack will not be symmetrical. Consider, now, a pair of self-equilibrating shear loads, Q, fig.43c. Suppose that along the crack axis, at some general point remote from the crack, there is a finite displacement, B. Now rotate the plane of the crack through 180° about the crack axis. If the direction of the forces Q is reversed the problem is identical. However, to preserve an equivalent displacement, B, this too would have to be turned through 180° so that it faced in the opposite direction. The displacement B must therefore be zero, and the cracked space may be replaced by the upper half-space constrained as in fig.43d.



Roller constrained equivalents of crack face loading. Fig. 43.



Deformation of an elastic half-space due to a uniform contact load. Fig. 44.



Nomenclature used in determining shear deformation of an elastic half space. Fig. 45.

Solutions to the mixed boundary value problem of fig.43b,d are known (see Tiffin(124)), but are difficult to understand. Since other aspects of the calculation necessitated the use of a computer, an alternative numerical method was found. A freely deforming half space is adopted with loads applied either side the crack position, to ensure that displacement at such positions are zero. By Kirchoff's Uniqueness theorem, the set of forces found must be those which would have existed in a constrained half space, and so the solutions are identical, within the continuum. The tangential and normal loading cases are treated separately but in an entirely analogous manner. First it is necessary to find the influence coefficients, ie. the displacements of remote points of the boundary, due to the application of a unit load. For a normal load, the solution is given by Timoshenko and Goodier(125). In the notation of fig.44;

$$\frac{\delta_o}{p} = \frac{h}{\pi E}\left\{2\log\left(\frac{2d}{h}\right) + 1 - \nu\right\}$$
$$\frac{\delta_n}{p} = \frac{1}{\pi E}\left\{2\left[(h+s)\log\left(\frac{d}{h+s}\right) - s\log\left(\frac{d}{s}\right)\right] + h(1-\nu)\right\} \quad (36)$$

The deformation of a tangentially loaded half space may be obtained in an analogous manner. First the deformation due to a line load is required, fig.45.

$$\sigma_{rr} = -\frac{2P}{\pi r}\cos\theta \qquad \sigma_{\theta\theta} = \tau_{r\theta} = 0$$

Then;

$$\epsilon_{rr} = \frac{\partial u}{\partial r} = -\frac{2P}{\pi E}\frac{\cos\theta}{r}$$
$$\epsilon_{\theta\theta} = \frac{u}{r} + \frac{\partial v}{r\partial\theta} = \nu\frac{2P}{\pi E}\frac{\cos\theta}{r} \quad (37)$$
$$\gamma_{r\theta} = r\frac{\partial u}{\partial\theta} + \frac{\partial v}{\partial r} - \frac{v}{r} = 0$$

Thus;

$$u = -\frac{2P}{\pi E}\cos\theta\log r + f(\theta) \quad (38)$$
$$v = \frac{2\nu P}{\pi E}\sin\theta + \frac{2P}{\pi E}\sin\theta\log r - \int f(\theta)d\theta + F(r)$$

where $f(\theta)$ and $F(r)$ are arbitary functions of integration.

Differentiaing equations (38) gives;

$$\frac{\partial u}{\partial \theta} = \frac{2P}{\pi E}\sin\theta\log r + f'(\theta)$$
$$\frac{\partial v}{\partial r} = \frac{2P}{\pi E}\frac{\sin\theta}{r} + F'(r) \qquad (39)$$

Substituting these equations into the last of equations (37) gives;

$$\frac{2P}{\pi E} r\log r \sin + f'(\theta) + \frac{2P}{\pi E}\frac{\sin\theta}{r} + F'(r) - \frac{2\nu P}{\pi E}\frac{\sin\theta}{r}$$
$$- \frac{2P}{\pi E}\frac{\log r}{r}\sin\theta + \frac{1}{r}\int f(\theta)d\theta - \frac{F(r)}{r} = 0$$

Therefore; $f(\theta) = \frac{(1-\nu)P}{E}\theta\sin\theta + A\sin\theta + B\cos\theta$ & $F(r) = C.r$

Sustituting these back into (38) gives;

$$u = -\frac{2P}{\pi E}\cos\theta\log r - \frac{(1-\nu)P}{\pi E}\theta\sin\theta + A\sin\theta + B\cos\theta$$

$$v = \frac{2\nu P}{\pi E}\sin\theta + \frac{2P}{\pi E}\log r\sin\theta - \frac{(1-\nu)P}{\pi E}\theta\cos\theta + \frac{(1-\nu)P}{\pi E}\sin\theta$$
$$+ A\cos\theta - B\sin\theta + C.r$$

Suitable boundary conditions must be found to eliminate A,B,C:

I. At r=d, $\theta = \frac{\pi}{2}$, $u = v = 0$

$$\therefore A = \frac{(1-\nu)P}{2E}$$
$$B - C.d = \frac{P}{\pi E}\left\{1 + \nu + 2\log d\right\}$$

II. From a consideration of antisymmetry it is clear that:

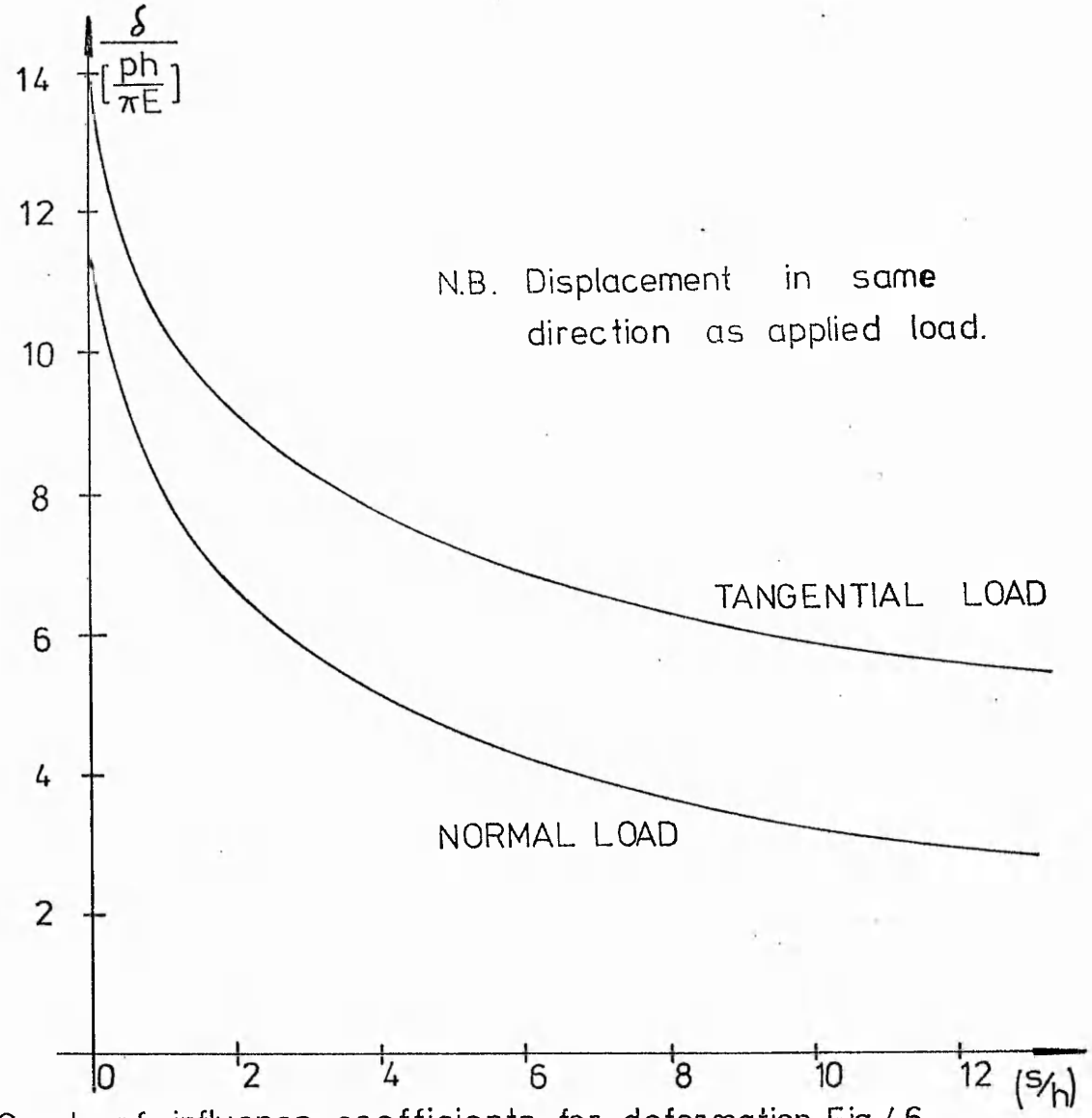
$$u|_{\theta=0} = -u|_{\theta=\pi} \qquad v|_{\theta=0} = v|_{\theta=\pi}$$

ie. $u(0) = -\frac{2P}{\pi E}\log r + B$
$u(\pi) = \frac{2P}{\pi E}\log r - B$
} so that the first condition is always satisfied

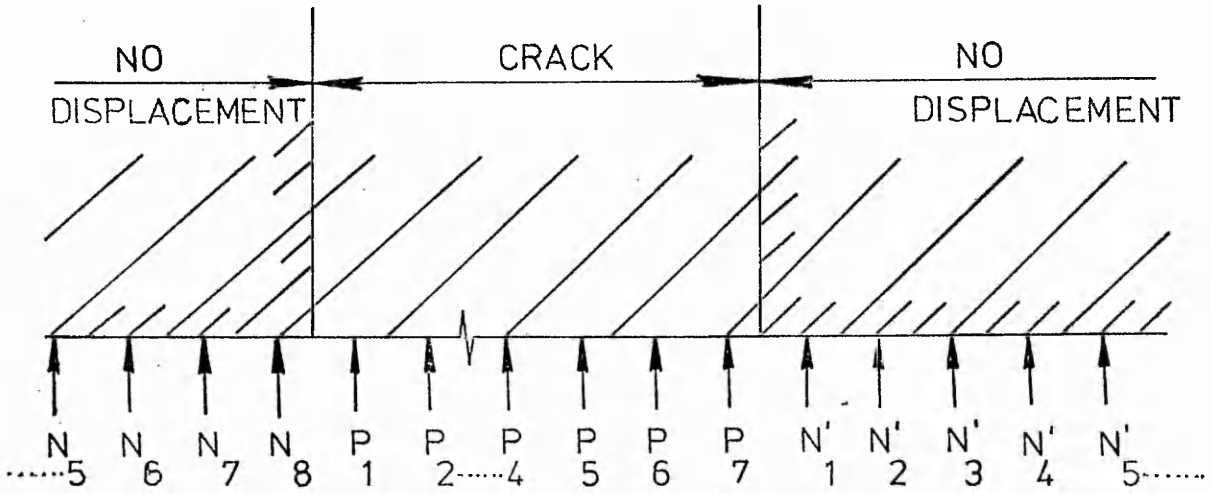
$v(0) = A + C.r$
$v(\pi) = \frac{(1-\nu)P}{E} - A + C.r$
} this gives the same value of A as above

III. Lastly, examine the slope as $r \longrightarrow \infty$. This should tend to zero: $\frac{dv}{dr} = \frac{2P}{\pi E}\frac{1}{r}\sin\theta + C \xrightarrow[\text{Lt } r\to\infty]{} 0$

$$\therefore C = 0$$
$$B = \frac{P}{\pi E}\left\{1 + \nu + 2\log d\right\}$$



Graph of influence coefficients for deformation of elastic half space. Fig.46.



Loads on crack face and additional loads need to simulate crack. Fig. 47

Thus; $-u|_{\theta=\pi} = u|_{\theta=0} = \frac{P}{\pi E}\left\{1+\nu + 2\log(\frac{d}{r})\right\}$

$$v|_{\theta=\pi} = v|_{\theta=0} = \frac{P(1-\nu)}{\pi E}$$

Everything is consistent except the deflexion at the origin, which is double-valued. This is to be expected at a singularity. The deflexions due to distributed loads may now be found. In the notation of fig.44 again;

$$\frac{\delta_n}{p'} = \frac{1}{\pi E}\left\{ 2\int_s^{s+h}\log(\frac{d}{r})dr + \int_s^{s+h}(1+\nu)dr\right\}$$
$$\frac{\delta_o}{p'} = \frac{1}{\pi E}\left\{ 4\int_0^{h/2}\log(\frac{d}{r})\,dr + 2\int_0^{h/2}(1+\nu)dr\right\} \qquad (40)$$

where p' is now the distributed shear 'pressure'.

ie.

$$\frac{\delta n}{p'} = \frac{h}{\pi E}\left\{ 2\log(\frac{2d}{h}) + 3 + \nu\right\}$$
$$\frac{\delta_o}{p'} = \frac{1}{\pi E}\left\{ 2\left[(h+s)\log(\frac{d}{h+s}) - s\log(\frac{d}{s})\right] + h(3+\nu)\right\} \qquad (41)$$

The similarity between equations (36) and (40) is clear. A plot of values from these equations, indicating their gradual decrease with distance, is shown in fig.46 for d/h = 100 (values are also tabulated in table 5). It is evident that for a very accurate solution, boundary condition matching is necessary for a large distance either side the crack.

Consider now the half space of fig.47, and the loads applied to it. It represents a section through the crack centreline and the material above it, and the loads may represent either normal or tangential forces. The displacement at the first station is given by;

$$N_1\delta_0+N_2\delta_1+\ldots.N_8\delta_7+N_1'\delta_{15}+\ldots.N_8'\delta_{22}-P_1\delta_8-\ldots.P_7\delta_{14}=0 \qquad (42)$$

where N_i, P_i are the applied loads and δ_i are the influence coefficients. Similarly, at the second station;

$$N_1\delta_1+N_2\delta_0+\ldots N_8\delta_6+N_1'\delta_{14}+\ldots.N_8'\delta_{21}-P_1\delta_7-\ldots.-P_7\delta_{13}=0 \qquad (43)$$

Table 5. List of Influence Coefficients for the Deformation of an elastic half-space under normal and shear loads.

$\frac{s}{h}$	$\frac{\delta}{(\frac{ph}{\pi E})}$ shear	$\frac{\delta}{(\frac{ph}{\pi E})}$ normal	$\frac{s}{h}$	$\frac{\delta}{(\frac{ph}{\pi E})}$ shear	$\frac{\delta}{(\frac{ph}{\pi E})}$ normal
0	13·90	11·30	7	6·62	4·02
1	10·60	8·CC	8	6·35	3·75
2	9·14	6·55	9	6·12	3·52
3	8·32	5·72	10	5·91	3·31
4	7·74	5·14	11	5·72	3·12
5	7·30	4·70	12	5·54	2·94
6	6·93	4·33	13	5·38	2·78

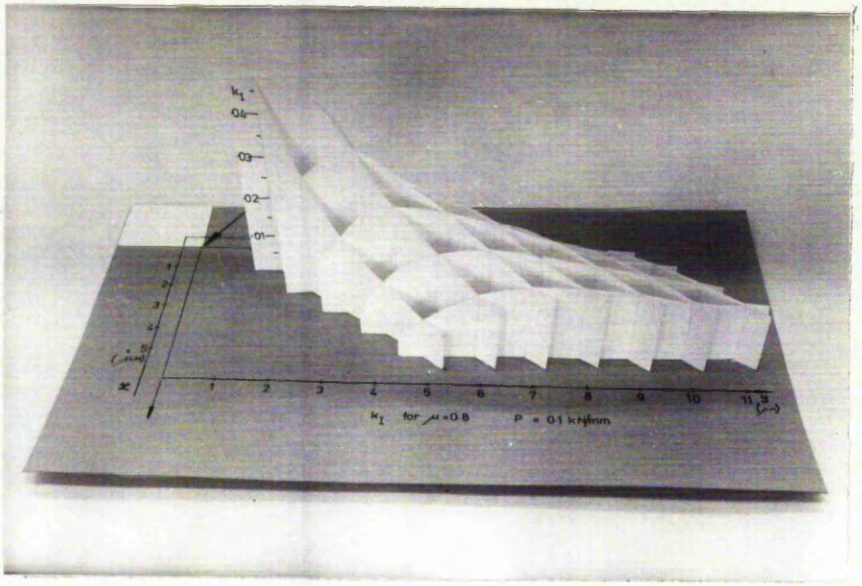
By continuing in this way it is possible to generate 16 simultaneous equations in the 16 unknowns N_1-N_8 and N_1'-N_8'. To facilitate solution, the equations may conveniently be written in matrix form. Let $[\Delta]$ be the symmetric matrix of influence coefficients, and $\{N\}$ the matrix of unknown loads. Let $\{B\}$ be the column vector of known loads and influence coefficients ($P_1\delta_8+P_2\delta_9+\ldots+P_7\delta_{14}$ &c).

Then;
$$[\Delta]\{N\} = \{B\}$$

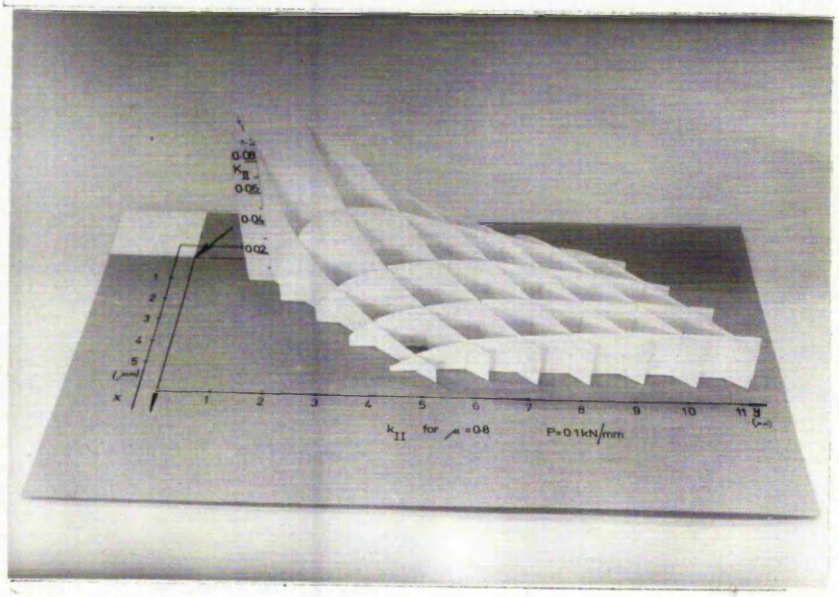
Solving;
$$\{N\} = [\Delta]^{-1}\{B\} \qquad (44)$$

Note that $[\Delta]^{-1}$ is a constant matrix and, once found, may be stored for use in each iteration cycle. All these equations apply equally to normal and tangential loads; it is necessary simply to use the correct set of influence coefficients.

The complete stress field above the crack may now be determined. This was done by using the Flamant solution (equations 33) for each load, both on the crack face and either side, and superimposing the results. Consequently, non-zero stresses appeared along the surface of the wearing



a. Mode I stress Intensification Factors



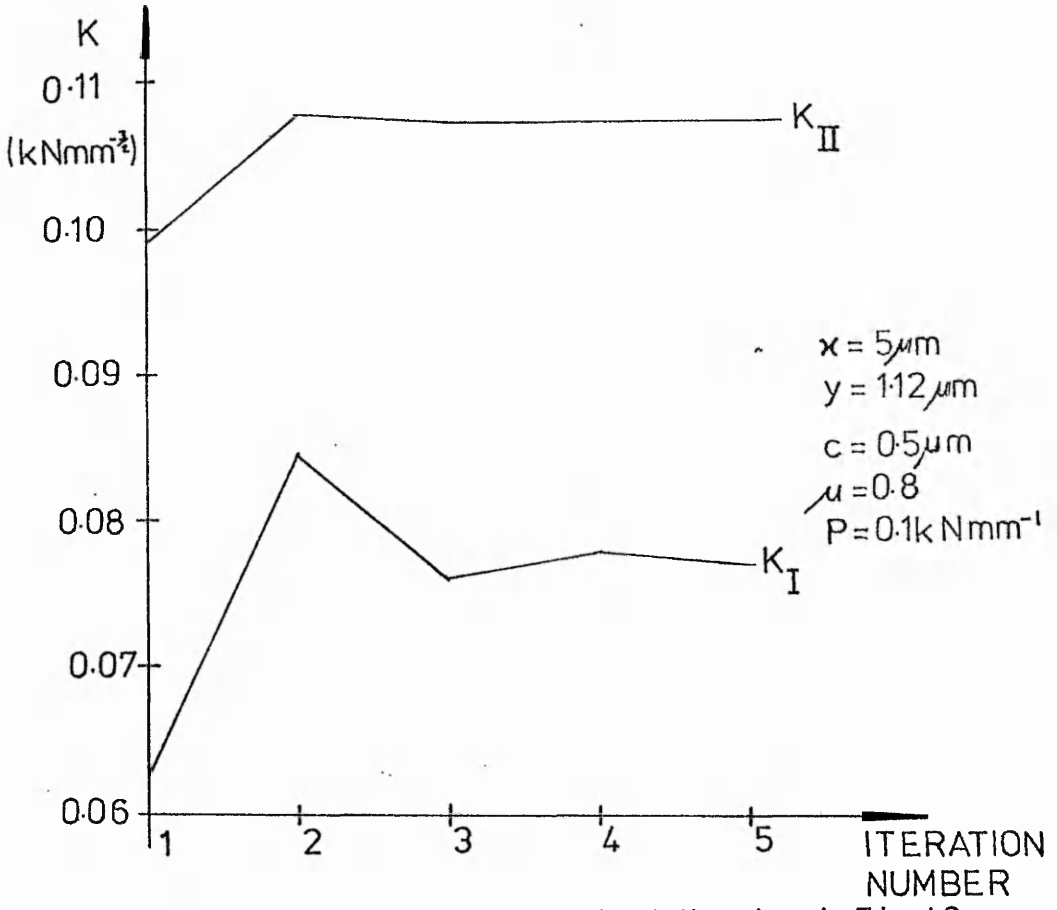
b. Mode II stress Intensification Factors

The photographs are of models of the variation of S.I.F. with position for a single crack inserted within a an elastic half space. The base of a model represents a vertical section, and values are shown for the region in the wake of the applied line load. The crack half length is 1 μm.

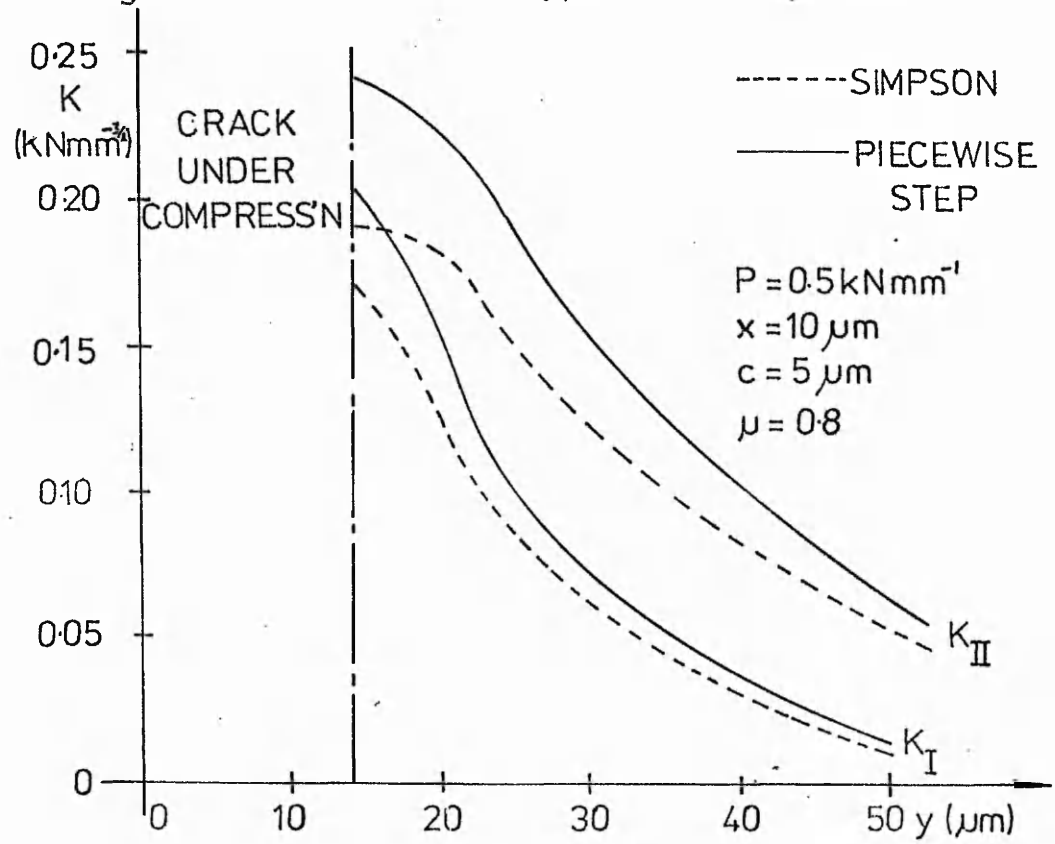
Fig.48.

half-space. At a number of points in the neighbourhood of the crack, on the surface, a set of equally spaces stations was chosen and corresponding array space allocated in the computer. The unsatisfied stress appearing at each station was noted, and an equal, opposite pressure applied. Thus the boundary conditions were again satisfied. A new pseudo-stress field was determined, again by superposition of the Flamant solution. Using the appropriate.Green's function the extra contributions to the S.I.F. were found. The process was repeated until convergence occurred. Because the iterative process required identical steps, after the determination of the inital stress field, it lent itself very well to machine computation. All work was carried out on a mini-computer having only about 8k of usable core, but with a large backing store. The technique just presented was the subject of a paper (126).

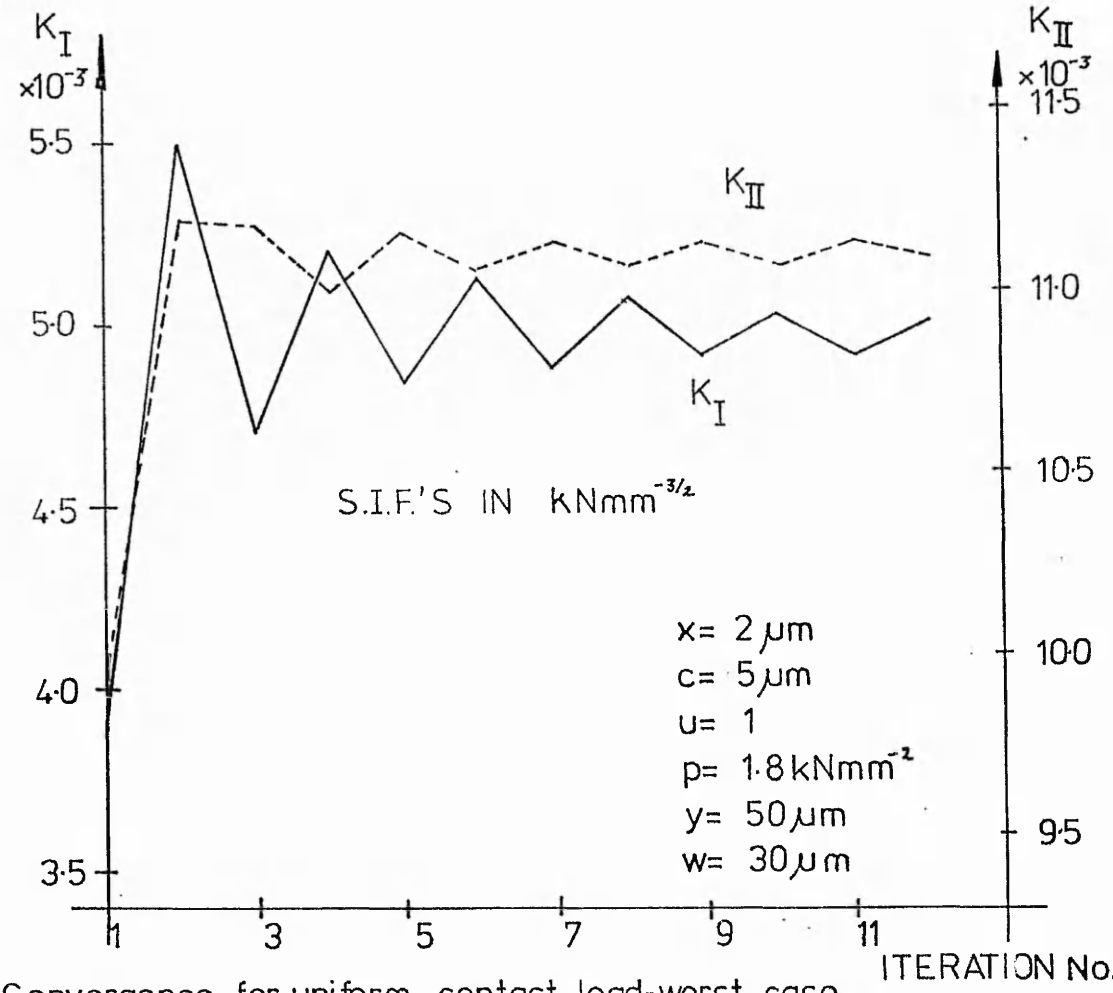
In fig.48 is shown the variation of modes I and II S.I.F. within the tensile region, for an applied line load. The largest S.I.F. is attained, as might expected, at or near the surface. For the same configuration, fig.49 shows the rate of convergence upon the final value, which is achieved almost immediately for mode II and within 5 iterations for mode I. A small improvement which was made was to improve the numerical integration of Green's functions. This was originally done simply by a piecewise-step process, but, because of the large contribution of forces applied near the ends of the crack (b→c,eqn.34), some smoothing was indicated. The assumption that crack loads fall continuously to zero at the ends enables the Repeated Simpson's Rule to be written in a slightly mod-



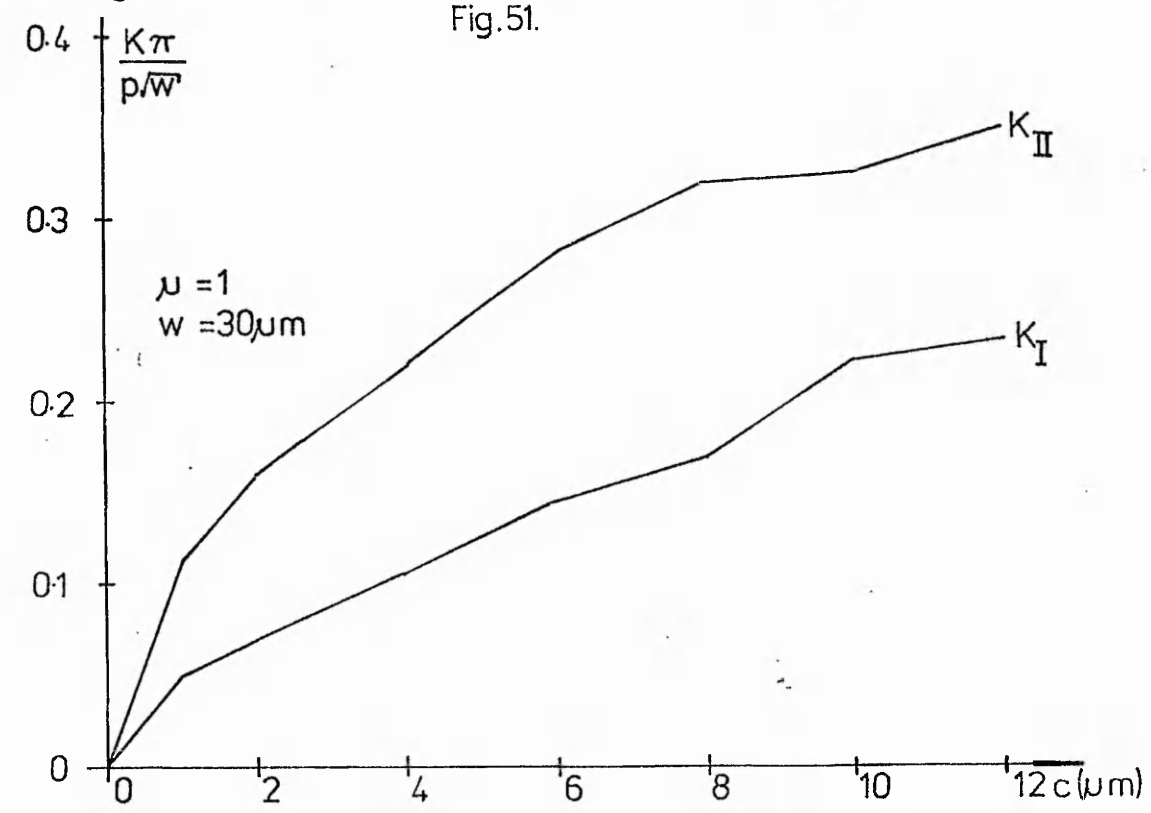
Convergence of solution for typical line load. Fig.49.



The effect of using numerical integration. Fig.50



Convergence for uniform contact load-worst case.
Fig.51.



Maximum SIF found for various cracks under uniform load. Fig.52

ified form, which is particularly convenient for computation;

$$I = \frac{c}{12}\left\{4y_1+2y_2+4y_3+.....+4y_7\right\} \qquad (45)$$

where y_i is the product of the ith load and Green's function. The effect of this improvement is shown for one particular configuration in fig.50.

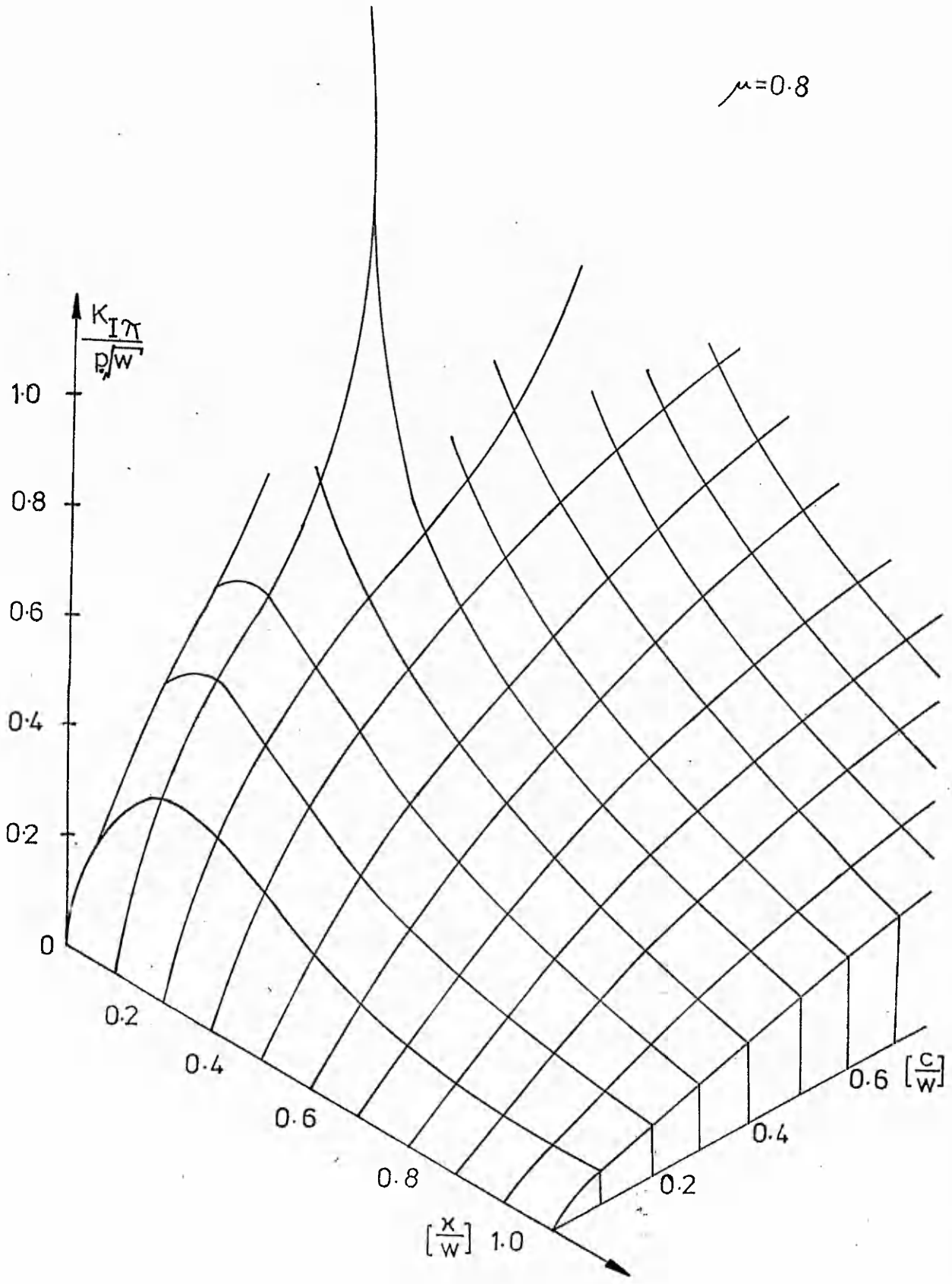
Calculations were also performed using a uniformly distributed load. This might be looked upon as the load applied (in two dimensions) by a plastically deformed asperity, or by two contacting surfaces where the surface roughness was not negligible in comparison with the contact width (16). Fig.51 and fig.52 show the rather poorer convergence experienced, and the S.I.F. as a function of crack half-length for one particluar configuration. Fig.53 attempts to summarise the effect of crack length and depth upon S.I.F., for one particular coefficient of friction. Calculations were also performed using Hertzian loading conditions. The results of these will be presented in the next chapter when the behaviour of a crack within the compression region has been determined.

Conclusions which may be drawn so far are;

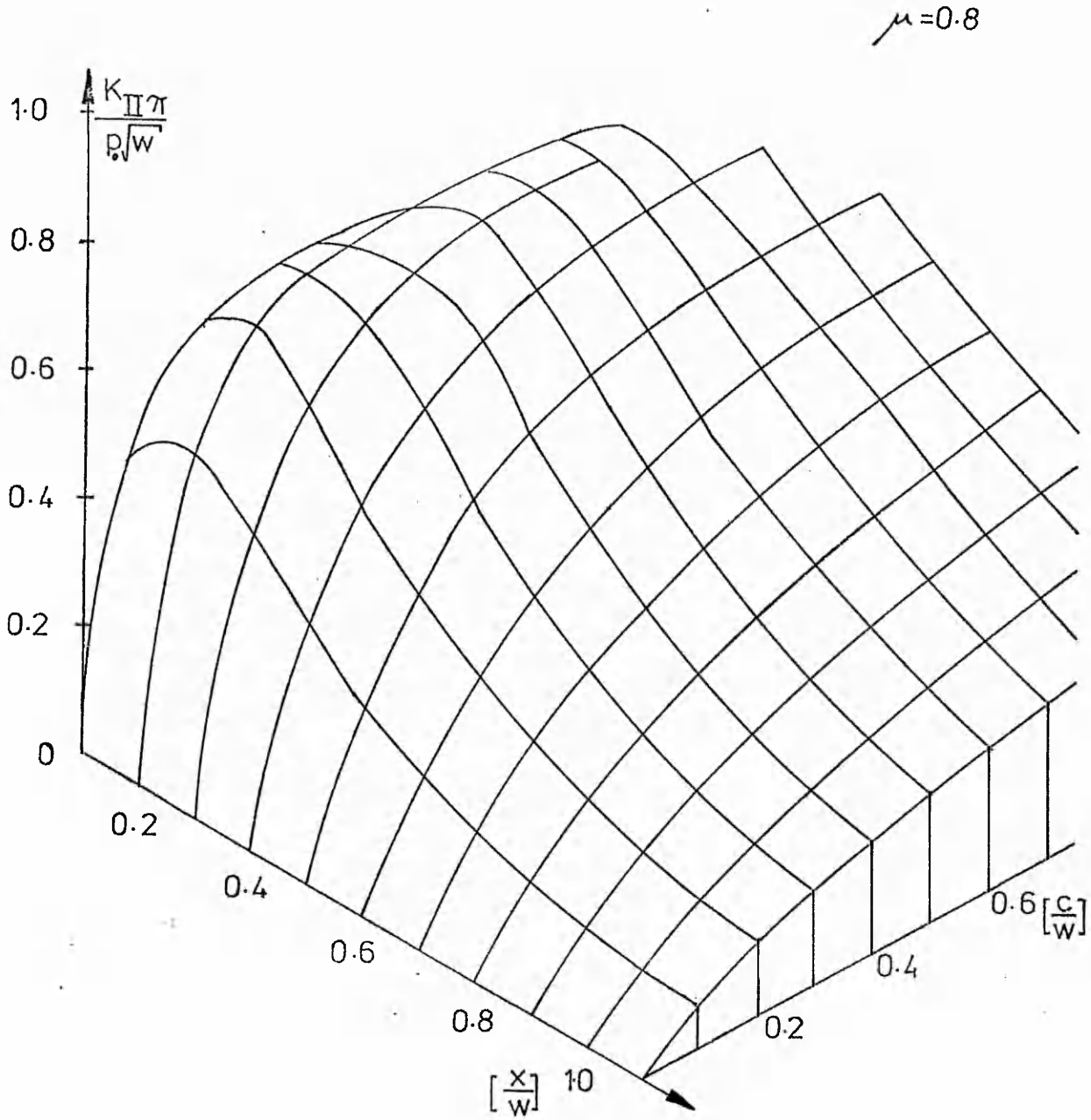
A. The result of including the effect of the free surface is to increase the magnitude of the S.I.F.. Thus, the nearer to the surface a crack lies, the greater will be the correction.

B. With the two loading arrangements so far considered, the maximum S.I.F. is at or near the surface. This is largely a feature of the pseudo-stress field assumed.

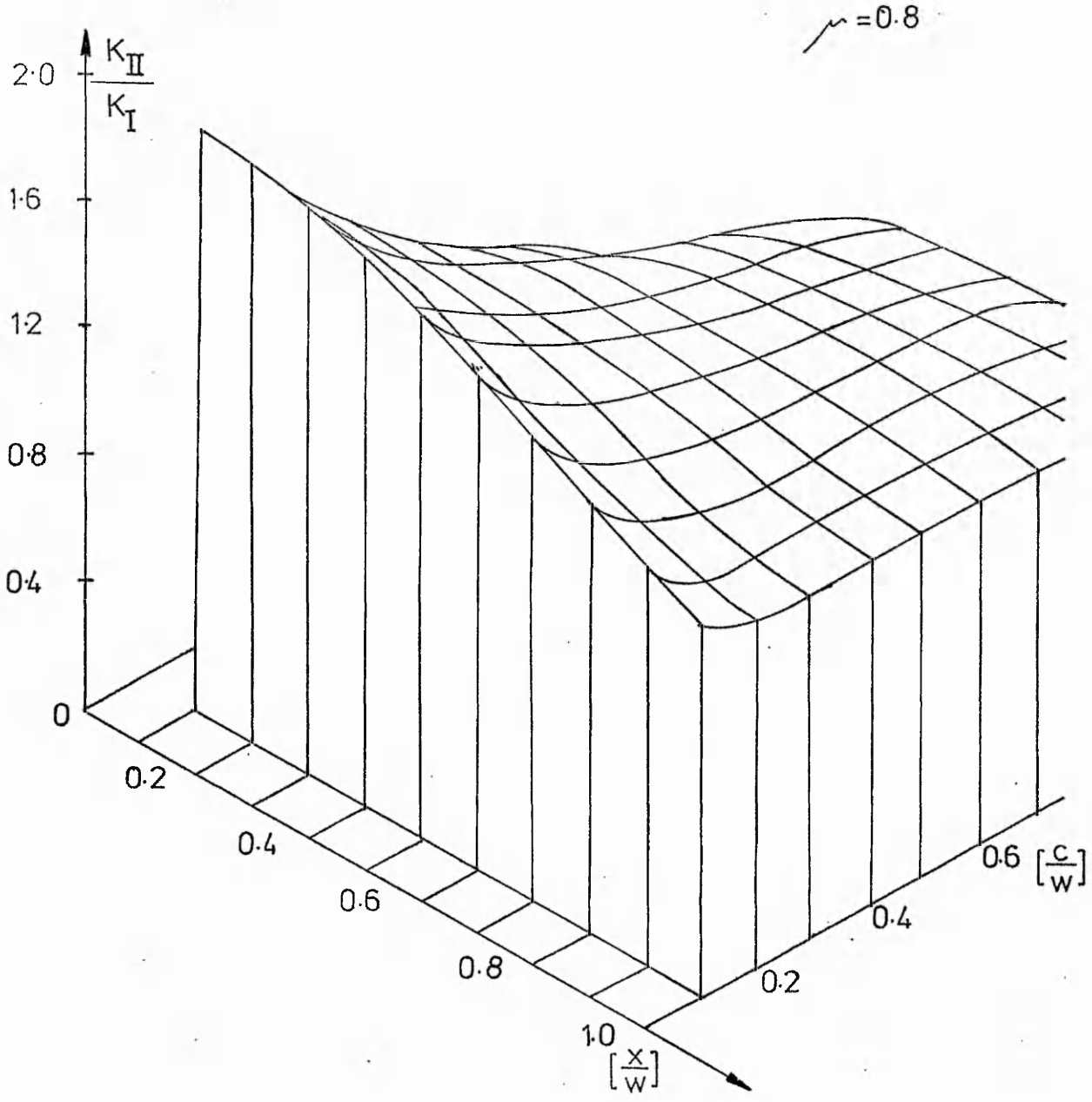
C. The solution described provides fairly rapid convergence, though, because of the small computer used, computing time was very long (about 3 mins. per iteration). It would have been impossible to obtain any finite element solution on such a machine.



Variation of mode I S.I.F. with depth & crack size. Fig. 53a.



Variation of mode II S.I.F. with depth & crack size. Fig. 53b.



Variation of ratio K_{II}/K_I with depth & crack size. Fig.53c.

4. Extensions of the Fracture Problem

4.1 Cracks under Compression

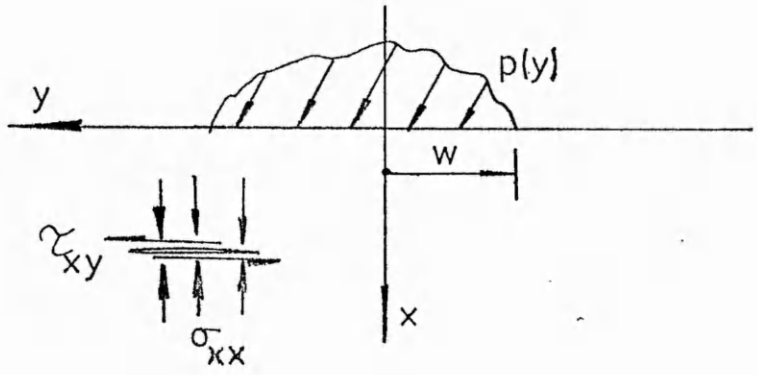
In the previous chapter the tentative assumption was made that cracks grow only when opened, ie. when there is a tensile component of stress normal to the crack faces. In order to have a significant period of opening, and therefore of mode 1 loading, it is necessary to assume very large coeffiients of friction- coefficients of the order of unity, which cannot realistically be expected to occur over the entire contact patch. Further, as the tractive loading component vanishes there becomes no region at all where a subsurface crack may be held open whilst a shear traction is applied. Such a loading arrangement (as found in any bearing) would apparently cause no wear. Because of these unrealistic conclusions the shear available to propel a crack was investigated more carefully. Fig.54 shows a closed crack under the compressive action of a normal stress σ_{xx}, and also loaded by a shear stress τ_{xy}. If the coefficient of friction between the crack faces is μ_c, then the crack might as well not exist if;

$$\tau_{xy} < \mu_c \cdot \sigma_{xx} \qquad (45)$$

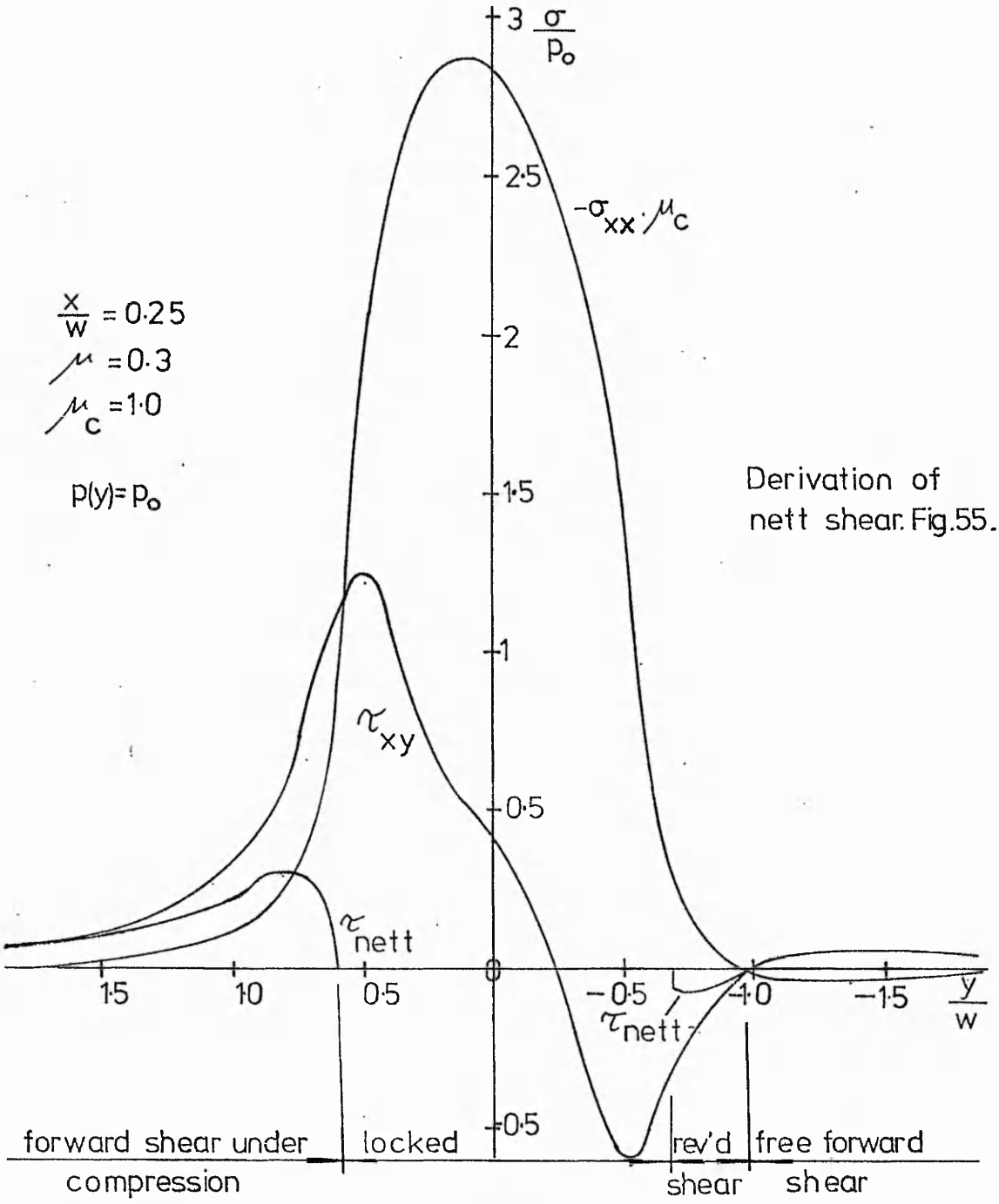
However, if this criterion is exceeded there is an excess shear stress which cannot be satisfied by frictional forces and this will contribute to mode II loading of the crack tips. The nett shear available to propel the crack is given by;

$$\begin{aligned} \tau_{xynett} &= \tau_{xy} + \mu_c \cdot \sigma_{xx} \quad \tau_{xy} > 0 \\ \tau_{xynett} &= \tau_{xy} - \mu_c \cdot \sigma_{xx} \quad \tau_{xy} < 0 \end{aligned} \qquad \sigma_{xx} < 0 \qquad (46)$$

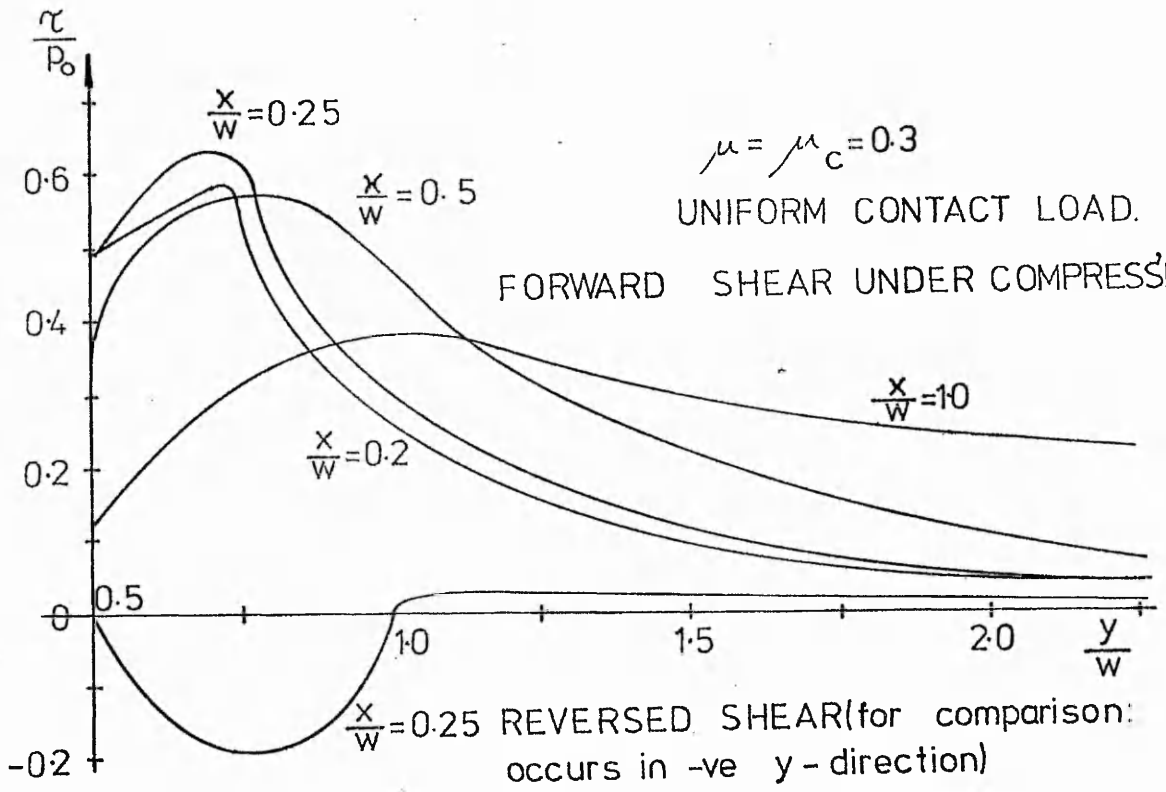
The derivation of this nett shear stress is illustrated



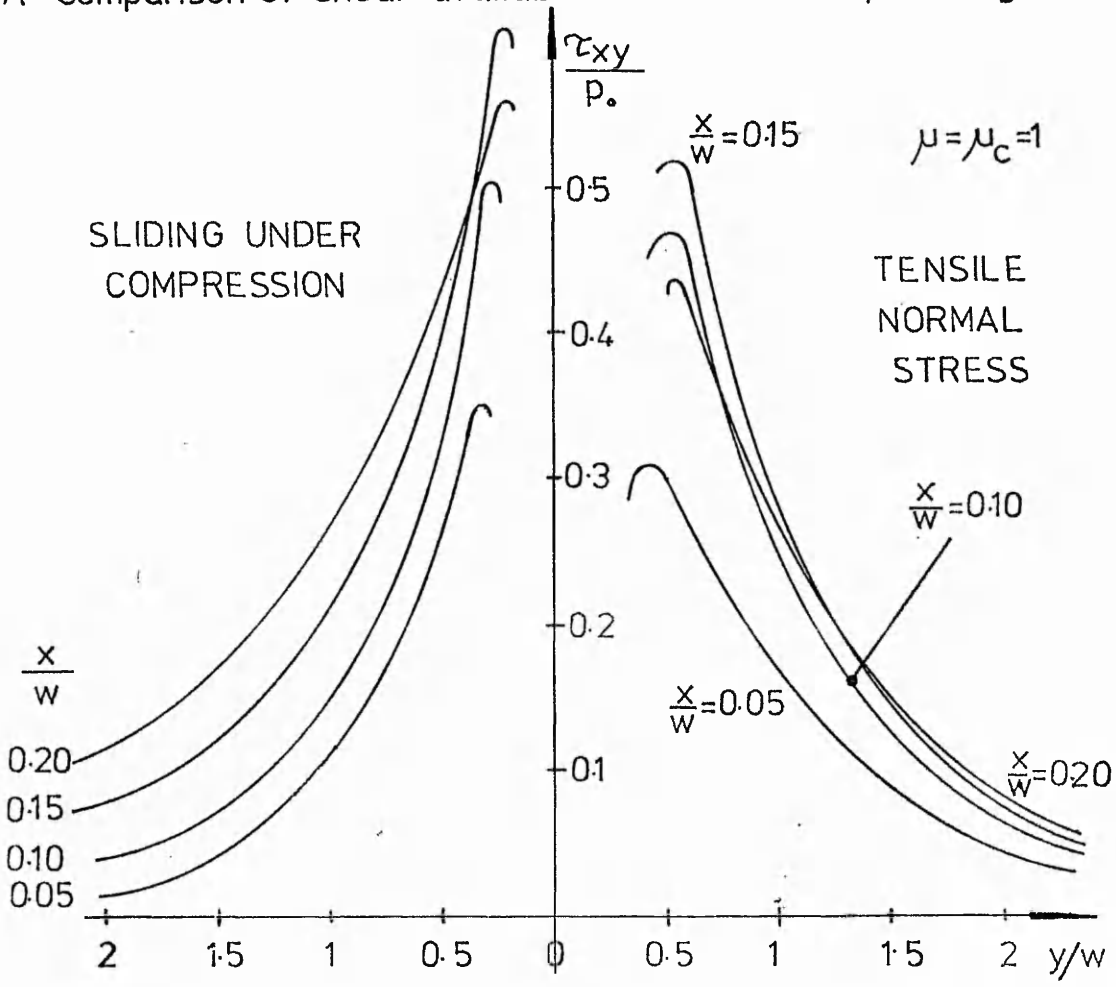
Crack under compression and shear. Fig.54.



Derivation of nett shear. Fig.55.



A Comparison of shear available at several depths. Fig.57.



Nett shear available to propel crack under uniform pressure. Fig.56.

for a uniformly distributed load in fig.55. It should be noted that for the case shown the coefficient of friction between the crack faces was assumed to be very much greater than the coefficient of friction at the surface, and this gave rise to the rather small shear stresses shown. It should nevertheless be recognised that the shear stress available in the compression region is rather greater than that in the tension zone. A comparison ~~of the propelling~~ of the propelling shear stress at various depths is shown in fig.56, which shows the greater importance of the shear-under-compression zone at all depths. Also to be noted in fig.55 is the small zone of reversed shear under compression. This is not present at small depths, but further within the material this too may be important (fig.57). Thus, as the slider passes over a crack, it experiences up to four regimes;

A. Forward shear umder compressive normal loading.

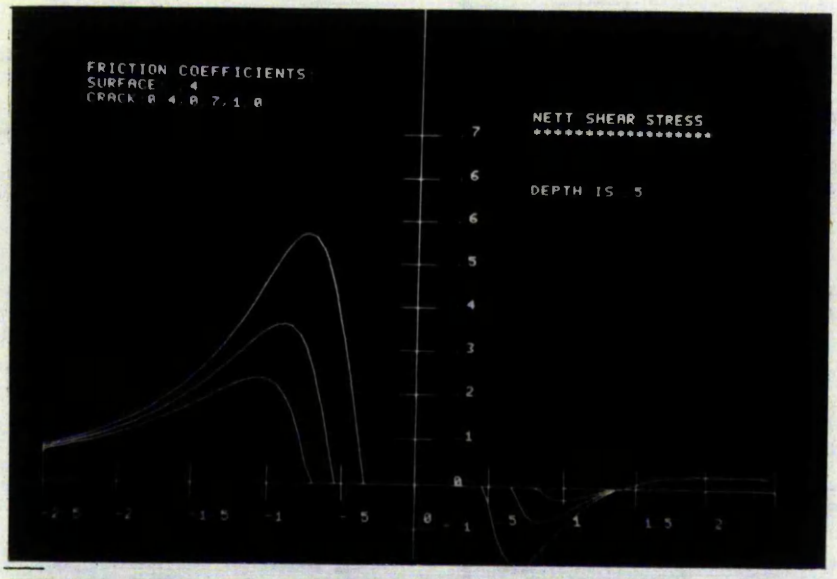
B. "Locking", where all shear is carried by frictional forces, and there is no relative motion between crack faces.

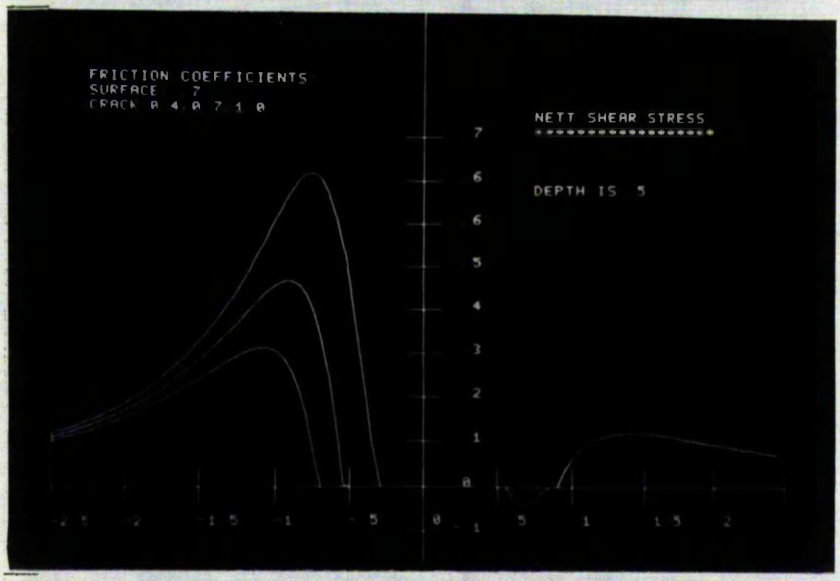
C. Reversed shear under compression. This does not occur near the surface, where the clamping stress is too large, and should not be important owing to its small magnitude.

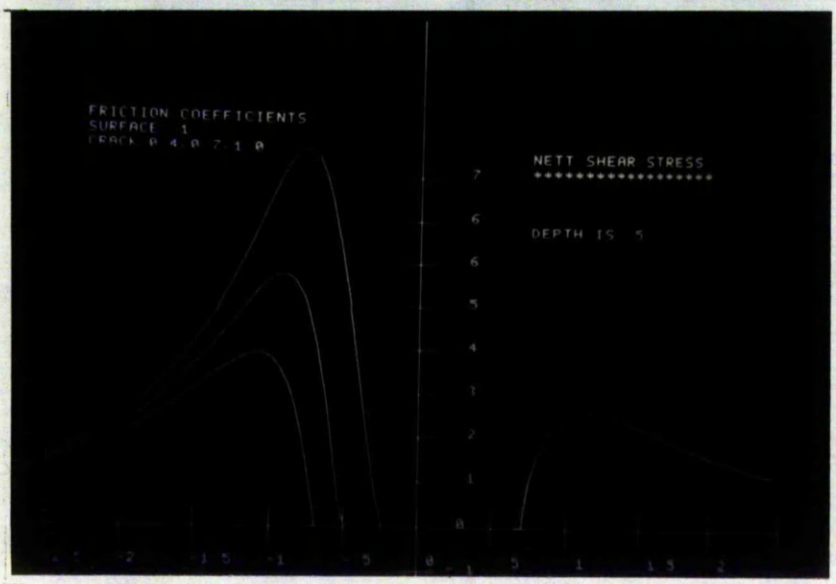
D. Free forward shear, which is always in the wake of the rider and accompanied by mode I loading.

The shear stress available to propel a crack under a variety of surface and crack coefficients of friction is shown in fig58, again for a uniformly distributed load.

Using these results and the iterative technique described in chapter three, the complete S.I.F. field for a uniformly distributed load was determined, and is shown in fig.59.

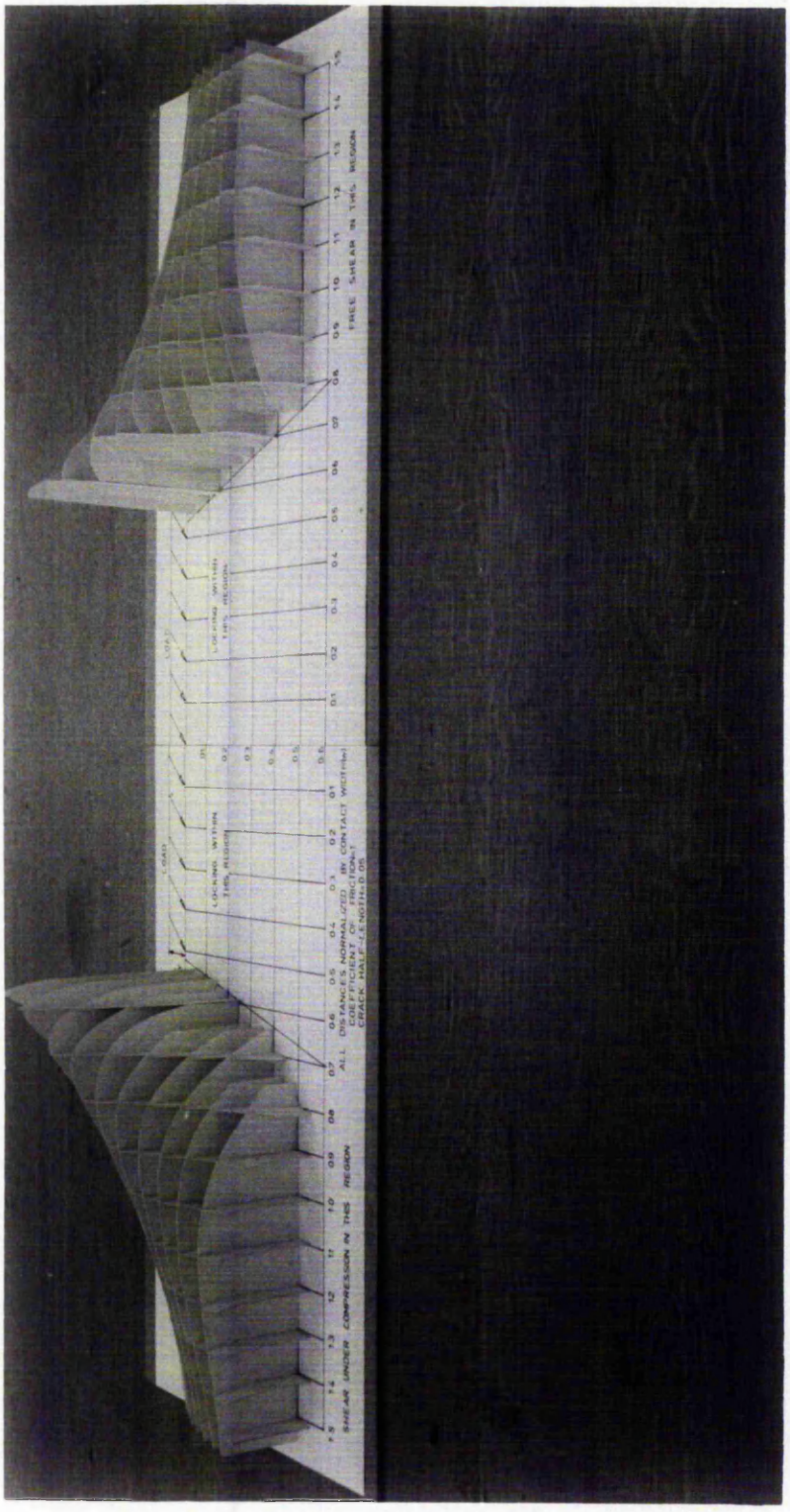






Load acts from right to left, and is uniform.
Nett shear is normalised by contact pressure.
Distances are normalised by contact half-width.
Note that the tallest peak corresponds to the lowest coefficient of friction between the crack faces, and vice versa.
The zone of shear on the right is not under compression.

More distributions of nett shear for uniform load. Fig. 58

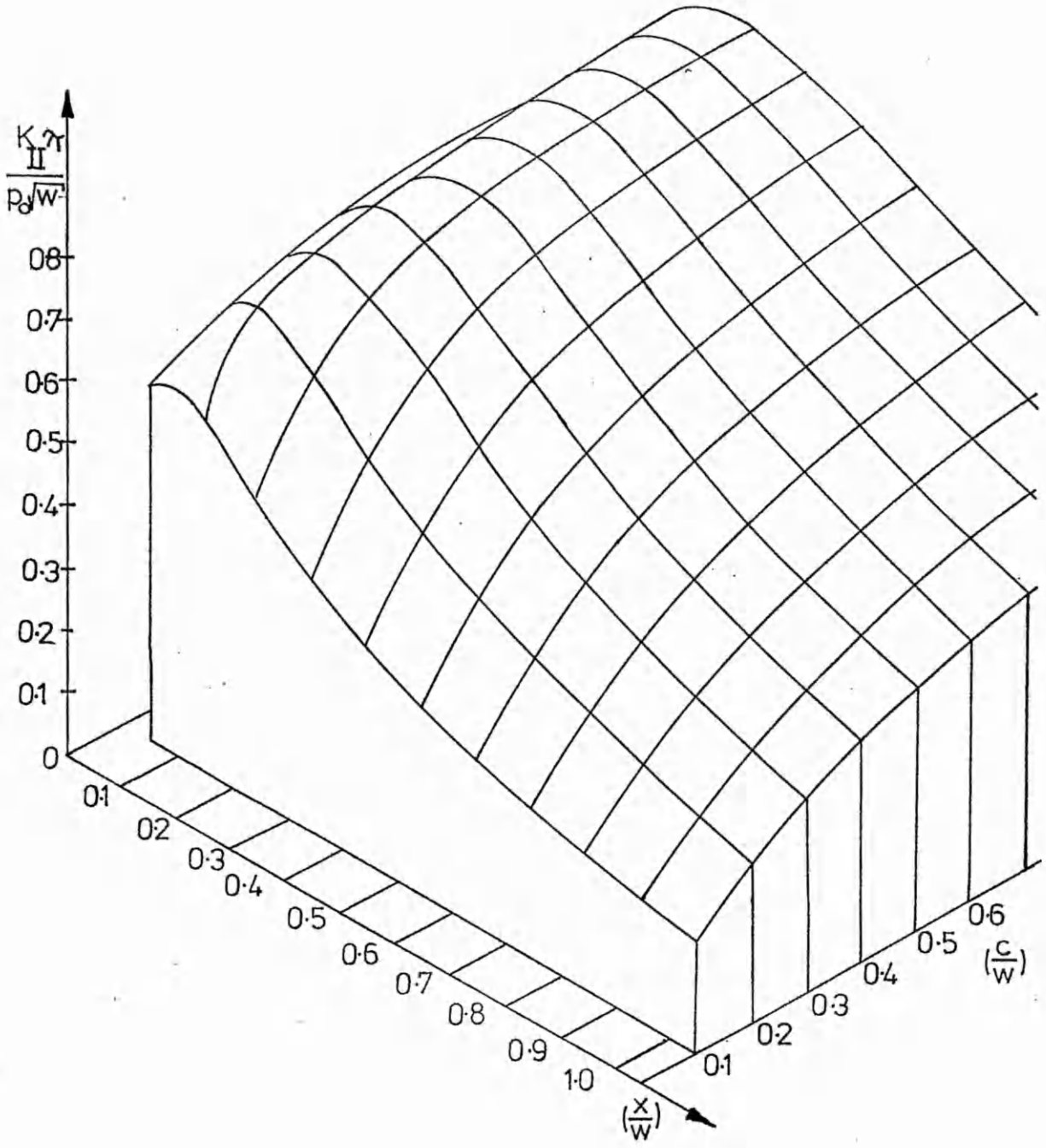


Model of mode II S.I.F.s for uniform load. Fig.59

As can be seen, for this case, the two shear zones are of approximately equal importance. Also, they act in the same (forward) direction. A summary of maximum mode II S.I.F. values in the compression zone is shown in fig.60.

Because of the severe state of stress produced near the ends of a uniform load distribution, making the estimation of S.I.F.'s difficult, a Hertzian distribution with shear was also studied. The pseudo-stress field used was the one described earlier, derived by Smith and Liu(93), equation 25. The results of these calculations are shown in fig.61. It can be seen that largest forward-acting S.I.F's occur at about half to three quarters of the semi-contact width, whilst the backward shear has its maximum at a depth at or below the semi-width of contact.

Recognising that subsurface cracks probably grow whilst suffering compression raises extra questions. First, should the same coefficient of friction be assumed between the crack faces as between the wearing pair? Since, in vacuo, the coefficient of friction between two clean metals is very high ($\sim$10), it might be expected that the same conditions exist at a crack not exposed to the atmosphere. However, when the crack underwent severe compression in the "locking" regime it would probably be cold-welded back together again, so that the wear crack would continually heal. Schijve(127) has recently performed some rotating bending fatigue tests on internally flawed specimens, and found that cracks grew regardless of whether he vented the crack to atmosphere. In each case it is uncertain whether any gases remaining within the material after steelmaking provided lubrication or a means of surface oxidation. The notion that the inclusion

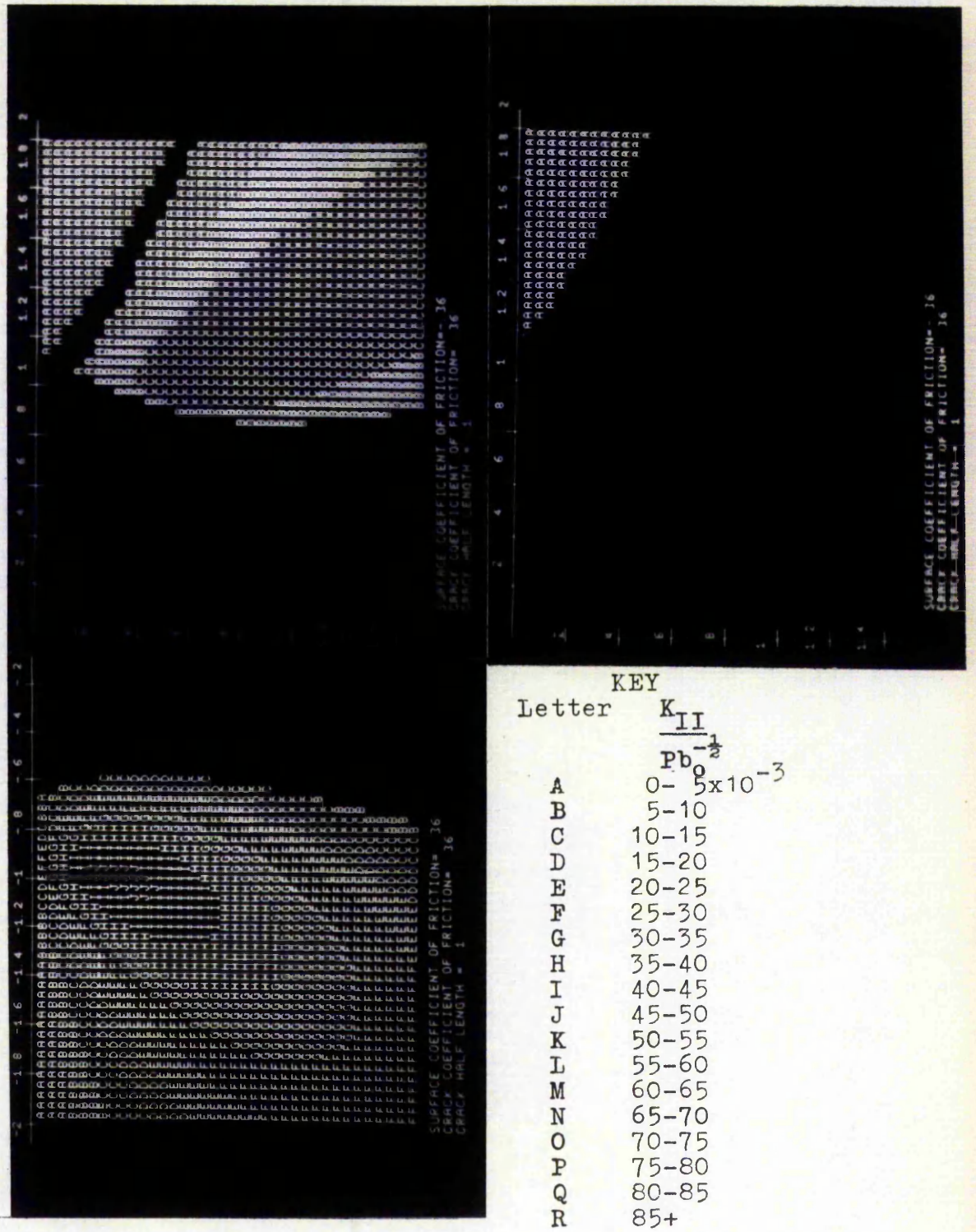


Mode II S.I.F. as a function of depth & crack size in compression zone.
Fig. 60.

For key see overleaf.

S.I.F. MAP HERTZIAN LOAD WITH TRACTION

Fig.61a



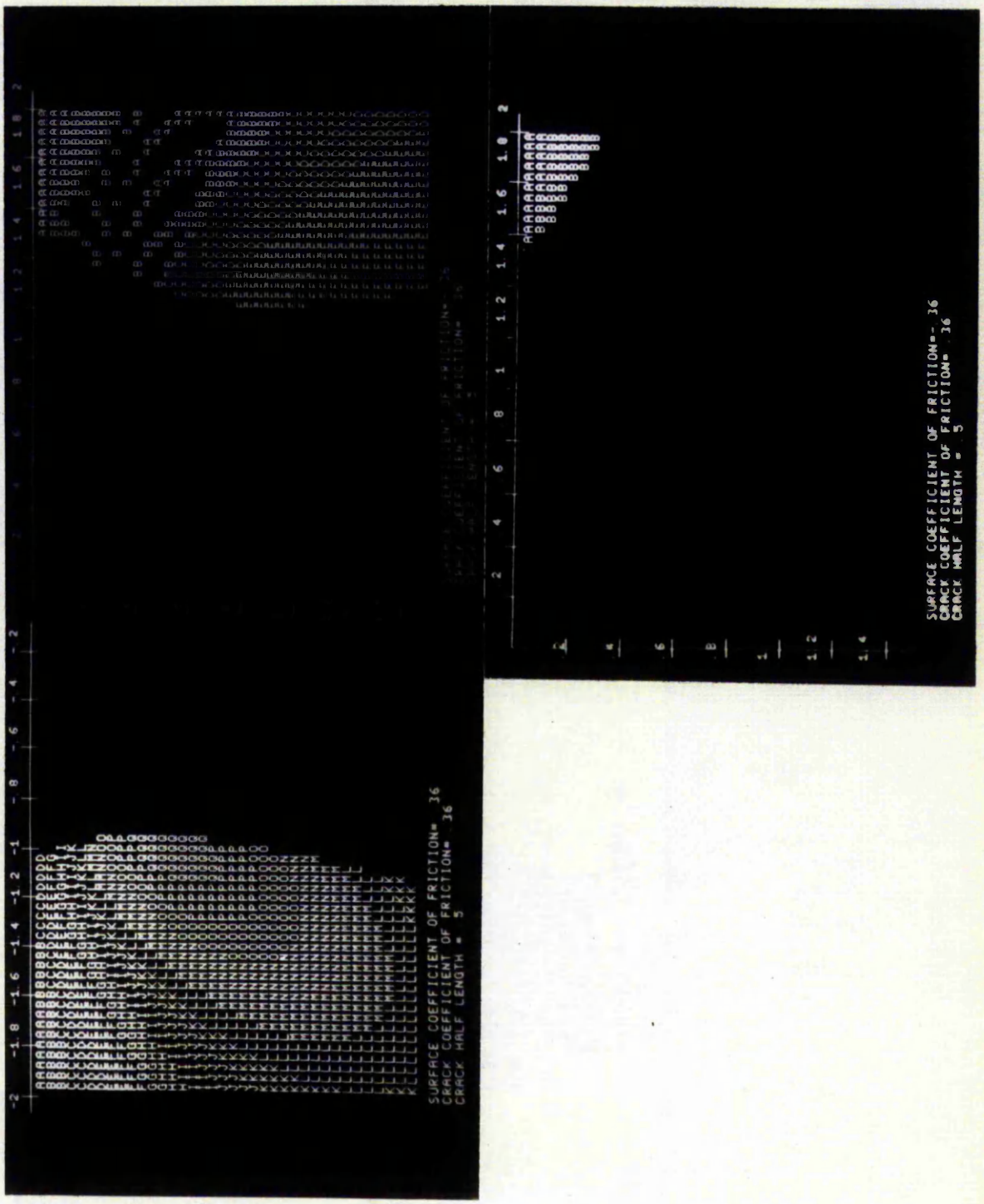
KEY

Letter	$\frac{K_{II}}{Pb_o^{-\frac{1}{2}}}$
A	$0-5\times10^{-3}$
B	5-10
C	10-15
D	15-20
E	20-25
F	25-30
G	30-35
H	35-40
I	40-45
J	45-50
K	50-55
L	55-60
M	60-65
N	65-70
O	70-75
P	75-80
Q	80-85
R	85+

If no letter is shown in a particular zone then the crack faces are locked. All dimensions and crack lengths are normalized with respect to the semi contact width, b_o.

S.I.F. MAP HERTZIAN LOAD WITH TRACTION

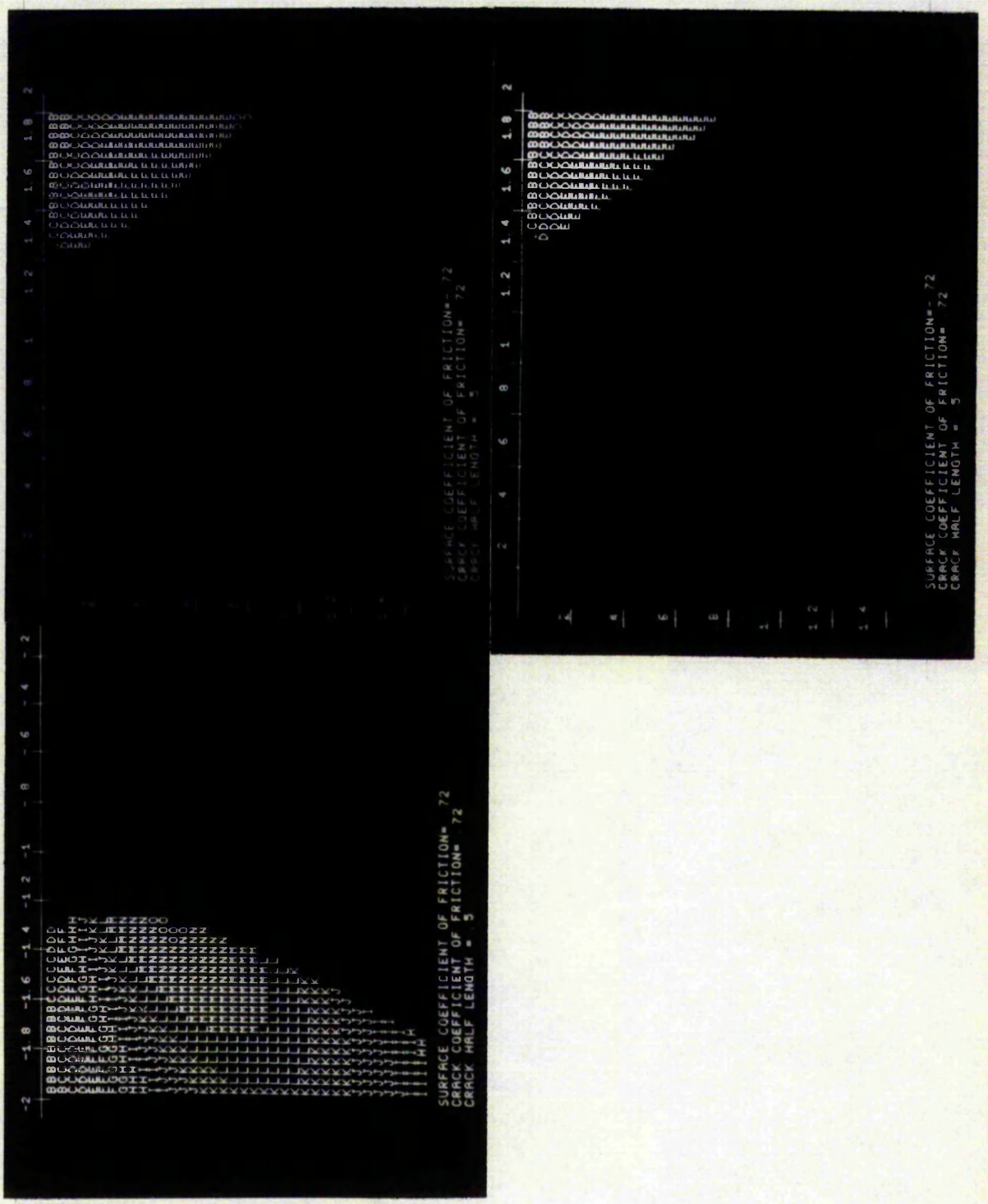
Fig.61b



Note that the load is always acting towards the left, and that the samekey is used for the pure rolling case, fig.67, to facilitate comparison.

S.I.F. MAP HERTZIAN LOAD WITH TRACTION

Fig.61c



S.I.F. MAP HERTZIAN LOAD WITH TRACTION

Fig.61d

of gases is an important detrimental factor is consistent with the results of Scott(128,129,130) who found a considerably improved life in bearing steels which had been degassed. It is expected, then, that the coefficient of friction will be higher than that found at the 'dirty' free surface but will not attain the adhesive values found under vacuum conditions.

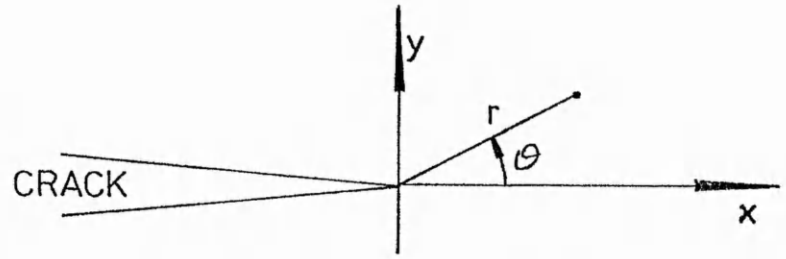
A second aspect of mode II loading with a clamping force is the degradation of the crack faces by a type of fretting action. Corresponding to the singular stress solutions (equation 29), there are equations describing the displacement of material in the neighbourhood of the crack tip. For mode II they are (108);

$$\left.\begin{matrix} u_x \\ u_y \end{matrix}\right\} = \left\{\frac{K_{II}}{2E}\right\}\left\{\frac{r}{2\pi}\right\}^{\frac{1}{2}} \left\{\begin{matrix} (1+\nu)\left[(9-8\nu)\sin(\theta/2)+\sin(3\theta/2)\right] \\ -(1+\nu)\left[(3-8\nu)\cos(\theta/2)+\cos(3\theta/2)\right] \end{matrix}\right\} \quad (47)$$

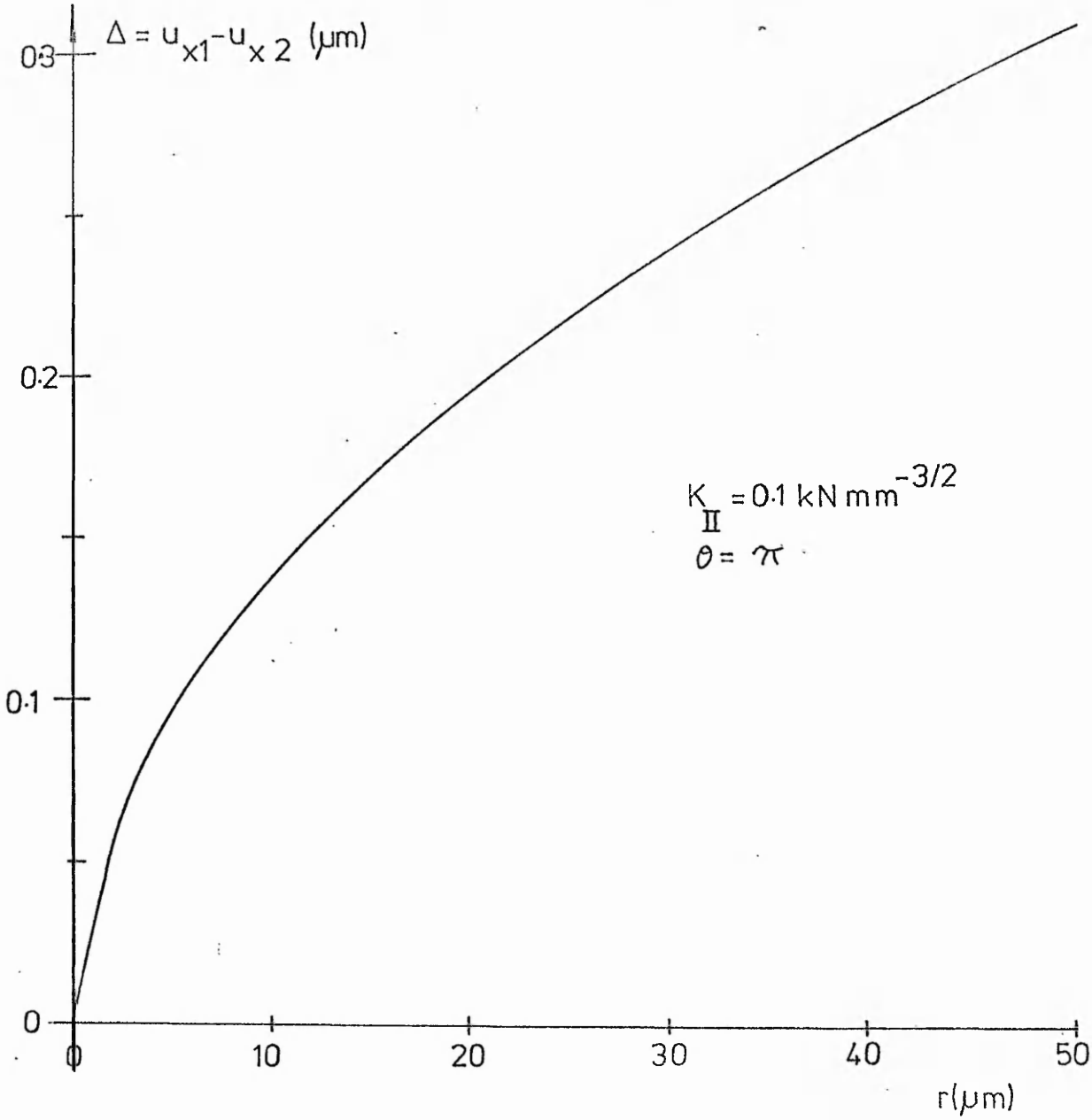
where the crack tip coordinates are shown in fig.62.
To find the displacements on the crack faces substitute in $\theta = \pm\pi$. Thus;

$$\begin{aligned} u_y &= 0 \\ u_{x1} &= \left\{\frac{K_{II}}{2E}\right\}\left\{\frac{r}{2\pi}\right\}^{\frac{1}{2}} \left\{\begin{matrix} (1+\nu)8(1-\nu) \\ -(1+\nu)8(1-\nu) \end{matrix}\right\} \\ u_{x2} &= \end{aligned} \quad (48)$$

So that the relative displacement between the crack faces is given by $u_{x1}-u_{x2} = \left\{\frac{K_{II}}{2E}\right\}\left(\frac{r}{2\pi}\right)^{\frac{1}{2}} \times 16(1-\nu^2)$ (49)
A graph of this function is shown in fig.63. It is therefore suggested that the result of this relative motion under compression is an acceleration of the degradation of the crack faces, and the debris and loss of surface integrity may help in preventing re-welding as mentioned in the previous paragraph. Whilst there is no direct evidence for this, it is interesting to speculate on the role such a phenomenon might play in the development of a transformed



Crack tip coordinate system. Fig.62.



Example of shear displacement near crack tip. Fig.63.

'white etching layer' which is often seen along the edges of cracks in sectioned bearings, fig.64 (these micrographs were kindly supplied by the RHP bearing company, Newark). As well as the compression and mechanical action, these crack faces undergo a steep temperature rise caused by frictional heating, in a limited gaseous atmosphere. A recent paper by Fujita and Yoshida(131) identified the white etching layer on cracks found within nitride-hardened gears as iron carbide.

Lastly, it should be borne in mind that the very surface layers of a wearing material will contain more absorbed gases which have diffused down grain boundaries and faults, and that the concentration will fall off rapidly beneath the surface. Their presence may enable some oxidation of subsurface cracks to occur.

Some attention has been paid recently to the formation of spherical wear debris. Rabinowicz(132) considered that their smoothness was caused by their becoming burnished in a three body wear process, but Loy and McCallum(133) associate the formation of spherical debris with white etching areas. They show micrographs of sectioned bearing material illustrating the nucleation of spherical debris between two cracks growing parallel to the surface , and anti-parallel to each other. When an already approximately spherical particle is detached it is rolled into an even smoother shape by the oscillatory rolling action of the crack faces. Direct evidence for this has been observed by Smith(134) who has conducted fatigue tests in compression for a slant-cracked specimen, and found wear debris of a similar morphology in one set of resulting cracks. This

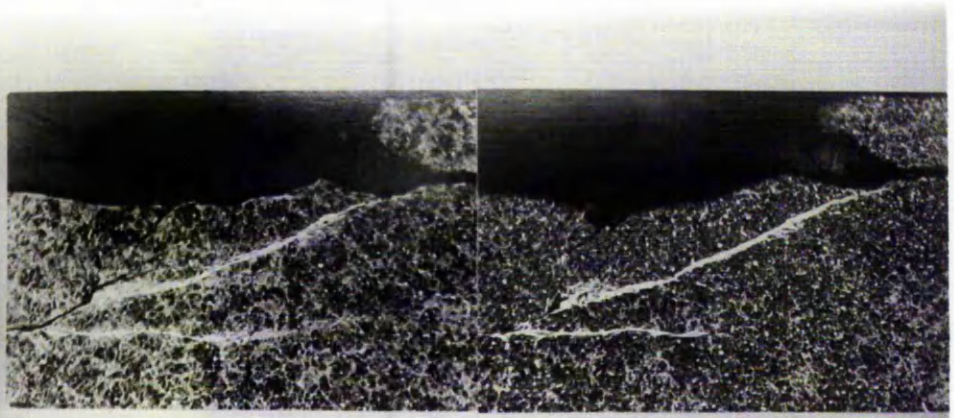


Fig.7. Untempered 500x

Fig.8. Tempered 2 hrs 200°C 500x

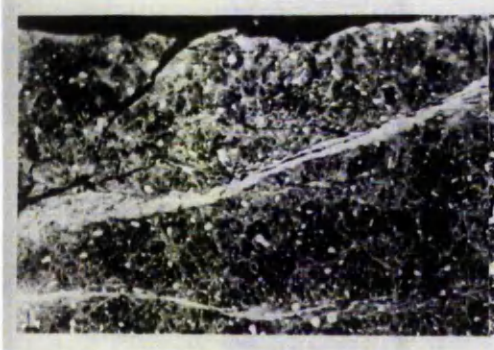


Fig.9. Untempered 1000x

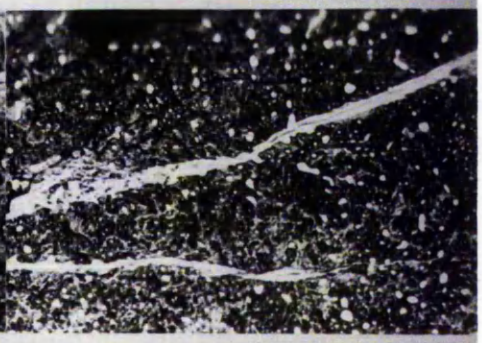


Fig.10. Tempered 2 hrs 200°C 1000x



Fig.11. Untempered 2000x



Fig.12. Tempered 2 hrs 200°C 2000x

Vertical section through failed bearing showing white etching layer. Fig. 64.

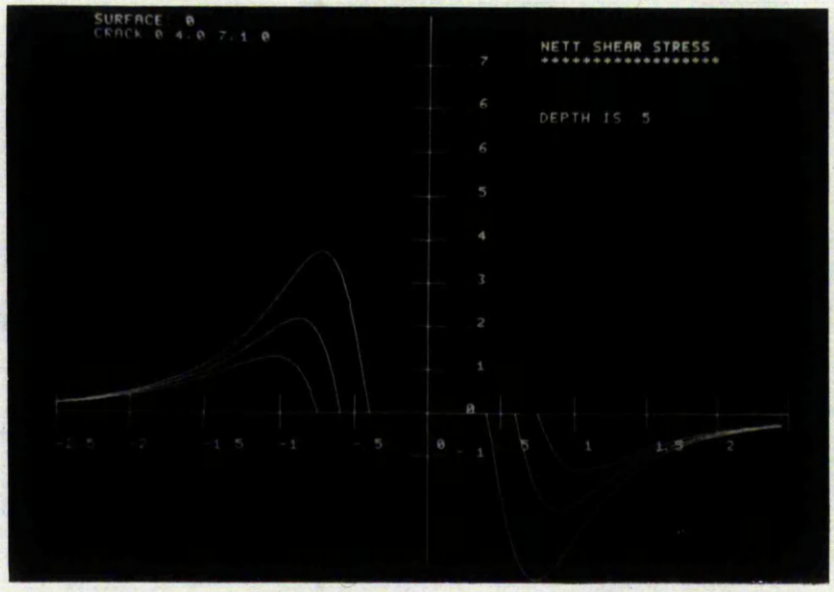
experiment also provides support for the view that the shear-under-compression mode of crack growth is important.

The results of this section were summarised in a paper (135).

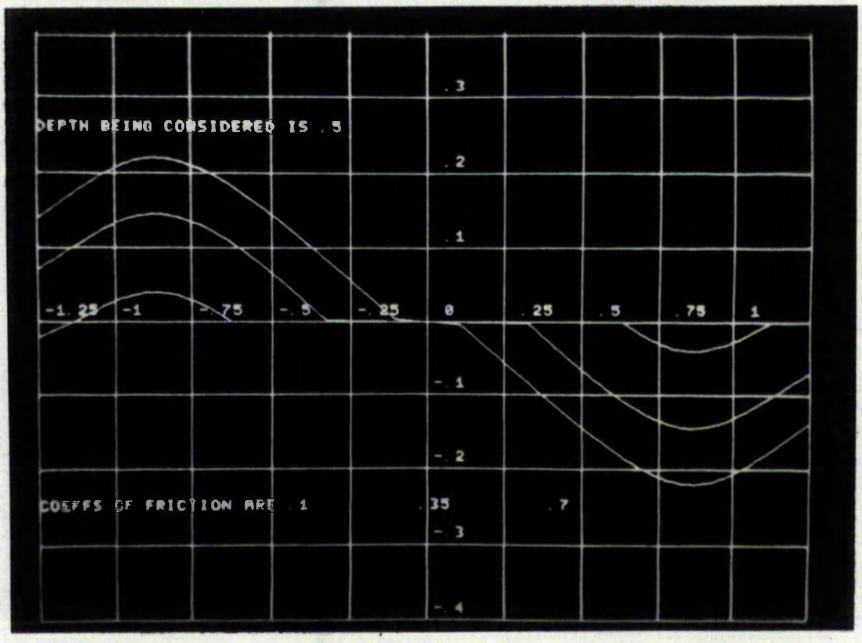
4.2 The Application of Fracture Mechanics to Pure Rolling

If attention is restricted to the problem of pure rolling it is easier to draw general conclusions about the fatigue strength conditions, because the number of parameters is reduced considerably. First consider the case of a uniformly distributed load, with no friction. Using the same method as described in 4.1, the nett shear was found, as shown in fig.65. The shear available is, of course, antisymmetrical, and a locking region exists at the centreline of contact. For a roller, the pressure distribution is Hertzian, and the nett shear under these conditions is shown in fig.66. In a private communication, Professor K.L.Johnson noted the similarity between the regions where cracks were likely to grow, and the zones of slip between a steel wheel and tyre, which he had calculated (136). Johnson modelled the zones in two ways; first, he used a continuum solution similar to that presented but based on Flamant's lineload solution, and secondly, an array of dislocations within the non-locking regions was inserted to accommodate slip. It is interesting to note the similarity between the second technique of Johnson, and the zones of high dislocation density experimentally observed by Swain(137) and Dufrane(138) in single salt crystals, under Hertzian load conditions.

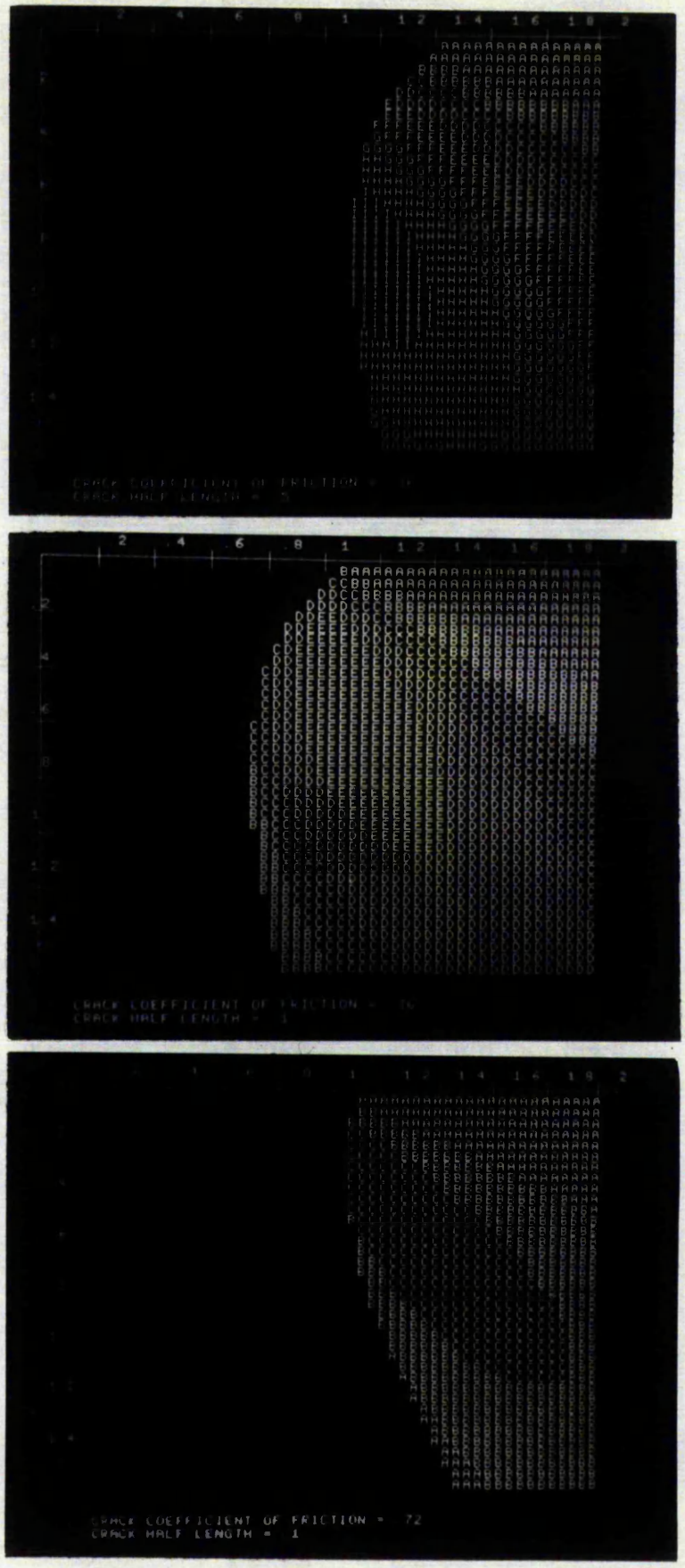
Returning to the fracture mechanics problem, the field of stress intensification factors was determined in exactly



Nett shear available for uniformly loaded half-space. Vertical axis normalised with respect to contact pressure, Horizontal axis normalized with respectto contact width,w, as is depth. Tallest peak corresponds to lowest coefficient of friction and vice versa. Fig.65.



Nett shear available for half-space supporting Hertzian load. All distances normalized with respect to contact half-width, b_o, and stress normalized with respect to peak contact pressure, p_o. Fig.66.



Map of mode II S.I.F. for a crack lying beneath a roller. Centreline of roller is to left of diagrams; for key see fig.61d. All lengths normalised with respect to contact half-width, b_o. Frictional quantity is between crack faces

Fig.67

the same way as previously described, but this time for only a quarter-space, since anti-symmetry was guaranteed. The results are shown in fig.67. The reason for such an abrupt truncation of S.I.F. as one moves towards the centre-line, which might not be expected from fig.66, is that the computer programme does not attempt to calculate an S.I.F. if part of the crack is within the compression zone. This was done to simplify the programme, which does not need to work out the effective crack length, but uses only the full crack length. The simplification is not as drastic as might at first appear, since reducing the effective crack size leads to a rapid reduction in S.I.F., and hence the results shown certainly locate the maxima. With a crack length of 0·5 of the semi contact width , the largest S.I.F. found for a coefficient of friction μ_c of 0·36 was;

$$\frac{K_{II}\sqrt{b_o}}{P} = 0{\cdot}043$$

and was located at $\frac{x}{b_o}$ =0·8, $\frac{y}{b_o}$ = 1·1

For a similar coefficient of friction but a normalised crack length of 0·1, the largest value found was;

$$\frac{K_{II}\sqrt{b_o}}{P} = 0{\cdot}024$$

located at $\frac{x}{b_o}$ =0·5, $\frac{y}{b_o}$ =1·1

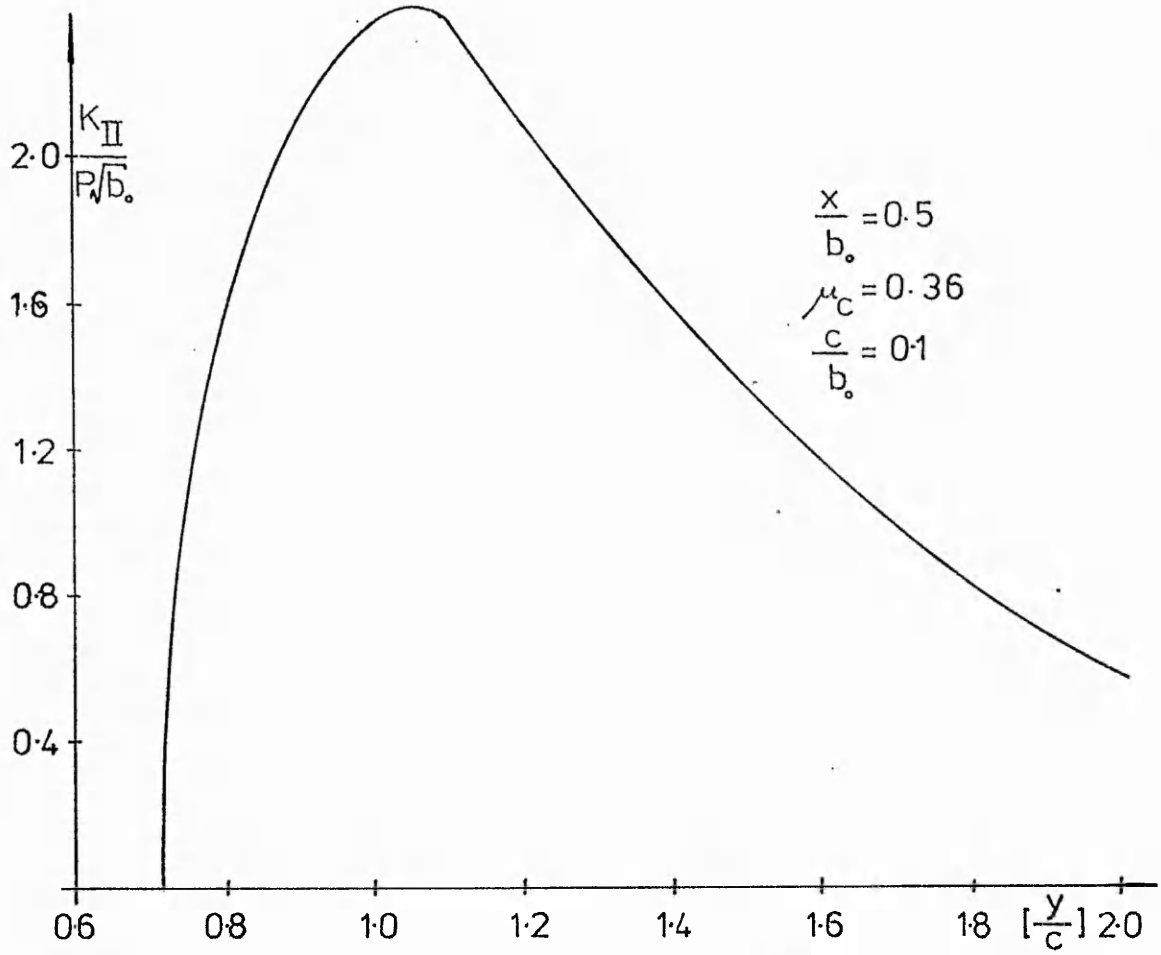
Thus the point of greatest S.I.F. varies according to crack length, which is to be expected with cracks of appreciable length, because it is the weighted average of nett shear which contributes to the S.I.F., rather than the point of greatest shear. It is worth comparing the depths found above with those determined from an examination of bulk shear (equations 9,10). Since the range of depths involved is roughly the same it appears that a fracture mechanics model is not at variance with the plethora of experimental

evidence accumulated over the years.

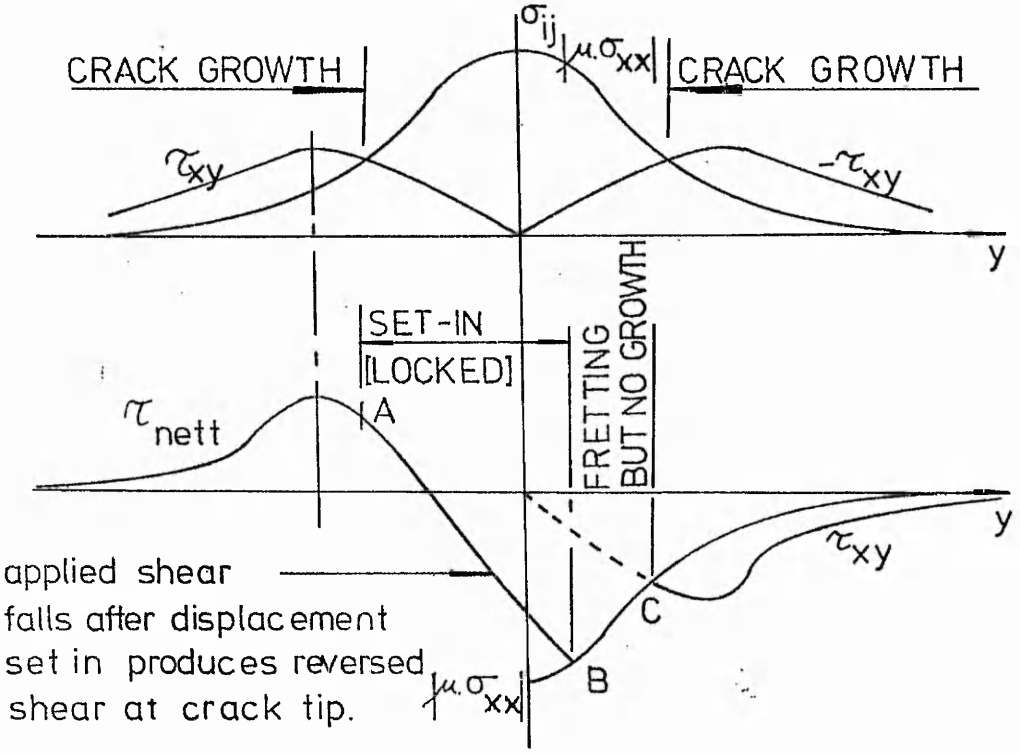
The rolling configuration differs from sliding in that a crack experiences (apparently) equal and opposite values of S.I.F. as a load passes over (fig.68). Each growth period causes the crack to deviate slightly from a horizontal trajectory, since a crack propelled by shear does not normally grow in its own plane. Because the S.I.F.s are of opposite sign it might be expected that a crack beneath a roller would weave up and down, and this is observed in practice (unpublished work by RHP bearings, Newark). However, this apparent confirmation of the above theoretical work poses two more questions;

A. A crack growing under the influence of a shear load is not normally stable (139) and as soon as it starts to grow out of its own plane a mode I (or even III) loading is added which is stable, and which tends to dominate the shear loading. Why, then, does a subsurface crack not turn upwards (or downwards) immediately, rather than growing a considerable distance horizontally first?

B. It is not quite true to say that a rolling wear crack experiences equal and opposite periods of shear, as will become apparent from a critical examination of fig.69: as the load approaches the crack, sliding between the crack faces occurs and the maximum nett shear is attained,(point A) The applied stress relaxes shortly afterwards and as it does so the "locked-in" relative displacement between the crack faces manifests itself as a propelling shear in the opposite direction, which reaches a maximum just after the load has passed over the crack. As the load moves further on an augmenting shear is applied while the clamping



Variation of S.I.F. with lateral distance for crack under roller.
Fig. 68.



Growth regimes experienced by crack beneath a roller. Fig. 69

force slowly decays.When point B is reached limiting friction is attained and the set-in shear is gradually relaxed until point C is reached when all residual shear has subsided. Subsequently the crack experiences a propelling shear due to the applied load alone. This rather complicated cycle is, in reality, even more difficult to determine when a crack of finite extent is considered and different parts of the crack are undergoing different types of loading on the figure.

From these remarks it is clear that wear cracks should be rather unstable, and one might therefore expect them to be rather shorter than is often the case. One possible reason for this is the development of residual tensile stresses normal to the free surface. The conditions under which such stresses might form are discussed in detail in the chapter on rolling shakedown. Under sliding conditions the opening mode growth in the wake of the rider would, in any case, provide some stability.

Before leaving rolling contact it is probably worthwhile making use of the results of fracture mechanics to formulate design criteria. First, an upper bound of what constitutes a fully-developed crack is needed,ie. the shortest crack must be considered where the assumptions of fracture mechanics are valid. Although shorter cracks may well be able to grow, the critical length must be chosen so that unmodified fracture mechanics is applicable. For simplicity choose $c=0{\cdot}1b_o$. Now, the S.I.F. generated must be less than the threshold, ie.

$$\Delta K_{II} < \Delta K_{IIC}$$

It will later be shown that $\Delta K_{IIC} \simeq 0{\cdot}867\Delta K_{IC}$, and it is

known from Hertzian mechanics that for a roller moving over a flat plane; $b_o = 1{\cdot}52\sqrt{\frac{QR}{E}}$

Also; $K_{II} = n\frac{Q}{\sqrt{b_o}}$ where n is dependent on crack friction, and may be found from fig.67 or similar calculations. Assembling these equations gives;

$$\frac{Q}{R} < \frac{(0{\cdot}867\Delta K_{IC}\ 1{\cdot}52)^4}{n^4 E} \qquad (50)$$

A further condition which is desirable is that there should not be continued plastic flow at any depth. For the time being, the necessary condition will be stated, ie. $p_o < 4\tau_o$

From Hertz' relations;

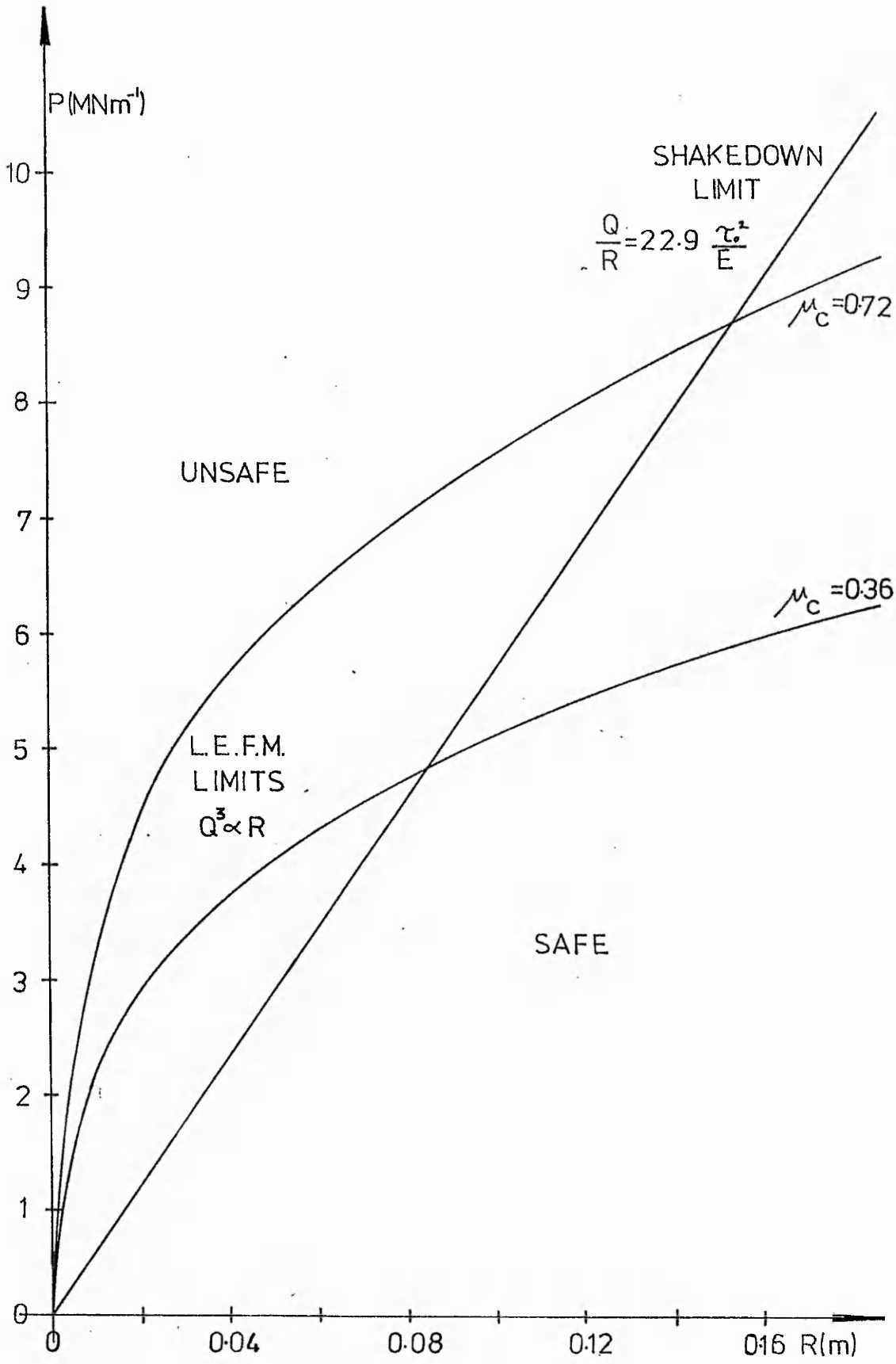
$$p_o = 0{\cdot}418\sqrt{\frac{QE}{R}}$$

$$\text{ie. } \frac{Q}{R} < \left(\frac{4\tau_o}{0{\cdot}418}\right)^2 \times \frac{1}{E} \qquad (51)$$

These criteria are plotted for a specific case in fig.70. As can be seen, continued plasticity is the limiting factor for rollers of small radii, whilst for larger rollers the possibility of fatigue crack growth is the severer limitation.

4.3 The Initiation of Cracks

Before fracture mechanics can be used, a well-developed crack must be present, ie. it must be larger than the grains in which it exists, and it must not be so short that the singular solution fields overlap or are distorted significantly by crystallographic effects. The initiation of cracks under fatigue conditions is not a subject which lends itself to a continuum approach, occurring as it does on an atomic scale. However, some insight may be gained by considering the stress raising effect of inclusions or second phase particles, and by examining the energy expended by plasticity and hysteresis.



Failure criterion diagram for titanium roller. Fig.70

It is natural to assume that cracks initiate when the ductility of a material is exhausted. The point of fracture under monotonic loading is strongly dependent on the confining pressure ($\bar{\sigma}$) for most polycrystalline metals, because premature separation of the metal and any flaw is prohibited. However, some early ideas of 'toughness' were based on the amount of energy a material could absorb before failure. Making the very crude assumption that the energy under the stress-strain curve is the energy absorbed which would cause cracking, the number of passes needed to initiate a crack in a nickel-plated roller was estimated and is shown in fig.71. Several energy absorbed curves were obtained, using a standard tensile test, at different stress levels, and the energy absorbed evaluated, using an Amsler planimeter. The energy absorbed was found to be related to the stress approximately by;

$$E(mJmm^{-3}) = 9{\cdot}38 \times 10^{-4} \times \sigma^{2} \ (Nmm^{-2})$$

When considering the roller the value of stress substituted was twice the largest shearing stress in the plane of symmetry. The graph does nothing more than to show where the greatest energy of distortion is expended.

Evaluating the stress concentration factor for a rigid inclusion within an elastic matrix will help show where initiation is most probable, though it cannot determine the number of passes needed to cause initiation. It is thought that an initiation criterion may be established using one of these parameters; the interfacial tensile stress, the local strain gradient or the local elastic energy. A review of these suggestions was made by Mogford(140) and by Rosenfield(141). The local energy criterion, ie. that

the strain energy released by decohesion should be at least as great as the surface energy needed turns out to be a necessary but not a sufficient condition for particles larger than 25 nm. Finite element studies of the stress field within an ideal elastic-plastic & extended elastic matrix were conducted by Argon(142,143), for the case of cylindrical inclusions. He found that the stress concentration, as might be expected,was greater for the extended elastic behaviour. An interfacial stress criterion was studied by Goods and Brown(144), who presented experimental evidence in support of such a suggestion. Jahanmir and Suh (85) pursued this line of thought in relation to delamination wear. They used the stress concentration factor for a rigid cylindrical inclusion and used the far-field created by a sliding roller. They also took forward flow into account, but their analysis seems defective in several respects;

A. They assumed that the hydrostatic stress component was unaffected by the presence of the inclusion.

B. Even though they used an elastic stress concentration factor the yield criterion was clearly exceeded.

C. A linear relation between the forward shear of the surface and the stresses generated was assumed-no allowance was made for the 'back stress' caused by the inclusion itself. The accumulated forward shear was used to create a cycle dependent separation criterion;this is unsatisfactory.

D. The interfacial shear stress was neglected.

The author chose a much simpler configuration, ie. a rolling cylinder, but examined the stress raising effect of an elliptical inclusion. This is convenient because by altering its eccentricity anything between a cylinder and

a flat plate may be modelled. The elastic stress concentration factors for stiff cylinders and spheres has been found by Goodier(145), whilst some guidelines on elliptical inclusions are given by Muskhelishvili(117). It is these which will be followed.

Consider fig.72. It will be assumed that a small cell AAAA may be found such that the stresses along its boundary due to the stress field generated by the contact loading are substantially constant. At the same time, the inclusion within the cell must be much smaller still, so that the local disturbances to the stress field caused by the inclusion do not extend to the bounds of the cell. Suppose that the stresses along the edges of the cell are given by σ_{xx}, σ_{yy}, τ_{xy}. These could be replaced by a "hydrostatic" stress (2-D) and a pure shear, ie.

$$\begin{aligned} \overline{\sigma} &= \tfrac{1}{2}(\sigma_{xx}+\sigma_{yy}) \\ \tau &= \sqrt{\left\{\tau_{xy}^2+\tfrac{1}{4}(\sigma_{xx}-\sigma_{yy})^2\right\}} \end{aligned} \qquad (52)$$

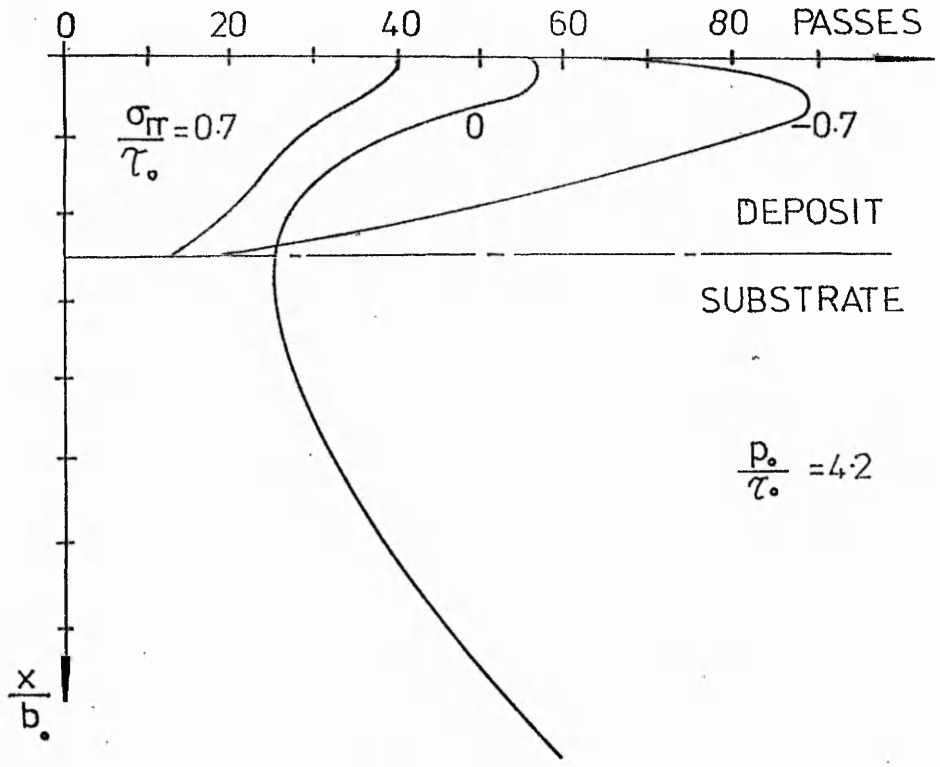
Since only elastic stress concentrations are being considered superposition is acceptable, and all that is required is the concentration caused by each of stresses (52). Fig.73 shows a detail of the ellipse as contained within the matrix (L-space) and its mapping (S-space). For the pure shear field $N_1=-N_2=\tau$, whilst for the 'hydrstatic' field $N_1=+N_2=\overline{\sigma}$. The mapping used is;

$$z = w(\zeta) = R(\zeta + \frac{m}{\zeta}) \qquad (53)$$

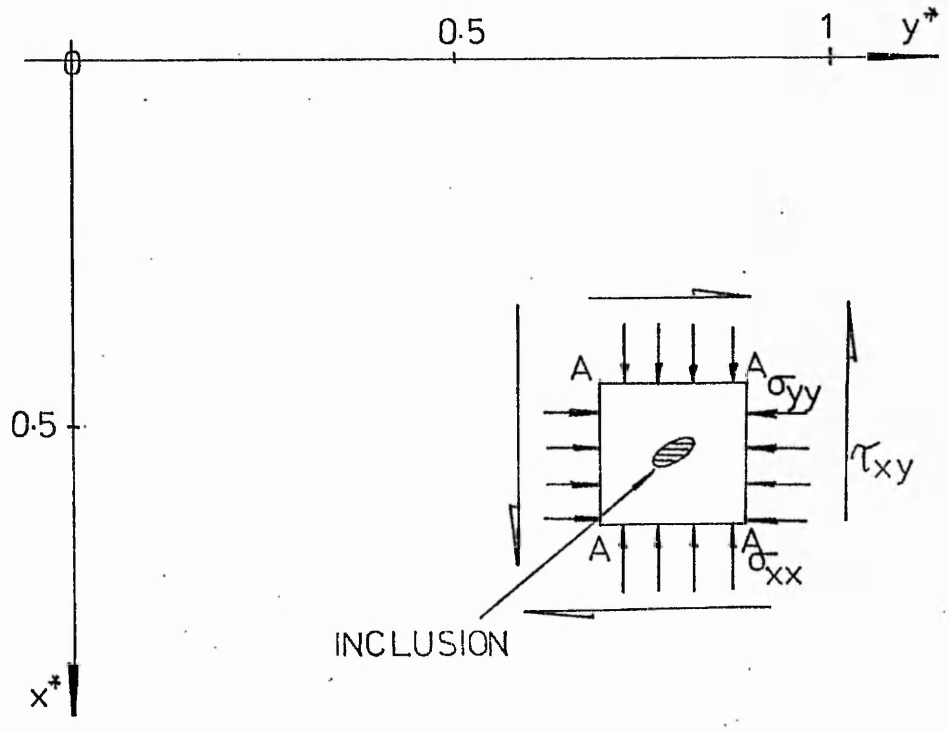
where $z= x+iy$ and $\zeta = \rho e^{i\theta}$

The eccentricity of the ellipse is defined in an unusual way, ie. $\begin{matrix} a = R(1+m) \\ b = R(1-m) \end{matrix}$ $0 \leq m < 1$ which maps to unit circle

By equation (53) coordinates map as;



Number of passes needed to initiate cracks in nickel, based on a maximum energy criterion. Fig.71



Scale of inclusion relative to contact patch. Fig.72

$$x = R.Re\ (\rho e^{i\theta} + \frac{1}{m\rho} e^{-i\theta}) = R(\rho + \frac{m}{\rho})\cos\theta$$
$$y = R.Im\ (\rho e^{i\theta} + m\frac{1}{\rho} e^{-i\theta}) = R(\rho - \frac{m}{\rho})\sin\theta \qquad (54)$$

Muskhelishvili shows that the correct stress functions are derived by way of;

$$\Gamma = \tfrac{1}{4}(N_1 + N_2)$$
$$\Gamma' = \tfrac{1}{2}(N_1 - N_2)e^{-2i\alpha} \qquad (55)$$

They are: $\phi(\zeta) = (2Gm\epsilon i + \overline{\Gamma'})\frac{R}{\chi\zeta}$

$$\psi(\zeta) = \Gamma' R\zeta + \frac{2G\epsilon Ri}{\zeta} + (2Gm\epsilon i + \overline{\Gamma'})(\frac{1+m\zeta^2}{\zeta^2 - m})(\frac{R}{\chi\zeta}) \qquad (56)$$

where ϵ is the rotation of the inclusion, and $\chi = 3-4\nu$

The stresses are given by;

$$\sigma_{\rho\rho} + \sigma_{\theta\theta} = 4\ Re\{\Phi(\zeta)\}$$
$$\sigma_{\theta\theta} - \sigma_{\rho\rho} + 2i\tau_{\rho\theta} = \frac{2\zeta^2}{\rho^2 \omega'(\zeta)}\{\overline{\omega(\zeta)}\,\Phi'(\zeta) + \omega'(\zeta)\Psi(\zeta)\} \qquad (57)$$

where:

$$\Phi(\zeta) = \frac{\phi'(\zeta)}{\omega'(\zeta)} \qquad \Psi(\zeta) = \frac{\psi'(\zeta)}{\omega'(\zeta)}$$

where $w'(\zeta)$ means $\frac{dz}{d\zeta} = R(1 - \frac{m}{\zeta^2})$

So far these results are general. Each loading must now be considered individually.

Consider the shear loading case first. From equations (55) are obtained;

$$\Gamma = 0 \qquad \Gamma' = -pe^{-2i\alpha}$$

Therefore $\Phi(\zeta) = -\frac{(2Gm\epsilon i - pe^{2i\alpha})}{\chi(\zeta^2 - m)}$

Since $\Psi(\zeta) = \frac{\psi'(\zeta)}{\omega'(\zeta)}$

the second of equations (57) may be re-written as;

$$\sigma_{\theta\theta} - \sigma_{\rho\rho} + 2i\tau_{\rho\theta} = \frac{2\zeta^2}{\rho^2 \overline{w'(\zeta)}}\left\{\overline{w(\zeta)}\,\Phi'(\zeta) + \psi'(\zeta)\right\} \qquad (58)$$

$$\psi'(\zeta) = \Gamma' R - \frac{2G\epsilon Ri}{\zeta^2} + \phi'(\zeta)(\frac{1+m\zeta^2}{\zeta^2 - m}) - \phi(\zeta)\,2\zeta\left\{\frac{1+m^2}{(\zeta^2 - m)^2}\right\}$$

It is now possible to write down expressions for the stresses:

$$\sigma_{\rho\rho} + \sigma_{\theta\theta} = 4\,\mathrm{Re}\left\{\Phi(\zeta)\right\} = 4\,\mathrm{Re}\left\{\frac{(pe^{2i\alpha} - 2G_m\epsilon i)(\rho^2 e^{-2i\theta} - m)}{(\rho^2 e^{2i\theta} - m)(\rho^2 e^{-2i\theta} - m)\chi}\right\} \quad (59)$$

$$= \frac{4}{\chi}\left\{\frac{-mp\,\mathrm{Re}(e^{2i\alpha}) - 2G_m\epsilon\rho^2 i\,\mathrm{Im}(e^{-2i\theta}) + p\rho^2\,\mathrm{Re}(e^{i2(\alpha-\theta)})}{\rho^4 - 2m\rho^2\cos 2\theta + m^2}\right\}$$

$$= \frac{4}{\chi}\left\{\frac{-mp\cos 2\alpha - 2G_m\epsilon\rho^2\sin 2\theta + p\rho^2\cos 2(\alpha-\theta)}{\rho^4 - 2m\rho^2\cos 2\theta + m^2}\right\}$$

$$\sigma_{\theta\theta} - \sigma_{\rho\rho} + 2i\tau_{\rho\theta} = \frac{2\zeta^2}{\rho^2 R\left(1 - \frac{m}{\rho^4}\zeta^2\right)}\left\{R\left(\frac{\rho^2}{\zeta} + \frac{m}{\rho^2}\zeta\right)\cdot\frac{2\zeta^2\phi(\zeta)}{R(\zeta^2-m)^2} + \Gamma' R\right.$$

$$\left. - \frac{2G\epsilon R i}{\zeta^2} - \frac{\phi(\zeta)}{\zeta}\left\{\frac{1+m\zeta^2}{\zeta^2-m}\right\} - 2\zeta\phi(\zeta)\left[\frac{m^2+1}{(\zeta^2-m)^2}\right]\right\}$$

$$= \frac{2\rho^2}{(\rho^4 + m^2 - 2m\rho^2\cos 2\theta)}\left\{\left(\frac{\phi}{R}\right)\left(\frac{2\zeta}{\zeta^2-m}\right)\left[\rho^2 + \frac{m}{\rho^2}\zeta^2 - (m^2+1)\right] - \left(\frac{\phi}{\zeta R}\right)(1+m\zeta^2)\right.$$

$$\left. + (\zeta^2 - m)\left(\Gamma' - \frac{2G\epsilon i}{\zeta^2}\right)\right\}$$

Restricting attention to the interface, ie. $\rho = 1$

$$= \frac{2}{(1+m^2-2m\cos 2\theta)}\left\{\frac{1}{\chi}\left[2G_m^2\epsilon i - mpe^{2i\alpha} - 2G_m\epsilon i e^{-2i\theta} + pe^{2i(\alpha-\theta)}\right]\right.$$

$$\left. - \left[pe^{2i(\theta-\alpha)} + 2G\epsilon i - mpe^{-2i\alpha} - 2G_m\epsilon i e^{-2i\theta}\right]\right\} \quad (60)$$

Taking the real part;

$$\sigma_{\theta\theta} - \sigma_{\rho\rho} = \frac{2}{1+m^2-2m\cos 2\theta}\left\{mp\cos 2\alpha + 2G_m\epsilon\sin 2\theta - p\cos 2(\alpha-\theta)\right\}\left(1 - \frac{1}{\chi}\right) \quad (61)$$

Solving equations 59 and 60 gives;

$$\frac{\sigma_{\rho\rho}}{\left(1+\frac{1}{\chi}\right)} = \frac{\sigma_{\theta\theta}}{\left(-1+\frac{3}{\chi}\right)} = -\left\{\frac{mp\cos 2\alpha + 2G_m\epsilon\sin 2\theta - p\cos 2(\alpha-\theta)}{1+m^2-2m\cos 2\theta}\right\} \quad (62)$$

Taking the imaginary part of equation 60;

$$2i\tau_{\rho\theta} = \frac{2i}{(1+m^2-2m\cos 2\theta)}\left\{\frac{1}{\chi}\left[2Gm^2\epsilon - mp\sin 2\alpha - 2Gm\epsilon\cos 2\theta + p\sin 2(\alpha-\theta)\right]\right.$$
$$\left. - \left(p\sin 2(\theta-\alpha) + 2G\epsilon + mp\sin 2\alpha - 2Gm\epsilon\cos 2\theta\right)\right\}$$

$$\tau_{\rho\theta} = \left\{\frac{(p\sin 2(\alpha-\theta) - mp\sin 2\alpha)(\frac{1}{\chi}+1) - 2Gm\epsilon\cos 2\theta(\frac{1}{\chi}-1) + 2G\epsilon(\frac{m}{\chi}-1)}{1+m^2-2m\cos 2\theta}\right\} \quad (63)$$

Specialising to the case of a cylindrical inclusion, ie. $m=\alpha=\epsilon=0$ gives the following relations, in agreement with Goodier(145)

$$\sigma_{\rho\rho} = p(1+\tfrac{1}{\chi})\cos 2\theta$$
$$\sigma_{\theta\theta} = -p(1-\tfrac{3}{\chi})\cos 2\theta$$
$$\tau_{\rho\theta} = -p(1+\tfrac{1}{\chi})\sin 2\theta$$

Muskhelishvili found the solution for ϵ. It is;

$$\epsilon = \frac{p\sin 2\alpha}{4G}$$

The variation of stress concentration factor as the inclusion is turned within a shear field is shown in fig.73. The maximum tension occurs when $\alpha=0$ and is located at $\theta=0$. Substituting into equation 62. the much simplified value results;

$$\frac{\sigma_{\rho\rho}}{p} = (1+\frac{1}{\chi})\times\frac{1}{(1-m)} \quad (64)$$

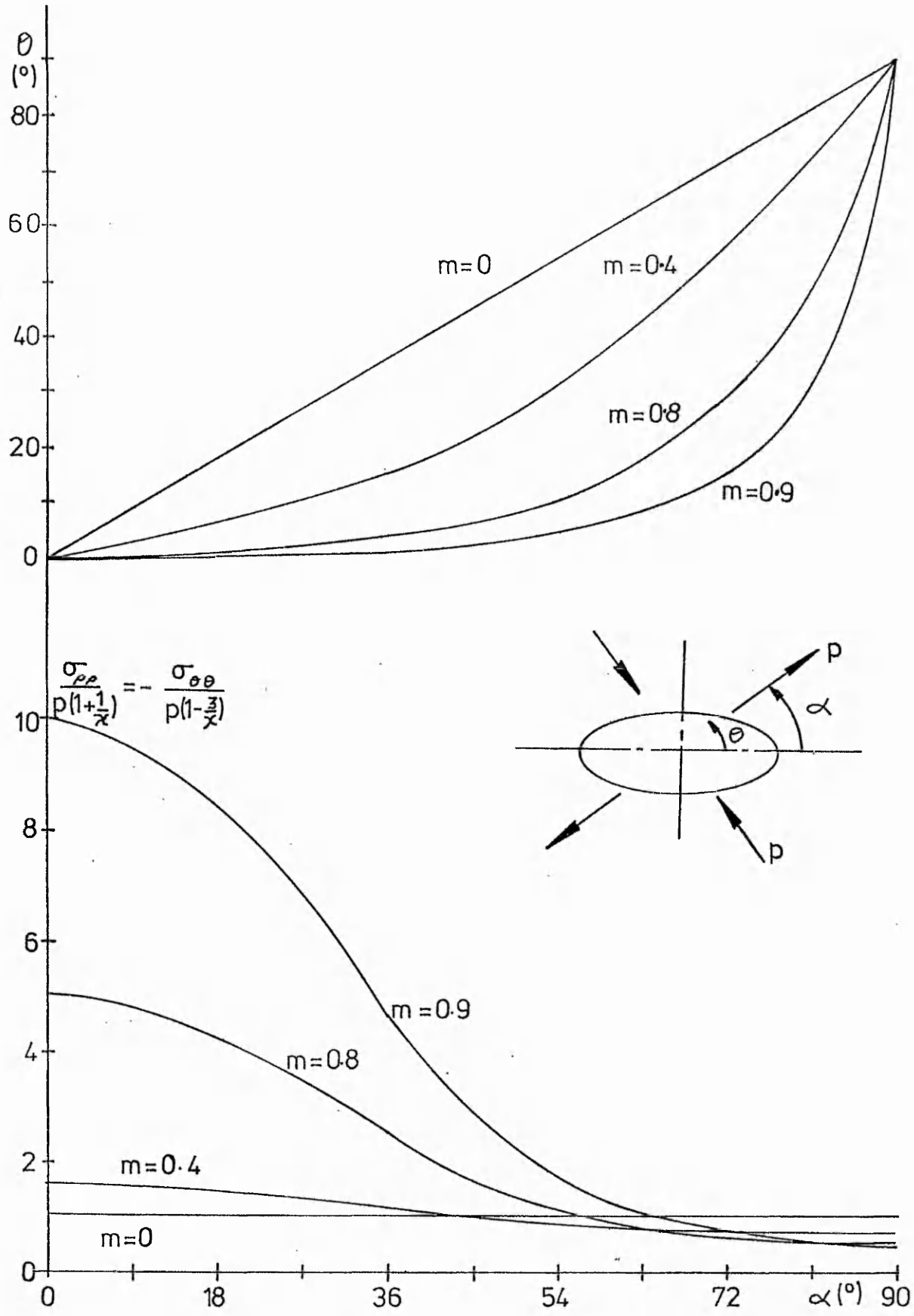
Let us return now to the 'hydrostatic' field. From equations 55 are obtained;

$$\Gamma = \tfrac{1}{2}p \qquad \Gamma' = 0$$

Therefore $\Phi(\zeta) = \dfrac{p(\zeta^2 - \frac{m}{\chi})}{(\zeta^2-m)}$

The resulting stresses may be found by making use of equations 57 and 58:

$$\sigma_{\rho\rho} + \sigma_{\theta\theta} = 4\,Re\{\Phi(\zeta)\} = 4\,Re\left\{\frac{p(\rho^2e^{2i\theta} - \frac{m}{\chi})(\rho^2e^{-2i\theta} - m)}{2(\rho^2e^{2i\theta}-m)(\rho^2e^{-2i\theta}-m)}\right\}$$
$$= 2p\frac{\left[\rho^4 + \frac{m^2}{\chi} - m\rho^2\cos 2\theta(\frac{1}{\chi}+1)\right]}{\rho^4 - 2m\rho^2\cos 2\theta + m^2} \quad (65)$$



Value and position of largest stress concentration . Fig.73

$$\Psi(\zeta) = \frac{pR}{2}\left\{-\frac{\chi}{\zeta^2} + \frac{(m+\zeta^2)(1+m^2)}{(\zeta^2-m)^2} - 2\left(\frac{m}{\chi}\right)\frac{(1+m^2)}{(\zeta^2-m)^2} - \frac{m}{\chi\zeta^2}\left[\frac{1+m\zeta^2}{\zeta^2-m}\right]\right\}\frac{d\zeta}{dz}$$

$$= \frac{p}{2}\left\{-\chi + \zeta^2\frac{(1+m^2)}{(\zeta^2-m)^2}\left[m\left(1-\frac{2}{\chi}\right)+\zeta^2\right] - \left(\frac{m}{\chi}\right)\left[\frac{1+m\zeta^2}{\zeta^2-m}\right]\right\}\frac{1}{(\zeta^2-m)}$$

$$\sigma_{\theta\theta} - \sigma_{\rho\rho} + 2i\tau_{\rho\theta} = \frac{2\zeta^2}{\rho^2 R\left(1-\frac{m}{\rho^2}\zeta^2\right)}\left\{R\left(\frac{\rho^2}{\zeta} + \frac{m}{\rho^2}\zeta\right)\rho m\zeta\frac{\left(\frac{1}{\chi}-1\right)}{(\zeta^2-m)^2} + \frac{pR}{2}\left[-\frac{\chi}{\zeta^2} + \right.\right.$$

$$\left.\left. + \frac{(m+\zeta^2)(1+m^2)}{(\zeta^2-m)^2} - 2\left(\frac{m}{\chi}\right)\frac{(1+m^2)}{(\zeta^2-m)^2} - \frac{m}{\chi\zeta^2}\left(\frac{1+m\zeta^2}{\zeta^2-m}\right)\right]\right\}$$

Restricting attention to the interface, ie. $\rho = 1$;

$$= \frac{2\rho}{1+m^2-2m\cos 2\theta}\left\{\frac{1}{\left(e^{2i\theta}-m\right)}\left[\left(\frac{m}{\chi}-m\right)\left(1+me^{2i\theta}\right) + \frac{1}{2}(1+m^2)\left(e^{2i\theta}+m\right) - \left(\frac{m}{\chi}\right)(1+m^2)\right]\right.$$

$$\left. - \frac{1}{2}\chi\left(1-me^{-2i\theta}\right) - \frac{1}{2}\left(\frac{m}{\chi}\right)\left(e^{-2i\theta}+m\right)\right\}$$

$$= \frac{\rho}{\left(1+m^2-2m\cos 2\theta\right)}\left\{1 - m^2 - \chi + \frac{m^2}{\chi} + e^{-2i\theta}\left(m\chi - \frac{m}{\chi}\right)\right\} \qquad (66)$$

Taking the real part;

$$\sigma_{\theta\theta} - \sigma_{\rho\rho} = \frac{\rho}{1+m^2-2m\cos 2\theta}\left\{1 - m^2 - \chi + \frac{m^2}{\chi} + m\left(\chi - \frac{1}{\chi}\right)\cos 2\theta\right\} \qquad (67)$$

Taking the imaginary part;

$$\tau_{\rho\theta} = \frac{-\rho m\left(\chi - \frac{1}{\chi}\right)\sin 2\theta}{2\left(1+m^2-2m\cos 2\theta\right)}$$

Solving equations 65 and 67;

$$\sigma_{\rho\rho} = \frac{\rho}{2\left(1+m^2-2m\cos 2\theta\right)}\left\{1 + \chi + m^2\left(1+\frac{1}{\chi}\right) - m\left(2+\chi+\frac{1}{\chi}\right)\cos 2\theta\right\} \qquad (68)$$

$$\sigma_{\theta\theta} = \frac{\rho}{2\left(1+m^2-2m\cos 2\theta\right)}\left\{3 - \chi + m^2\left(\frac{3}{\chi}-1\right) + m\left(\chi - \frac{3}{\chi} - 2\right)\cos 2\theta\right\} \qquad (69)$$

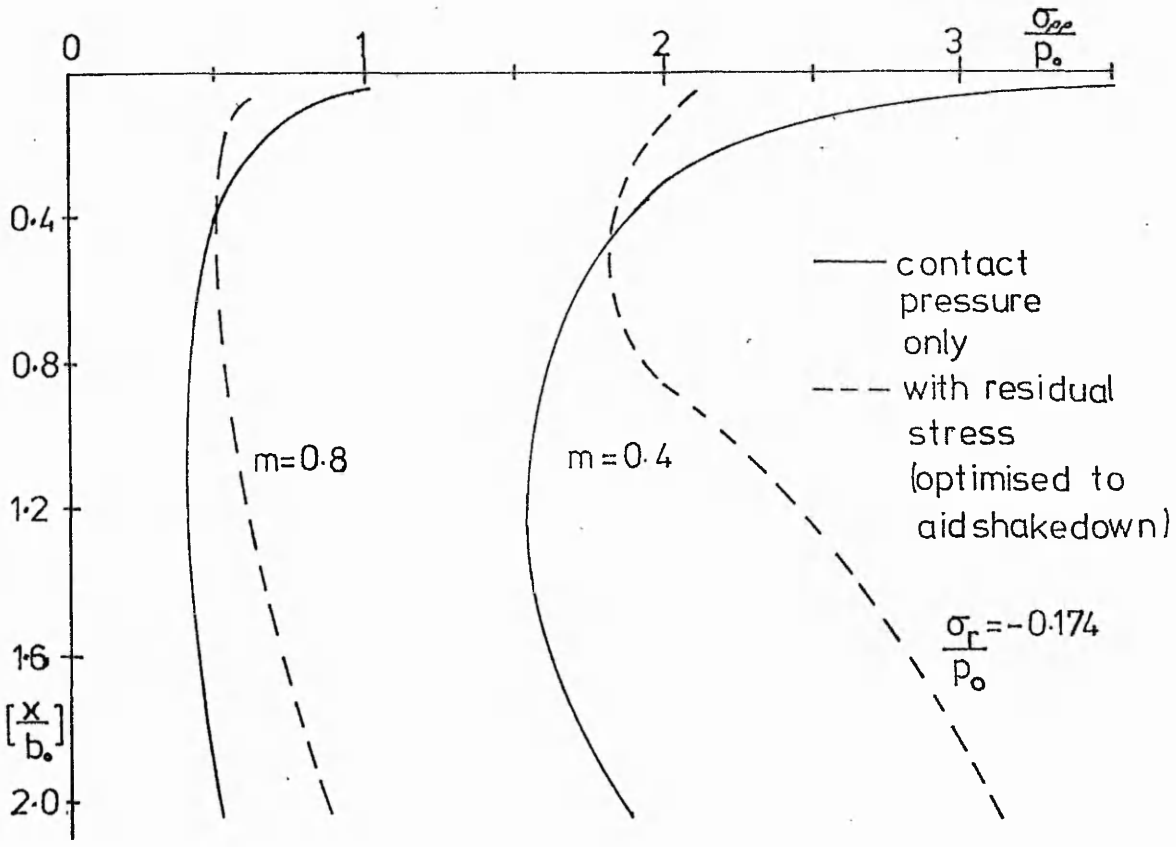
The concentration of hydrostatic stress is independent of the orientation of the inclusion. Note, too, that both components of the stress concentration are independent of

the size of the inclusion, providing continuum and yield conditions are satisfied. Combining equations 62 and 68 and maximising the result with respect to θ still predicts that the greatest tensile stress will be at the tip, ie. $\theta = 0$. The required result is therefore;

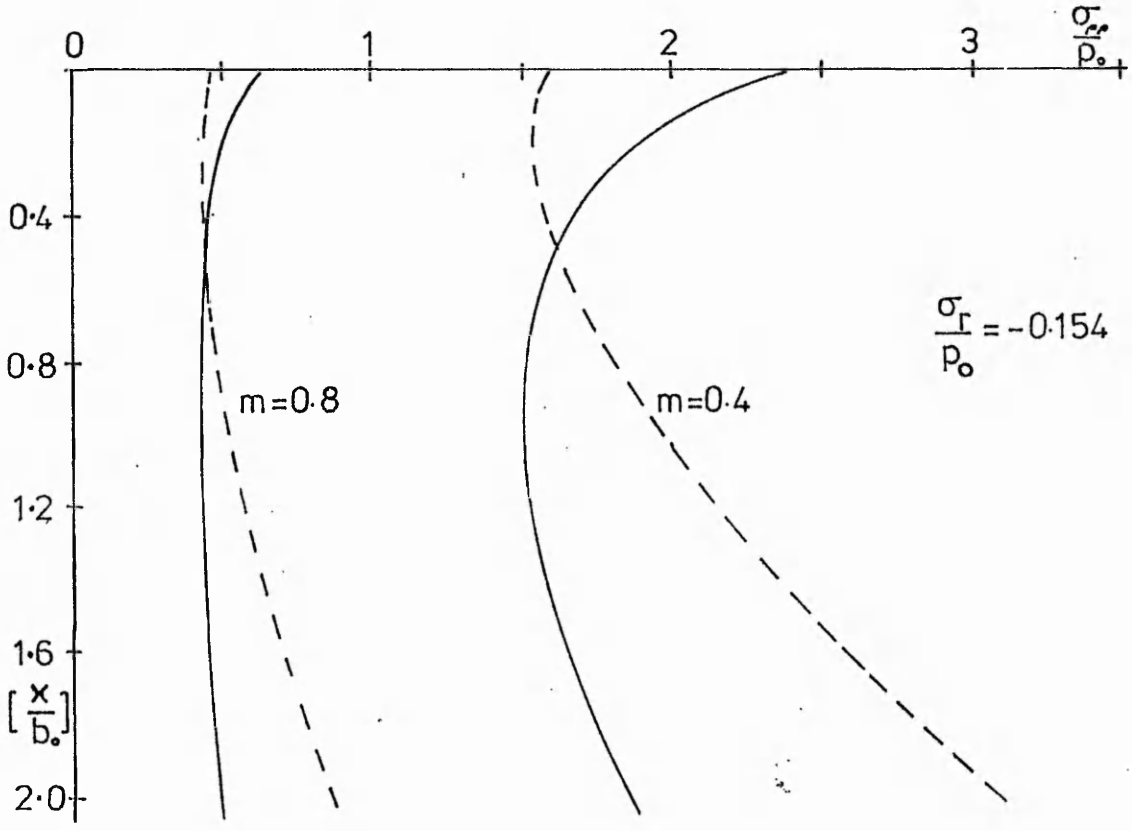
$$\sigma_{\rho\rho} = \left(\frac{1}{1-m}\right)\left(p_s \chi_1 + \tfrac{1}{2} p_h (\chi_0 - \chi_1 m)\right) \qquad (\alpha = 0) \qquad (70)$$

where; p_s is the shear component of load
p_h is the hydrostatic component of load
$\chi_0 = 1 + \chi$ and $\chi_1 = 1 + \frac{1}{\chi}$

The elliptical inclusion was then considered when lying within the pseudo-stress field generated by a roller. It was assumed that the inclusion always lay at the worst possible orientation, ie. parallel to the most positive principal stress direction. A computer programme was written to determine the largest ratio of the interfacial tensile stress to the peak contact pressure which could be tolerated at any particular depth, fig.74. At low eccentricities (nearly cylindrical inclusions) the beneficial effect of a residual stress is clear, but this vanishes as the inclusion becomes plate-like. The value of stress superimposed is that found later to be optimum for suppressing plasticity, and is probably not ideal for minimising the interfacial tensile stress. For the case of a small applied surface traction the results are shown in fig.75. The position of worst stress concentration is moved by applying the optimum residual stress and the severest trajectories are shown in fig.76. At the surface the location is always on the trailing edge of contact, where the state of greatest hydrostatic tension exists. Beneath the surface the trajectories follow a compromise between the point of greatest shear and the line of



Tolerable ratio $\frac{\sigma_{\theta\theta}}{p_o}$ at various depths, $\mu=0$. Fig.74



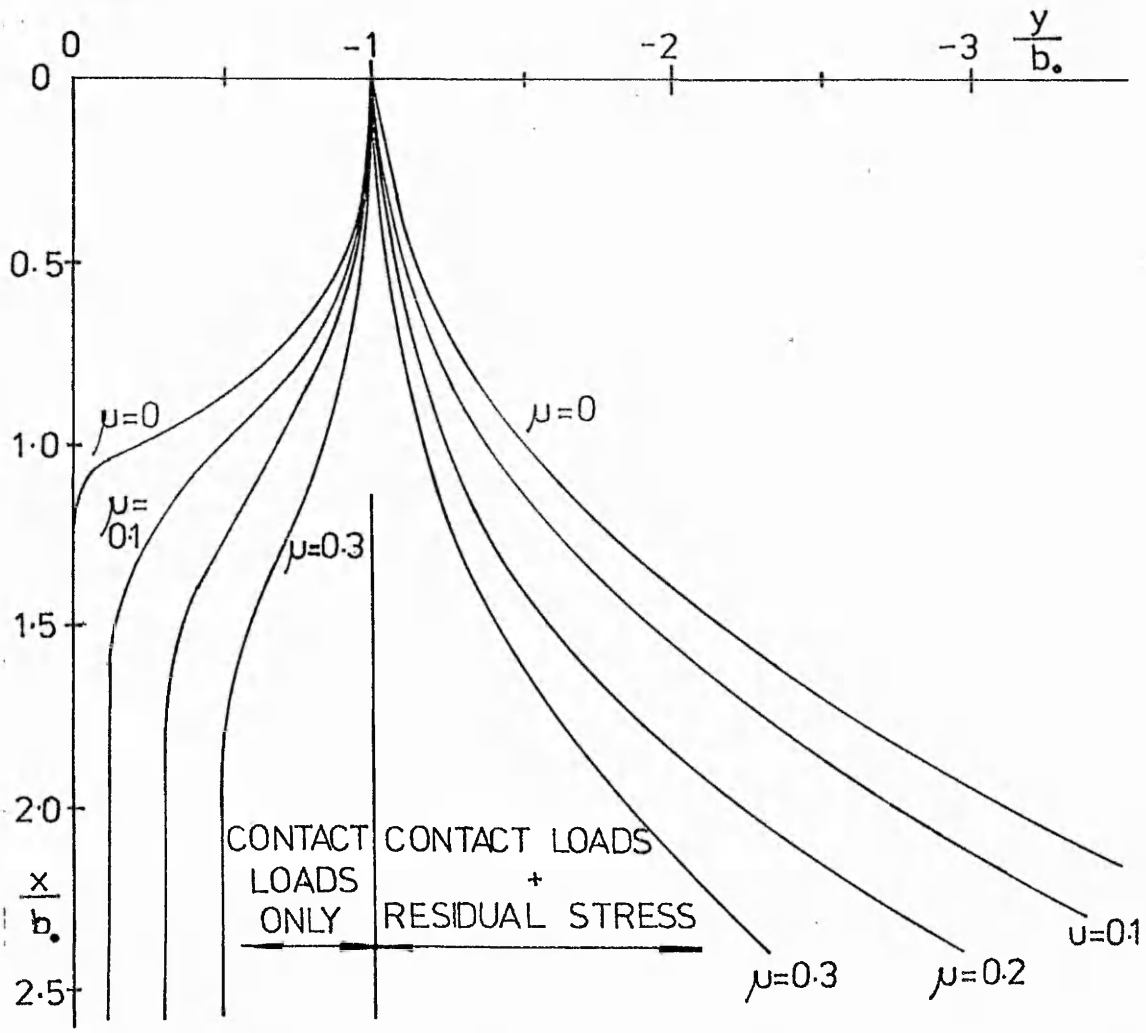
Tolerable ratio $\frac{\sigma_{\theta\theta}}{p_o}$ at various depths, $\mu=0.1$ Fig.75.

maximum hydrostatic stress. It is clear that the topography of the inclusion dominates the problem,ie. that tribological components containing flake-like second phase particles are more likely to begin cracking than those containing approximately equi-axed flaws. Also, since the influence of residual stresses on reducing the likelihood of initiation is marginal, it may be concluded that if residual stresses do control wear in any particluar case then that system is propagation controlled.

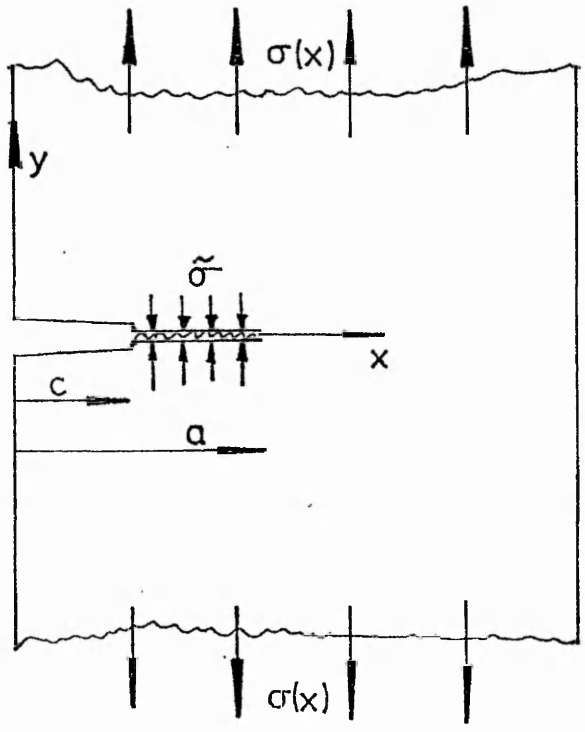
In this section only materials containing a rare dispertion of rigid inclusions have been considered. The interaction between inclusions have been ignored, as has any localized plasticity. Stress concentration factors for various flaws in a work-hardening (Ramberg-Osgood) material have recently be found by Huang(146), which might be more appropriate in some wear corfigurations bearing in mind the large strains found. However, it is worth noting that the wear tests conducted and reported earlier were done with electroplate which is very pure, and they showed a strong interdependence between wear rate and residual stress. If this were a propagation controlled system with plenty of crack sites available the size of a fully developed crack must be very small.

4.4 Non-linear aspects of Crack Propagation

This topic was not treated extensively, but is worth mentioning because of the exceptional conditions in which a wear crack lies. It has been stated that wearing surfaces often undergo large plastic deformations: the limitations of linear elastic fracture mechanics state that any plasticity must be confined to a small zone around the crack tip, and



Worst location of inclusion beneath a cylinder, m=0·4 .Fig.76



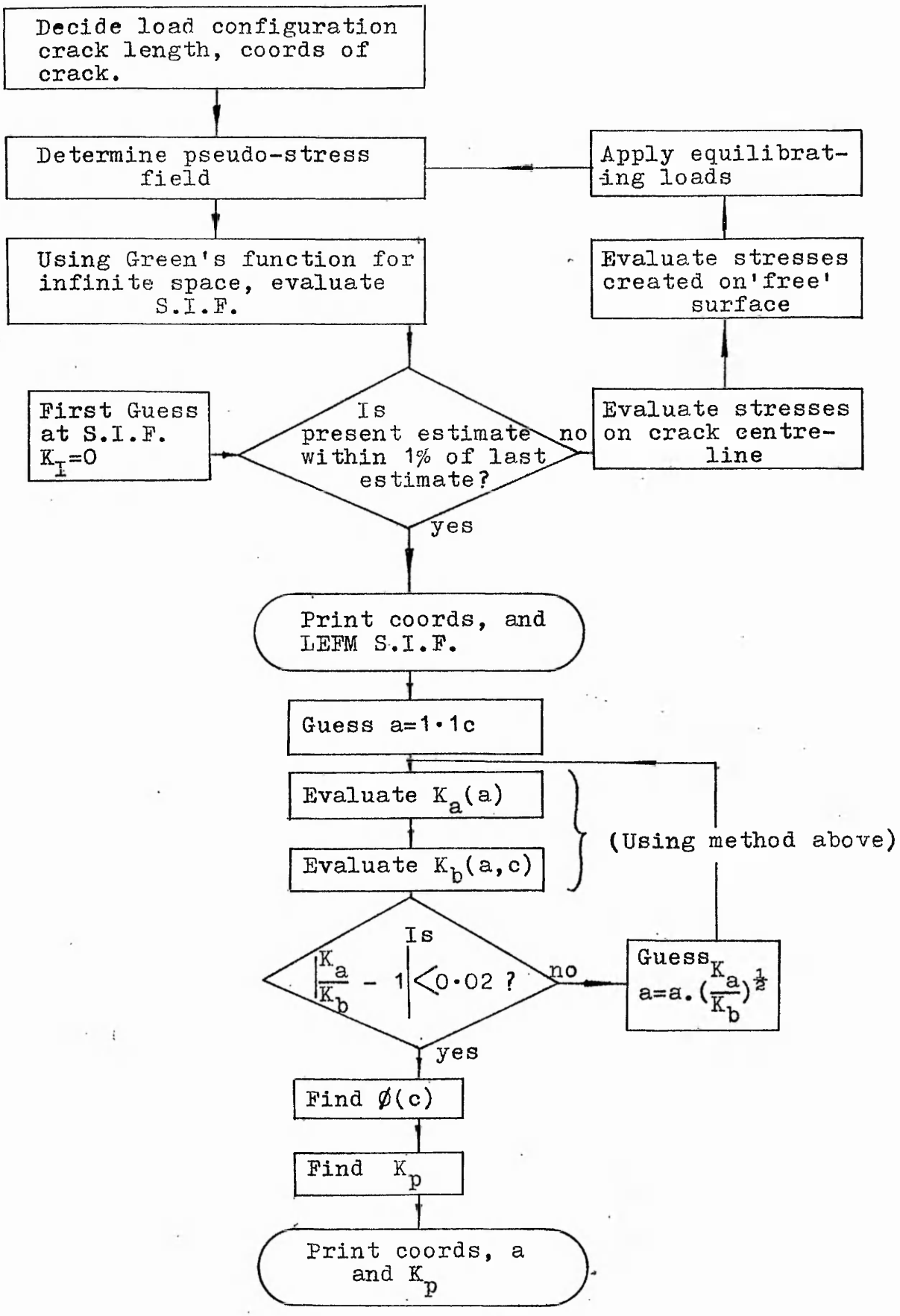
Arbitrarily loaded cracked plate. Finite plastic zone.

Fig.77.

be negligible in extent compared with the crack length. If forward flow occurs within the crack tip plasticity zones, then they must be larger in extent than L.E.F.M. permits.

Most approaches to post yield fracture mechanics use the so-caleed HRR solution, which was found independently by Hutchinson(147) and Rice & Rosengren(148). It deals with the stress state at the crack tip as if it were a non-linear elastic material, and, by implication, the solution is taken to be accurate for deformation plasticity (in spite of the irreversibilities). The method is difficult to implement and necessitates using the J-contour integral (120). A second method suitable for experimental purposes is to measure the crack opening displacement (C.O.D.) and to relate this to the failure stress.

Where there is only limited yielding a third method is available. In its simplest form a larger effective crack length is assumed when calculating the S.I.F.. If the plastic zone size predicted by L.E.F.M. is r_p then the effective crack half-length is $c+r_p$ and so $K_I=K_I(c+r_p)$. This method is only very rough and provides a safe upper bound. However, in assuming that the crack length extends to the end of the plastic zone the cohesive stresses within that portion are neglected. The simplest way to allow for them is to assume that within the plastic zone $\sigma = \sigma_o$, as was done in early versions of the Dugdale model (106). A direct way of obtaining S.I.F.'s making use of this principle has been developed by Chell (149,150).Fig.77 shows a cracked plate and a model plasticity zone emanating from the crack tip. Chell analyzed the plate, under arbitary mode I loading, under conditions



Flow chart for the Determination of post yield S.I.F.'s, using Chell's Method. Fig.78

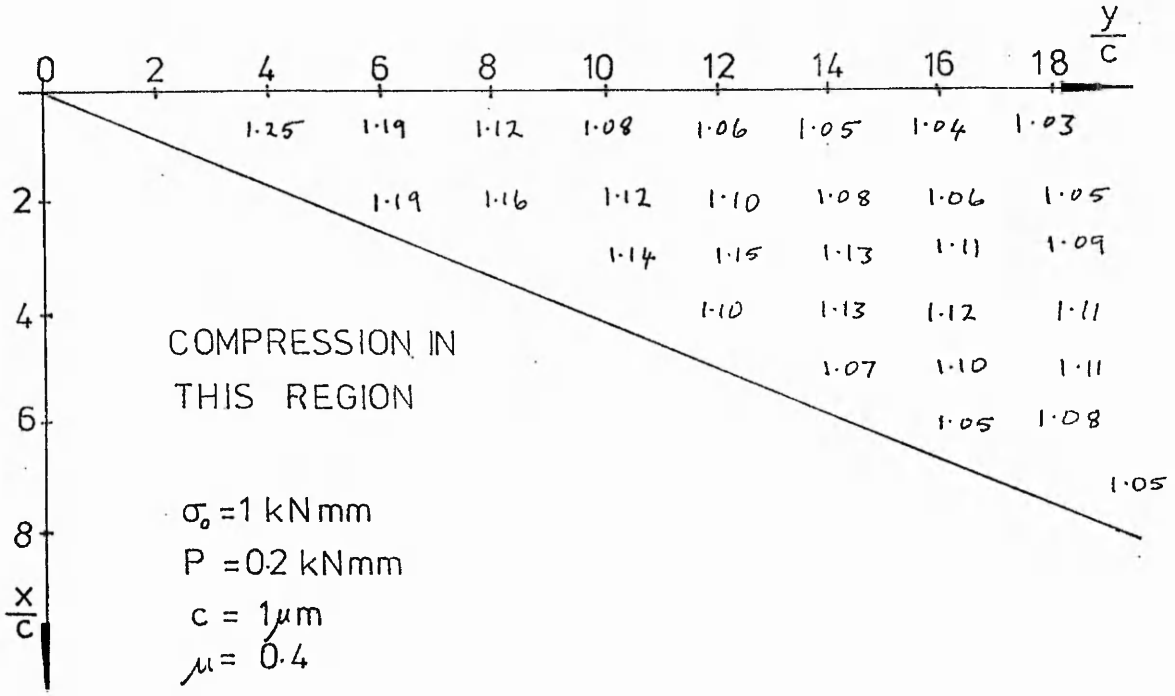


Table of values of the ratio a/c due to line load. Fig 79a

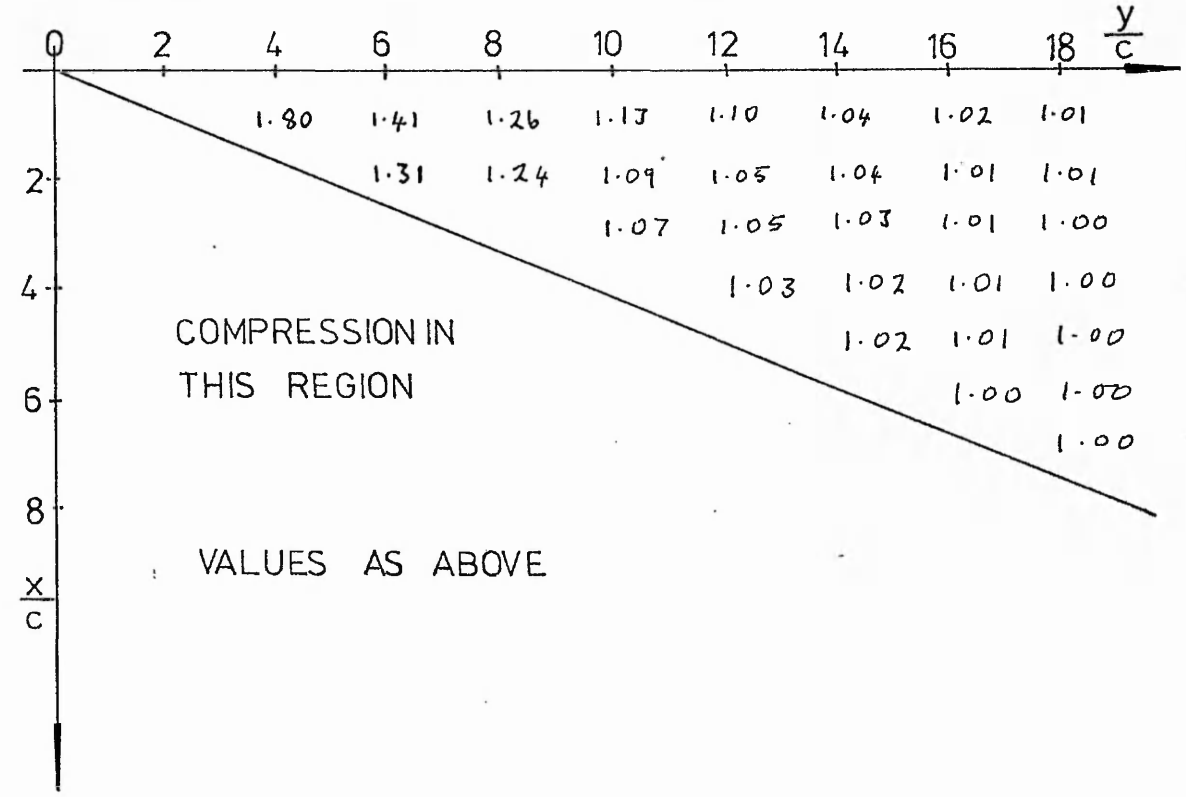


Table of values of the ratio $\frac{K_{Ip}}{K_I}$ for a line load. Fig. 79 b

where the plastic zone size is not negligible. The crack-opening displacement is given by;

$$\phi(c) = \frac{2}{E}\int_{c}^{a} G(x,c)\ K_a(x) - K_b(x,c)\ dx \qquad (71)$$

where, in this case, the Green's function G(x,c) is approximated by equation 34a. Note that here the 'variable' is $x > c$, the real crack length. The S.I.F.'s are given by;

$$K_a(x) = \int_0^x G(x,x')\ \sigma(x')dx$$
$$K_b(x,c) = \int_0^x G(x,x')\ \tilde{\sigma}\ dx \qquad (72)$$

where (x') is the pseudo stress and $\tilde{\sigma}$ is the stress component in the y direction in the yield condition. The plasticity zone, s=a-c is determined by the relation;

$$K_a(a) = K_b(a,c) \qquad (73)$$

Also, the 'plastic' S.I.F. may be found from;

$$K_p = \sqrt{E\tilde{\sigma}\phi(c)}$$

Failure is predicted when $K_p = K_{IC}$, in uniformity with L.E.F.M. The solution of the above family of equations was attempted on the same mini-computer used for earlier calculations, and a block diagram is shown in fig.78. The results of applying the method to one loading configuration, viz. a line load, are shown in fig.79. There was insufficient capacity available to attempt a more realistic load. Also, it was felt that because fracture mechanics has not yet progressed to the stage where mode II loading can be handled in the post-yield regime, any results would only be indicative of material behaviour under wear conditions.

It can be seen from fig.79 that at most depths the correction to post yield mechanics has only a small effect on the S.I.F., and zone sizes never exceed about 0·25 of the crack half length.

5. An Estimation of Crack Growth Rates

5.1 Difficulties unique to Wear

Now that the relation between applied load, crack size, loading geometry and S.I.F. has been established, it will be valuable to find the rate of crack growth. There are two features of wear crack growth which make estimation by established methods difficult, viz. stress intensification factors encountered are low, being little in excess of the threshold value. Secondly, the crack suffers combined modes I and II loading for part of the cycle, and pure mode II growth in a second part.

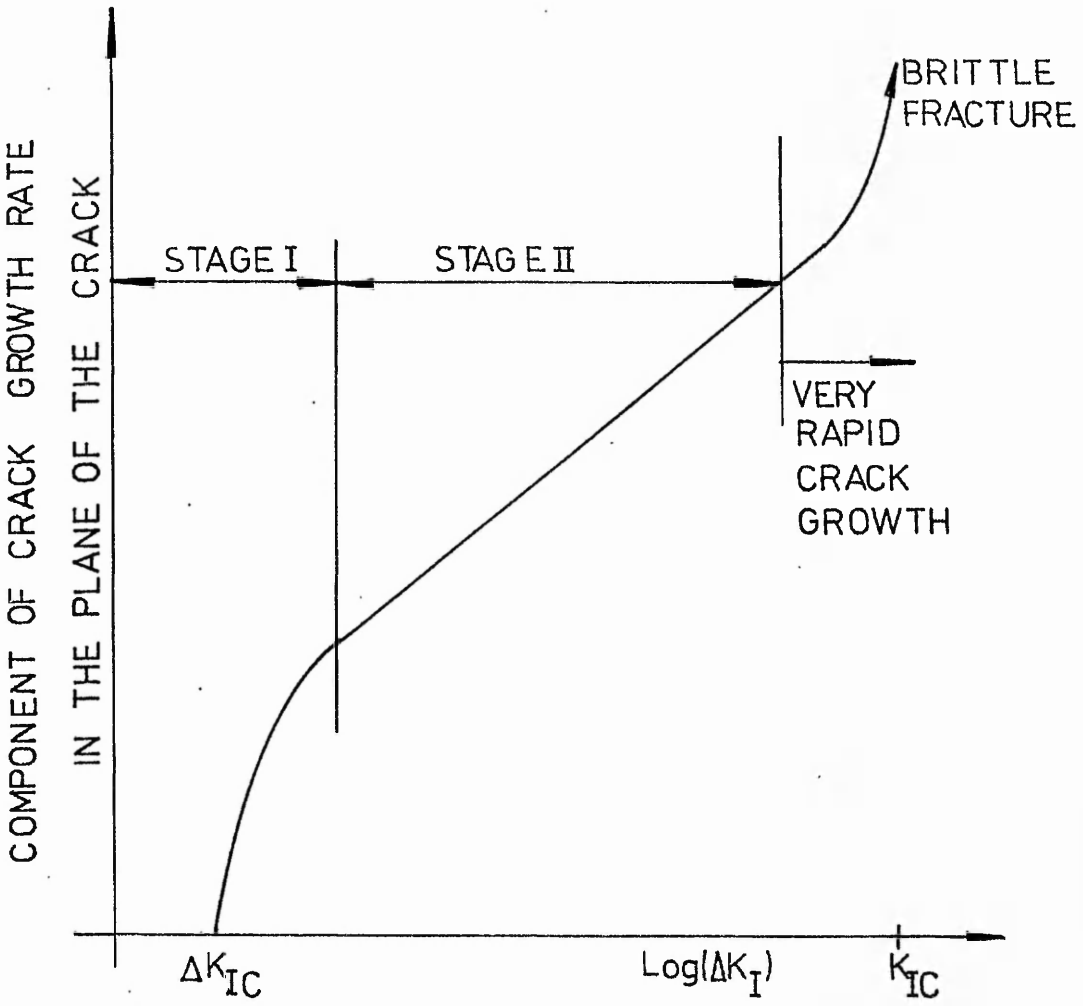
When an ordinary fatigue crack undergoes pure mode I loading the relationship between the S.I.F. and the crack growth per cycle can be represented by a graph of the type shown in fig.80. There are three regions of interest;

A. Stage I Growth

Here the crack is still small compared with the grain size, and crystallographic effects are present. The crack grows by a shear mode action , along lines at $\theta = \pm 70^{\circ}$, so that progress in the plane of the crack is low. Note that the crack growth rate is extremely sensitive to the value of the applied load.

B. Stage II Growth

As the crack grows much longer than the grains, the continuum approach becomes valid. The crack now grows by an opening mode mechanism. Within this region the relation between the crack growth and S.I.F. can adequately be represented by Paris' equation,ie.;



The three stages of crack growth. Fig.80

$$\frac{dc}{dN} = A.(\Delta K)^m \qquad (74)$$

C. 3rd Stage of Growth

Eventually the crack tends towards the critical size. As it does so the crack grows rather more quickly than predicted by Paris, and a power relation is no longer valid.

Since stage II occupies the majority of the crack's life, it is usual to predict time to failure by substituting the relation for the S.I.F. into equation 74, and integrating;

$$\frac{dc}{dN} = A.\ (K(\sigma, c))^m$$

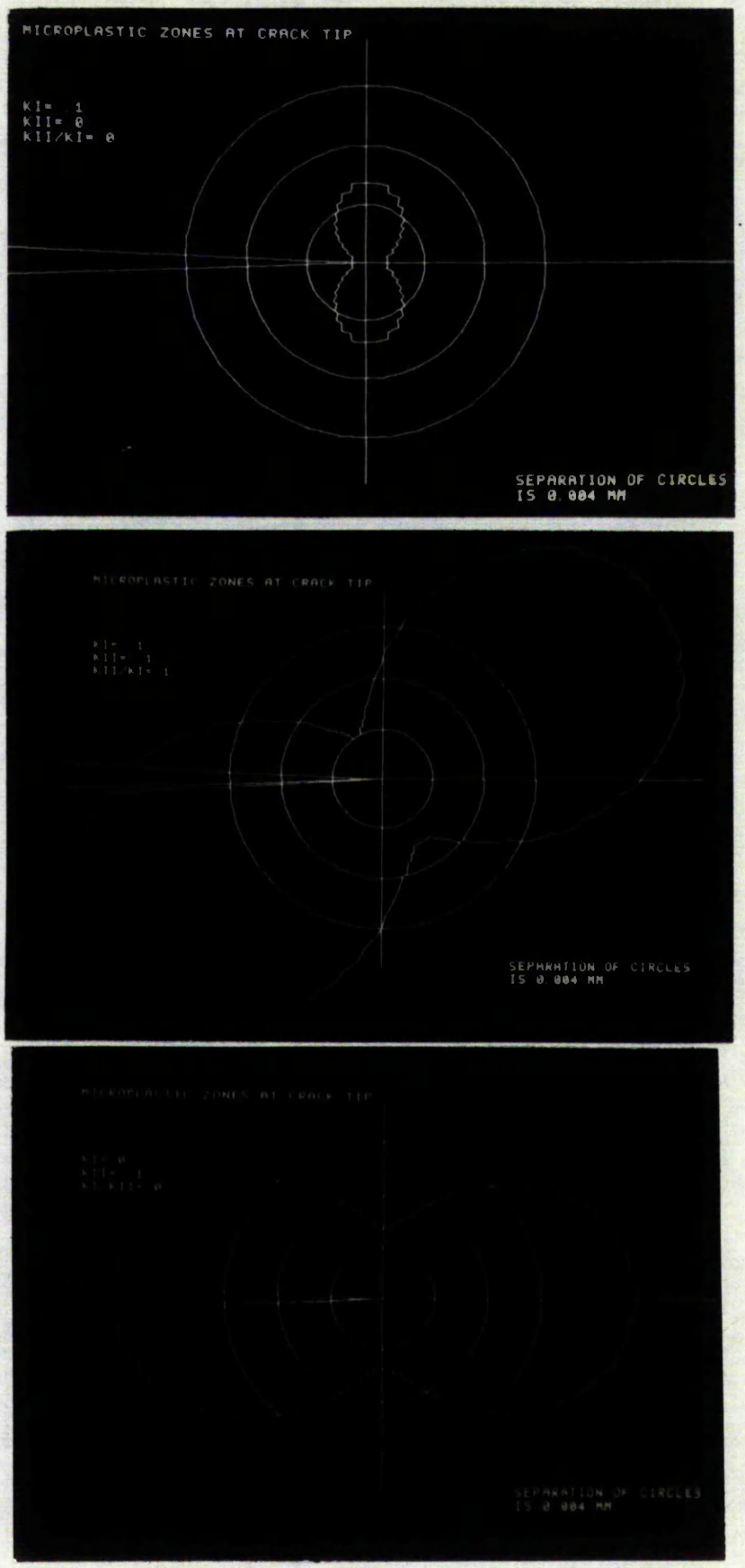
$$N = \frac{1}{A}\int_{c_1}^{c_2} \frac{dc}{K(\sigma, c)^m}$$

where c_1 is the length of the crack found at any particular time, c_2 is the largest crack length which can be tolerated and N is the number of fatigue cycles needed to make the crack grow from c_1 to c_2.

The distinction between a fully developed stage II crack and the intiating period associated with stage I is due to Forsyth(151). Wear cracks, because they are so short, are more likely to exist for a long time in the first stage of growth. An examination of fig.80 will show that under these conditions use of equation 74 will under estimate crack growth rate considerably, because of the greatly increased shear component present in the plane of the crack. There is currently no simple way of estimating what the growth rate might be.

Combined modes I and II loading presents difficulties because there is no universally acceptable equation, together with data, available. A review of the available proposed laws was made by Toor(152). All require the experimental

Note that the S.I.F.'s are given in $kNmm^{-3/2}$



Idealized plasticity zones found at crack tips. Concentric circle are for scaling only. $\sigma_o = 0 \cdot 5 kNmm^{-2}$

Fig.81.

determination of a large number of empirical coefficients, and it is far from certain whether the results obtained in one configuration are applicable in another. Thus, a method is needed which determines:

A. Whether a crack is growing by opening or shearing.

B. The most probable direction of crack growth.

C. The rate of growth.

Erdogan(153), Kanazawa(154) and Antolovich et al (155) have suggested using the microplastic zones at crack tips as a means of predicting propagation rates. The equations deduced also involve many arbitary constants, and their use is considered only for mode I growth. However, much experimental data are available for mode I (see, for example Pook(156)). Therefore, these data may be used to eliminate some of the constants, and hence combined mode propagation rates may be deduced. The method to be described is applicable only when the loads are applied in phase; cumulative damage caused by out of phase loading cannot be properly taken into consideration.

First, the nature of the plastic zones at crack tips should be visualised. The stress field in the neighbourhood of the tip has been shown to obey a relation of the form of equation 28. The angular distribution of stresses is given by the Irwin-Kolosov singular solution. This is:

$$\begin{Bmatrix} \sigma_{rr} \\ \sigma_{\theta\theta} \\ \tau_{r\theta} \end{Bmatrix} = \frac{K_I}{\sqrt{2\pi r}} \begin{Bmatrix} \cos(\theta/2)\left[1+\sin^2(\theta/2)\right] \\ \cos^3(\theta/2) \\ \sin(\theta/2)\cos^2(\theta/2) \end{Bmatrix}$$

$$\sigma_{zz} = (\sigma_{rr} + \sigma_{\theta\theta}) \qquad \epsilon_{zz} = 0 \qquad (75)$$

$$\begin{Bmatrix} \sigma_{rr} \\ \sigma_{\theta\theta} \\ \tau_{r\theta} \end{Bmatrix} = \frac{K_{II}}{\sqrt{2\pi r}} \begin{Bmatrix} \sin(\theta/2)\ 1-3\sin^2(\theta/2) \\ -3\sin(\theta/2)\cos^2(\theta/2) \\ \cos(\theta/2)\ 1-3\sin^2(\theta/2) \end{Bmatrix}$$

There is a similar solution for mode III loading.

If it is assumed that the elastic stresses are given by equations (75) right up to the value where the yield criterion is exceeded, ie. $J_2=\tau_0^2$, then the plastic zones are of the form shown in fig.81. It should be noted that for a given S.I.F. the plastic zone is larger for mode II loading than for mode I, and that linear superposition is permissible if it is assumed that the strains are given by the extended elastic strains.

5.2 Estimating Stage and Rate of Crack Growth

Two criteria have been proposed for deciding the stage of crack growth; the maximum energy release criterion due to Wu(157), and the local stress criterion due to Otsuka et al (158). The latter is followed here since the parameters derived also enable the most probable direction of growth to be found. Consider the following parameters, found from equations (75):

$$K\sigma=\sigma_{\theta\theta}\sqrt{2\pi r}=\cos^2(\theta/2)\{K_I\cos(\theta/2)-3K_{II}\sin(\theta/2)\} \quad (76)$$
$$K\tau=\tau_{r\theta}\sqrt{2\pi r}=\cos(\theta/2)\{K_I\sin(\theta/2)\cos(\theta/2)+K_{II}(1-3\sin^2(\theta/2))\}$$

It is assumed that the transition from stage I to stage II occurs when $K\sigma$ reaches some critical value. Therefore this must be maximised with respect to θ. This gives;

$$K_I\sin(\theta/2)+2K_{II}(1-3\sin^2(\theta/2))=0 \quad (77)$$

Similarly, to obtain the boundary between no-growth and stage I $K\tau$ is maximised with respect to θ giving;

$$K_I\cos(\theta/2)(1-3\sin^2(\theta/2))-3K_{II}(3\cos^2(\theta/2)-1)\sin(\theta/2)=0 \quad (78)$$

Solving equations 76 with equations 77 and 78 enables the form of the boundaries to be found. Otsuka et al then used their experimental results to determine the relative positions of the boundaries. This, however, should not be

necessary. If, in equation 76a, the value $\theta=0$ is inserted then it is obvious that;

A. This corresponds to pure mode I, and therefore the values to be substituted are $K_I=\Delta K_{IC}$, $K_{II}=0$

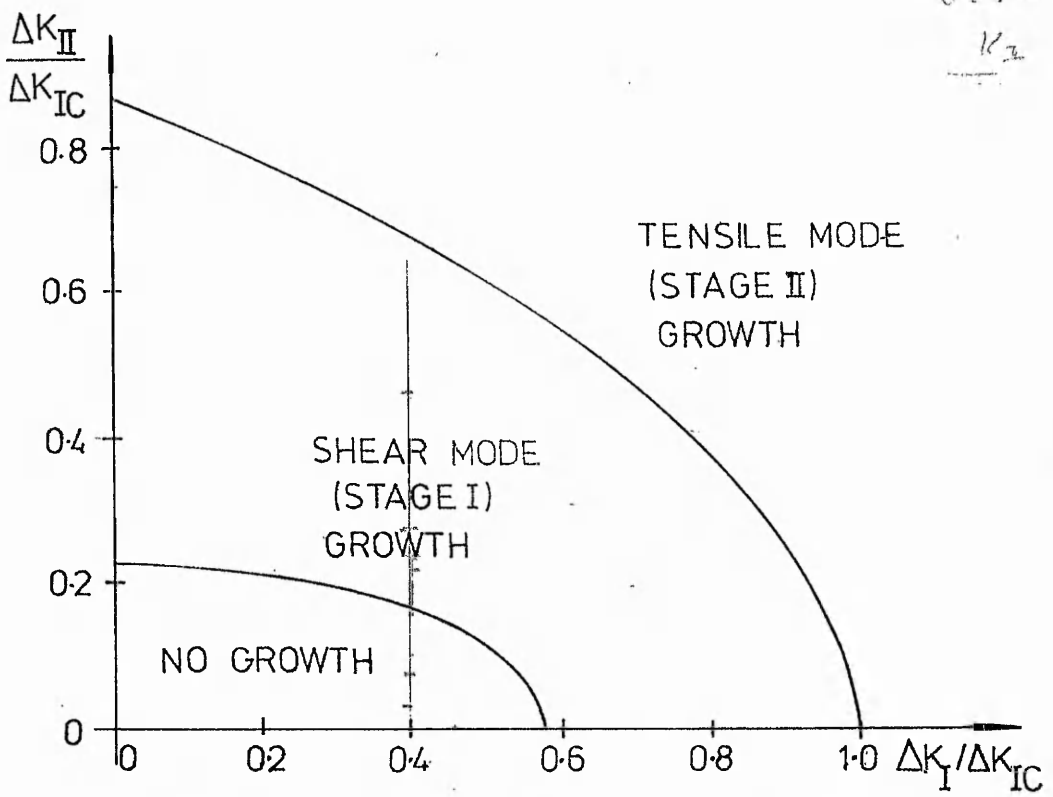
B. Form the singular solutions, with values substituted as above, $\tau_{r\theta}=0$, so that $\sigma_{\theta\theta}$ is a principal stress.

Thus, for the case of plane stress, yielding occurs in front of the crack when the hoop stress $\sigma_{\theta\theta}$ reaches the yield value σ_o. This occurs when the maximum shear exceeds the yield stress in pure shear. If von Mises' criterion is assumed, $\tau_o=\frac{\sigma_o}{\sqrt{3}}$ and growth will begin when K_I reaches $0{\cdot}577\Delta K_{IC}$. This value differs only slightly from that used by Otsuka, and gives very similar curves (fig.82). The form of the stage I-stage II boundary is in good agreement with that derived from experimental work by Pook (139,159).

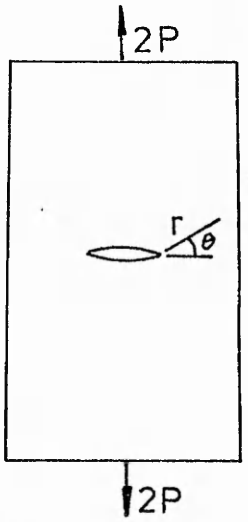
Now that the most likely growth mechanism has been established, the propagation rate must be found. Before doing this, the errors introduced by using an elastic stress field and a plasticity criterion are illustrated. Consider the centrally cracked plate of fig.83. Clearly, the ligaments either side the crack must each carry a load P, regardless of the value of P, ie. no matter what the size of the plastic zone. Since the ligaments lie on the crack centre-line, and assuming plane stress, the extended stresses may be written down immediately;

$$\sigma_{xx}=\sigma_{yy}=\frac{K_I}{\sqrt{2\pi r}}, \qquad \sigma_{zz}=0 \tag{78}$$

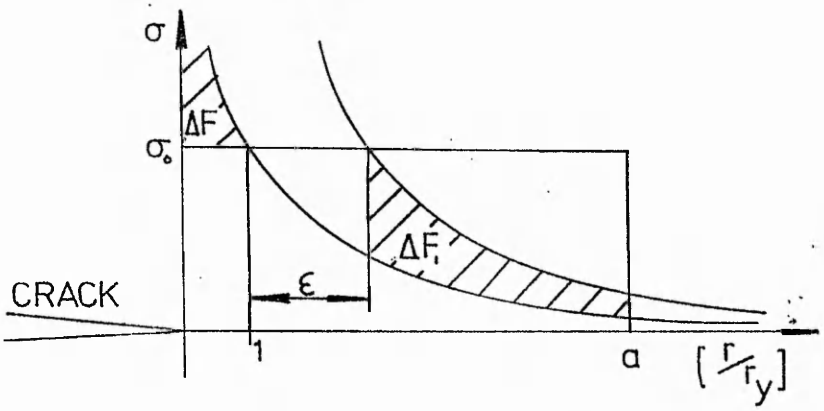
Using Tresca's criterion, it is clear that yielding occurs when σ_{yy} reaches σ_o. In limiting the stress to the yield value the contribution made by higher stress levels, ΔP, is lost. In order to maintain equilibrium the part of the



Prediction of most probable type of crack growth. Fig. 82.



A large, centrally cracked plate.
Fig. 83.



Stresses near crack tip showing 'lost' force due to yielding. Fig. 84.

force which would be supported by these higher stresses must now be catered for by extending the yielded zone further, as shown in fig.84. The 'lost' force is given by;

$$\Delta F = K_I\sqrt{\frac{2r_y}{\pi}} - \sigma_o r_y \qquad (79)$$

The extra contribution of force made by extending the yield zone by ϵ is $\Delta F'$;

$$\Delta F' = \epsilon.\sigma_o + K_I\sqrt{\frac{2r_y}{\pi}} \times \left\{\sqrt{a}\left(1 - \frac{\epsilon}{a.r_y}\right)^{\frac{1}{2}} - \sqrt{a}\right\} \qquad (80)$$

But $\Delta F = \Delta F'$, ie.

$$\epsilon + r_y = \frac{K_I}{\sigma_o}\sqrt{\frac{2r_y}{\pi}}\left\{\sqrt{a} + 1 - \sqrt{a}\left(1 - \frac{\epsilon}{a.r_y}\right)^{\frac{1}{2}}\right\} \qquad (81)$$

Taking the limit $a \to \infty$;

$$\frac{\epsilon}{r_y} = \frac{K_I}{\sigma_o}\sqrt{\frac{2}{\pi r_y}} - 1 \qquad (82)$$

Putting in the plane stress plastic radius;

$$r_y = \left(\frac{K_I}{\sigma_o}\right)^2 \cdot \frac{1}{2\pi} \qquad (83)$$

gives;

$$\frac{\epsilon}{r_y} = 1 \qquad (84)$$

This result and its implications for accuracy should be borne in mind, because it will subsequently be neglected, ie. $\epsilon = 0$. Work hardening is also ignored.

The following method will be used to find the size of the reversed plastic zones: first, the monotonic zones will be found. It will be assumed that within this plastic zone all stresses maintain the same value, and do not fall off towards the crack tip. (This cannot be true since tractions would appear on the crack face which would be unsatisfied. However, since the exact form of the fall-off is not known, and this assumption will, to some extent, cancel the effect of neglecting the correction to the zone size, it will be ignored consistently). Secondly, the reversed zone size will then be found by observing when, having relaxed a certain fraction 'p' of the original load,

the new nett shear stress exceeds the yield criterion. First, though, p must be found.

This is done by considering one ligament of fig.83. Assume that the stress ratio is zero, so that upon relaxation the value of P falls to zero. The stress system is shown in fig.85. If the load P falls to zero, so does the sum of the stresses across the ligament. From fig.85, it can be seen that this is equivalent to saying that the two areas A and B are equal.

First, the monotonic plastic radius r_p is found as described above. It is then substituted back into the singular solutions to give the 'saturation' stress level, $\tilde{\sigma}$, corresponding to yielding. The nett stresses after the reversed stress field is superimposed are then given by;

$$\sigma_{xx}=\sigma_{yy}=\frac{K_I}{\sqrt{2\pi}}\left\{\frac{1}{\sqrt{r_p}}-\frac{p}{\sqrt{r}}\right\} \qquad \tau_{xy}=\frac{K_{II}}{\sqrt{2\pi}}\left\{\frac{1}{\sqrt{r_p}}-\frac{p}{\sqrt{r}}\right\}$$
$$\sigma_{zz}=K_I\sqrt{\frac{2}{\pi}}\nu\left\{\frac{1}{\sqrt{r_p}}-\frac{p}{\sqrt{r}}\right\} \qquad (85)$$

Substituting these equations (which are for plane strain) into von Mises' criterion and putting;

$$A^2=\tfrac{1}{3}K_I^2(1-2\nu)^2+K_{II}^2$$

gives the relation

$$\pm\sigma_0=\sqrt{\frac{3}{2\pi}}\left\{\sqrt{\frac{2\pi}{3}}\left(\frac{\sigma_0}{A}\right)-\frac{p}{\sqrt{r'_p}}\right\}A \qquad (86)$$

The only solution which is not trivial is associated with $-\sigma_0$, giving;

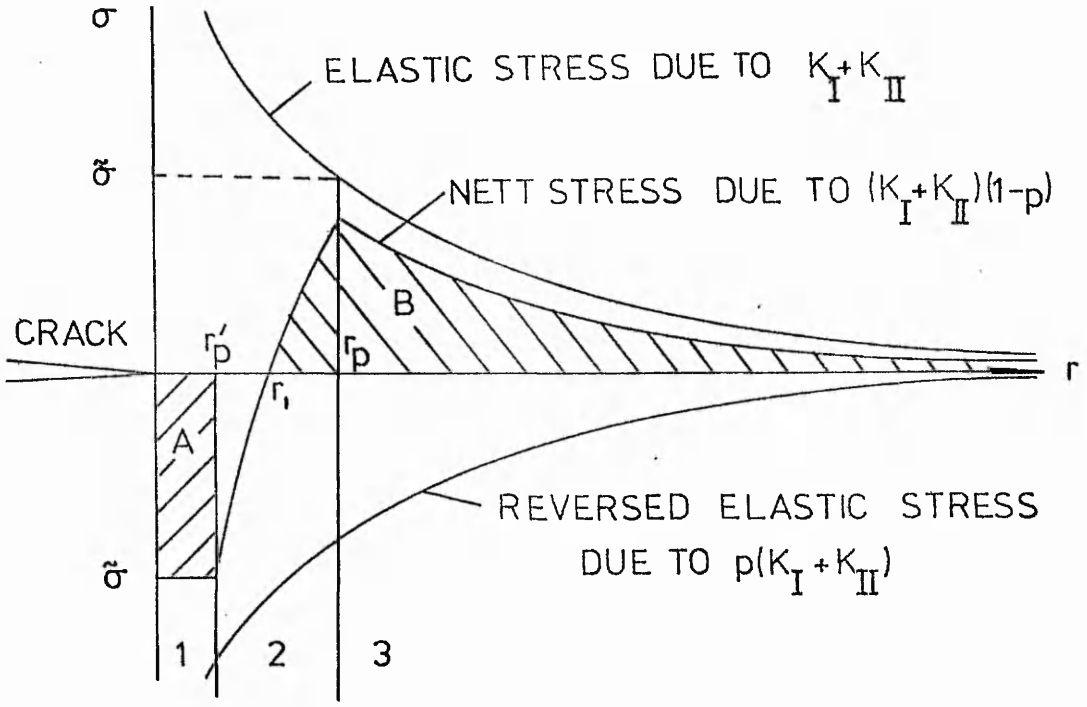
$$r'_p=\frac{3p^2A^2}{8\sigma_0^2\pi} \qquad (87)$$

To find p, return to fig.85 and equations 85. The σ_{yy} stress will cross the zero-stress axis when;

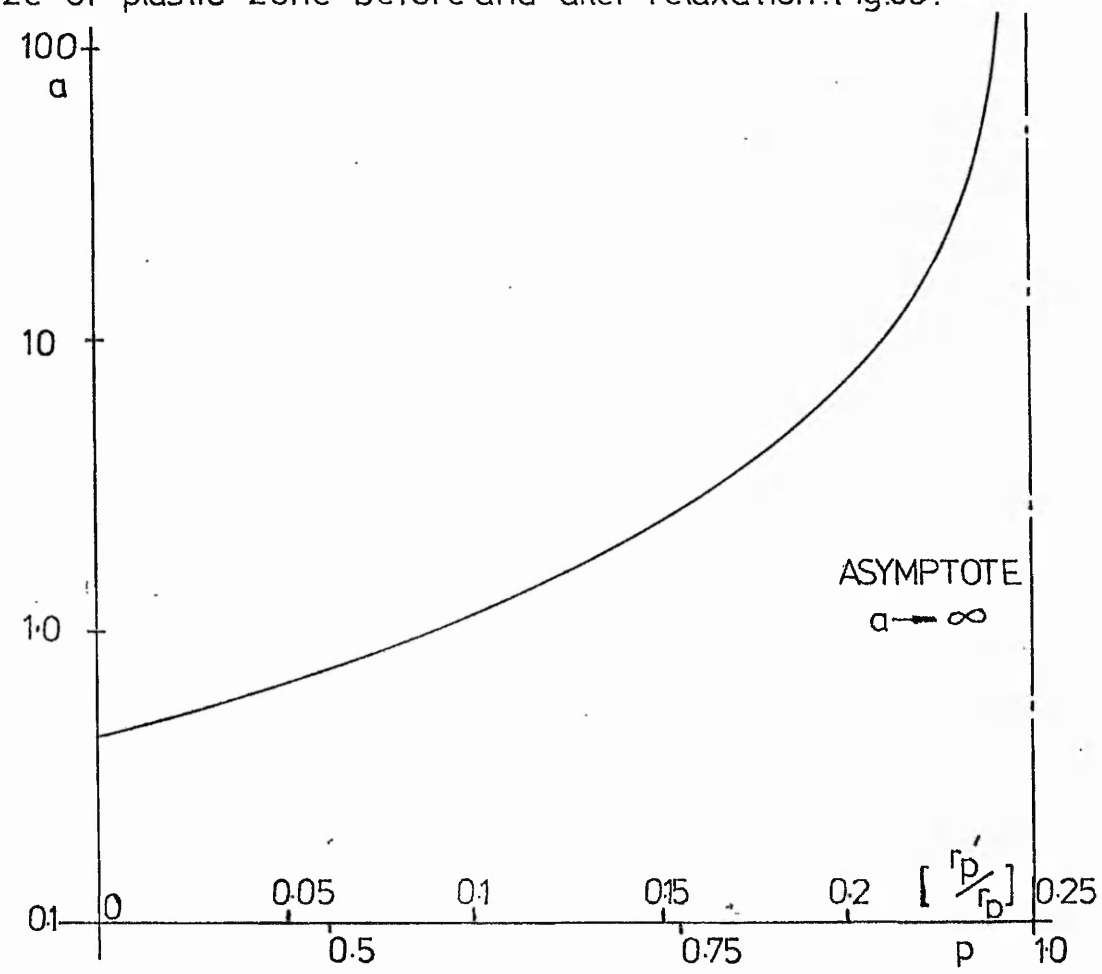
$$p^2=\left(\frac{r_1}{r_p}\right) \qquad (88)$$

The force contributions can now be found;

$$F_1=\left\{K_I r'_p\right\}\Big/\sqrt{2\pi r_p}$$



Size of plastic zone before and after relaxation. Fig.85.



Effect of modifying outer limit of integration. Fig. 86.

$$F_{2A}=\frac{K_I}{\sqrt{2\pi}}\left\{p^2\sqrt{r_p}\ -\ 2p\sqrt{r'_p}+\frac{r'_p}{\sqrt{r_p}}\right\}$$

$$F_{2B}=\frac{K_I}{\sqrt{2\pi}}\sqrt{r_p}\ (1-p)^2 \qquad (89)$$

$$F_3\ =\ K_I(1-p)\sqrt{\frac{2r_p}{\pi}}\ (\sqrt{a}\ -\ 1)$$

Assembling these with attention to signs gives;

$$2\left\{\frac{r'_p}{\sqrt{r_p}}\ -\ p\sqrt{r'_p}\right\}=\sqrt{r_p}\left\{\ 2\sqrt{a}\ (1-p)\ -\ 1\right\} \qquad (90)$$

Rearranging and taking the limit $a\rightarrow\infty$ gives $p\rightarrow 1$. Substituting this value into equation 87;

$$r'_p=\frac{3A^2}{8\sigma_o^2\pi} \qquad (91)$$

whereas the monotonic plastic zone size is;

$$r_p=\frac{3A^2}{2\sigma_o^2\pi} \qquad (92)$$

Therefore;

$$\frac{r'_p}{r_p}=\tfrac{1}{4} \qquad (93)$$

Two equilibrium problems have now been solved by arbitrarily taking the outer limit at infinity. This is convenient for converging quantities and gives simple ratios. However, it cannot really be justified on elasticity grounds, since the singular solutions are valid only for a given distance from the crack tip, and further away the stress field is influenced by the boundary conditions on the component. The effect of taking finite limits on p and $(\frac{r'_p}{r_p})$ is shown in fig.86. Though the analysis is not repeated here, because it is rather tedious, it is easy to show that the monotonic and reversed plastic zones are geometrically similar. The plastic radius is now known for both the reversed and monotonic zones, for any combination of mode I and II loading, and for any angle, θ. It is now necessary to find the most likely direction of propagation. There are two possible criteria; the maximum energy release condition due to Cotterell(160), and the stress

criterion mentioned before, due to Erdogan and Sih(161). For simplicity, and because it is consistent with the threshold work done earlier, the second idea will be adopted. It is sometimes suggested that it is the largest tensile principal stress which determines the stage II direction- the present work will utilise the tensile hoop stress, which lies in a principal direction only for $\theta = 0$, pure mode 1.

To find the most probable direction of crack propagation for either stage equations 77 & 78 must be solved and the correct maxima selected. Equation 77 may be solved straightforwardly to give;

$$\theta = 2 \arctan\left\{\frac{1 - \sqrt{1+8n^2}}{4n}\right\} \qquad (94)$$

Equation 78 is much more difficult. Note, instead, that solutions lie in three possible regions;

$$0 \leqslant \theta \leqslant 70{\cdot}53$$

$$-109{\cdot}47 \leqslant \theta \leqslant -70{\cdot}53$$

$$109{\cdot}47 \leqslant \theta \leqslant 180$$

Only the first two are important since the last is unfavourable energetically and gives very low propagation rates. The most favoured directions as a function of the ratio $\frac{K_{II}}{K_I}$ are shown in fig.87

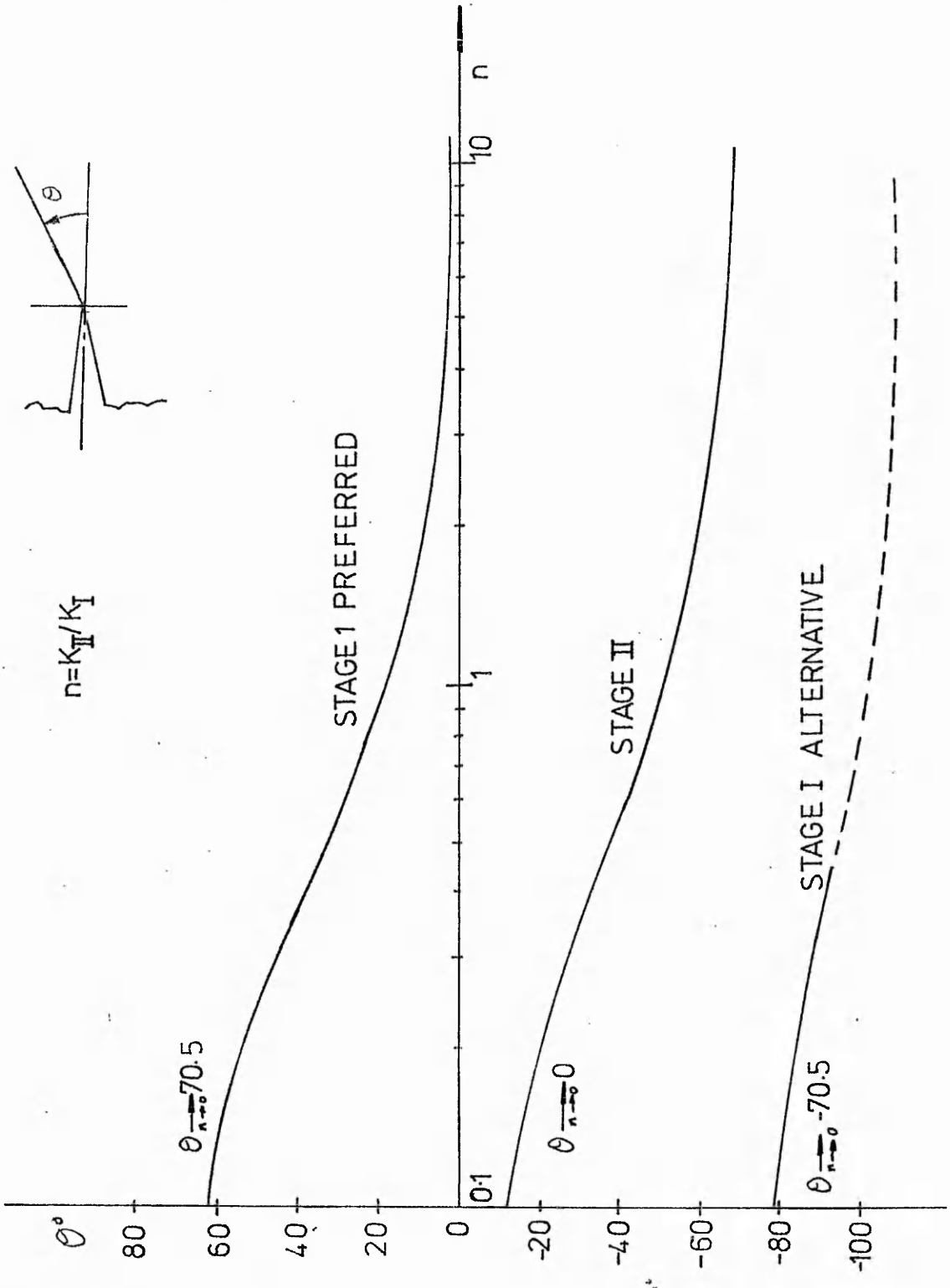
From Antolovich et al's work (155), which seems to tie in well with available data, the fatigue crack growth rate may be written as;

$$\frac{dc}{dN} = B.(r'_p)^{1/\beta} \qquad (95)$$

Note that $2/\beta$ is equivalent to m, the exponent in the Paris equation. A new general growth rate equation may be written as;

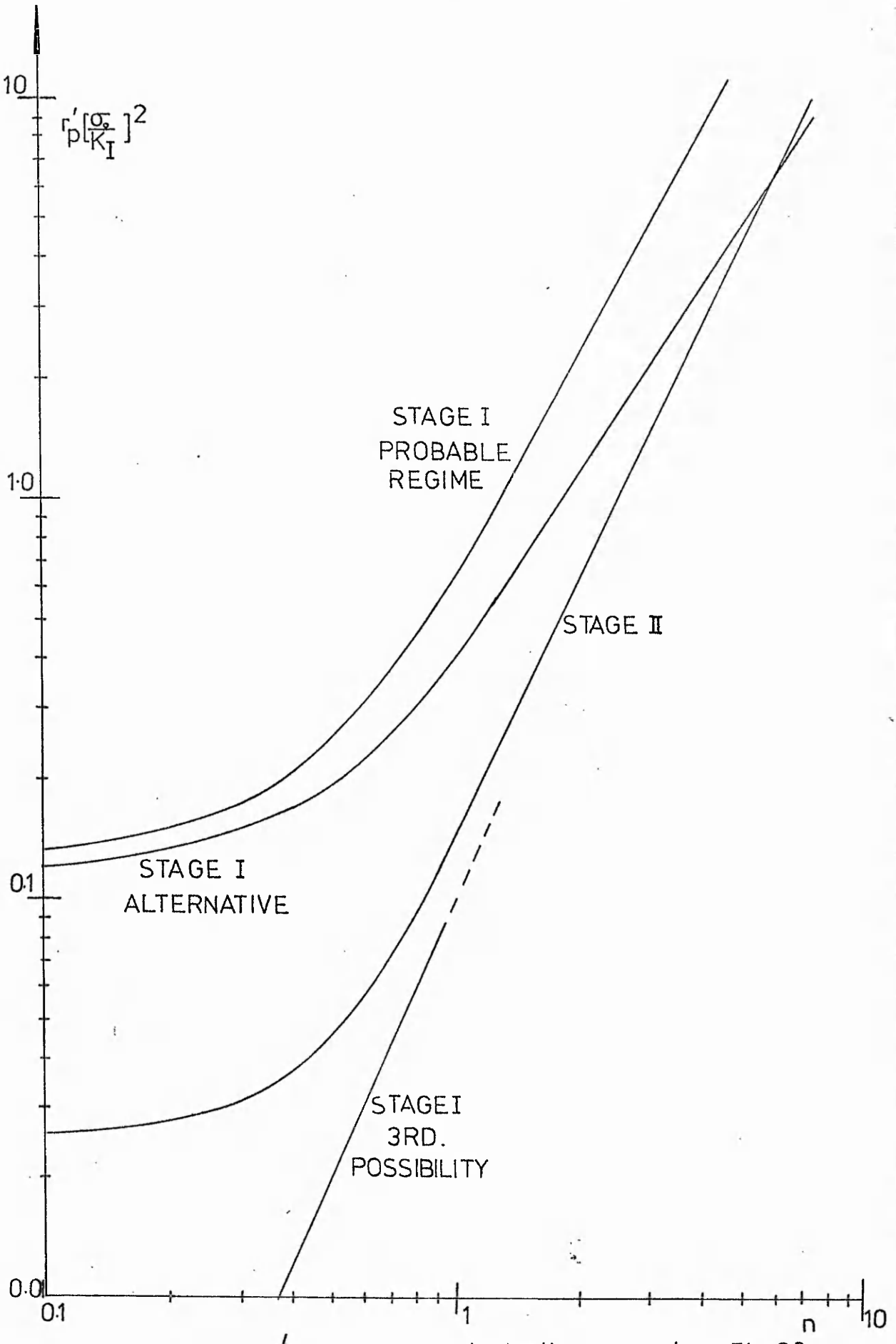
$$\frac{dc}{dN} = B.(r'_p)^{m/2} \quad \text{where } r'_p \text{ is found from fig.88} \qquad (96)$$

Fig.88 was constructed to be most useful over the range



Most likely direction of crack growth for various K_{II}/K_I

Fig. 87.



Effect of ratio K_{II}/K_I on reversed plastic zone size. Fig.88.

n=0 to 7, but could easily be re-drawn to be more sensitive in other ranges. It was constructed by taking the values of θ given by equation 94 and the solutions of equation 78 and substituting them into the general plastic zone relation given by the singular solutions and von Mises' criterion. All that remains is to evaluate the constant in equation 96. This is done by using n=0 (pure mode I) and subsituting data given by Pook (156). Additional values to fig.88 are shown in table 6.

Table 6. Additional values of plastic zone sizes

Stage	$r'_p(\frac{\sigma_o}{K_I})^2$	$r'_p(\frac{\sigma_o}{K_{II}})^2$
2	0·026	0·168
1 (probable)	0·123	0·477
1 (alternative)	0·123	0·176

To use the idea one first determines the constants m and B as described above. The ratio of stress intensification n is found for the particular loading being considered. Fig.82 is then consulted to find the most likely stage of crack growth obtaining. The most likely angle of crack extension is found from fig.87, and the reversed plastic zone size from fig.88. The value for r'_p may now be substituted into equation 96 to determine the crack growth rate.

5.3 Applying the results found to Wear

The method may be applied to sliding wear. Assume a crack half-length, normalised by the contact half-width, of 0·2, and a coefficient of friction of 0·2. Then, from fig.53, the following results are obtained;

$\frac{K_{II}}{p_o\sqrt{w}} = 0·622$ -free shear $\quad n = \frac{K_{II}}{K_I} = 1·43$

$\frac{K_I}{p_o\sqrt{w}} = 0{\cdot}434$ -free shear $\frac{x}{w} = 0{\cdot}1$ $\frac{y}{w} = 0{\cdot}7$

$\frac{K_{II}}{p_o\sqrt{w}} = 0{\cdot}677$ -shear + compression $\frac{x}{w}=0{\cdot}2$ $\frac{y}{w}=0{\cdot}8$

Let the applied force be 5kgf, and the material hardness be 300 VHN (ie. $\sigma_o=10^3 Nmm^{-2}$). Then the contact half-width $w \simeq 0{\cdot}12mm$. Thus the depths of fastest crack growth are about 12μm in the free shear mode and 24μm in the shear plus compression mode.

The next step is to eliminate the constants from equation 96. If the wearing material is hard nickel electroplate, the following data, from Pook(156) may be used;

$\Delta K_I = 0{\cdot}278\ kNmm^{-3/2}$ These values give $B=3{\cdot}88$

$\frac{dc}{dN} = 1x10^{-6} mm/cycle$ ie. $\frac{dc}{dN}=3{\cdot}88 \times r_p'^2$

$m = 4$

$\sigma_o = 10^3\ Nmm^{-2}$

$\Delta K_{IC} = 0{\cdot}187\ kNmm^{-3/2}$

The actual S.I.F.'s encountered are found;

Free shear: $K_I = 0{\cdot}070\ kNmm^{-3/2} \approx 0{\cdot}37\ \Delta K_{IC}$

Compression shear: $K_{II}=0{\cdot}108\ kNmm^{-3/2} \approx 0{\cdot}58\ \Delta K_{IC}$

By comparing these with fig.82 it is clear that both phases of crack growth occur in stage I. Using values from fig.86, the following crack growth rates result;

$r_p'(\frac{\sigma_o}{K_I})^2=1{\cdot}15$ ie. $\frac{dc}{dN} = 123\ nm/cycle$ -free shear

$r_p'(\frac{\sigma_o}{K_I})^2=0{\cdot}48$ ie. $\frac{dc}{dN} = 123\ nm/cycle$ -shear + compression

It is quite by chance that the two growth rates should be so similar. However, a nett growth per slider pass of about $0{\cdot}25\mu m$ seems reasonable, but cannot be interpreted in terms of wear volume without knowing the number of cracks growing at any instant, and the critical crack length. This will almost certainly be much less than the crack length

corresponding to K_{IC}, since the trailing edge of the crack usually appears at the surface first. In this condition the platelet is held only by the front edge, and is therefore elastically unstable when loaded by a shear traction.

It is expected that cracks from several differnt planes will grow simultaneously, though clearly the growth rate will fall off with depth. Thus, when one layer of delamination sheets has detached, there will already be several short cracks in subsequent layers, ready to grow more quickly as the S.I.F. suddenly increases. This will not happen during running-in.

5.4 Further Aspects of Crack Growth

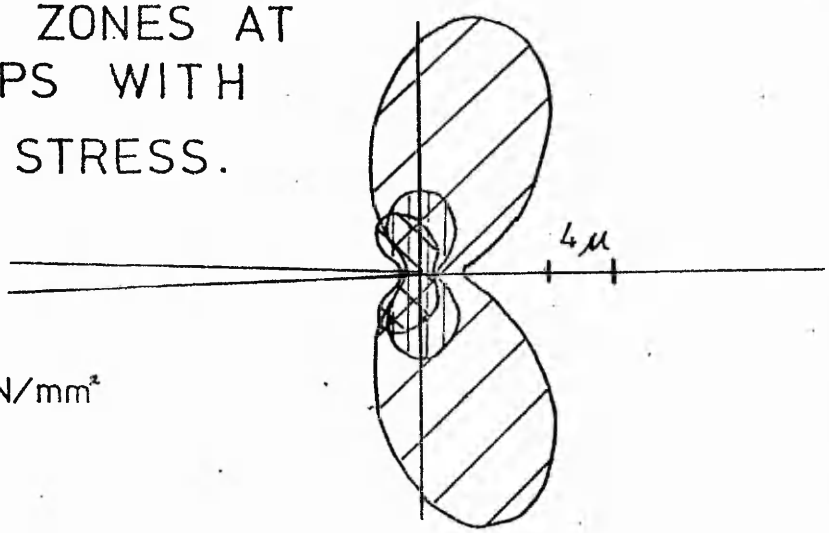
Stresses in a plane parallel to the surface, and therefore 'in-plane' with the crack, do not contribute to any stress intensification factor, and therefore, to a first approximation, do not modify the crack growth rate. However, it should be noted that the singular solution (equation 75) whilst adequate for all normal purposes, is really only the first term in a series expansion, and a corrected solution for a biaxially loaded crack, taking higher order effects into account, has been determined (162,163). The solutions are mathematically difficult, but a rough estimate of the effect of in-plane stresses may be obtained by superposition. Aurich(164) mentions this, but fails to give any examples. Physically, the reason for inaccuracy in performing straightforward superposition is that, once a mode I load has been applied, the in-plane stress does not 'see' an infinitely sharp crack, but one which has been opened slightly. In the case of a wear crack the mode I S.I.F. is small compared with any residual stress present, and

PLASTIC ZONES AT CRACK TIPS WITH "IN-PLANE" STRESS.

(a)
PURE MODE I

$K_I = 0.1\ kN/mm^{3/2}$

Applied stress $= \pm 0.2\ kN/mm^2$





No stress

Tensile stress

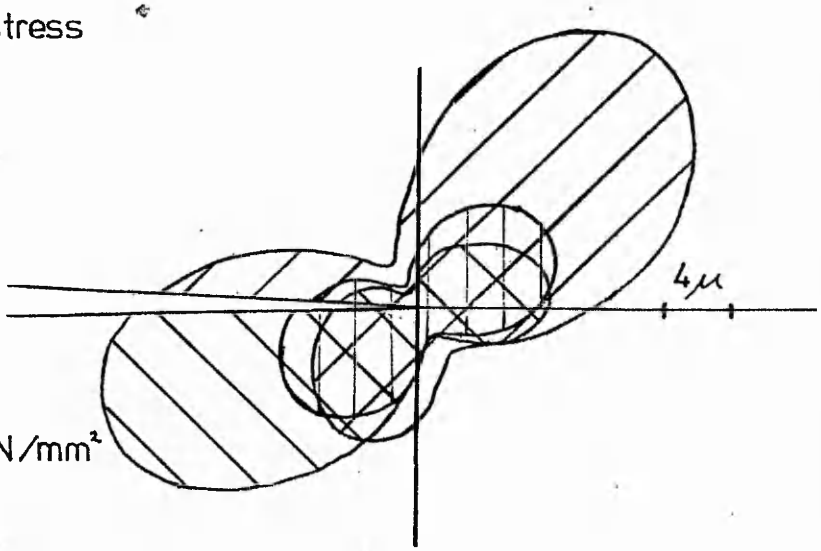
Compressive stress

(b)
MIXED MODE

$K_I = 0.06\ kN/mm^{3/2}$

$K_{II} = 0.06\ kN/mm^{3/2}$

Applied stress $= \pm 0.2 kN/mm^2$



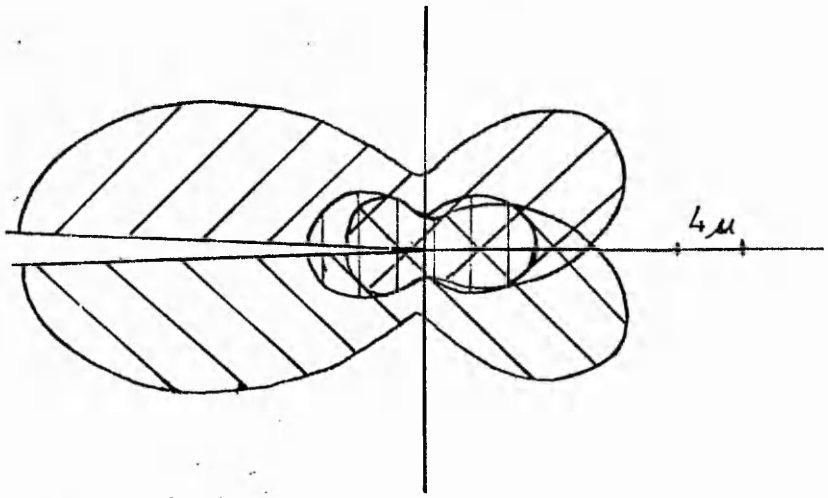
ZONE YIELDING "SIGN"

MODE:	I	II	MIXED
	t | c t | c	c | c t | t	? | c t | ?

(c)
PURE MODE II

$K_{II} = 0.06\ kN/mm^{3/2}$

Applied stress
$= \pm 0.25\ kN/mm^2$

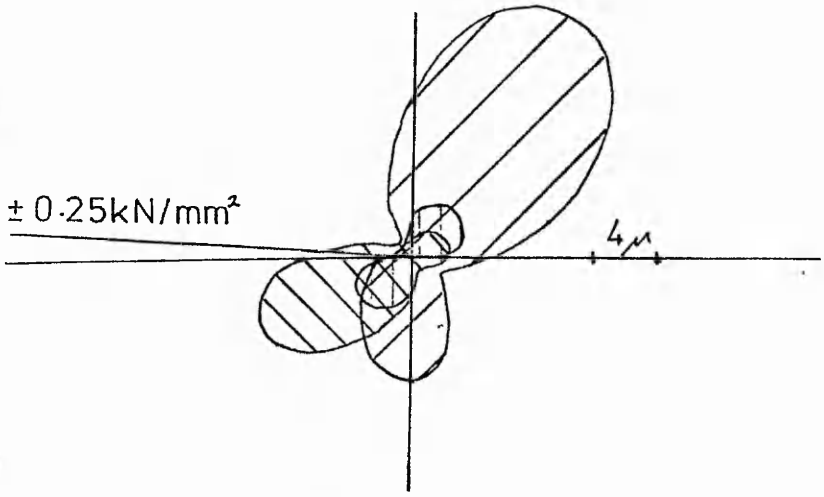


(d)
MIXED MODE

$K_I = 0.06\ kN/mm^{3/2}$

$K_{II} = 0.03\ kN/mm^{3/2}$

Applied stress = $\pm 0.25 kN/mm^2$

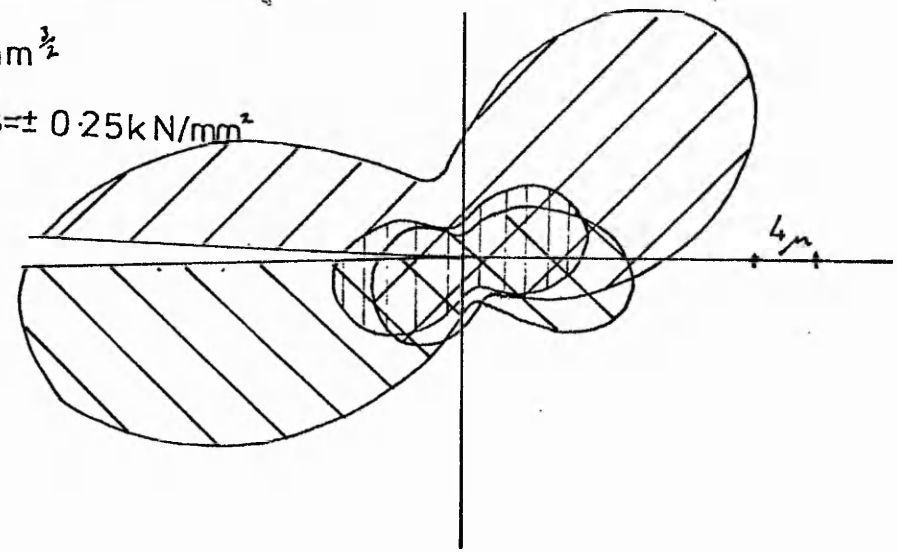


(e)

$K_I = 0.03\ kN/mm^{3/2}$

$K_{II} = 0.06\ kN/mm^{3/2}$

Applied stress = $\pm 0.25 kN/mm^2$



The effect of in plane residual stress on plastic zone size.
Fig. 89.

therefore superposition is acceptable, fig.89. As can be seen, the plastic zones at crack tips may be modified very considerably, and, further, they completely lack symmetry. Following an argument similar to that presented in the previous section, it must be true that the crack growth rate is modified. The nature of the modification is difficult to quantify because of the asymmetry of the plastic zones with respect to the crack centre-line. A fracture mechanics explanation for the modified wear rates of chapter two might be interpreted as the reduction in size of the plastic zone on one side of the crack by either tensile or compressive residual stresses. This is only speculation.

Under mode I conditions the value of the stress ratio $R = \frac{\sigma_{min}}{\sigma_{max}}$ has some influence on the rate of crack growth, as well as on the threshold level. For $R > 0$, ΔK_{IC} falls as R increases for nickel, though for steel the rate of crack growth seems independent of R (165). A complete independence from R is reported by Ohta and Sasaki(166). However, all these experiments were performed for R in the range -1 to +1, and for the wear case $R \approx -10$, for which no values are available. Thus values used above were obtained in vastly different environments from those occurring under wear conditions, so that their suitability is in question.Recent work by Francois(167) on the influence of hydrostatic stress on fracture may eventually facilitate better predictions.

A paper was written on the determination of crack growth rates from mode I data, explained in section 5.2,(168).

6. Shakedown

6.1 Concept of Shakedown

In previous chapters, the stress distribution beneath various sliding and rolling contact geometries has been investigated, together with the influence of a pre-existing static stress system. If the yield criterion is never exceeded, it is reasonable to assume that any pre-existing stresses will persist, and the shape of the contact patch will change only steadily, as material is worn away. However, if the yield criterion is exceeded, three things will occur so that the system may quickly reach a state of elastic equilibrium;

A. In the case of some geometries, such as a ball rolling on a flat block, plastic flow of the block will occur to produce a shallow groove. The contact patch will now be much larger, so that the mean contact pressure is lower, reducing the resultant stresses.

B. Work hardening will occur, increasing the yield stress, and therefore increasing the size of the yield envelope.

C. The system will tend towards a shakedown state. This involves the creation of residual stresses, which, together with the applied stresses, may produce a state of stress which lies within the yield surface. It should be noted that a system may shake down without any increase in yield stress, and throughout this chapter models will be presented based on ideally elasto-plastic behaviour.

Shakedown in continuous media occurs because as a component, loaded beyond the elastic limit, is unloaded, stresses develop which are of opposite sign to those produced by the load. These stresses are maintained by elastic recovery of the

surrounding material, and reduce the nett value of stresses produced by a subsequent application of the load.

The "shakedown limit" is the largest load which may be applied, which, together with the optimum residual stress system, lies within the yield criterion. The "elastic limit" is the largest load which may be applied, without exceeding the yield criteion, in the absence of residual stresses. Use will be made of Melan's theorem, an explanation of which is given in English by Symonds(169). This states that if some residual stress system (even if rather contrived) may be found, which, together with the applied stress system, lies within the yield surface, the system will shake down, though not necessarily in the way proposed,ie. the residual stresses may differ from those speculated.

Shakedown has two important implications for wear. First, whilst tribological components should not be over designed, for economy, it is desirable that plastic flow should not persist. In rolling components this would not be catastrophic immediately, but would acceleate fatigue failure, and give rise to the forward flow of surface layers, as observed by Crook(170) and later by Hamilton(171). Secondly, the nature of the self-generated stresses may be very important. Fujita and Yoshida(172,173) found that when two cylinders of different widths were rolled together, a tensile stress developed perpendicular to the surface-this would accelerate mode I growth. Various studies of residual stresses in railway lines have also found deleterious tensile stresses perpendicular to the free surface (174,175).

The first contribution to shakedown theory in tribology was made by Johnson(176) who showed that the shakedown

limit for two cylinders rolled together is;

$$\frac{p_o}{\tau_o} \leqslant 4{\cdot}00 \qquad (97)$$

Johnson obtained this result by an examination of the stress history projected onto the deviatoric (π) plane, but a simpler proof which may immediately be extended to a sliding cylinder is as follows: consider the sliding or rolling cylinder of fig.3. The problem is strictly two-dimensional and it should be noted that the residual stresses must, when the load has passed, satisfy the equilibrium equations themselves. These are;

$$\begin{aligned} \frac{\partial \sigma_{xx}}{\partial x} + \frac{\partial \tau_{xy}}{\partial y} + \frac{\partial \tau_{xz}}{\partial z} &= 0 \\ \frac{\partial \tau_{xy}}{\partial x} + \frac{\partial \sigma_{yy}}{\partial y} + \frac{\partial \tau_{yz}}{\partial z} &= 0 \\ \frac{\partial \tau_{zx}}{\partial x} + \frac{\partial \tau_{yz}}{\partial y} + \frac{\partial \sigma_{zz}}{\partial z} &= 0 \end{aligned} \qquad (98)$$

Because stresses cannot vary with respect to y or z, we note that; $\frac{\partial \sigma_{ij}}{\partial y} = \frac{\partial \sigma_{ij}}{\partial z} = 0$ Thus;

$$\frac{\partial \tau_{xz}}{\partial x} = \frac{\partial \tau_{yz}}{\partial x} = \frac{\partial \sigma_{xx}}{\partial x} = 0 \qquad (99)$$

Since the free surface must remain clear of all tractions, and stresses do not vary with depth;

$$\tau_{xz} = \tau_{yz} = \sigma_{xx} = 0 \quad \forall x \qquad (100)$$

Because there can be no residual orthogonal shear, the shakedown limit for these cases may be expressed as;

$$\tau_{xy} \leqslant \tau_o \qquad (101)$$

For a rolling cylinder $\tau_{xymax} = 0{\cdot}25\ p_o$, giving equation 97.

Later, Johnson proposed an explanation for the forward flow phenomenon, and at the same time worked out the nature of the residual stresses (177). He did this by assuming that the strains were given by the extended elastic strains,

if the yield criterion were not greatly exceeded, and using the Prandtl-Reuss flow rules. These results were then generalized to a sliding cylinder (178).

It is possible to extend this technique and examine the 'no-plasticity' condition when there is a pre-existing residual stress system. The essential difference between shakedown and previously built in stresses is that the former are totally independent (subject to the yield criterion and equilibrium requirements), whereas the latter are, of course, cylindrical, ie. $\sigma_{yyr} = \sigma_{zzr} = \sigma_r$ (where the added subscript r just refers to a residual stress). Consider now the second invariant of the stress deviator tensor;

$$J_2 = \frac{1}{6}\left\{ (\sigma_{xx}-\sigma_{yy})^2+(\sigma_{yy}-\sigma_{zz})^2+(\sigma_{zz}-\sigma_{xx})^2 \right\} + \tau_{xy}^2 + [0] \quad (102)$$

If the shakedown limit of equation 101 is to be attained it is clear that the term within the braces must be zero. Since $\sigma_{xxr}=0$, we have;

$$\sigma'_{xx} = \sigma'_{yy} + \sigma_{yyr} = \sigma'_{zz} + \sigma_{zzr}$$

$$\text{or} \quad \sigma_{yyr} = \sigma'_{xx} - \sigma'_{yy} \qquad \text{where ' indicates stress}$$
$$\sigma_{zzr} = \sigma'_{xx} - \sigma'_{zz} \qquad \text{due to contact load alone} \quad (103)$$

If the residual stresses are not independent the term within the braces must instead simply be minimised.

$$\text{ie.} \quad \frac{d}{d\sigma_r}\left\{ (\sigma'_{xx}-\sigma'_{yy}-\sigma_r)^2+(\sigma'_{yy}-\sigma'_{zz})^2+(\sigma'_{zz}+\sigma_r-\sigma'_{xx})^2 \right\} = 0$$

$$\text{ie.} \quad -2(\sigma'_{xx}-\sigma'_{yy}-\sigma_r) + 2(\sigma'_{zz}+\sigma_r-\sigma'_{xx}) = 0$$

$$\sigma_r = \tfrac{1}{2}(2\sigma'_{xx}-\sigma'_{yy}-\sigma'_{zz}) \quad (104)$$

The new effective value of J_2 is;

$$J_2^* = \frac{1}{6}\left\{ (\tfrac{1}{2}\sigma'_y-\tfrac{1}{2}\sigma'_z)^2+(\sigma'_z-\sigma'_y)^2+(\tfrac{1}{2}\sigma'_y-\sigma'_z)^2 \right\} + \tau_{xy}^{2\prime}$$
$$= \tfrac{1}{4}(\sigma'_z-\sigma'_y)^2+\tau_{xy}^{2\prime} \quad (105)$$

When the shakedown condition is reached at the surface first, ie $\mu \geq 0{\cdot}367$ the worst stresses occur at the origin

and are;

$$\sigma_{xx} = \sigma_{yy} = \frac{\sigma_{zz}}{2\nu} = \frac{\tau_{xy}}{\mu} = -p_o \qquad (106)$$

Subtituting these values into equation 101 it is clear that the shakedown limit is;

$$\frac{p_o}{\tau_o} \leqslant \frac{1}{\mu} \qquad (107)$$

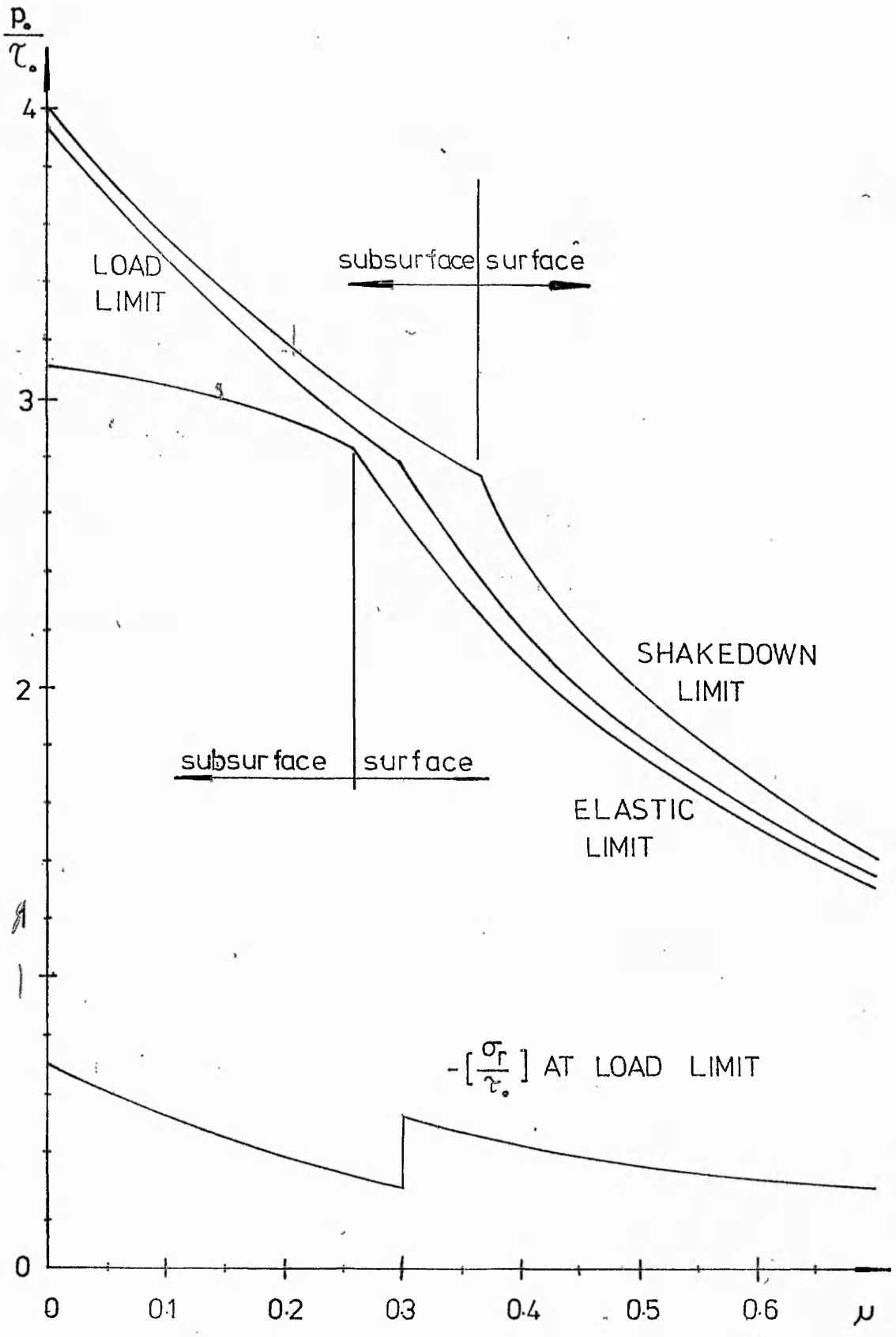
and the load limit is; (see below for definition)

$$\frac{p_o}{\tau_o} \leqslant \frac{1}{\sqrt{0{\cdot}04+\mu^2}} \qquad (\nu=0{\cdot}3) \qquad (108)$$

so that as μ becomes large the two quantites tend to the same value.

A computer programme was written, based on Smith and Liu's solution (equation 25) to determine the elastic limit, shakedown limit and "load limit", the last quantity being the largest load which may be applied, in addition to the optimum cylindrical residual stress system, without causing plasticity. The results are summarised in fig.90. The elastic limit based on Tresca's criterion, found by Johnson, is omitted for clarity. Note, too, that a load limit based on Tresca's criterion would coincide with the shakedown limit, since only one degree of freedom is required to maintain the largest principal shear stress equivalent to τ'_{xy}. Table 7 summarises the results found, and it should be noted that the optimum residual stress depends on the applied load. This is not too serious, because the value of the applied stresses will not become critical until near the load limit, and therefore residual stresses based on this pressure should be used.

A graph of the optimum residual stresses is shown in fig.91, and an illustration of the contraction of the plastic zones caused by these residual stresses is given



GRAPH OF ELASTIC, SHAKEDOWN & LIMIT LOADS - CYLINDER

Fig. 90.

in fig.33.

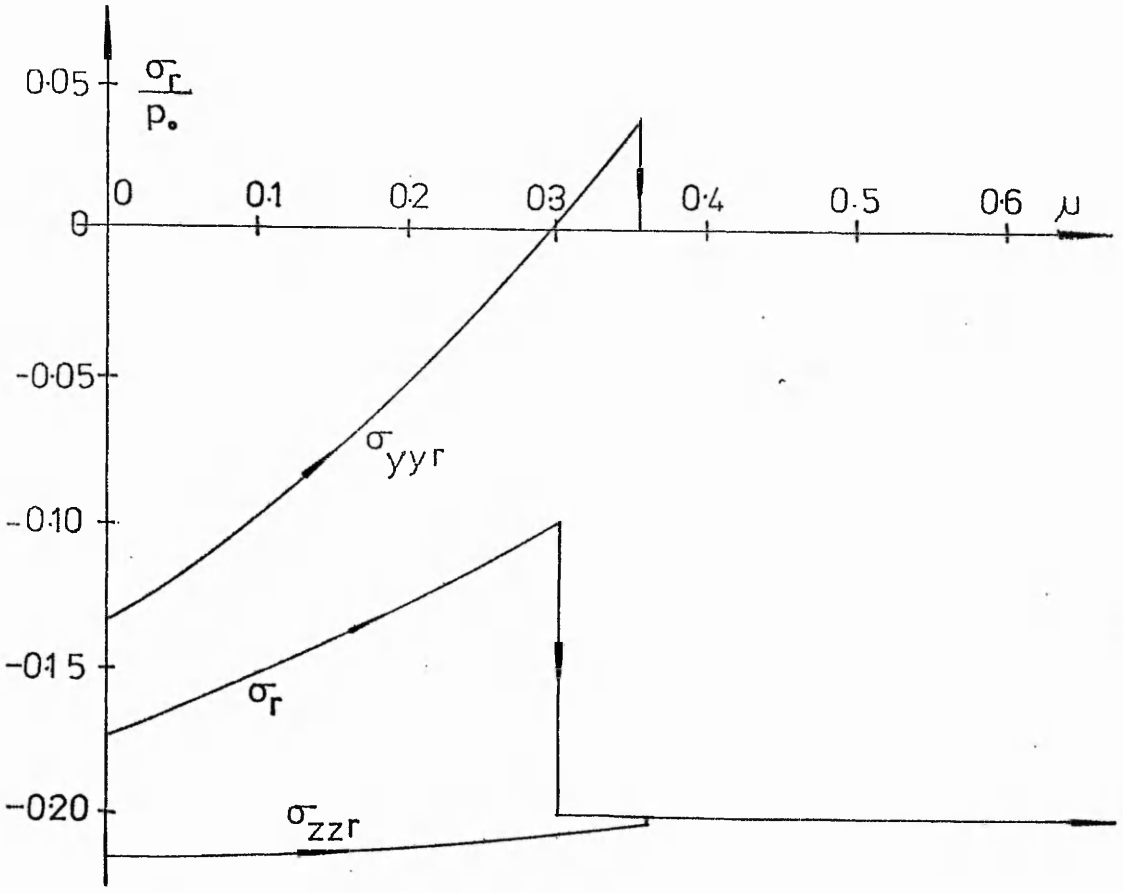
Table 7. Shakedown results for Sliding Cylinder

μ	y^*	x^*	$\frac{\tau_{xymax}}{p_o}$	S.L.$(\frac{\tau_o}{p_o})$	L.L.$(\frac{\tau_o}{p_o})$	$\frac{\sigma_r}{p_o}\Big\|_{optimum}$
0	$\pm$0·866	-0·500	0·250	4·00	3·95	-0·174
0·1	0·866	-0·452	0·281	3·56	3·49	-0·152
0·2	0·864	-0·415	0·312	3·20	3·10	-0·128
0·3	0·861	-0·384	0·345	2·90	2·78	-0·102
0·367	0·858	-0·366	0·367	2·73	2·59	-0·083

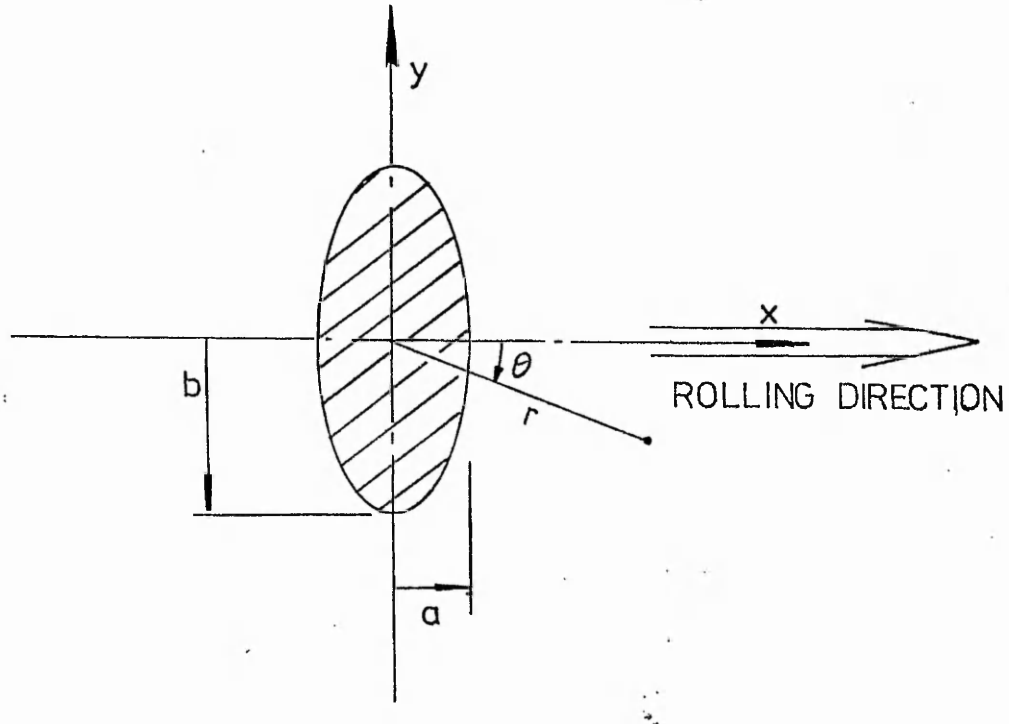
where S.L. = shakedown limit L.L.= load limit

Note that when μ = 0·367 the surface value of the shear stress is equal to that found subsurface, and subsequently higher values of μ are substituted into equations 107 and 108 respectively to find the S.L. and L.L.

A second configuration which was examined was that of two balls rolling or sliding together, or indeed any arrangement resulting in a circular contact patch and Hertzian loading. The elastic limit is clearly achieved on the plane of symmetry, ie. y=0, fig.21, and may be found by using the solution for the elastic stresses, found by Hamilton and Goodman(83). The shakedown condition presents extra problems. It has been shown that for two dimensional rolling or sliding contact, the shakedown limit is governed by the orthogonal shear (equation 101). It will now be shown that under a general elliptical contact patch, for rolling contact, the same limitation applies. It has not been possible to devise a line of argument to show that the same condition applies for a sliding three-dimensional contact, and this,regretably, has therefore been assumed. The results are entirely consistent with



Residual stresses beneath a cylinder – self generated & optimum.
Fig.91.



General elliptical rolling-contact patch. Fig.92

other cases treated more rigorously.

Fig.92 shows a plan view of one contacting body, with a general elliptical contact patch. By careful considerations of symmetry, the following relations are apparent;

$$\begin{aligned}
\tau_{xz}(\theta) &= \tau_{xz}(-\theta) = -\tau_{xz}(\pi-\theta) \\
\tau_{yz}(\theta) &= -\tau_{yz}(-\theta) = \tau_{yz}(\pi-\theta) \\
\tau_{xy}(\theta) &= -\tau_{xy}(-\theta) = -\tau_{xy}(\pi-\theta)
\end{aligned} \tag{109}$$

Thus, residual stresses τ_{xz} and τ_{xy} can be of no benefit. Two possible shakedown limits are therefore;

$$\tau_{xz} \leqslant \tau_o$$
$$\tau_{xy} \leqslant \tau_o$$

The solution for the elastic stresses in polar coordinates for a <u>circular</u> contact patch were given by Huber(87). These are (with dimensions normalized to the contact radius);

$$\frac{\sigma_{\theta\theta}}{p_o} = -\left\{ \frac{(1-2\nu)}{3r^{*2}} \left[1 - \left(\frac{z^*}{\sqrt{u}} \right)^3 \right] + \frac{z^*}{\sqrt{u}} \left[2\nu + \frac{(1-\nu)u}{1+u} - (1+\nu)\sqrt{u}\tan^{-1}\left(\frac{1}{\sqrt{u}} \right) \right] \right.$$

$$\frac{\sigma_{rr}}{p_o} = \left\{ \frac{(1-2\nu)}{3r^{*2}} \left[1 - \left(\frac{z^*}{\sqrt{u}} \right)^3 \right] + \left(\frac{z^*}{\sqrt{u}} \right)^3 + \frac{u}{u^2+z^{*2}} + \frac{z^*}{\sqrt{u}} \left[\frac{(1-\nu)u}{1+u} + (1+\nu)\sqrt{u}\tan^{-1}\left(\frac{1}{\sqrt{u}} \right) - 2 \right] \right\} \tag{110}$$

$$\frac{\sigma_{zz}}{p_o} = -\left\{ \left(\frac{z^*}{\sqrt{u}} \right)^3 \frac{u}{u^2+z^{*2}} \right\}$$

$$\frac{\tau_{rz}}{p_o} = -\left\{ \frac{r^* z^{*2}}{u^2+z^{*2}} \right\} \left\{ \frac{\sqrt{u}}{1+u} \right\}$$

And from symmetry, $\tau_{z\theta} = \tau_{r\theta} = 0$

where $u = \frac{1}{2}\left[r^{*2}+z^{*2}-1 \sqrt{\left\{ (r^{*2}+z^{*2}-1)^2 + 4z^{*2} \right\}} \right]$

Transforming now into Cartesian coordinates;

$$\begin{aligned}
\sigma_{xx} &= \sigma_{rr}\cos^2\theta + \sigma_{\theta\theta}\sin^2\theta \\
\sigma_{yy} &= \sigma_{rr}\sin^2\theta + \sigma_{\theta\theta}\cos^2\theta \\
\sigma_{zz} &= \sigma_{zz}
\end{aligned} \tag{111}$$

$$\tau_{xy} = \tfrac{1}{2}(\sigma_{rr} - \sigma_{\theta\theta})\sin 2\theta$$
$$\tau_{xz} = \tau_{rz}\cos\theta \qquad (111)$$
$$\tau_{yz} = \tau_{rz}\sin\theta$$

Maximising τ_{xy} with respect to θ ;

$$\frac{\partial \tau_{xy}}{\partial \theta} = (\sigma_{rr} - \sigma_{\theta\theta})\cos 2\theta = 0 \Rightarrow \theta = \frac{\pi}{4}$$

Substituting from equations 110 the maximum value of τ_{xy} is;

$$\frac{\tau_{xy}}{p_o} = \left\{ \frac{(1-2\nu)}{3r^{*2}}\left[1 - \left(\frac{z^*}{u}\right)^3 \right] + \left(\frac{z^*}{\sqrt{u}}\right)\left[\frac{z^{*2}}{2(u^2+z^{*2})} - \frac{(1-\nu)}{(1+u)} \right] \right\}$$

It tanspires that the maxima and their locations are;

$$\left.\frac{\tau_{xy}}{p_o}\right|_{max} = 0{\cdot}05 \quad \text{at } z^* = 0{\cdot}5 \;, \; r^* = 1{\cdot}11$$

$$\left.\frac{\tau_{xz}}{p_o}\right|_{max} = 0{\cdot}214 \text{ at } z^* = 0{\cdot}35 \;, \; r^* = 0{\cdot}848$$

It is clear that the orthogonal shearing stress again provides the shakedown limit, which is given by;

$$\frac{p_o}{\tau_o} \leqslant 4{\cdot}675 \qquad (112)$$

In the case of elliptical contact, as $\frac{b}{a} \longrightarrow \infty$ the shear τ_{xymax} falls continuously to zero, and it is therefore reasonable to assume that the orthogonal shear provides the limiting factor in all practical shakedown conditions under traversing contact loading.

Returning to the problem of shakedown with a circular sliding contact patch, great care must be taken when evaluating the stresses, because of the indeterminate nature of the equations given by Hamilton and Goodman. In their notation, consistent with fig.21;

$$y = 0, \quad r^* = x^*$$
$$\therefore R_1^{*2} = z_2^{*2} + x^{*2}$$
$$= (x^{*2} + z^{*2} - 1) + 2iz^*$$

Let $R_2^{*2} = J e^{i\lambda}$, then $J = \sqrt{\{(x^{*2} + z^{*2} - 1)^2 + 4z^{*2}\}}$

$\lambda = \tan^{-1}\{2z^* / (x^{*2} + z^{*2} - 1)\}$

If $R_2^* = \phi + i\psi$ (say)

then $\phi = \sqrt{J}\cos(\lambda/2)$

$\psi = \sqrt{J}\sin(\lambda/2)$

The imaginary parts of the functions F-H required are;

$$F = \tfrac{1}{2}(z^*\psi - \phi) + \tfrac{1}{2}x^{*2}\Gamma$$

$$F_x = -\frac{x^*}{2J}\alpha + x^*\Gamma - \frac{x^{*3}}{2JK}(2\phi\psi + \alpha)$$

$$F_z = \tfrac{1}{2}\psi(1 - (z^{*2} + x^{*2} + 1)/J)$$

$$G = -\frac{\psi}{3}\beta + \tfrac{1}{2}z^*\alpha - \tfrac{1}{3} + \tfrac{1}{2}z^*x^{*2}\Gamma$$

$$H = \tfrac{4}{3}z^* - \frac{\psi}{6}z^*\beta + \tfrac{1}{2}\phi\delta - \tfrac{1}{4}x^{*2}\alpha - \tfrac{1}{4}x^{*4}\Gamma$$

$$H_z = \tfrac{4}{3} - \frac{\psi}{6}\beta - \tfrac{1}{2}z^*\alpha + \tfrac{3}{2}(z^*\phi - \psi) - \frac{x^{*2}}{4}\left\{\psi + \frac{1}{J}[2z^*\phi - \psi(z^{*2} + x^{*2} - 1)]\right\}$$

$$H_{xz} = -x^*\psi\{1 - (z^{*2} + 1)/J\} + \frac{x^{*3}}{4J}\left\{5\psi + [\psi(1 - z^{*2})\beta + 2z^*\phi\delta]/J^2\right\} + \frac{x^{*5}\psi}{4J^3}\beta$$

where;

$$\alpha = z^*\psi + \phi$$

$$\beta = 3\phi^2 - \psi^2$$

$$\delta = \phi^2 - 3\psi^2$$

$$\Gamma = \tan^{-1}\left\{\frac{\psi + 1}{\phi + z}\right\}$$

$$K = (\phi + z^*)^2 + (\psi + 1)^2$$

The stresses due to the tractive force on the surface are;

$$\frac{\sigma_{xx}}{\mu p_0} = \frac{1}{x^{*3}}\left\{(H\nu - \tfrac{1}{2}z^*H_z) + (1 - \nu)x^*H_x + \tfrac{1}{2}x^*z^*H_{xz} - 2\nu x^{*2}F\right\}$$

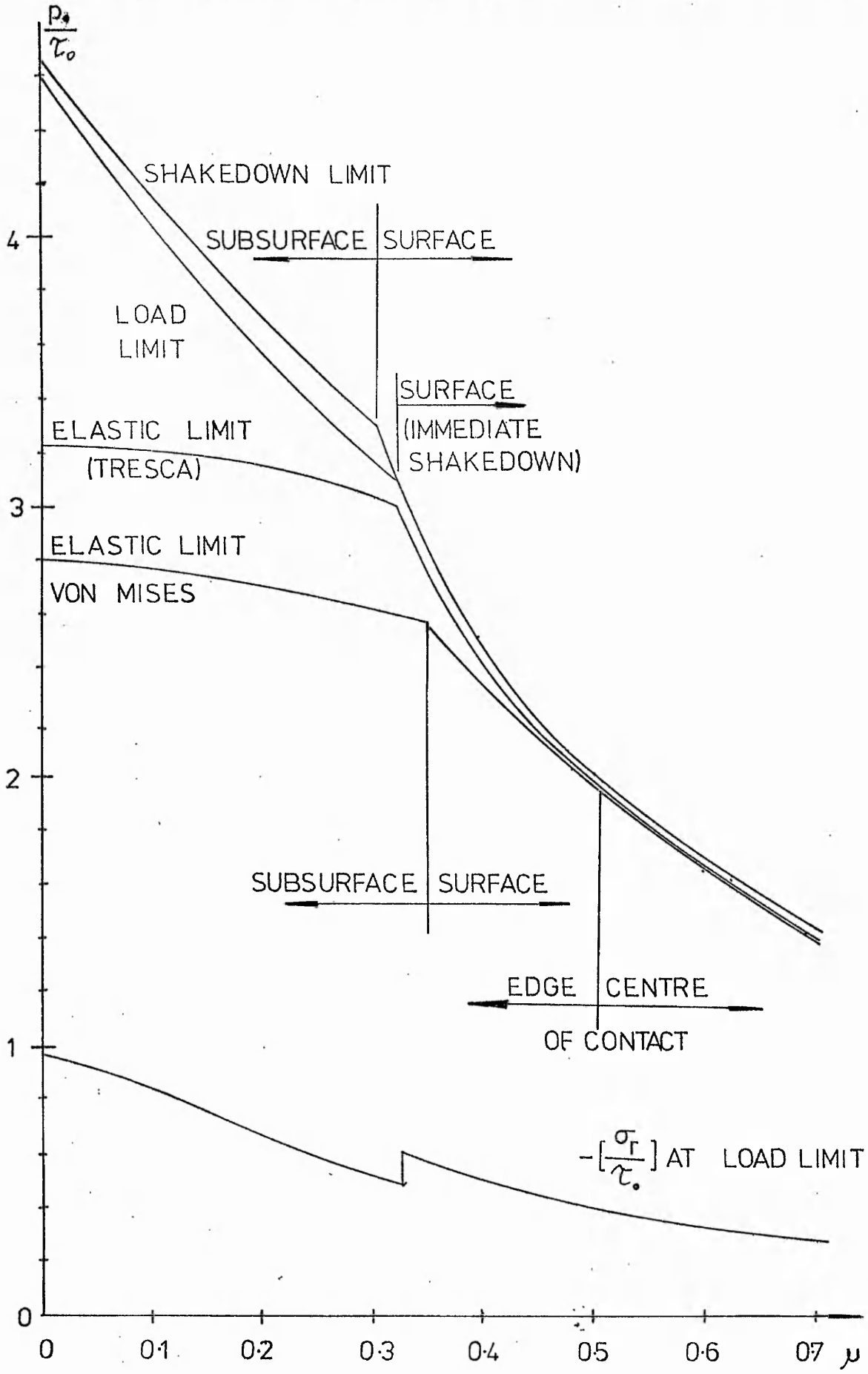
$$\frac{\sigma_{yy}}{\mu p_0} = \frac{1}{x^{*3}}\left\{-(H\nu - \tfrac{1}{2}z^*H_z) - 2\nu x^{*2}F\right\}$$

$$\frac{\sigma_{zz}}{\mu p_0} = \left(\frac{z^*}{x^*}\right)F_z \qquad (113)$$

$$\frac{\tau_{xz}}{\mu p_0} = \frac{1}{x^{*2}}\left\{2G + \tfrac{1}{2}H_z + z^*(F + x^*F_x) - 2\nu^*F\right\}$$

$$\tau_{xy} = \tau_{yz} = 0$$

The stresses due to the normal component of contact load may be found from equations 110 and superimposed.



Elastic, shakedown & load limits - circular contact patch. Fig 93.

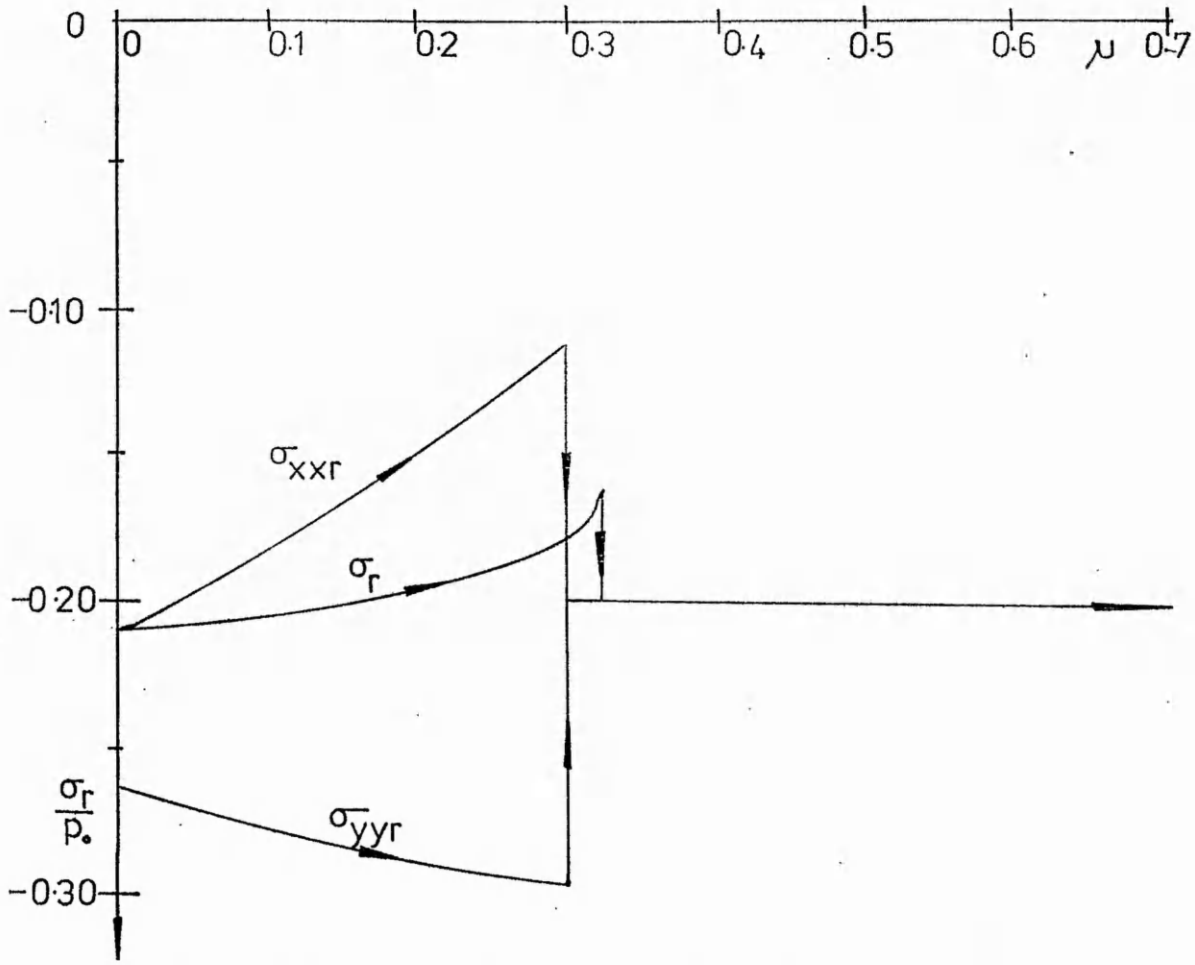
Fig.93 shows the variation of shakedown, elastic and limit loads found exactly as before, whilst fig.94 summarises the optimum residual stresses. Table 8 also summarises the results obtained, and fig.95 shows how the critical points vary with friction. The results found are generally similar to those obtained by finite elements by Rydholm and Fredriksson(179), who also deliberately assumed that the residual stresses need not obey any specific constitutive relation (Ponter's theorem). Their curves differ for the shakedown limit, when this is attained subsurface, and show higher values in this region. Because of their totally numerical method it is difficult to see where the discrepancy lies, but their higher values are consistent with fewer constraints imposed on the nature of the residual stresses.

Table 8.Shakedown Results for a Sliding Ball.

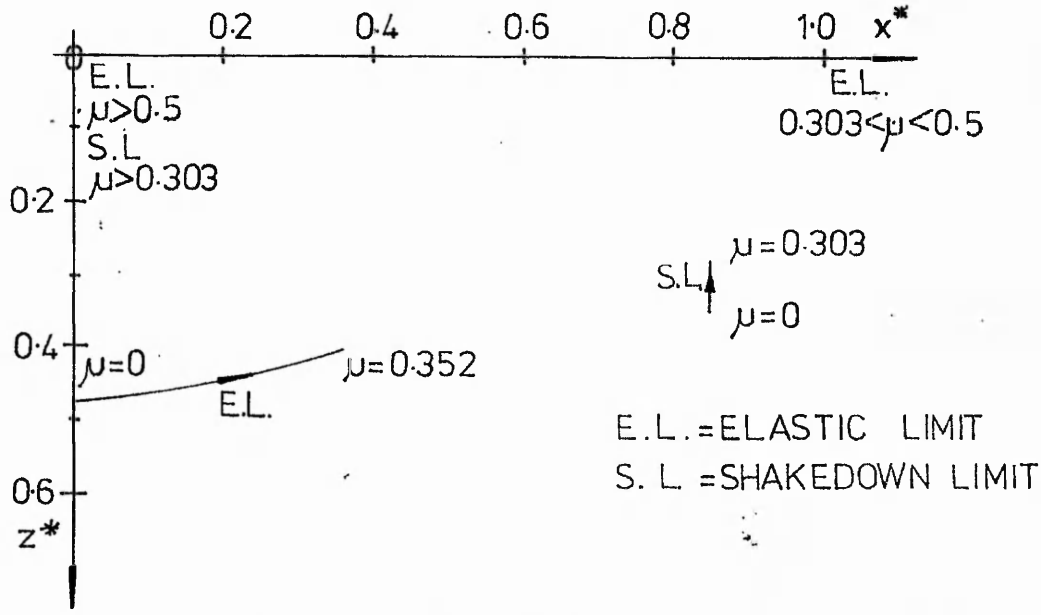
μ	x^*	z^*	S.L.$(\frac{\tau_o}{p_o})$	L.L.$(\frac{\tau_o}{p_o})$	$\frac{\sigma_r}{p_o}$ optimum
0	0·848	0·350	4·675	4·632	-0·208
0·1	0·849	0·321	4·129	4·054	-0·205
0·2	0·847	0·298	3·683	3·574	-0·187
0·3	0·842	0·278	3·315	3·170	-0·179
0·32	0·841	0·274	surface	3·077	-0·163

At higher coefficients of friction the shakedown and load limits both occur at the surface. Their values are easily found from the simple relations given by Hamilton and Goodman. The S.L. is given by; $\frac{\tau_o}{p_o} \geq \mu$

Although the foregoing results are of fundamental interest, their use is rather limited. This is because, as a rolling ball on a flat shakes down, a groove is created



Residual stresses beneath a circular contact-self generated and optimum. Fig 94.



Location of point of achievement of elastic & shakedown limits. Fig. 95

so that the contact becomes elliptical. This problem is now considered in detail.

6.2 Shakedown of a rolling ball in a Groove

It has been mentioned that a heavily loaded rolling ball creates a groove, and hence an elliptical contact contact patch,with repeated rolling passes. The minor axis of the ellipse is aligned with the direction of rolling. In the case of a railway carriage wheel rolling along a length of railway track the contact again is nearly elliptical, but with the major axis extending along the rolling direction (fig.96.). The solution of the "elliptical" shakedown problem is therefore of practical interest.

Since the shakedown condition has been established as $\tau_{xz} \leqslant \tau_o$, the problem is reduced to solving the Hertz problem on the plane y=0, for elliptical contact. The usual restrictions of isotropy and homogeneity apply, and it should be noted with reference to fig.96a that the larger contact semi-axis should be rather less than the smallest principal radius of curvature. Fessler and Ollerton(180) have experimentally shown that the Hertz conditions are certainly satisfied if;

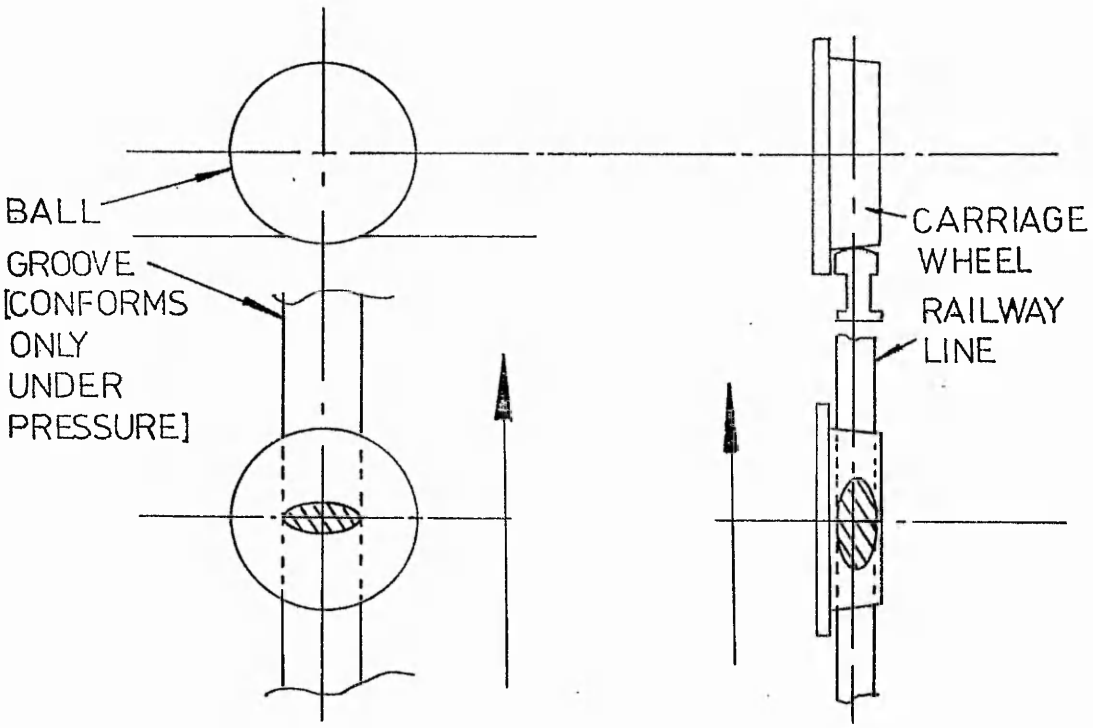
$$b < 0{\cdot}3\ R_{ball} \qquad (114)$$

In the same paper, the solution is also given for τ_{xz}; much of the theory is contained in Love(181), which should also be consulted. For the plane y=0, where the severest stresses act, the auxilliary variable γ, when normalized with respect to the semi-minor axis, becomes;

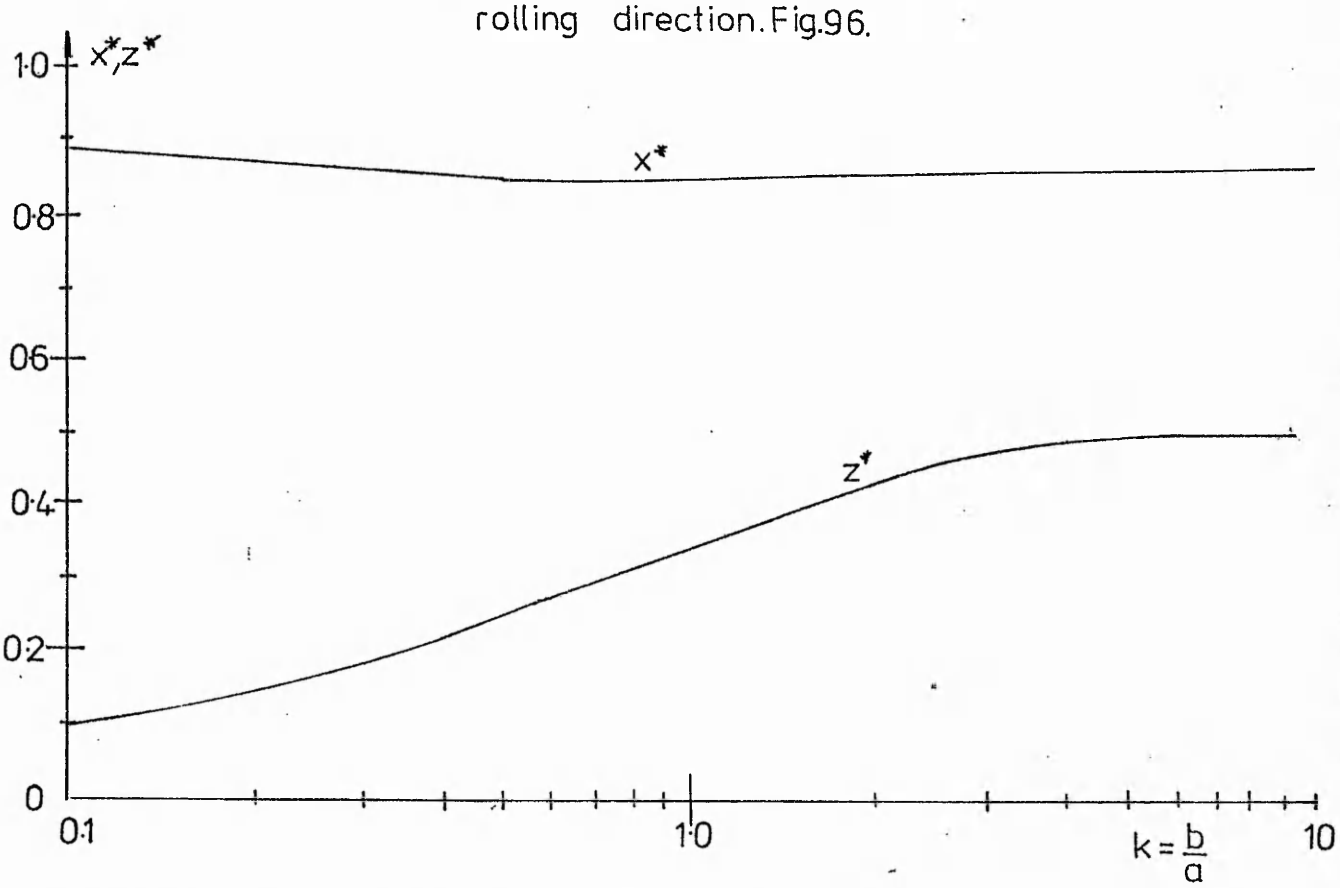
$$\gamma^* = \frac{1}{2}\left\{-\left(1 - x^{*2} - z^{*2}\right) + \sqrt{\left[\left(1 - x^{*2} - z^{*2}\right)^2 + 4z^{*2}\right]}\right\} \qquad (115)$$

Then;

$$Q = \frac{x^* z^{*2} \left(\gamma^* + \gamma^{*2}\right)^{-3/2} \cdot \left(k^2 + \gamma^*\right)^{-\frac{1}{2}}}{\left(\frac{x^*}{1+\gamma^*}\right)^2 + \left(\frac{z^*}{\gamma^*}\right)^2} \qquad (116)$$



Examples of contact ellipse aligned & perpendicular to rolling direction. Fig.96.



Location of maximum orthogonal shearing stress. Rolling direction parallel to 'a'. Fig.97.

and the shear stress is given by;

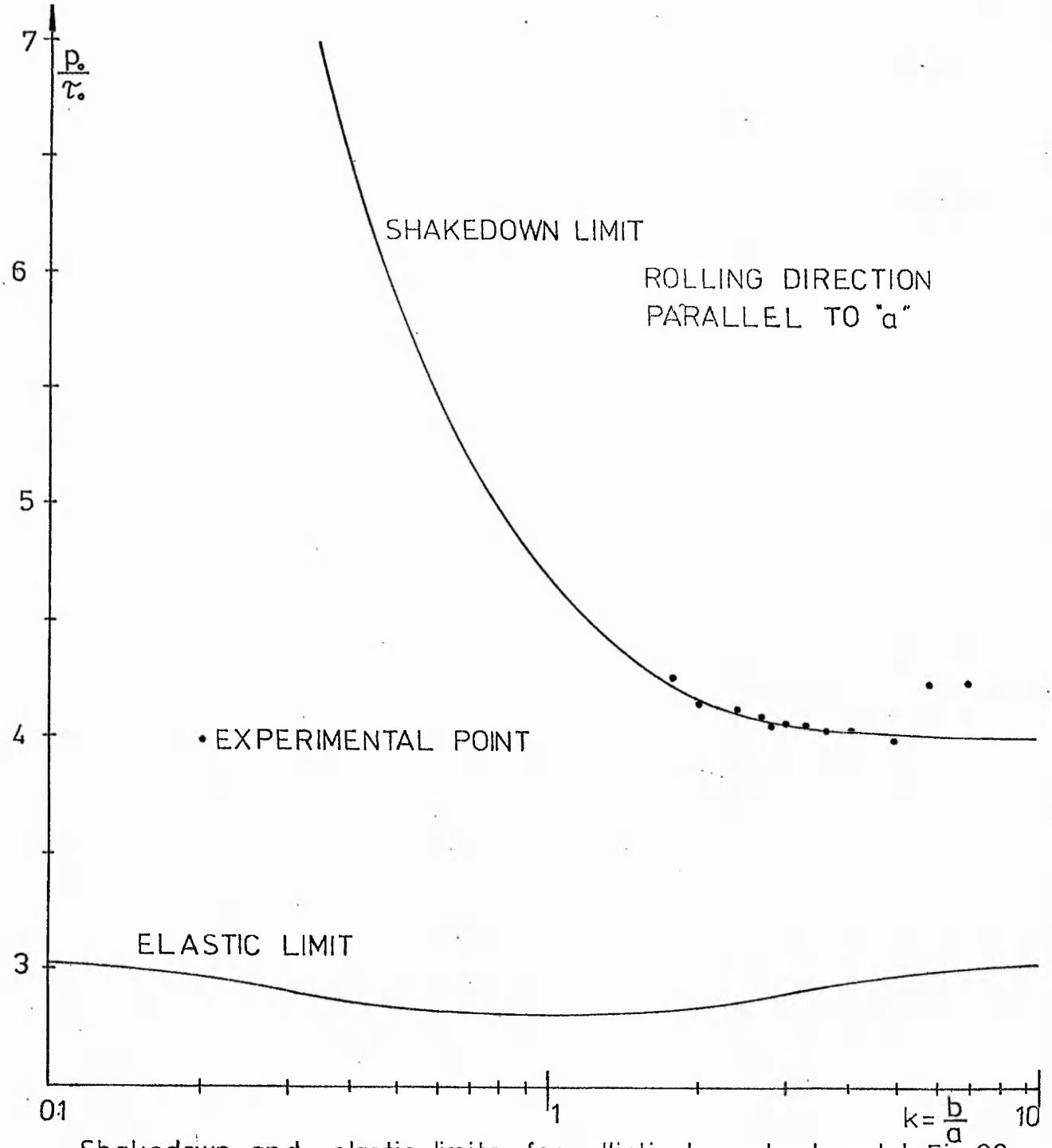
$$\tau_{xz} = -p_o kQ \qquad (117)$$

and the shakedown limit (equations 109) may be written;

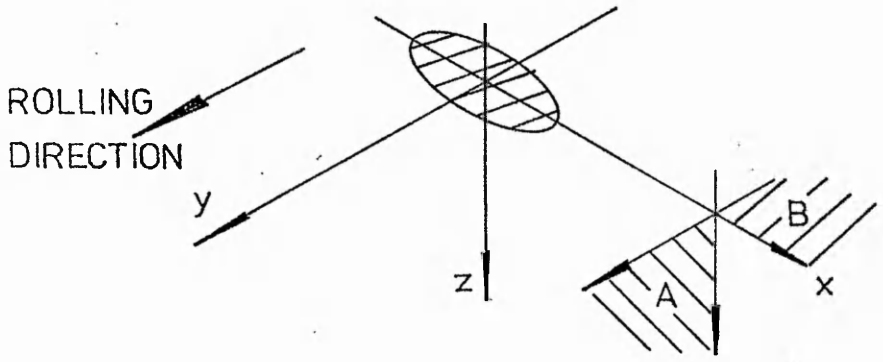
$$-kQ \leqslant \frac{\tau_o}{p_o} \qquad (118)$$

The results were checked for two special cases, viz. k=1 (circular contact) and $k \to \infty$ (strip contact of two cylinders) and the shakedown limits of equations 97 and 112 were confirmed. The depths of severest shearing stress found are shown in fig.97, and fig.98 shows the variation of shakedown limit with oblateness,k. From the figure it may be seen that the shakedown limit becomes very large as k becomes very small (very elongated contact length parallel with the direction of rolling). Under these circumstances the criterion of secondary plastic flow, ie. flow upon unloading,becomes limiting, so that $2J_2 \leqslant k^2$. The shakedown limit corresponding to this inequality is $p_o \leqslant 8\tau_o$. Also shown in the figure is the variation of elastic limit with oblateness.

It is easy to find the elastic limit when once the complete elastic solution is known, using a classical yield criterion. However, only limited solutions exist for the case of the Hertz problem with an elliptical contact. The stresses on the z-axis have been determined by Thomas and Hoersch(182) and are expressed in terms of elliptic integrals. These could be used to find the elastic limit, but in the present investigation the initial spread of plasticity at loads up to the shakedown limit was required. Although strictly speaking this requires a proper elasto-plastic solution, it is usual to accept that provided the plasticity is well contained by elastic material the elastic solution provides a good estimate of the elastic-plastic boundary.



Shakedown and elastic limits for elliptical contact patch. Fig. 98.



A change of axes. Fig. 99

Consider fig.99, with the rolling direction now along the y-axis. To determine the elastic limit and the spread of plasticity across the groove, attention may still be confined to the y=0 plane. Examination of the planes A and B shows that $\tau_{xy} = \tau_{yz} = 0$, because of symmetry. Since τ_{xz} is known (equation 117) the problem reduces to a determination of the three direct stresses. One solution is given by Ollerton and Morey(26);

$$\frac{\sigma_{zz}}{p_o} = \frac{-k z^{*3}\left[(1+\gamma^*)(k^2+\gamma^*)\right]^{-1/2}\gamma^{*-5/2}}{\left(\frac{x^*}{1+\gamma^*}\right)^2 + \left(\frac{z^*}{\gamma^*}\right)^2} \qquad (119)$$

The other stresses must be determined from first principles, using the method set out by Thomas and Hoersch(182), and by Love(181), qq.v.;

$$\sigma_{xx} = \frac{1}{2\pi}\left\{2\nu\frac{\partial\phi}{\partial z} - z\frac{\partial^2\phi}{\partial x^2} - (1-2\nu)\frac{\partial^2\chi}{\partial x^2}\right\}$$
$$\sigma_{yy} = \frac{1}{2\pi}\left\{2\nu\frac{\partial\phi}{\partial z} - z\frac{\partial^2\phi}{\partial y^2} - (1-2\nu)\frac{\partial^2\chi}{\partial y^2}\right\} \qquad (120)$$

where $\phi = \iint \frac{p'}{r}\,dx'dy' \quad \& \quad \chi = \iint p' l_3 (z+r)\,dx'dy'$

But $\sigma_{xx}, \sigma_{yy} \to 0$ as $z \to \infty$, so that;

$$\frac{\partial^2\chi}{\partial x^2} = -\int_z^\infty \frac{\partial^2\phi}{\partial x^2}\,dz \quad ; \quad \frac{\partial^2\chi}{\partial y^2} = -\int_z^\infty \frac{\partial^2\phi}{\partial y^2}\,dz \qquad (121)$$

If the assumption is made that the potential, ϕ, is a homogeneous ellipsoid;

$$\phi = \frac{3p}{4}\int_\gamma^\infty \left\{1 - \frac{x^2}{a^2+\psi} - \frac{y^2}{b^2+\psi} - \frac{z^2}{\psi^2}\right\}\frac{d\psi}{\left[(a^2+\psi)(b^2+\psi)\psi\right]^{1/2}} \qquad (122)$$

where γ is the positive root of the equation;

$$1 - \frac{x^2}{a^2+\gamma} - \frac{y^2}{b^2+\gamma} - \frac{z^2}{\gamma} = 0 \qquad (123)$$

Note that this is the same form as equation 115, when y=0, $\gamma^* = \frac{\gamma}{a^2}$. Differentiation of equation 122 may now be carried out for substitution into equations 120 and 121.

$$\frac{\partial\phi}{\partial z} = -\frac{3pz}{a^3}\int_{\sqrt{\gamma^*}}^\infty \frac{d\omega}{\omega^2(1+\omega^2)^{1/2}(k^2+\omega^2)^{1/2}} \qquad (124)$$

where $\psi = a^2\omega^2$, $k = b/a$

Similarly; $$\frac{\partial \phi}{\partial x} = -\frac{3P_x}{a^3}\int_{\sqrt{\gamma^*}}^{\infty}\frac{d\omega}{(1+\omega^2)^{3/2}(k^2+\omega^2)^{1/2}} \qquad (125)$$

$$\frac{\partial \phi}{\partial y} = -\frac{3P_y}{a^3}\int_{\sqrt{\gamma^*}}^{\infty}\frac{d\omega}{(1+\omega^2)^{1/2}(k^2+\omega^2)^{3/2}} \qquad (126)$$

The second derivatives may now be found;

$$\frac{\partial^2 \phi}{\partial z^2} = -\frac{3P}{a^3}\int_{\sqrt{\gamma^*}}^{\infty}\frac{d\omega}{\omega^2(1+\omega^2)^{1/2}(k^2+\omega^2)^{1/2}} + \frac{3P_z}{a^3\gamma^*(1+\gamma^*)^{1/2}(k^2+\gamma^*)^{1/2}}\frac{d\sqrt{\gamma^*}}{dz} \qquad (127)$$

$$\frac{\partial^2 \phi}{\partial x^2} = -\frac{3P}{a^3}\int_{\sqrt{\gamma^*}}^{\infty}\frac{d\omega}{(1+\omega^2)^{1/2}(k^2+\omega^2)^{3/2}} + \frac{3P_x}{a^3(1+\gamma^*)^{3/2}(k^2+\gamma^*)^{1/2}}\frac{d\sqrt{\gamma^*}}{dz} \qquad (128)$$

Restricting attention to the y=0 plane, advantage may be taken of this in writing the last second derivative;

$$\frac{\partial^2 \phi}{\partial y^2} = -\frac{3P}{a^3}\int_{\sqrt{\gamma^*}}^{\infty}\frac{d\omega}{(1+\omega^2)^{1/2}(k^2+\omega^2)^{3/2}} \qquad (129)$$

where, in equations 127 and 128;

$$\frac{d\sqrt{\gamma^*}}{dz} = \frac{z}{\gamma^{*3/2}}\left\{\frac{x^2}{(1+\gamma^*)^2} + \frac{y^2}{(k^2+\gamma^*)^2} + \frac{z^2}{\gamma^{*2}}\right\}^{-1} \qquad (130)$$

It may now be seen that the evaluation of the σ_{xx} stress presents very much greater difficulties than the σ_{yy} stress, since the integration of equation 128 in equation 121 presents a formidable challenge. The solution for σ_{yy} will be dealt with first, since it may be performed without recourse to numerical methods.

First note that the relevant equation 121 may be integrated by parts, thus;

$$\frac{\partial^2 \chi}{\partial y^2} = z\frac{\partial^2 \phi}{\partial y^2} + \int_z^{\infty} z\frac{\partial^3 \phi}{\partial y^2 \partial z}\,dz \qquad (131)$$

$\frac{\partial^2 \phi}{\partial y^2}$ is already known, and the third derivative may be written as;

$$\frac{\partial}{\partial z}\left\{\frac{\partial^2 \phi}{\partial y^2}\right\} = \frac{d\sqrt{\gamma^*}}{dz}\cdot\frac{d}{d\sqrt{\gamma^*}}\left\{\frac{\partial^2 \phi}{\partial y^2}\right\} \qquad (132)$$

The integral (I_1) of equation 131 may now be written as;

$$I_1 = \int_{\sqrt{\gamma^*}}^{\infty}\frac{3P_z\,d\sqrt{\gamma^*}}{a^3(1+\gamma^*)^{1/2}(k^2+\gamma^*)^{3/2}} = \frac{3P}{a^2}\int_{\sqrt{\gamma^*}}^{\infty}\frac{\sqrt{\gamma^*}(\gamma^*+1-x^{*2})^{1/2}d\sqrt{\gamma^*}}{(1+\gamma^*)(k^2+\gamma^*)^{3/2}} \qquad (133)$$

After several substitutions this transpires to be an elementary integral whose solution is;

$$I_1 = \frac{3P x^*}{a^2 (k^2-1)^{3/2}} \left[\boxed{H} - \tan^{-1} \boxed{H} \right] \qquad (134)$$

where $$\boxed{H} = \sqrt{\left\{ \frac{k^2-1}{x^{*2}} \right\}} \sqrt{\left\{ \frac{\gamma^* + 1 - x^{*2}}{\gamma^* + k^2} \right\}}$$

It will be noted that the solution is restricted to the open interval $k<1$, unless the inverse tangent is expanded as a series. However, an alternative solution suitable for numerical integration overa finite interval is;

$$I_1 = \frac{3P}{a^2} \int_0^{\sqrt{\gamma^*}} \frac{u \sqrt{\{1+u^2(1-x^{*2})\}}\, du}{(1+u^2)(1+k^2u^2)^{3/2}} \qquad (135)$$

The other integrals needed are elliptic and may be solved using the method given in Thomas and Hoersch;

$$\int_{\sqrt{\gamma^*}}^{\infty} \frac{d\omega}{\omega^2 (1+\omega^2)^{1/2} (k^2+\omega^2)^{1/2}} = \frac{\tau}{k^2 \gamma} - \frac{E(\phi, k')}{k^2}$$

$$\int_{\sqrt{\gamma^*}}^{\infty} \frac{d\omega}{(1+\omega^2)^{3/2} (k^2+\omega^2)^{1/2}} = \frac{1}{k'^2} \left\{ F(\phi, k') - E(\phi, k') \right\} \qquad (136)$$

$$\int_{\sqrt{\gamma^*}}^{\infty} \frac{d\omega}{(1+\omega^2)^{1/2} (k^2+\omega^2)^{3/2}} = \frac{1}{k'^2} \left[\left(\frac{1}{k^2}\right) E(\phi, k') - F(\phi, k') - \frac{\tau}{k^2 \sqrt{\gamma^*}} + \frac{1}{\tau \sqrt{\gamma^*}} \right]$$

where $$k'^2 = 1 - k^2 \,, \quad \sqrt{\gamma^*} = \cot \phi \,, \quad \tau = \sqrt{\frac{k^2+\gamma^*}{1+\gamma^*}}$$

Note that by making the modifications of substituting $\frac{1}{k}$ for k and (ak) for k, the same equations may be used for finding the σ_{xx} stress on the plane x=0.

To find the σ_{xx} stress on the y=0 plane, it is necessary to return to equations 121. Integrating by parts as before gives the result;

$$\frac{\partial^2 \chi}{\partial x^2} = z \frac{\partial^2 \phi}{\partial x^2} + \int_z^{\infty} z \frac{\partial^3 \phi}{\partial x^2 \partial z} \, dz \qquad (137)$$

In this instance there is no question of being able to

evaluate the integral (I_2) analytically. Instead, a convenient form of the integral was found, so that numerical integration could easily be applied, over a finite interval;

$$I_2 = \frac{3P}{a^2}\int_0^{\sqrt{s^*}} \left\{ \frac{(1+u^2)^2 - u^4 x^{*2}}{(1+k^2u^2)^{1/2}(1+u^2)^{7/2}} \right\} \left\{ u\left(\textcircled{H} + x^* \Phi\right) - x^* \textcircled{H}^2 \Gamma \right\} du \qquad (138)$$

where;

$$\Gamma = u^2 \left\{ \frac{3}{1+u^2} + \frac{1}{1+k^2u^2} \right\}$$

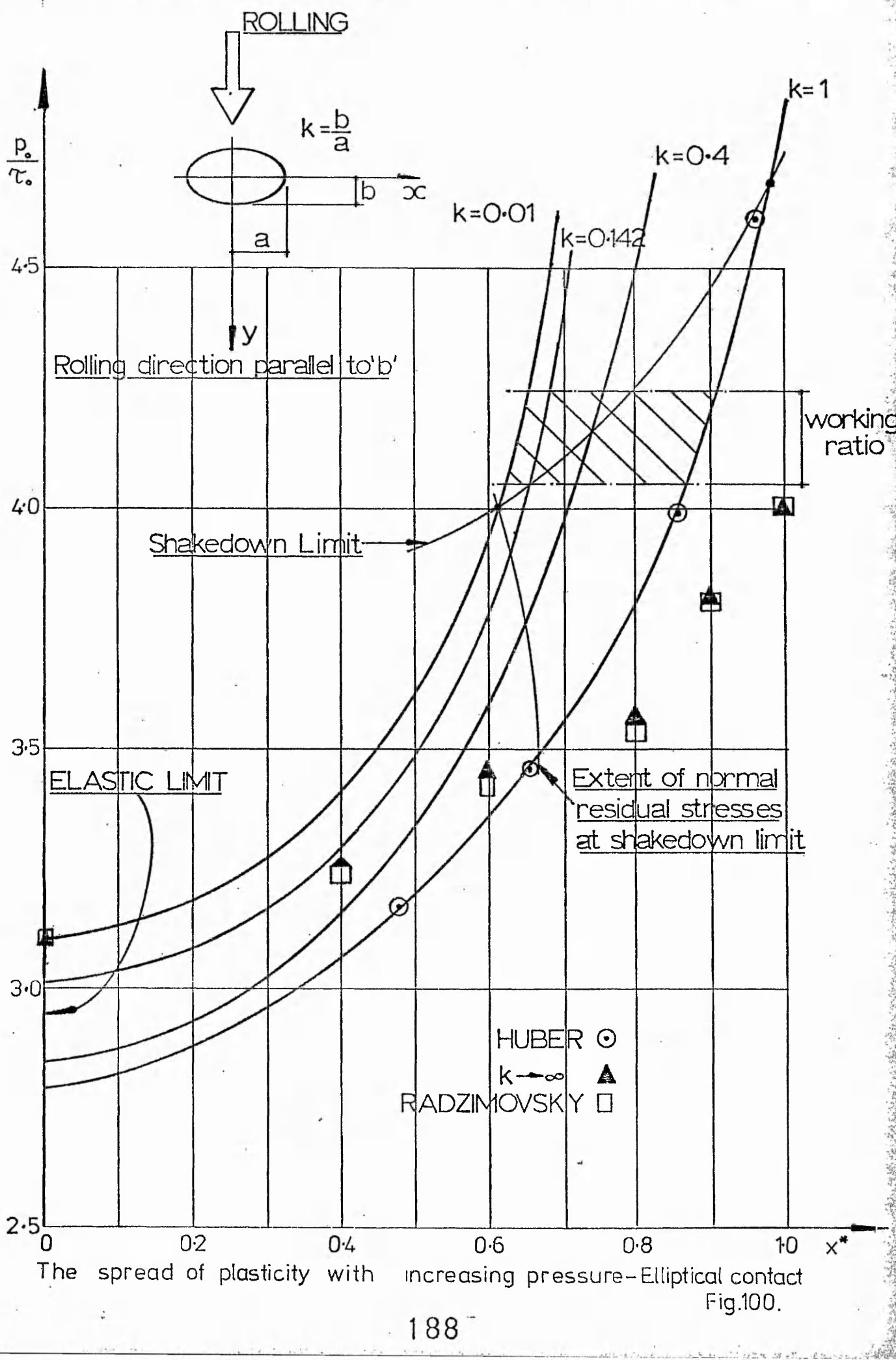
$$\textcircled{H} = \sqrt{\left\{ 1 - \frac{u^2 x^{*2}}{1+u^2} \right\} \frac{(1+u^2)}{\left[(1+u^2)^2 - u^4 x^{*2}\right]}}$$

$$\Phi = \frac{4(1+u^2)^6 \left(1 - \frac{u^2 x^{*2}}{1+u^2}\right)}{\left[(1+u^2)^2 - u^4 x^{*2}\right]^3} \left\{ \frac{x^{*2} u^3}{(1+u^2)^3} + u\left(1 - \frac{u^2 x^{*2}}{1+u^2}\right) \right\} +$$

$$+ \frac{u(1+u^2)^2}{\left[(1+u^2)^2 - u^4 x^{*2}\right]} - \frac{5u(1+u^2)^4 \left(1 - \frac{u^2 x^{*2}}{1+u^2}\right)}{\left[(1+u^2)^2 - u^4 x^{*2}\right]^2}$$

The other integrals present no problems and, as before, may be written down as elliptical integrals using equations 136. The solution for σ_{xx} on the y=0 plane may, mutatis mutandis, be used to find σ_{yy} on x=0.

All six stresses are now known on one plane of symmetry. Owing to the possibility of an algebraic or computing error a check on the solution was thought desirable. This was done by estimating the lateral spread of plasticity for loads above the elastic limit. Huber's solution (k=1) and Radzimovsky's solution (k→∞) were used for comparison, and the results are shown in fig.100. The fit is good, and is probably limited by round off error, as a 200-strip integration was used. With the soluion's accuracy established the elastic limit was determined for several values of k and these were plotted on fig.98. Since plasticity always starts on the z-axis it is immaterial whether the contact ellipse lies across or parallel to the direction of rolling,



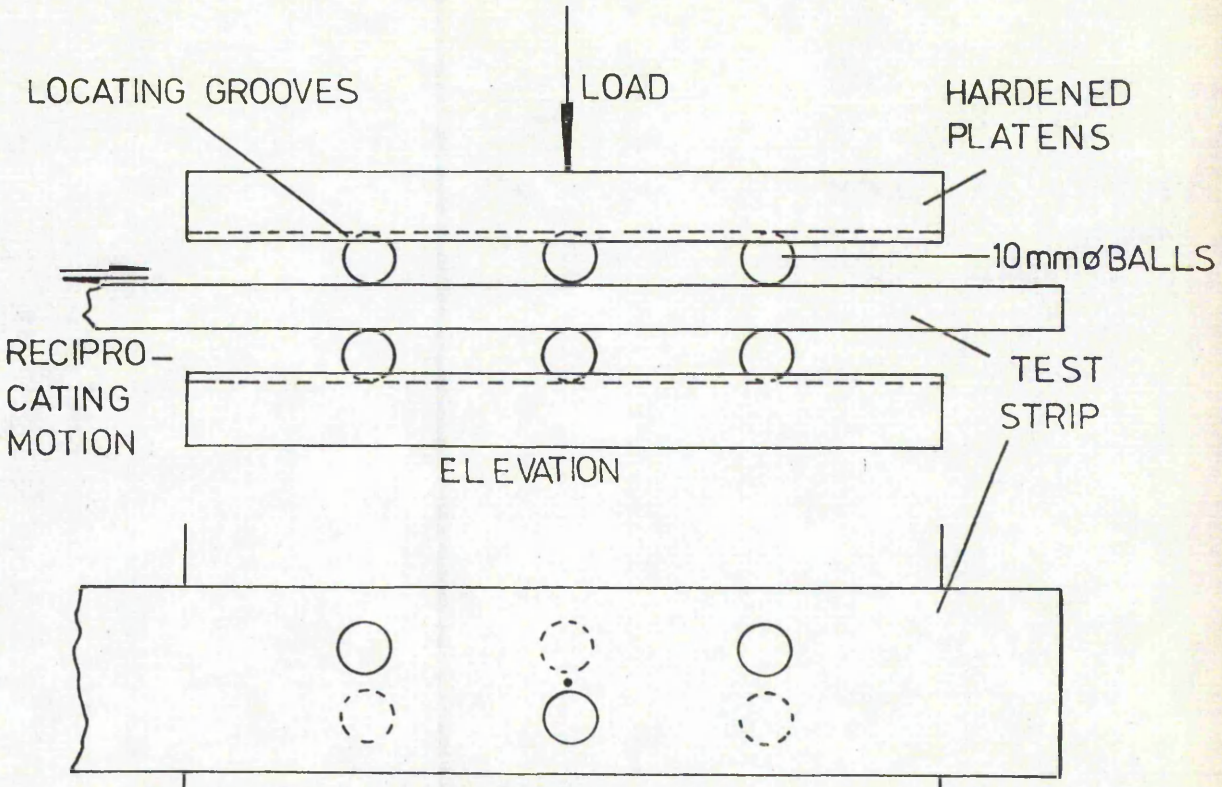
The spread of plasticity with increasing pressure – Elliptical contact

Fig.100.

as can be seen. Fig.100 also summarises the initial extent of plasticity for several oblatenesses, for the case of a ball rolling in a groove,ie. the shorter axis parallel to the direction of rolling. Shown on the same diagram are the shakedown limit, and the extent of the normal residual stresses, which will be discussed later. The relative extents of the inital plasticity zones, for different geometries is perhaps worth noting.

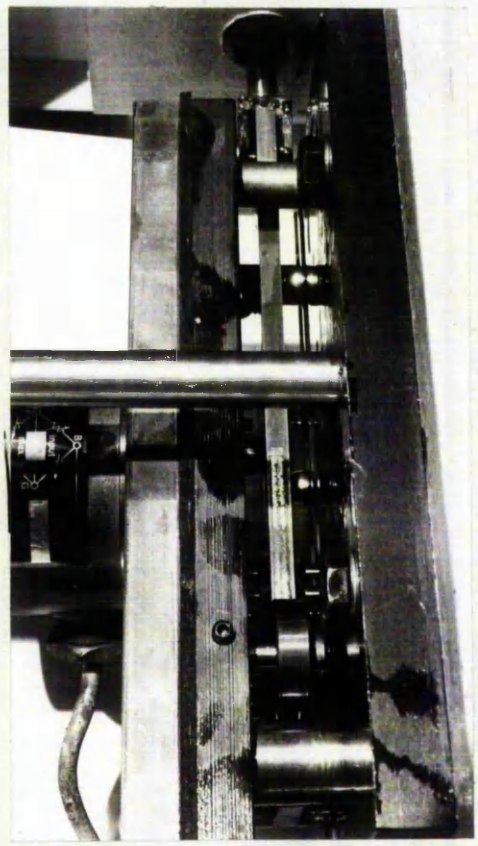
In their classic paper, Merwin and Johnson(177) were able quite accurately to estimate the residual stresses and strains occurring when two cylinders are rolled together. They used the Prandtl-Reuss rules to determine what the stresses would be if they were forced to return to their original dimensions after compression, and then permitted some stresses to relax to satisfy equilibrium with the free surface. A similar technique was tried for the geometry presently under consideration, but without success. This was because insufficient boundary conditions could be found to indicate how the material should be allowed to relax after compression; the Prandtl Reuss solution itself presented comparatively few difficulties. A theoretical treatment of the complete residual stress and strain field still, therefore, seems too difficult.

A check on the attainment of the shakedown limit was thought desirable, and fig.101 outlines the main part of the apparatus used. The loading platens are free to move vertically only, whilst the sample is oscillated over a distance of $2\frac{1}{2}$ inches, by a Scotch-Yoke arrangement. Because of the way the balls are arranged, the central ones carry a constant load, whilst the others are subjected to

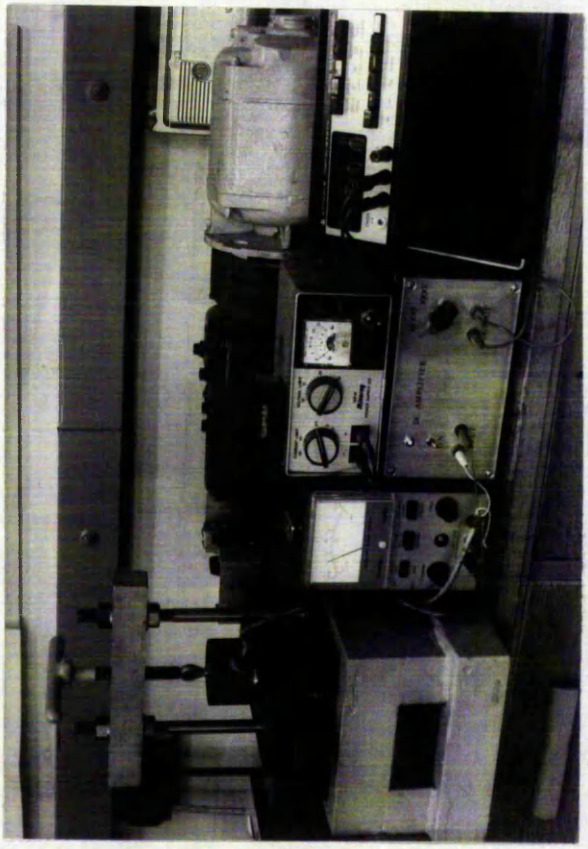


APPARATUS USED IN SHAKEDOWN TESTS

Fig.101.



DETAIL OF BALL ARRANGEMENT



GENERAL VIEW

Apparatus used in determining the shakedown limit of a Rolling Ball. Fig.102

a linearly varying load. Where possible a dead load was used, though for higher contact pressures a loading frame had to be used, which meant some variation in applied force because of the varying compliance of the apparatus as the balls moved to and fro (fig.102 shows load cell). Applied loads were chosen so that initially there was considerable plastic deformation, and a groove was formed. As the groove develops the contact area increases and so the peak pressure falls. At the same time, because of yielding, residual stresses develop. Eventually an equilibrium is reached when the rolling ball is supported completely elastically, and the configuration has shaken down.

At several stations along the groove, width measurements were taken using a Swiss Universal Measuring Instrument (which has a resolution of 0·1μm). Also, at each point, a profile of the cross-section of the groove was taken using a Talysurf profilometer. A typical trace, illustrating the flow of material to either side of the groove, and the continuity of the cross-section, even in the built-up ridge, is shown in fig.103. Careful measurements were taken from the profile traces and plotted in a normalised form so that the shape of the groove could be visualised (fig. 104). It is clearly parabolic.

Since the contact surfaces were second order, and the contact elastic,it seemed reasonable to use Hertzian mechanics to analyze the problem. However, it was recognised that the presence of subsurface residual stresses was probably altering the groove's profile, and so the measured radius was not used in calculations. (Note that Hertzian mechanics assumes that a small arc of a circle may adequately

be represented by a parabola, so no accuracy is lost when speaking of the "measured radius". It is simply given by $R_G^o = -\frac{a^2}{w_o}$).

To proceed, it was necessary to assume that the groove width was the same as the major axis of the contact ellipse. This may not be as bad an approximation as at first appears because, as can be seen from fig.103, the built-up ridges fall away quite abruptly, and are unlikely to contribute much support beyond the groove width. Thus, the load, one axis dimension and three principal curvatures are known;

$$\begin{aligned} &\text{Ball;} \quad R_1 = R_2 = R_B \\ &\text{Groove;} \quad R_1' = \infty \qquad R_2' = R_G \end{aligned} \tag{139}$$

The second axis dimension and groove radius may be determined using the standard relations for elliptical contact. In the usual nomenclature (see Timoshenko and Goodier, ref. (122));

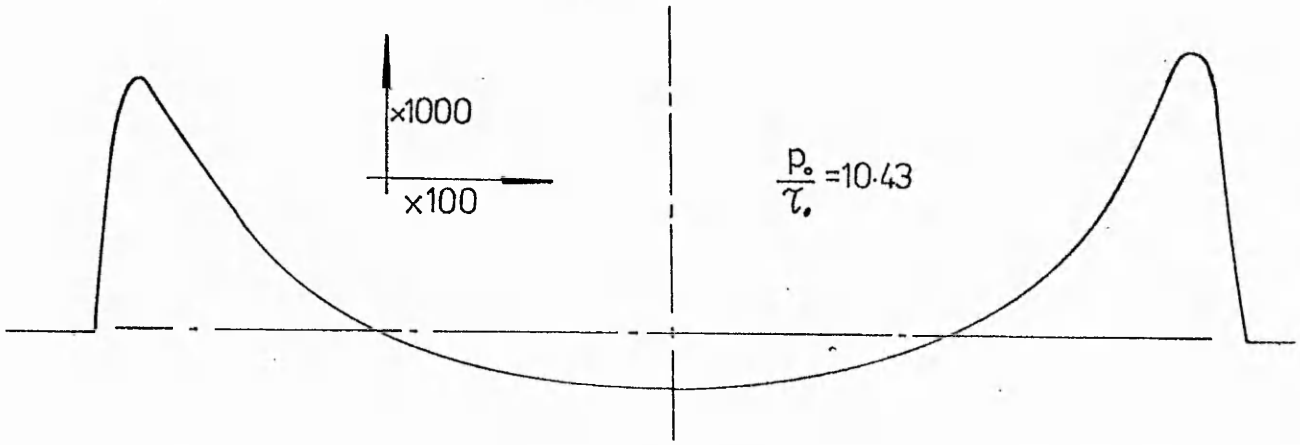
$$\begin{aligned} A + B &= \frac{1}{R_B} - \frac{1}{2R_G} \\ B - A &= \frac{1}{2R_G} \end{aligned} \tag{140}$$

$$a = m \sqrt[3]{\left\{ \frac{3\pi}{4} \frac{P(k_1 + k_2)}{A + B} \right\}} \qquad b = n \sqrt[3]{\left\{ \frac{3\pi}{4} \frac{P(k_1 + k_2)}{A + B} \right\}} \tag{141}$$

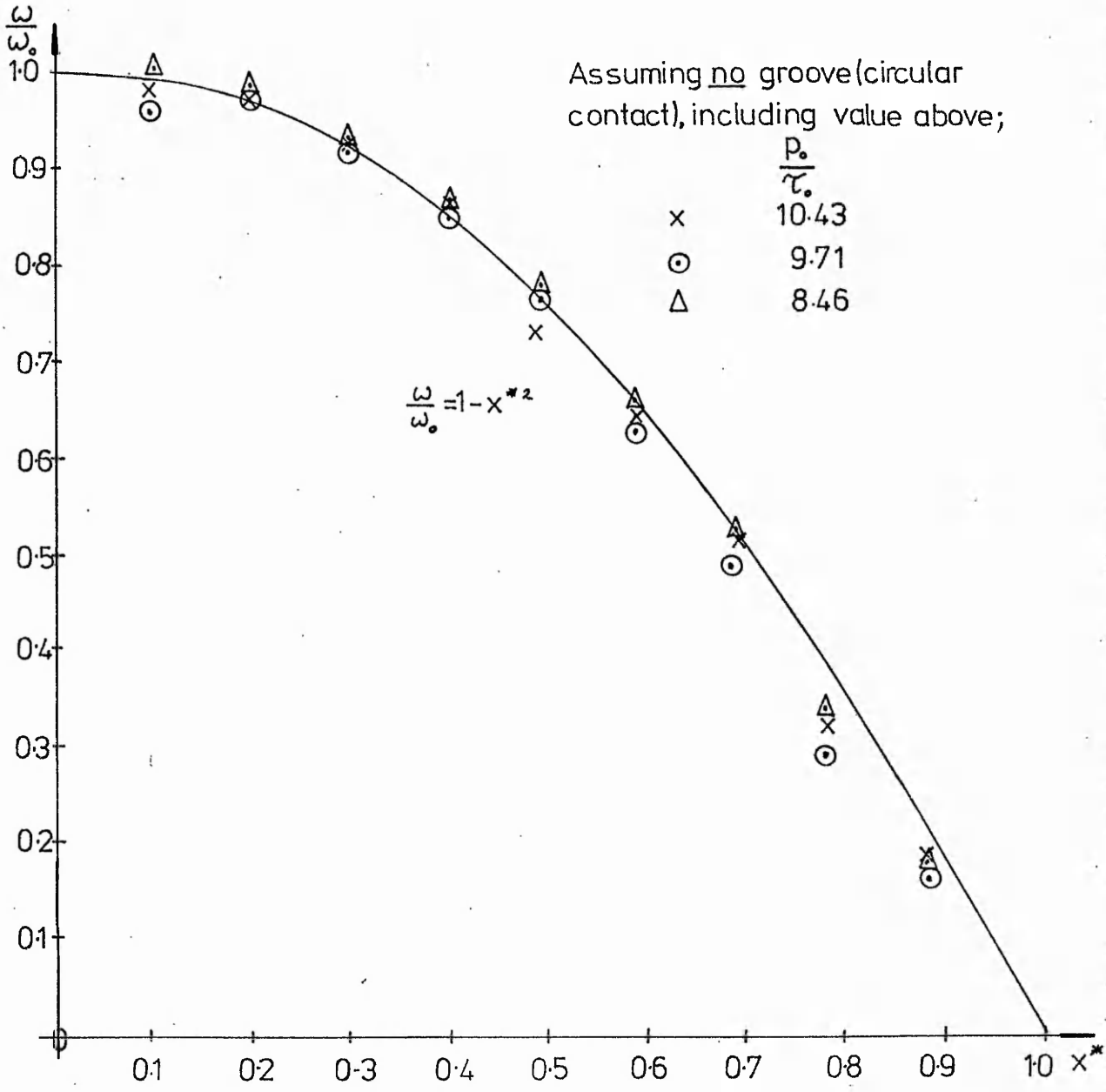
The auxilliary angle λ is introduced, defined by;

$$\cos\lambda = \frac{B-A}{B+A} \tag{142}$$

and the variables m, n and λ are related by a table such as that reproduced on p.416, ref.(122). An iterative solution procedure was adopted. A value of R_G was guessed and substituted into equations 140. Then, using equation 142 a value for λ was found. Using the table mentioned, m was determined and substituted into the first of equations 141, enabling a new estimate of (A+B), and hence R_G to be found. The procedure was repeated until convergence



A typical Talysurf trace of the Groove Cross Section Fig.103.



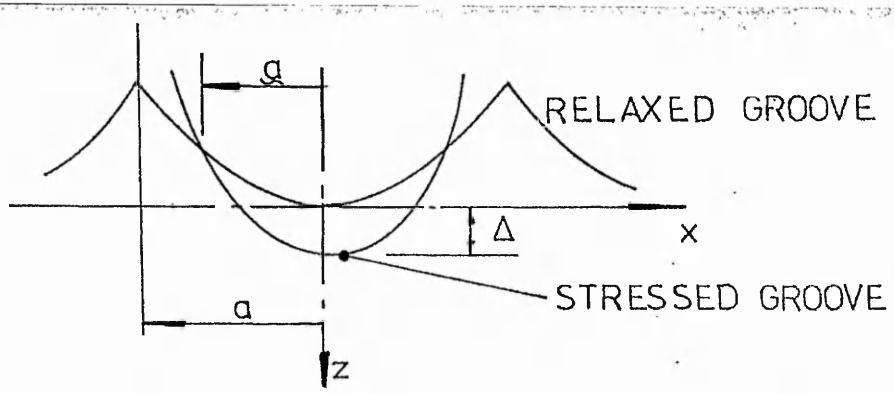
Form of the groove rolled into the specimen. Fig.104.

occurred. As the groove radius conformed more and more to the ball (under increasing load) the solution oscillated, and some care was required: also, the angle λ becomes small and an extension of the table cited, due to Kornhauser (183) was needed. When R_G and hence λ are known, it is simple to find the contact dimensions, and hence the peak contact pressure;

$$p_o = \frac{3P}{2\pi ab} \qquad (143)$$

A complicating factor which arises in the case of real materials is strain hardening of the surface layers due to plastic flow. This effect is naturally more pronounced when greater flow has occurred, and so micro-indentation tests were perfomed along the groove centre-line to determine the 'steady-state' yield stress. Table 9 summarises some of the experimental results obtained for copper (chosen because of its large yield strain), and the results for the shakedown limit are plotted on fig.98. It seems clear that the shakedown limit is reached, though the range of geometries which can be tested by this technique is rather limited.

As an extension to the conclusions drawn from this set of tests, some attempt was made at establishing the residual stresses. Since the shakedown results seemed internally consistent, some reliance might be placed on the associated (stress-free) groove radius. Consider fig.105 which illustrates the stress-free and residually stressed grooves. Since the stressed groove is always of a tighter radius, it is probable that a tensile residual stress is holding the groove down in the centre and an equilibrating compressive stress is pushing it up near the edges. Because



Geometry of stressed & relaxed Grooves. Fig.105.

$\frac{\sigma_{zzr}}{\tau_o}$

2·0

1·6

1·2

0·8

0·4

0

ROLLING DIRECTION
PARALLEL TO 'b'

k=0·56

CIRCULAR k=1

k=0·35

k=0·22

NEAR CYLINDER
k=0·1

INCREASINGLY CYLINDRICAL

0 0·2 0·4 0·6 0·8 1·0 x*

Suggested form of residual stresses for several geometries. Fig.106

there is no rucking of the surface, there can be no residual strain in the rolling direction, ie. $\epsilon_{yy}=0$, because any such strain could not depend on y. It is more difficult to quantify the residual strain in the transverse direction, because, although the material is certainly under overall plane strain, there is no necessity to prevent individual filaments moving in the x-direction. However, to a first approximation, it might be suggested that $\epsilon_{xx}=0$, so that the following relations between the residual stresses and strains exist, in terms of σ_{zzr} ;

$$\sigma_{xxr}=\sigma_{yyr}=\frac{\nu}{1-\nu}\times\sigma_{zzr}$$

$$\epsilon_{xxr}=\epsilon_{yyr}=0 \qquad \epsilon_{zzr}=\frac{\sigma_{zzr}}{E}\times\frac{(1-2\nu)(1+\nu)}{(1-\nu)} \tag{144}$$

Also, it was assumed that a residual shear stress τ_{xzr} could establish itself. For a selection of geometries, and with an applied load equal to the shakedown limit, the necessary residual stress distribution to maintain the effective stress within von Mises' yield surface was found. The results, summarised in fig.106, show the largest stress found beneath the surface. A check was made to ensure there was no secondary plastic flow; this does not occur because $\tau_{xzr} \rightarrow 0$ as $x \rightarrow 0$, where the severest direct stresses occur, and substituting equations 144 into von Mises' criterion gives;

$$\frac{\sigma_{zz}}{\tau_o} < 3{\cdot}03 \qquad \text{if } \nu=0{\cdot}3 \tag{145}$$

It is clear that the residual stresses left are amply large enough to propel a crack, as postulated rather earlier. While such a crack is small, it is probable that the residual stresses are dominated by the bulk field, as determined above. As the crack grows, however, the residual stress field

will alter considerably, to accommodate the boundary conditions of the crack. When this occurs, shear loading stresses might be expected to predominate, causing the crack to turn towards the free surface.

Returning to the question of the additional depression of the groove, the maximum depression, Δ, is given by;

$$\Delta = \int_0^\infty \epsilon_{zzr}(z) \cdot dz \qquad (146)$$

In practice the integral need only be extended a short distance beneath the surface, because the residual strains are zero further down.

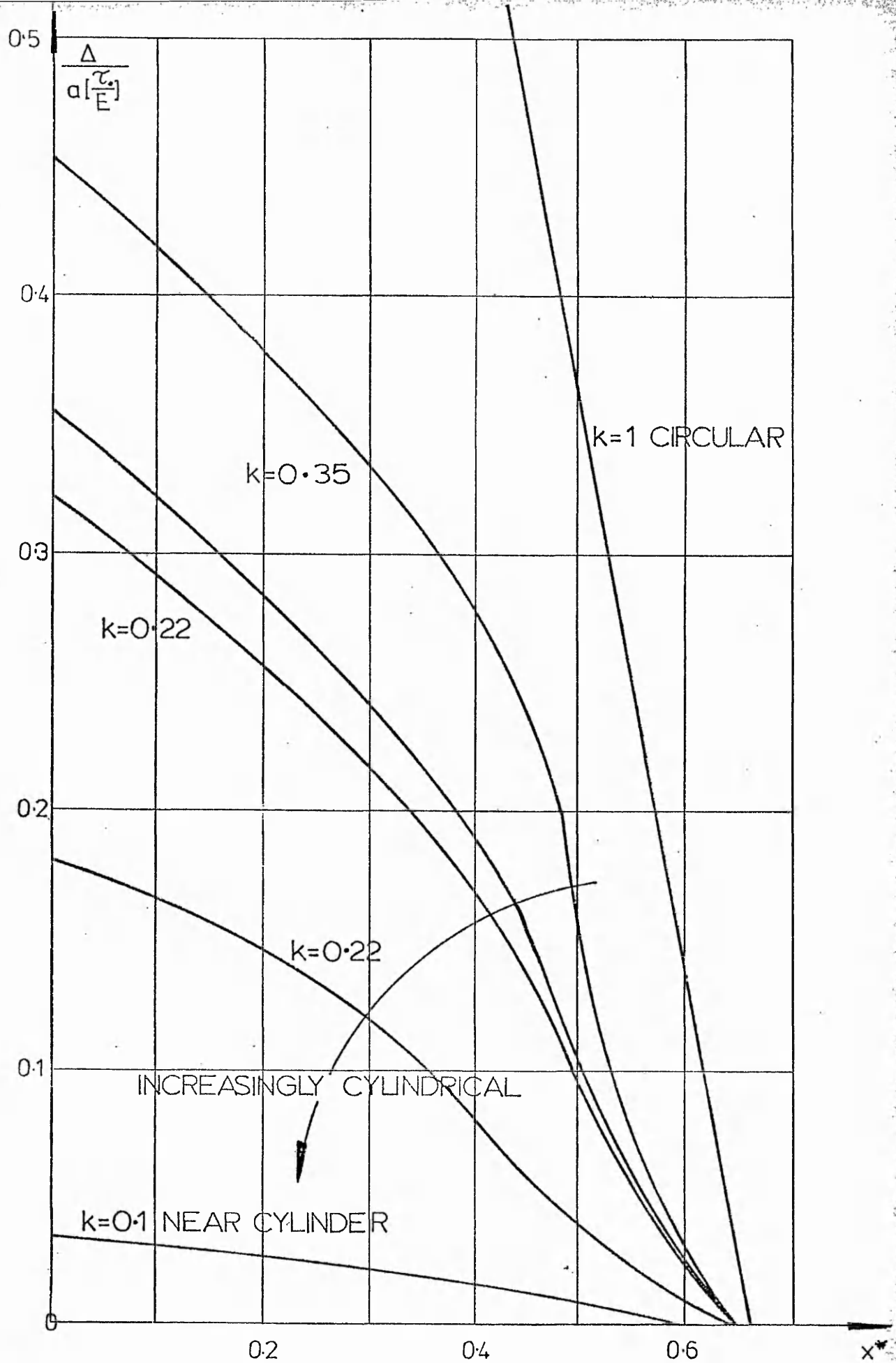
$$\frac{\Delta}{a\left(\frac{\tau_0}{E}\right)} = \int_{\substack{\text{plasticity} \\ \text{zone}}} \left(\frac{\sigma_{zzr}}{\tau_0}\right) \frac{(1-2\nu)(1+\nu)}{(1-\nu)} \, dz^* \qquad (147)$$

The results are plotted in fig.107. The form of the additional depression is approximately parabolic, as might be expected from an inspection of fig.105. An expression for Δ might be found from the same diagram;

$$\Delta = \tfrac{1}{2} \, a^2 \left(\frac{1}{R_G} - \frac{1}{R_G^0}\right) \qquad (148)$$

Substituting equation 148 into equation 147 permits a check to be made, since $\left(\frac{\tau_0}{E}\right)$ should be an invariant material property. The results are shown in table 9, and are rather variable. Probable reasons for this are that the quantity quoted is related to a small difference between two large quantities (the radii of curvature), and the lack of a distinct yield point for copper. This second point also hindered experiments on vertical shakedown, but copper is ideal from the point of view of having a high 'yield' strain, so that displacements are easily measured.

Pomeroy and Johnson(184) developed a method of finding residual strains due to rolling contact loads, but the results were not conclusive proof of Johnson's predicted



Additional depression of groove due to residual stresses. Fig.107

values (177,178). Krause and Jüke(185) used X-rays to measure residual strains, and noted different "ranges" of ordering, analogous to the macro- and micro-stresses found in electrodeposits. Any shakedown which had produced short range order stresses would be reflected in a hardness test, rather than a mechanical deformation technique, as used by Pomeroy and Johnson.

Table 9. Some Results obtained in Rolling Shakedown Tests

Measuring Station	Groove Width b(mm)	Load P(N)	Groove R_G(mm)	$\frac{p_o}{\tau_o}$	$\frac{\tau_o}{E}$
1	0·494	78·3	6·10	4·008	
2	0·458	73·8	6·28	4·08	$10·3 \times 10^{-3}$
3	0·429	69·2	6·45	4·15	
4	0·413	64·7	6·52	4·08	$10·4 \times 10^{-3}$
5	0·381	60·1	6·79	4·18	
6	0·364	55·6	6·90	4·13	$10·6 \times 10^{-3}$
7	0·344	51·0	7·07	4·12	
8	0·312	46·5	7·54	4·21	$7·4 \times 10^{-3}$
9	0·294	41·9	7·77	4·11	
10	0·261	37·4	8·64	4·23	$5·3 \times 10^{-3}$
11	0·257	32·8	8·28	4·09	
12	0·723	111·2	5·54	3·95	$6·5 \times 10^{-3}$

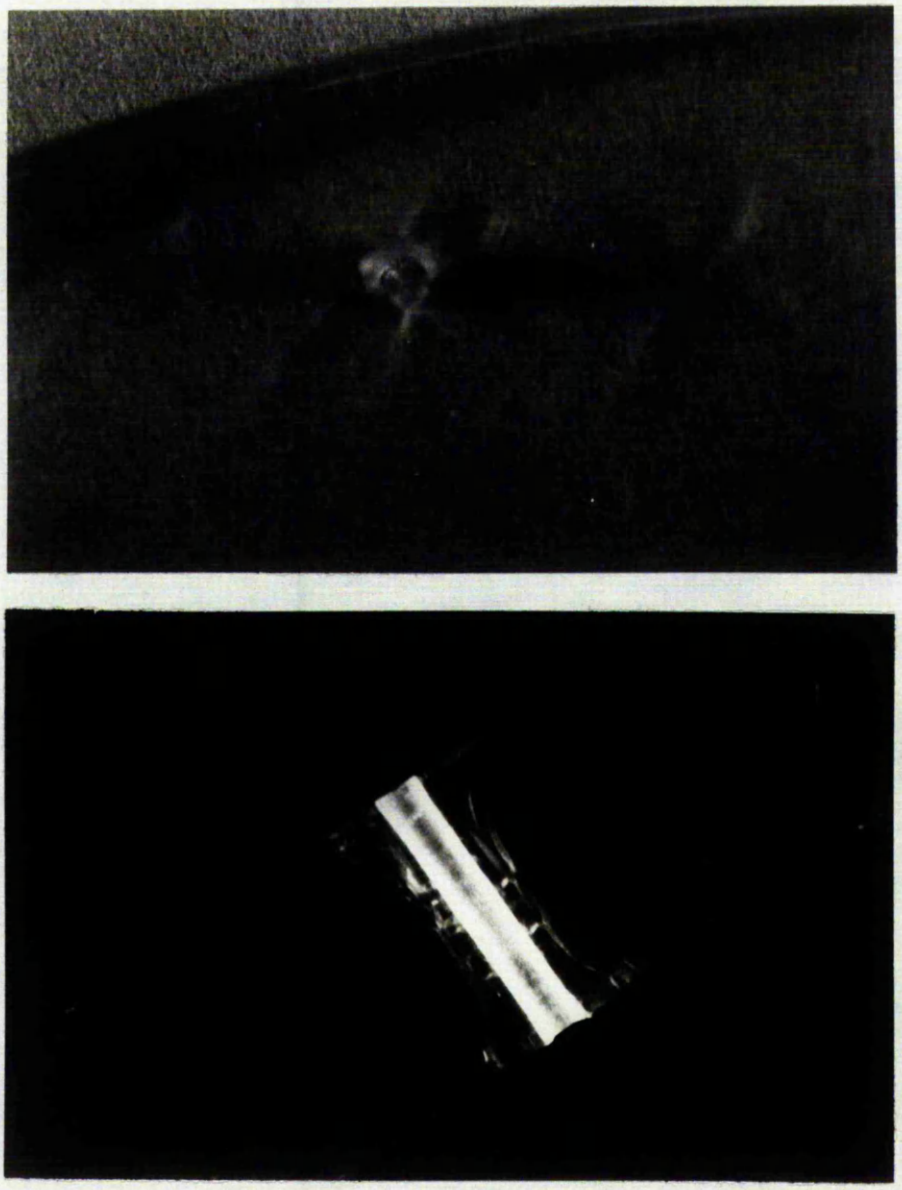
6·3 Vertical Shakedown of two Cylinders

Earlier work on the evaluation of stress intensification factors prompted an experimental investigation using two thick segments of Perspex, intended to represent parts of two cylinders rolled together. Small holes were drilled to 'seed' cracks, and these were placed at the point of

largest S.I.F. (fig.67), and on or near the axis of symmetry where the shear is lower and 'locking' occurs. It was anticipated that by cyclically compressing the segments together in an 'Instron' test machine the simulated rolling conditions would cause the first set of holes to initiate and grow cracks, whilst the second set in the locking region would initiate cracks which would fail to grow. This is not what happened. Cracks seeded in the non-locking region failed to grow, whilst those on-axis did grow ! Fig.108 shows a growing crack, and the principal shear planes, which are seen to be at 45° to the plane of the crack. Clearly, tensile stresses were being developed, causing the cracks to grow, and these were identified using a polariscope, fig.109. The discovery and its relation to fracture mechanics work was reported (186).

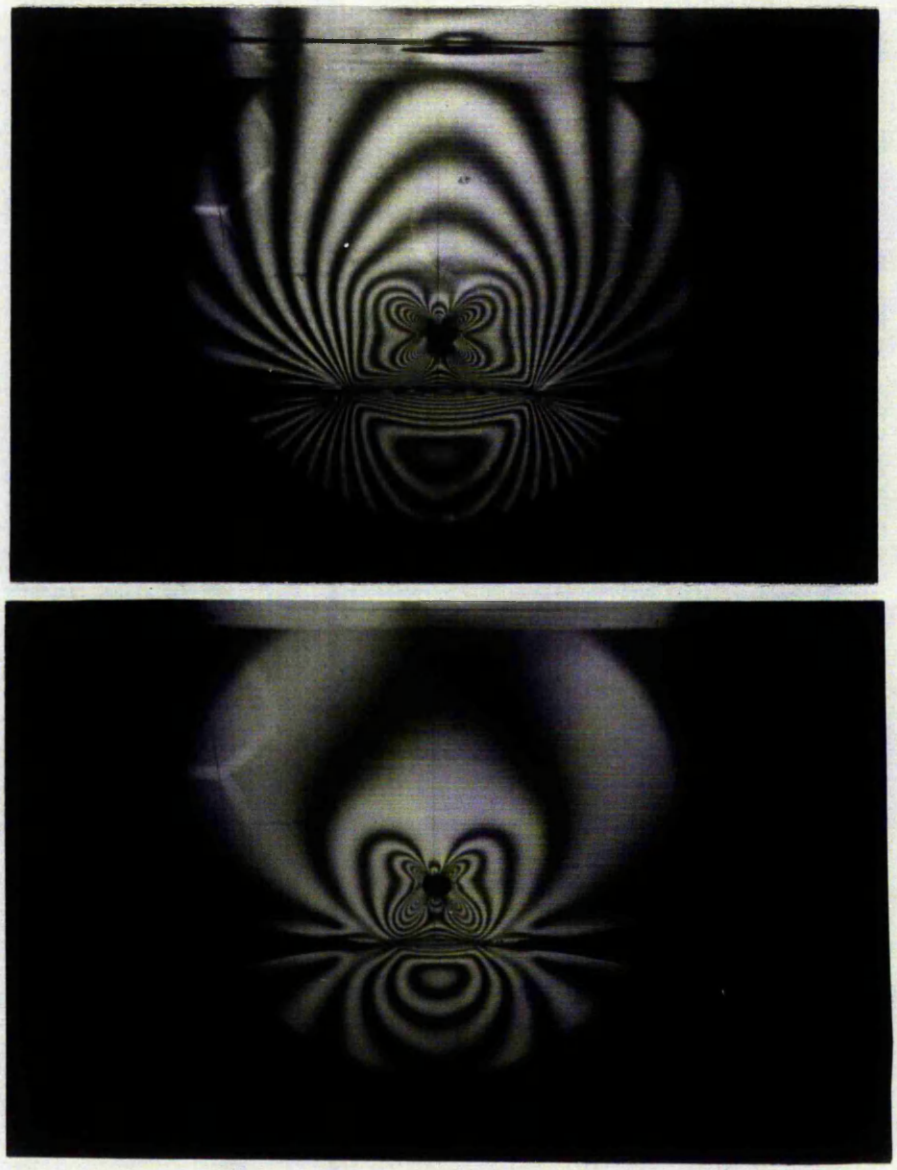
Lawn(187) has discovered a similar effect in indented soda glasses, where cracks grow after removal of the load. However, it must be stated that the simple loading configuration used does not cause the same residual stresses to develop as those which would be found beneath a rolling cylinder. The stresses actually generated were estimated using a novel approach based on deformation plasticity.

The key assumption of deformation plasticity is that the effective stress and effective strain values should have some fixed relation between them, fig.110. Another way of stating this is to say that the total plastic strain is proportional to the stress deviator. Although often used to model work hardening materials, there is no objection to its being used to model an ideally elasto-plastic material. If the assumption, now often accepted in contact theory,



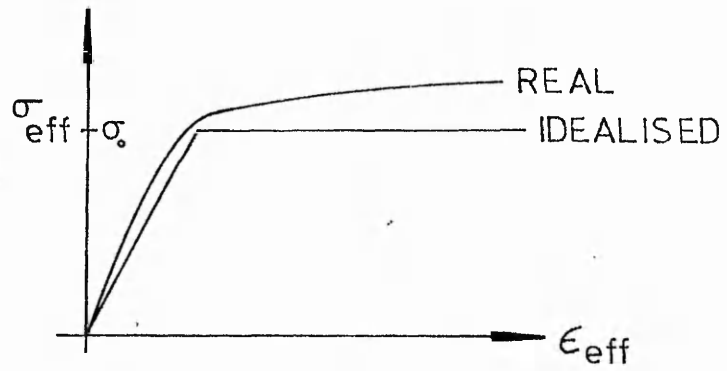
Elevation and 'plan' views of a horizontal crack emanating from a drilled hole. The cracks attained a length of about 3-4 times the diameter of the hole before arresting owing to a re-distribution of the residual stresses. Further support for the importance of residual stresses is the observation that the crack has grown further under plane stress, where its fracture toughness is higher, but where lower constraint means the generation of higher residual stresses normal to the surface.

Fig. 108.

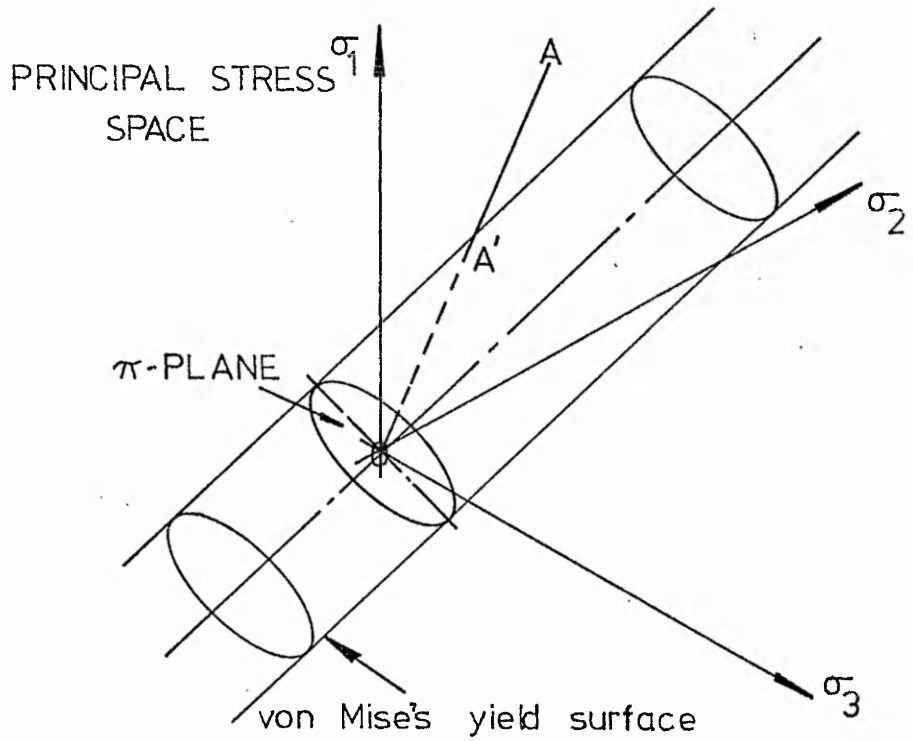


Applied and residual stress systems of a cracked Perspex segment. The dark contours represent lines of constant shear and show the classic Hertz distribution with a superimposed stress-raising hole. In the neighbourhood of the crack/hole the residual stresses are of nearly the same magnitude as the applied stresses, but are of opposite sign, ie. there is a large tensile stress normal to the crack.

Fig. 109.



Effective stress – effective strain curve. Fig.110.

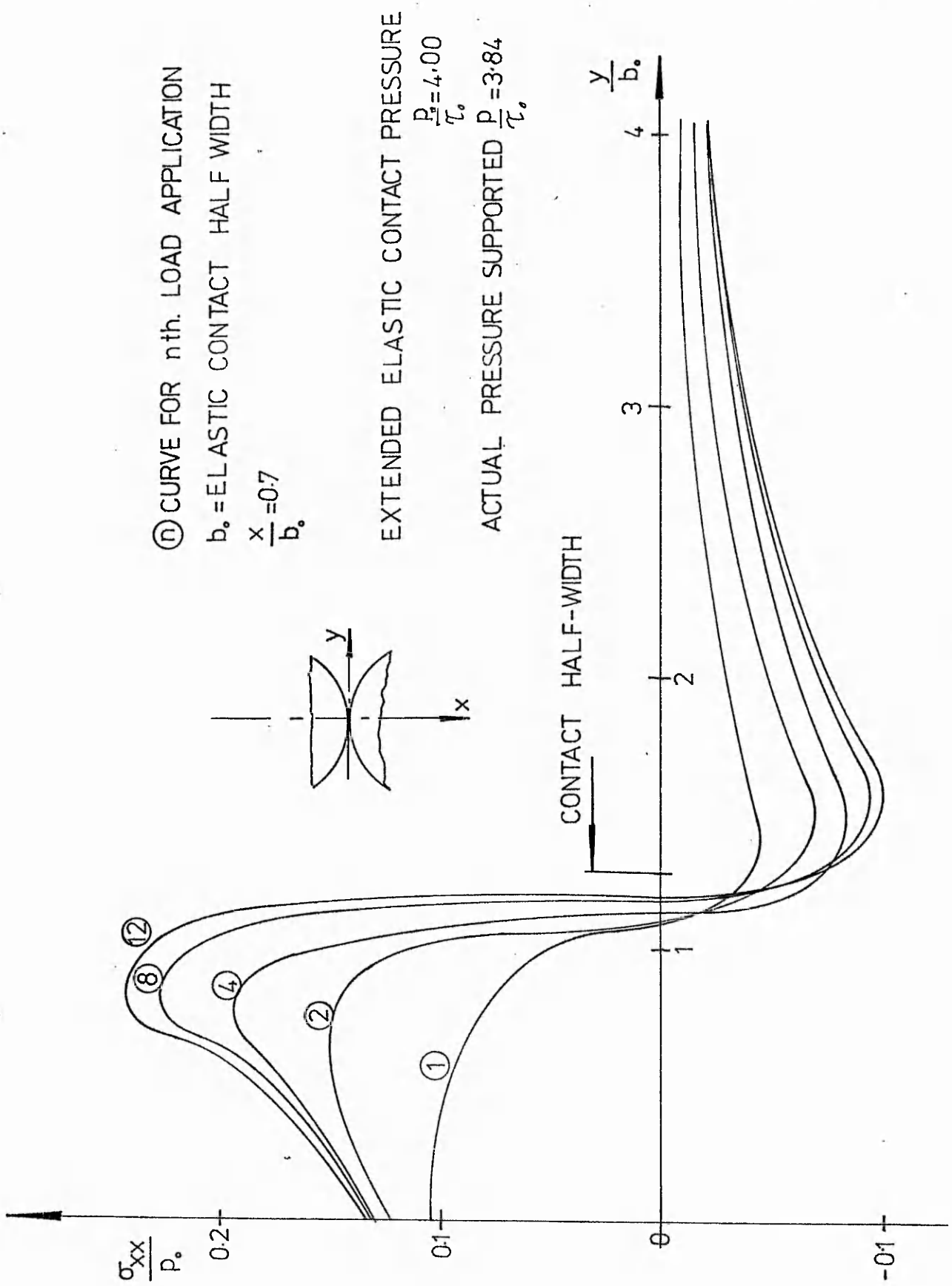


Yield criterion, infinitely elastic & elastic-plastic stress vectors. Fig111.

Note that under uniaxial conditions, the effective stress becomes equal to the direct stress applied, and the effective strain simplifies to the resulting strain. Thus, fig.110 is equivalent to a standard stress-strain curve. In fig.111 it is assumed that the principal stress directions and the principal strain directions coincide. This will certainly be true for small strain in an isotropic material.

is made that the strains are given by the extended elastic strains, the deformation plasticity rules take a very simple form. Fig.111 shows the yield surface of von Mises in Haigh-Westergaard stress space, and the extended elastic stress vector, OA. Since there is some fixed relation between the effective stress and effective strain quantities, the direction cosines of each must be the same. Thus the plastic stress vector, OA' must be collinear with the extended elastic stress vector (which may be looked upon as a 'strain' vector). Because an ideal elastic-plastic material was assumed, the point A' must lie on the yield surface. In practise then, when once the extended elastic stresses are known, all that need be done is to reduce then in proportion to each other until von Mises' criterion is just satisfied.

Two segments pressed together were analyzed assuming Hertzian extended elastic stresses (Perspex is nearly Hookean) and making use of the above result. Elastic unloading was performed so that equilibrium was maintained with the free surface, and the results of one set of calculations are shown in fig.112. A steady state condition is only approached and is not actually reached. This might be expected from some of the rather rough approximations made, the gravest of which is probably the use of deformation plasticity when the loading is not truly proportional. Nevertheless, the results are adequate to show the development of a considerable tensile stress, easily capable of propelling a crack, and the creation of compressive stresses further from the centre-line, which would hinder the growth of cracks in the shear zone. An examination of the results found from the approximate analysis bears comparison with the experimental results of



Residual stresses beneath contacting Cylinders. Fig.112.

Johnson(188).

6.4 Vertical Shakedown of a Ball

Though amenable to a similar treatment to that used in the previous section, this problem was tackled using standard incremental plasticity, for improved accuracy. It was first brought to the fore by Dr Ruff of the National Bureau of Standards, Washington, who had used a single indentation to try and calibrate a SEM modified for SACP work (20). There are, of course, great difficulties assciated with attempting an analysis of elasto-plastic indentation by a rigid ball, and only finite element studies have so far been completed (189,190). The repetition of such calculations did not seem a very satisfactory calibration technique. In his classic paper, Tabor(191) postulated that the unloading of hardness test ball was elastic, but later Johnson proved ingeniously that plastic flow also occurred upon unloading (192). However, after several loadings it was thought that a completely reversible elastic state persisted throughout the operation. Therefore it must have shaken down.

Since the residual stresses persisting after shakedown would provide a very adequate calibration, this problem was pursued. First, the actual shakedown limit was found. The on-axis stresses beneath a ball under elastic conditions have been quoted earlier (equations 21). Converting these into spherical and deviatoric components gives;

$$\frac{\bar{\sigma}}{p_o} = -\frac{2}{3}(1+\nu)(1-z^*\cot^{-1}z^*)$$

$$\frac{s_{\theta\theta}}{p_o} = \frac{s_{rr}}{p_o} = \frac{1}{2}\frac{1}{1+z^{*2}} - \frac{1}{3}(1+\nu)(1-z^*\cot^{-1}z^*) = \frac{s_o}{p_o} \qquad (149)$$

$$\frac{s_{zz}}{p_o} = -\frac{1}{1+z^{*2}} + \frac{2}{3}(1+\nu)(1-z^*\cot^{-1}z^*) = -2\frac{s_o}{p_o}$$

As a ball is pressed into a flat ideally elasto-plastic semi-infinite space, the stresses are given by equations 149 until the elastic limit is reached, ie. until;

$$J_2 = \tfrac{1}{2}\,(s_{rr}^2 + s_{\theta\theta}^2 + s_{zz}^2) = 3\,s_o^2 = \tau_o^2 \qquad (150)$$

or $\dfrac{s_o}{\tau_o} = \dfrac{1}{\sqrt{3}}$

Subsequently, the stresses will be given by the Prandtl-Reuss rules. In a private communication, Professor K.L. Johnson provided some notes showing that, during subsesquent loading, $\dfrac{ds_o}{dz^*} = 0$, ie. that the stresses were constant.

Thus, in the plastic zone,;

$$s_{rr} = s_{\theta\theta} = \frac{\tau_o}{\sqrt{3}} \qquad s_{zz} = -\frac{2\tau_o}{\sqrt{3}} \qquad (151)$$

The extent of the residual stresses, upon unloading, is given by the roots of the equation;

$$0 = -\frac{1}{3}(1+\nu)(1 - z^* \cot^{-1} z^*) + \frac{1}{2}\frac{1}{1+z^{*2}} - \frac{1}{\sqrt{3}}\left(\frac{\tau_o}{p_o}\right) \qquad (152)$$

and the magnitude of the residual stresses is found by subtracting the value given by equation 149 from that given by equation 151.

A possible shakedown limit is the onset of secondary plastic flow upon unloading. The stresses during the unloading phase are given by;

$$\sigma'_{rr} = \sigma'_{\theta\theta} = -s_o + \frac{\tau_o}{\sqrt{3}}$$
$$\sigma'_{zz} = 2\,s_o - \frac{2\tau_o}{\sqrt{3}} \qquad (153)$$

Secondary flow will occur when these stresses exceed von Mises' criterion, ie;

$$J_2 = \frac{1}{6}\left\{(\sigma'_{rr} - \sigma'_{\theta\theta})^2 + (\sigma'_{\theta\theta} - \sigma'_{zz})^2 + (\sigma'_{zz} - \sigma'_{rr})^2\right\} = \tau_o^2 \qquad (154)$$

ie. $s_o = \dfrac{2\tau_o}{\sqrt{3}}$

This corresponds to a load given by;

$$\frac{p_o}{\tau_o} = 5{\cdot}54 \qquad (155)$$

To test this possible shakedown limit experimentally, a hardened steel ball, 10 mm diameter, was repeatedly pressed into a mild steel block, using an 'Instron', for 100 cycles, using a range of loads, but all above the elastic limit. The impressions were then measured, as in the rolling ball experiment, and the results are shown in table 10.

Table 10 Results of Vertical Ball-shakedown Tests

Station	P(kN)	Dia(mm) Impression	V.H.N.	$p_o(\frac{kN}{mm^2})$	$\frac{p_o}{\tau_o}$
1	0·823	0·870	213	2·078	5·14
2	1·357	1·090	213	2·175	5·38
3	2·346	1·342	233	2·488	5·63
4	2·624	1·484	221	2·276	5·43
5	3·899	1·777	221	2·342	5·59
6	4·537	1·965	215	2·224	5·45
7	5·026	2·068	213	2·221	5·50
8	5·871	2·203	215	2·285	5·60
				Mean	5·46 ± 0·15

The shakedown limit guessed therefore seems to be confirmed. A major source of error was the susceptibility of the loading machine to changes in the specimen compliance: as shakedown occurred the arrangement became stiffer, and consequently the load applied fell slightly.

It might be worthwhile, here, to contrast the result obtained with hardness. Dieter(89) quotes the relation between the mean contact pressure, p_m, and yield stress as;

$$p_m = 2{\cdot}66\,\sigma_o \qquad (155)$$

whereas the shakedown limit proposed is equivalent to;

$$p_m = \frac{2}{3}p_o = 2{\cdot}15\,\sigma_o \qquad (156)$$

The main difference between the two load arrangements is that under shakedown conditions the pressure distribution is Hertzian, whereas under hardness test conditions the contact pressure is rather more uniform, since the ball is supported on almost fully plastic material.

The complete residual stress field is now considered. First the stresses produced as the half-space is loaded must be found. Within the elastic region these will be given by equations 149. Subsequently, they will be determined by the Prandtl-Reuss rules. It will be necessary to adopt several modifications to the usual symbols, viz.;

$\sim$ Denotes quantity evaluated when system is on the point of yield

$*$ Dimension normalized with respectto the current radius of contact

$\wedge$ Quantity normalized with respect tc the yield in pure shear

e As a superscript denotes extended elastic quantity

If a fixed point is chosen beneath the surface, this may be denoted by;

$$\underset{\sim}{r^*} = \frac{r}{\underset{\sim}{a}} \qquad \underset{\sim}{z^*} = \frac{z}{\underset{\sim}{a}} \qquad (157)$$

Note that;

$$p_o \propto \sqrt[3]{P}$$

$$a \propto \sqrt[3]{P}$$

Hence;

$$\frac{\hat{p}_o}{\underset{\sim}{\hat{p}_o}} = \frac{a}{\underset{\sim}{a}} \quad \text{and} \quad r^* = \underset{\sim}{r^*}\,\frac{\hat{p}_o}{\underset{\sim}{\hat{p}_o}} \qquad z^* = \underset{\sim}{z^*}\,\frac{\hat{p}_o}{\underset{\sim}{\hat{p}_o}} \qquad (158)$$

Von Mises' criterion may be written in terms of normalized variables as (noting $\tau_{r\theta} = \tau_{\theta z} = 0$);

$$\tfrac{1}{2}(\hat{s}^2_{\theta\theta} + \hat{s}^2_{rr} + \hat{s}^2_{zz}) + \hat{\tau}^2_{rz} = 1 \qquad (159)$$

Consider now the Prandtl-Reuss equations, given by Prager and Hodge in the form (193);

$$\dot{s}^p_{ii} = 2G(\dot{e}^e_{ii} - \frac{\dot{W}}{2k^2}s^p_{ii}) \qquad \dot{\tau}^p_{rz} = G(\dot{\gamma}^e_{rz} - \frac{\dot{W}}{k^2}\tau^p_{rz}) \qquad (160)$$

where $\dot{W} = \sum_{\theta,r,z}^{i}\left\{s^p_{ii} \times \dot{e}^e_{ii}\right\} + \tau^p_{rz} \times \dot{\gamma}^e_{rz}$

In these equations, the extended elastic strains have been substituted for the plastic strains, following Merwin and Johnson(177). This sweeping simplification is permissible if the elastic limit is not greatly exceeded. Also, the dot over some quatities denotes a variation with respect to time. Two sets of manipulations enable the problem to be cast in a simpler form;

A. Note that; $\hat{s}^e_{ii} = \hat{s}^e_{ii}(r^*, z^*, p_o)$ (equations 110)

Therefore;

$$\dot{\hat{s}}^e_{ii} = \frac{d\hat{s}^e_{ii}}{dt} = \frac{dr^*}{dt}\frac{\partial \hat{s}^e_{ii}}{\partial r^*} + \frac{dz^*}{dt}\frac{\partial \hat{s}^e_{ii}}{\partial z^*} + \frac{dp_o}{dt}\frac{\partial \hat{s}^e_{ii}}{\partial p_o} \qquad (161)$$

But; $\frac{dr^*}{dt} = \frac{d}{dt}\left(\frac{r}{a}\right) = -\frac{r^*}{p_o}\frac{dp_o}{dt}$ $\frac{dz^*}{dt} = \frac{d}{dt}\left(\frac{z}{a}\right) = -\frac{z^*}{p_o}\frac{dp_o}{dt}$

Therefore;

$$\dot{\hat{s}}^e_{ii} = \left[-\left\{ \frac{r^*}{p_o}\frac{\partial \hat{s}^e_{ii}}{\partial r^*} + \frac{z^*}{p_o}\frac{\partial \hat{s}^e_{ii}}{\partial z^*} \right\} + \frac{\partial \hat{s}^e_{ii}}{\partial p_o} \right] \times \frac{d\hat{p}_o}{dt} \qquad (162)$$

A similar relation exists for the shear stress, τ_{rz}.

B. Return to the flow equations, 160.

The following relations exist for the elastic quantities, from Hooke's Law;

$$2Ge^e_{ii} = s^e_{ii} \qquad G\gamma^e_{rz} = \tau^e_{rz} \qquad (163)$$

By making use of these identities, the flow rules may be written in a form which obviates the need to determine the strains explicitly;

$$\dot{\hat{s}}^p_{ii} = \dot{\hat{s}}^e_{ii} - \phi\,\hat{s}^p_{ii} \qquad \dot{\hat{\tau}}^p_{rz} = \dot{\hat{\tau}}^e_{rz} - \phi\,\hat{\tau}^p_{rz} \qquad (164)$$

where; $\phi = \frac{1}{2}\sum_{\theta,r,z}^{i} \left\{ \dot{\hat{s}}^e_{ii}\,\hat{s}^p_{ii} \right\} + \dot{\hat{\tau}}^e_{rz}\,\hat{\tau}^p_{rz}$

Note, further, that the time derivative of the plastic stress is a total derivative, so that;

$$\frac{d\hat{s}^p_{ii}}{dt} = \frac{d\hat{p}_o}{dt}\frac{ds^p_{ii}}{d\hat{p}_o} \qquad (165)$$

The flow rules may now be re-written in a form suitable for solution by a numerical technique:

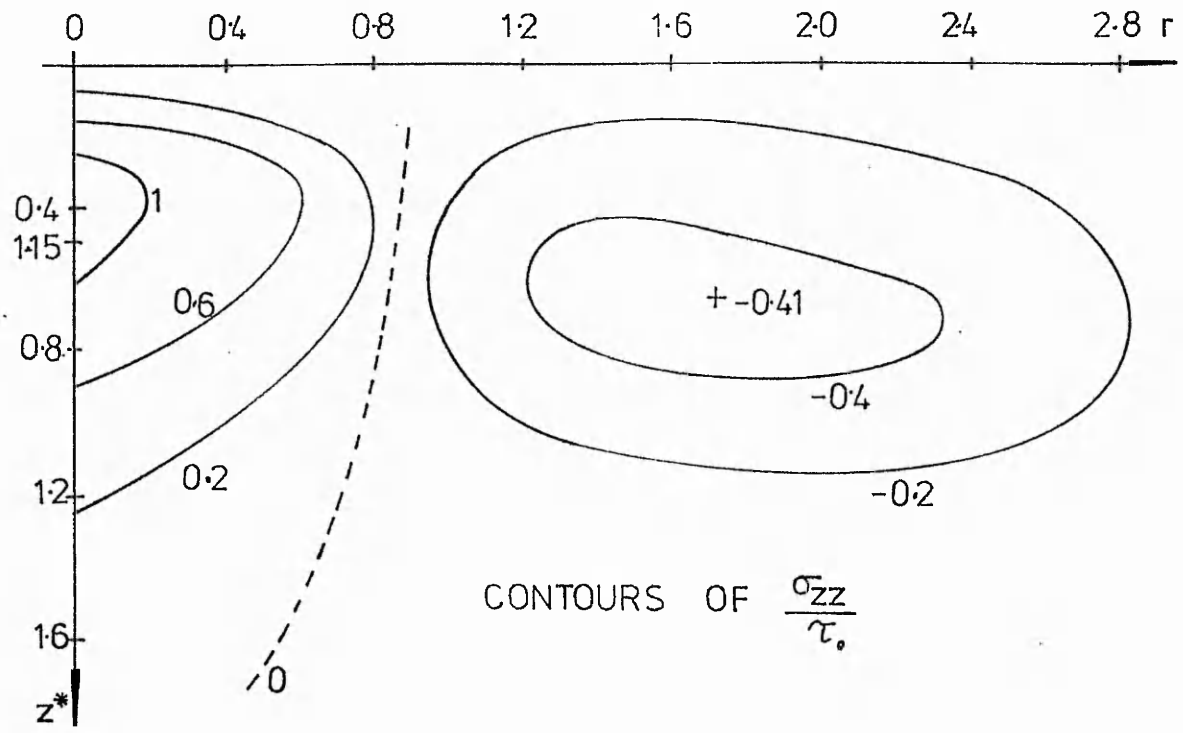
$$\frac{d\hat{s}^{p}_{ii}}{d\hat{p}_o} = \left\{ F_{ii}(p_o) - \phi_o s^{p}_{ii} \right\} \qquad \frac{d\tau^{p}_{rz}}{dp_o} = \left\{ F_{rz}(p_o) - \phi_o \, {}^{p}_{rz} \right\}$$

where; $\phi_o = \frac{1}{2}\Sigma\left\{ F_{ii}(\hat{p}_o)\hat{s}^{p}_{ii} \right\} + F_{rz}(p_o)\hat{\tau}^{p}_{rz}$ (166)

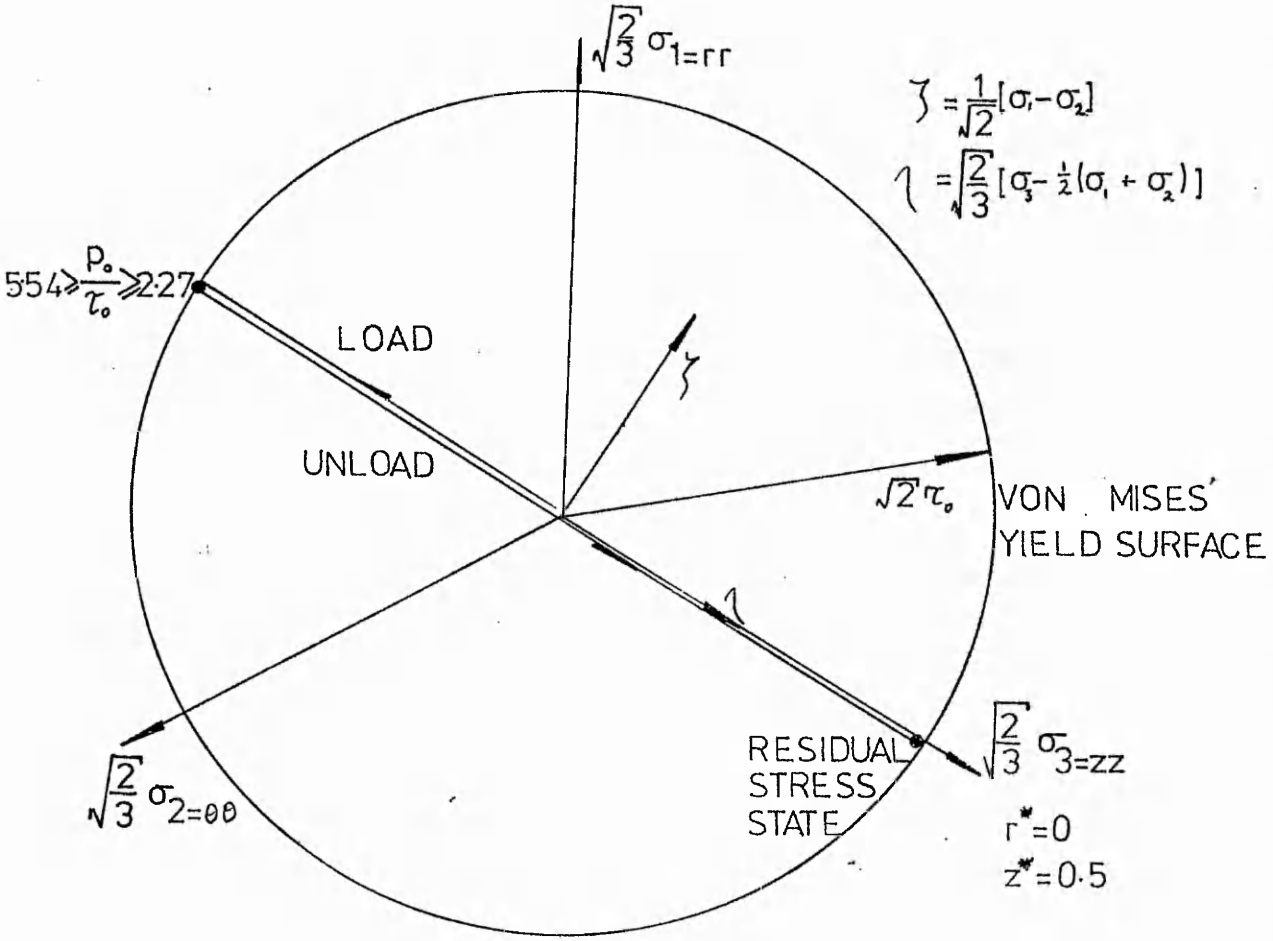
And; $F_{ii} = -\left\{ \frac{r^*}{\hat{p}_o}\frac{\partial \hat{s}^{e}_{ii}}{\partial r^*} + \frac{z^*}{\hat{p}_o}\frac{\partial \hat{s}^{e}_{ii}}{\partial z^*} \right\} + \frac{\partial \hat{s}^{e}_{ii}}{\partial \hat{p}_o}$ &c.

The deviatoric stresses at the point of yield, as the load is incremented, provide the starting point for the solutions. Subsequently, the Runge-Kutta method may be used to solve equations 166, and hence describe the plastic stresses. At first, it was thought that the contact pressure to which the stresses should be taken was given by the shakedown-limit, equation 155, but because of the truncation of stresses by plastic flow, equilibrium with the shakedown load is no longer satisfied. The computer programme written to solve the overall problem was therefore modified so that for each depth, a check was made so that the sum of the σ_{zz} stresses was in equilibrium with the intended load. Thus, to support a true load of $\frac{p_o}{\tau_o} = 5{\cdot}54$, a larger extended elastic load was applied, determined by iteration. When this had been achieved, the system was permitted to unload elastically. Note that during this process the contact patch decreases, so that care is required in calculating the 'unload' part of the stress trajectory.

The residual stresses predicted are shown in fig. 113, whilst the stress trajectory for a sample point projected onto the deviatoric plane (see Hill(194)) is given in fig. 114. There will inevitably be some inaccuracy, mainly caused by assuming that the strain field is unmodified by a small excursion into the plastic regime. This will lead to a re-distribution of the contact pressure during the first



Residual stresses found under shaken down Ball .Fig.113



Stress history projected onto Deviatoric Plane Fig.114

loading or two, but will not affect subsequent loadings very much. The same assumption also leads to the (incorrect) conclusion that shakedown will be complete after just one loading, and it is directly responsible for having to assume a strain field associated with an artificially high contact pressure, to maintain equilibrium. Notwithstanding these objections, the assumption of identical strain fields under elastic and elastic-plastic loads is the best way available at the moment to solve this type of problem, and the residual stress field should not be greatly in error. It is regrettable that, except at the point of severest stress, the residual stress field needed to contain the material within the yield surface is not unique, for such a uniqueness would enable the exact solution to be found.

7. Conclusions

Even with some of the sweeping simplifications made at the beginning of the thesis, it is difficult to draw general conclusions from what has been deduced about the remaining variables.If fracture mechanics is accepted as a possible explanation for wear (and the evidence is still rather tentative), the two phases of particle detachment must be considered separately.

During the initiation stage, it is reasonable to split the stress system into deviatoric and spherical components, and to say that both contact loads and any static residual stresses contribute to both parts. The spherical or average stress then controls the material's ductility, whilst the deviatoric stress governs the tendency towards plasticity, or the separation of any second phase particles from the matrix. The sensitivity of the material to a reduction of deviatoric stress would appear to depend greatly on the shape of second phase particles present (though not on their size); flake-like inclusions cause so much stress raising that a reduction of shear is of little benefit.

When well developed cracks are present, it would be better to split the stress system up in a different way, viz.;

1. Stress component normal to the crack.
2. Stress component in shear parallel with the crack.
3. Remaining direct stresses parallel with the crack.

The influence of stresses(1) & (2) can be quantified, but the influence of (3), which for wearing surfaces is often considerable, cannot at present be found. It is clear that (1) only causes crack growth when positive, and that

very negative values of normal stress inhibit shear growth by stresses (2).

Unfortunately, in a real wearing material, cracks are present which are growing in each phase contemporaneously. It is difficult to devise experiments which split up the life of a crack into each part, since they are so inter-dependent. It would appear that a residual compressive stress in-plane with the cracks (ie. parallel to the surface) would, ceteris paribus, be beneficial, since it both reduces the deviatoric stress, and makes the spherical stress more negative. Regretably its influence on crack growth rate is unknown.

When loading is strictly two-dimensional, the shake-down stresses are beneficial, since they always reduce plasticity to the absolute minimum. This is really an example of Le Chatelier's principle: putting in stresses before wear can reduce the initial plasticity, but the ideal stresses develop eventually. It is uncertain whether serious damage is done to the surface before shakedown is complete. Under three-dimensional conditions, the shake-down stresses are much more difficult to predict, but it seems highly probable that in the equilibrium state tensile stresses remain which are normal to the surface, and which encourage cracks to grow. Therefore, when the wearing pair are loaded to some point between the elastic and shakedown limits, the inclusion of in-plane compressive stresses could well be beneficial, since they would prevent the normal tensile stress from developing.

It is usual to suggest avenues of further work, and many present themselves. First, it would seem pointless

to make the fracture model more sophisticated until it has been confirmed experimentally that fracture mechanics is applicable under such odd loading. Dr R.A.Smith of Cambridge University is currently working on this, but there is a vast amount of work to be done. Also, more data are needed on combined mode crack growth in conjunction with cumulative damage criteria, before realistic crack growth rates can be predicted with any certainty.

Information is also needed on very short cracks, where fracture mechanics under-estimates the growth rate, and on the effect of an in-plane stress on propagation. To obtain actual volume wear rates, it will also be necessary to form a model of the number of cracks growing at any time, and on their stage of development.

Some progress has been made on the shakedown limits of a few simple geometries, but one which remains is that of a shear and normally loaded elliptical contact patch, such as that found beneath a locomotive wheel.High oblateness ellipses need also to be considered in greater detail. Ultimately, it oughtto be possible to take work-hardening and the Bauschinger effect into account. Some progress is being made in this area by Professor Ponter of Leicester University.

References

1. Eyre,T.S. "Wear characteristics of some Metals". Tribology International.Oct.1976,203-212
2. Bowden,F.P. and Tabor,D. "The Friction and Lubrication of Solids". Oxford University Press. Part I pub. in 1950 and Part II pub. in 1964
4. Rabinowicz,E. "Friction and Wear of Materials". John Wiley and Sons. Pub.1966
5. Neale,M.J.(ed) "Tribology Handbook". Butterworths. Pub. 1973
6. Sarkar,A.D. "Wear of Metals". Pergamon Press. Pub.1976 as vol.18 in series 'Materials Science and Technology'
7. Halling,J.(ed) "Principles of Tribology". McMillan. Pub.1975
8. Sakamoto,T. and Tsukizoe,T. "Metal transfer in the Frictional contact of a rough hard surface". Wear, 1978,44,301-303
9. Suh,N.P. "The Delamination theory of Wear". Wear, 1973,25,111-124
10. Rice.S.L. "Variations in Wear Resistance due to Microstructural condition in high strength steel under repetitive Impact".Tribology International,Feb.1979, 25-29
11. Doyle,E.D. and Turley,D.M. "Delamination Effects in Grinding". Wear,1978,51,269-278
12. Archard,J.F."Contact and Rubbing of flat surfaces". Jnl.Appl.Phys.,Aug.1953,24,8,981-988
13. Welsh,N.C. "The dry Wear of Steels". Phil.Trans.Roy. Soc.Ser.A. Jan.1965.No.1077,257,31-70
14. Bayer,R.G. and Sirico,J.L. "The Influence of Surface

Roughness on Wear". Wear, 1975, 35, 251-260

15. Halling, J. and Brothers, E.G. "The effect os surface finish on the creep and wear of a Rolling Ball subjected to Normal and Tangential Surface Tractions". Wear, 1966, 9, 199-208

16. Greenwood, J.A. and Tripp, J.H. "The Elastic Contact of Rough Spheres". Jnl. Appl. Mech., 1967, 34, 153-159

17. Gerlach, H.D. and Lokhamp, F. "Effect of Surface Defects on Contact Stresses". Ball Bearing Jnl., 1977, 176, 1-4

18. Kirk, J.A. and Swanson, T.D. "Surface Effects during Sliding Wear". Wear, 1975, 35, 63-67

19. Ruff, A.W. "Deformation Studies at Sliding Wear tracks in iron". Wear, 1976, 40, 59-74

20. Ruff, A.W. "Studies of deformation at sliding Wear tracks in iron". Inst. for Matls. Res., Nat. Bur. Stds, Washington, report no. NBSIR76-992

21. Hull, D. "Introduction to Dislocations". Pergamon Press. Pub. 1975

22. Suh, N.P. and Saka, N. "The stacking fault energy and Delamination Wear of single phase f.c.c. metals". Wear, 1977, 44, 135-143

23. Kayaba, T. and Kato, K. "The analysis of Adhesive Wear Mechanisms by Successive observations of the Wear Process in SEM". Wear of Matls. 1979, Bearbon, Michigan, 45-56

24. Johnson, K.L. "A review of the theory of Rolling Contact stresses". Wear, 1966, 9, 4-19

25. Radzimovsky, E.I. "Stress Distribution and Strength Condition of two rolling Cylinders pressed together". Univ. of Illinois, Eng. Exptl. Sta., Bull No. 408

26. Ollerton,E. and Morey,J.E.W. "Fatigue Strength of Rail Steel in Rolling Contact". Proc.Instn.Mech.Engrs. Conf.'Fatigue in Rolling Contact'.1963,177,25,11-22

27. Jain,V.K. and Bahadur,S. "Development of a wear equation for polymer-metal sliding in terms of fatigue and topography of sliding surfaces". Wear of Matls. Conf.,Dearbon,Michigan,1979.

28. Moore,M.A. and Douthwaite,R.M. "Plastic Deformation Beneath worn surfaces".Metall.Trans.1976,7A,1833-1839

29. Polk.C.J. and Rowe,C.N. "Crack growth rate:its measurement and a controlling factor in rolling contact fatigue".ASLE Preprint 74LC-SA-1

30. Soda,N.,Kimura,Y and Tanaka,A. "Wear of some f.c.c. metals during unlubricated sliding". Part IV. Wear, 1977,43,166-174

31. Halling,J. "A contribution to the theory of Mechanical Wear".Wear,1975,34,239-249

32. Fleming,J.R. and Suh,N.P. "Mechanics of Crack Propagation in Delamination Wear".Wear,1977,44,39-56

33. Hornbogen,E. "The role of fracture toughness in the wear of Metals".Wear,1975,33,251-259

34. McClintock,F.A. "plastic flow around a crack under friction and combined stress".Fracture,1977,ICF4, Waterloo,49-64

35. Fegredo,D.M. and Pritchard,C. "A Metallographic examination of rollers subjected to Wear under Rolling-Sliding conditions",Wear,1978.49,67-78

36. Muro,H.,Tsushima,T, and Nagafuchi,M. "Initiation and Propagation of Surface Flaws in rolling contact fatigue of high hardness steel".Wear,1975,35,261-282

37. Zum Gahr,K-H. "Fracture Mechanics aspects of abrasive friction wear, and Chip Formation of a -Fe-Ni-Al Steel". Fracture,1977,ICF4,Waterloo,735-739

38. Kolozsvary,Z. "The Study of Surface Fatigue in Sliding Wear".Wear,1973,25,215-224

39. Finkin,E.F. "An explanation of the Wear of Metals". Wear,1978,47,107-117

40. Roberts,J.C. et al"An empirical equation including fracture toughness and describing friction of Dental Restorative materials".Wear,1978,47,139-146

41. James,D.H.,Smart,R.F. and Reynolds,J.A. "Surface treatments in Engine component technology".Wear,1975,34, 373-382

42. Hurricks,P.L. "Review:Some aspects of the Metallurgy and wear Resistance of Surface Coatings".Wear,1972,22, 291-320

43. Rajasekariah,R. and Vaidyanathan,S. "Increasing the Wear resistance of steel components by Ball Burnishing" Wear,1975,34,185-188

44. Waterhouse,R.B. and Saunders,D.A. "The effect of shot peening on the fretting behaviour of an austenitic stainless steel and a mild steel".Wear,1979,53,381-386

45. Jahanmir,S.,Suh,N.P. and E.P. Abrahamson II "The Delamination theory of Wear and the Wear of a Composite Surface".Wear,1975,32,33-49

46. Jahanmir,S.,E.P.Abrahamson II and Suh,N.P. "Sliding Wear resistance of metallic coated surfaces".Wear,1976 40,75-84

47. Takagi,R. and Liu,T. "The Lubrication of Steel by Electroplated Gold".Trans.ASLE,1967,10,115-123

48. Antler,M. and Solomon,A.J. "Mechanisms of wear of gold electrodeposits".Plating,Aug.1970,812-816

49. Fenton,F.A.D.,Oolbekkink,A. and Assmuss,W. "Electroplating in marine engineering".Europort Conf.,1973, 26-34

50. Ricks,H.E."Building up worn shafts by nickel plating" Met.Fin.,Oct.1972,47-48

51. Roberts,W.H. "Chromium plate as a bearing surface at elevated temperatures". Proc.Conf. on Lub.&Wear.I.Mech.E. 1963,247-257

52. Scott,D. "Hollow rolling elements".Trib.Int.Dec1976, 261-264

53. Briscoe,B.J.,Eyre,T.S. and Gologan,V. "Assessing the durability of Electrodeposited Metal Films".Wear,1974, 28,271-275

54. Gologan,V. and Eyre,T.S."Friction and Wear of some engineering materials against hard Chromium plating". Wear,1974,28,49-57

55. Lawn,B.R. and Wilshaw,T.R. "Fracture of brittle solids". Cambridge University Press.Pub.1975,p.25

56. Ledford,R.F. and Dominik,E.A. "Comparative wear characteristics of some electrodeposited metals". Plating,April 1952,360-365

57. Wiegand,H. and Heinke,G. "The wear resistance of electrodeposited nickel and chromium and electroless nickel deposits, and comparison with the behaviour of some steels".Metalloberfläche,1970,24,163-170

58. Williams,C. "Internal stress and its measurement". Met.Fin.Jnl.,Jan.1962,5-12

59. Walker,R. "Internal stress in electrodeposited metallic coatings". Met.Fin.Jnl.Monograph,1968

60. Borchert,L.C. "Invesigation of methods for the Measurement of stress in electrodeposits". Proc.Am. Electroplaters Soc.,1963,50,44-50

61. Weil,R. "The measurement of Internal stresses in electrodeposits".Proc.Symp.Electrostress Soc. of New York,14th Oct.1974,319-327

62. Begh.F.R. et al "The Measurement of stress on electro-deposited silver by holographic Interferometry". Jnl.Less Common Metals.1975,43,243-248

63. Hoar.T.P. and Arrowsmith.D.J. "An instrument for the continuous measurement of stress in electrodeposits". Trans.Inst.Met.Fin.,1957,34,354-363

64. Hoar,T.P. and Arrowsmith,D.J. "Stress in nickel electro-deposits".Trans.Inst.Met.Fin.,1958,36,1-6

65. Gabe,D.R. and West,J.M. "The Measurement of Internal Stress in electrodeposits".Trans.Inst.Met.Fin.,1963 40,6-12

66. Norris,P.J. "A compact unit for the Measurement of stress in electrodeposited Coatings".Electroplating and Met.Fin.,March 1968,85-88

67. Sykes,J.M. and Rothwell,G.P. "Relaxation of Internal stresses in Electrodeposits during Measurement by null deflexion methods".Jnl.Electrochem.Soc:electro-chemical science,Jan.1971,91-93

68. Brenner,A. and Senderoff,S. "A Spiral Contractometer for Measuring Stress in Electrodeposits".U.S. Nat. Bur.Stds.,1949,42,RP1953,89-104

69. Brenner,A. and Senderoff,S. "Calculation of Stress in electrodeposits from the Curvature of a Flated Strip".U.S. Nat.Bur.Stds.,1949,42,RP1954,105-123

70. Cleghorn,W.H.,Gnanasekaran,K.S.A. and Hall,D.J. "Measurement of Internal Stress in Electrodeposits by a Dilatometric method".Met.Fin.Jnl.,April 1972, 92-95,+109

71. Gabe,D.R. "Calculation of internal stress for the Dilatometer I.S. meter".Trans.Inst.Met.Fin.,1973,51, 39-40

72. Kushner,J.B. "Factors affexting Residual stress in electrodeposited metals".Met.Fin.,April 1958,46-51

73. Perakh,M. "Calculation of Macrostress in Electrodeposits" Proc.Symp.Electrostress Soc. of New York,14thOct.1974, 328-352

74. Koch,F.B. et al "An electronic plating stress monitor" Plating and Surface Fin.,Jan.1976,46-50

75. Sykes et al "An apparatus for recording internal stress in Electrodeposits during plating".Jnl.Phys.E.,1970, 3,941-942

76. Hills,D.A. and Ashelby,D.W. "An automated plating stress monitor".Jnl.Phys.E.,1979,12,177-178

77. Ramskill,P. "The dry wear of Steels".BSc thesis,Trent Polytechnic,June,1976.

78. Broszeit,E.,Hess,F.J. and Wagner,E. "An electrochemical investigation of corrosive wear of electroplated nickel ".Wear,1974,30,311-319

79. Kendrick ,R.J. "The effects of a.c. on the Properties of Nickel Electrodeposits from an all-chloride solution".Trans.Inst.Metal Fin.,1966,44,78-83

80. Kendrick,R.J. "The effects of some aromatic sulphonic acids on the stress,structure and composition of electrodeposited nickel".Trans.Inst.Met.Fin.,1963, 40,19-27

81. Georges,J.M. and Rabinowicz,E. "The effect of film thickness on the wear of hard electrodeposits".Wear, 1969,14,171-180

82. Paul,B. "Macroscopic Criteria for plastic flow and brittle failure".In Liebowitz,H."Fracture,and Advanced Treatise",vol.II,315-489.Academic Press.Pub.1968

83. Hamilton,G.M. and Goodman,L.E. "The stress field created by a circular sliding contact".Jnl.Appl.Mech. June 1966,371-378

84. Jaeger,J.C. "Elasticity,Fracture and Flow;with engineering and geological applications".Science Paperbacks.Pub.1974

85. Jahanmir,S. and Suh,N.P. "Mechanics of subsurface void nucleation in Delamination Wear".Wear,1977, 44,17-38

86. Fujita,K. and Yoshida,A. "The effect of changing Rolling direction on the Rolling Contact fatigue lives of annealed and case-hardened steel rollers". Wear,1977,43,315-327

87. Huber,M.T. "Zur Theorie der berührung fester elasticher Körper".Annalen der Physik,1904,14,152-163

88. Toor,P.M. "A unified approach to the prediction of Multiaxial fatigue fracture of Aircraft Structures" Eng.Fract.Mech.,1975,7,731-741

89. Dieter,G. "Mechanical Metallurgy".McGraw Hill.Pub.1961

90. Williams,C. and Hammond,R.A.F. "The change of fatigue limit on chromium or nickel plating with particular reference to the strength of the steel base".Trans. Inst.Met.Fin.,1957,34,317-349

91. Dennis,J.K. "Decorative electro-deposited Metallic coatings".Int.Met.Rev.,1972,17,43-65

92. Hartley,N.E.W. "The tribology of Ion Implanted Metal Surfaces".Trib.Int.,April 1975,8,2,65-72

93. Smith,J.O. and Liu,C.K. "Stresses due to Tangential and Normal loads on an Elastic Solid with application to some contact stress problems".Jnl.Appl.Mech.,1953, 157-166

94. Poritsky,H. "Stresses and Deflexions of Cylindrical bodies in contact with Application to contact of Gears and of Locomotive Wheels".Jnl.Appl.Mech.,1950, 72,191-201

95. Hills,D.A.,Ashelby,D.W. and Waterhouse,R.B. "The Physical Influence of Surface treatments on Wear". Wear of Matls.1979,Dearbon,Michigan,396-402

96. Soda,N. et al "Wear of some f.c.c. metals during unlubricated sliding".Part III.Wear,1976,40,23-35

97. Bates,T.R. and Kudema,K.C. "Comments on 'The Delamination theory of Wear'".Wear,1974,28,141-142

98. Beagley,T.M. "Comments on 'The delamination theory of Wear'".Wear,1978,47,417-419

99. Suh,N.P. "An overview of the Delamination theory of Wear".Wear,1977,44,1-16

100. Suh,N.P. and Sridharan,P. "Relationship between the coefficient of friction and the Wear rate".Wear,1975, 34,291-299

101. Mitchell,L.A. and Osgood,C. "A theory of friction and wear based on a new characterisation of asperity interactions".Wear,1976,40,203-222

102. Bayer,R.G. et al "Applying the wear model to design problems".ASME Design Eng. Conf.Paper No.66MD-12 (May 1966)

103. Palmgren,A. "Ball and roller bearing Engineering". English trans. by Palmgren,G. and Ruley,B..Burbank and Co.,Philadelphia.2nd. ed.,pub.1946

104. Fleming,J.R. and Suh,N.P."The relationship between crack propagation rates and wear rates".Wear,1977, 44,57-64

105. Hertzberg,R.W. "Deformation and Fracture of Engineering Materials".John Wiley and Sons.Pub.1967

106. Knott,J.F. "Fundamentals of Fracture Mechanics". Butterworths.Pub.1973

107. Broek,D. "Elementary Engineering Fracture Mechanics". Noordhoff International Publishing.Pub.1974

108. Lawn,B.R. and Wilshaw,T.R. "The fracture of Brittle Solids".Cambridge University Press,Solid State Series Pub.1975

109. Knott,J.F. "An Introduction to Fracture Mechanics". Pub. in 'The Welder',nos.197-206,1977-1978

110. Rolfe,S.T. "Use of fracture mechanics in design". Int.Met.Rev.,1974,19,183-198

111. Hayes,D.J. "Origins of the S.I.F. approach to Fracture Mechanics".Jnl.Strain Anal.,1975,10,4,198-200

112. Hayes,D.J. "Origins of the Energy Balance approach to Fracure".Jnl.Strain Anal.,1975,10,4,195-197

113. Turner,C.E. "Yielding Fracture Mechanics".Jnl. Strain Anal.,1975,10,4,207-216

114. Rooke,D.P. and Cartwright,D.J. "Compendium of Stress Intensity Factors".HMSO.1st.ed.Pub.1976

115. Cartwright,D.J. and Rooke,D.P."Evaluation of stress intensity factors". Jnl. Strain Anal.,1975,10,4, 217-224

116. Westergaard,H.M."Bearing Pressures and Cracks".Jnl. Appl.Mech.,June 1939,A49-A53

117. Muskhelishvili,N.I."Some basic Problems of the Mathematical theory of Elasticity".English trans. by J.R.M.Radok.Pub. by Noordhoff,Gronigen,1953,3rd.ed.

118. Williams,M.L. "On the stress distribution at the base of a stationary crack".Jnl.Appl.Mech.,1957,24,109-128

119. Cartwright,D.J. and Rooke,D.P. "Green's Functions in Fracture Mechanics".Paper presented at'Fracture Mechanics-Current Status,future prospects',Cambridge,1979

120. Rice,J.R. "A path independent integral and the approximate analysis of strain concentration by Notches and Cracks".Jnl.Appl.Mech.,June 1968,379-386

121. Shaw,K.G."Fracture path determination using finite element methods".PhD thesis,Nottingham University,1975

122. Timoshenko,S.P. and Goodier,J.N. "Theory of Elasticity" McGraw Hill.3rd.ed.Pub.1970

123. Tada,H.,Paris,P.C. and Irwin,G.R. "The Stress Analysis of Cracks Handbook".Del Research Corp, Hellertown,Pa,1973

124. Tiffin,R. "Plane Elastic Deformation".Longmans,1970

125. Timoshenko,S.P. and Goodier,J.N. "Theory of Elasticity" 2nd.Ed.Note that these results do not appear in the third ed.,ref.122

126. Hills,D.A. and Ashelby,D.W. "On the Determination of Stress Intensification Factors for a Wearing Half-Space".Accepted for publication in Engineering Fracture Mechanics

127. Schijve,J."Internal cracks are growing in a Vacuum" Eng.Fract.Mech.,1978,10,359-370

128. Scott,D. "Ball Bearing steels-Factors influencing rolling contact fatigue".NEL Report No.360,Aug.1968

129. Scott,D. and Blackwell,J. "Steel refining as an aid to Improved roller bearing life".NEL Report No.354 May,1968

130. Scott,D. and McCullagh,P.J. "The effect of Residual Gas content on the performance of Rolling Bearing Materials".NEL Report No.551,Nov.1973

131. Fujita,K. and Yoshida,A. "Surface fatigue failure of nitride-hardened aluminium-chromium-molybdenum steel rollers under pure rolling and rolling-sliding contacts".Wear,1979,53,61-68

132. Rabinowicz,E. "The formation of spherical Wear particles".Wear,1977,42,149-156

133. Loy,B. and McCallum,R. "Mode of formation of spherical Wear particles".NEL Report No.536,Jan 1973

134. Smith,R.A. Unpublished work. Cambridge University Engineering Department

135. Hills,D.A. and Ashelby,D.W. "On the application of Fracture Mechanics to wear".Wear,1979,54,321-330

136. Anscombe,H. and Johnson,K.L. "Slip of a thin, solid tyre press-fitted onto a wheel".Int.Jnl.Mech.Sci., 1974,16,329-334

137. Swain,M.W. "Dislocation Generation beneath static and rolling contact with a sphere".Wear,1978,48, 173-180

138. Dufrane,K.F. "Influence of adsorbed fluids on the rolling contact deformation of magnesium oxide single crystals". Wear of matls. Conf.,St.Louis,1977

139. Pook,L.P. "An observation on mode II fatigue crack growth threshold behaviour".Int.Jnl.of Fract.,1977, 13,867-869

140. Mogford,I.L. "The Deformation and Fracure of two-phase Metals".Metall.Rev.,1967,12,114,49-68

141. Rosenfield,A.R. "Criteria for ductile fracture of two-phase materials".Metall.Rev.,1968,13,121,29-40

142. Argon,A.S. "Formation of Cavities from nondeformable second phase particles in low temperature ductile fracture".Jnl.Eng.Matls.& tech.,1976,60-68

143. Argon,A.S.,Im,J and Safoglu,R. "Cavity formation from Inclusions in ductile fracture".Metall.Trans., April 1975,6A,825-837

144. Goods,S.H. and Brown,I.M. "The nucleation of Cavities by plastic deformation".Acta Metallurgica,1979,27, 1-15

145. Goodier,J.N. "Concentration of stress around spherical and cylindrical Inclusions and flaws".Jnl.Appl.Mech., APM-55-7,39-44

146. Huang,W-C "Theoretical study of stress concentrations at circular holes and inclusions in Strain-hardening Materials".Int.Jnl.Solids Structures,1972,8,149-192

147. Hutchinson,J.W. "Singular behaviour at the end of a tensile crack in a hardening material".Jnl.Mech. Phys.Solids,1968,16,13-31

148. Rice,J.R. and Rosengren,G.F. "Plane strain deformation near a crack tip in a power law hardening material".

149. Chell,G.G. "B.C.S. Model solutions for Centre and Edge cracked plates subject to arbitary mode I loading" Int.Jnl.Fract.,1976,12,1,135-147

150. Chell,G.G. "A combined linear elastic and post yield Fracture Mechanics theory and its Engineering Applications".In 'Fracture Mechanics in Engineering Practice' Ed.P.Stanley,Applied Science publishers,1977

151. Forsyth,P.J.E. "A two-stage process of crack growth" Proc.Crack Propagation Symp.,Cranfield College of Aeronautics,1961,76-94

152. Toor,P.M. "On fracture mechanics under Complex Stress" Eng.Fract.Mech.,1975,7,321-329

153. Erdogan,F.In Fracture,an Advanced Treatise,ed.H.Liebowitz Academic Press,New York.Pub 1968,p.497

154. Kanazawa,T. and Machida,S. "On the effect of cyclic Stress Ratio on the Fatigue Crack propagation".Eng. Fract.Mech.,1975,7,445-455

155. Antolovich,S.,Saxena,A. and Chanani,E. "A Model for Fatigue crack propagation".Eng.Fract.Mech.,1975,7, 649-652

156. Pook,L.P. "Analysis and Application of Fatigue Crack Growth Data".Jnl.Strain.Anal.,1975,10,4,242-250

157. Wu,C-H "Fracture under combined loads by Maximum Energy release rate criterion".Jnl.Appl.Mech.,Sept. 1978,45,553-558

158. Otsuka,A.,Mori,K. and Miyata,T. "The condition of Fatigue crack growth in Mixed Mode condition".Eng. Fract.Mech.,1975,7,429-439

159. Pook,L.P. "Practical Implications of the Fatigue Crack growth threshold".Metal Science,Aug-Sept.1977,382-389

160. Cotterell,B. "On brittle fracture paths".Int.Jnl. Fract.,1965,1,2,96-103

161. Erdogan,F. and Sih,G.C. "On Crack Extension in Plates under plane loading and Transverse Shear".Jnl.Basic Eng.,1963,82D,4,519-527

162. Eftis,J. and Subramonian,N. "The Inclined crack under Biaxial Load".Eng.Fract.Mech.,1978,10,43-67

163. Liebowitz,H.,Lee,J.D. and Eftis,J. "Biaxial load effects in Fracture Mechanics".Eng.Fract.Mech.,1978, 10,315-335

164. Aurich,D. "The Influence of the Stress State on the Plastic Zone size".Eng.Fract.Mech.,1975,7,761-765

165. Frost,N.E.,Pook,L.P. and Denton,K. "A fracture mechanics Analysis of fatigue crack growth data for various Materials".Eng.Fract.Mech.,1971,3,109-126

166. Ohta,A. ans Sasaki,E. "A method for determining the stress intensity Threshold for fatigue crack Propagation".Eng.Fract.Mech.,1977,9,805-820

167. Francois,D. "The Influence of hydrostatic pressure on Fracture".Fracture,1977,1CF4,Waterloo,805-820

168. Hills,D.A. and Ashelby,D.W. "Combined Mode Fatigue crack propagation Predictions using Mode I data". Accepted for publication in Engineering Fracture Mechanics

169. Symonds,P.S. "Shakedown in Continuous Media".Jnl. Appl.Mech.,1951,85-89

170. Crook,A.W. "Simulated Gear Tooth Contacts;Some experiments on their Lubrication and Deformation". Proc.Instn.Mech.Engrs.,1957,171,5,187-214

171. Hamilton,G.M."Plastic Flow in Rollers loaded above

the yield point".Proc.InstnMech.Engrs.,1957,171,5, 187-214

172. Fujita,K. and Yoshida,A. "Surface Fatigue of case-hardened nickel-chromium steel rollers under pure rolling and sliding-rolling conditions".Wear,1979, 52,365-374

173. Fujita,K. and Yoshida,A. "Surface durability of case-hardened nickel-chromium steel rollers under pure rolling and rolling-sliding conditions".Wear,1979, 52,37-48

174. U.S. Dept. of Commerce, National Information Center "A Preliminary Description of Stresses in Railroad Rail". No. PB-272054,Nov.1976

175. Martin,G.C. and Hay,W.W."The Influence of Wheel-Rail contact forces on the formation of Rail Shells" ASME Preprint No.72-WA/RT-8

176. Johnson,K.L. "A Shakedown limit in Rolling Contact" Proc.4th.Nat.Conf.Appl.Mech.,Berkeley,California, June,1962,971-975

177. Merwin,J.E. and Johnson,K.L. "An analysis of plastic Deformation in Rolling Contact".Proc.Instn.Mech.Engrs. 1963,177,25,676-685

178. Johnson,K.L. and Jefferis,J.A. "Plastic Flow and Residual Stresses in Rolling and sliding contact". Proc.Instn.Mech.Engrs.,1963,177,25,54-65

179. Rydholm,G. and Fredriksson,B. "Shakedown in Rolling Contact Problems". International Conference on Applied Mechanics,Sweden,1978.

180. Fessler,H. and Ollerton,E. "Contact Stresses in Toroids under Radial Loads".Brit.Jnl.Appl.Phys., 1957,8,387-393

181. Love,A.E.H. "The Mathematical theory of Elasticity" Pub. by Oxford University Press.4th.ed,p.192-198

182. Thomas,H.R. and Hoersch,V.A. "Stresses due to the pressure of one Elastic Solid upon another". Univ. of Illinois Eng.Exptl.Station.Bull No.212,1930

183. Kornhauser,M. "A note on Elastic Surface Deformation" Jnl.Appl.Mech.,1951,18,251-252

184. Pomeroy,R.J. and Johnson,K.L. "Residual Stresses in Rolling Contact".Jnl.Strain Anal.,1969,4,3,208-218

185. Krause,H. and Juke,H-H "Internal Stresses during rolling friction and their Evaluation".Wear,1977,41, 15-23

186. Hills,D.A. and Ashelby,D.W. "A Fracture Mechanics Approach to Rolling Contact Fatigue".Tribology Int. June 1979,12,3,115-119

187. Marshall,D.B. and Lawn,B.R. "Residual Stress Effects in sharp-contact cracking":Part I Indentation Fracture Mechanics".To be pub. in Jnl.Mat.Sci.

188. Johnson,K.L. "An Experimental determination of the contact stresses between plastically deformed Cylinders" in 'Engineering Plasticity' ed. J.Heyman & F.A.Leckie, Cambridge University Press,1968

189. Hardy,C.,Baronet,C.N. and Tordion,G.V. "The elastic-plastic indentation of a Half-space by a Rigid Sphere". Int.Jnl.Num.Methods in Eng.,1971,3,451-462

190. Lee,C.H.,Masaki,S. and Kobayashi,S. "Analysis of ball Indentation".Int.Jnl.Mech.Sci.,1972,14,417-426

191. Tabor,D."A Simple theory of Static and Dynamic Hardness". Proc.Roy.Soc. Ser.A,1948,247-274

192. Johnson,K.L. "Reversed Plastic Flow during the unloading of a Spherical Indentor".Nature,1963,199, 4900,1282.

193. Prager,W. and Hodge,P.G. "Theory of Perfectly Plastic Plastic Solids".Pub. by John Wiley and Sons, New York,1951

194. Hill,R."The Mathematical Theory of Plasticity". Pub. by Oxford University Press,1950

J. Phys. E: Sci. Instrum., Vol. 12, 1979. Printed in Great Britain

An automated plating stress monitor

D A Hills and D W Ashelby
Department of Mechanical and Production Engineering,
Trent Polytechnic, Nottingham NG1 4BU, UK

Received 27 April 1978, in final form 6 October 1978

Abstract An automated bent-strip method for assessing the internal macrostresses in electrodeposits is described. True null deflection of the strip is maintained and an electrical output is available which can be recorded continuously, and processed. A modified calibration technique is described.

1 Introduction

Macrostresses in deposits are ordered, long-range forces which tend to distort thin components. Of apparatus designed to measure them, the manual Hoar and Arrowsmith (1957, 1958–9) method is fundamentally the most attractive since the elastic constants of the substrate do not need to be known. Little relaxation of the deposit is permitted and the apparatus is, in principle, frictionless. The specimens are much easier to make than those for its main rival, the Brenner and Senderoff (1949) spiral contractometer.

Automated stress monitors have been described by Koch *et al* (1976) and Sykes *et al* (1970), though both lack the accuracy of the Hoar and Arrowsmith method. The apparatus developed combines the accuracy of the last-mentioned technique with the convenience of automated methods.

2 Apparatus

A significant objection to the use of an optical lever to determine the null position, pointed out by Perakh (1974), is that the equilibrium position is not uniquely determined (figure 1). The improved instrument uses a light beam shone across the plane of swing of the strip, with a pair of closely

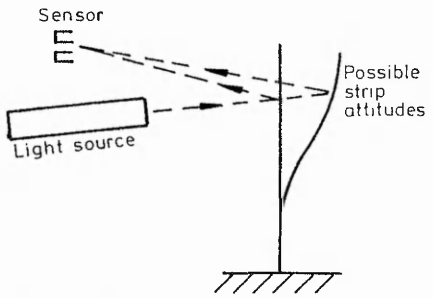


Figure 1 Diagram of optical lever showing lack of uniqueness in null position.

mounted phototransistors in the shadow of the strip (figure 2). The apparatus is immersed in a tank so that the electrolyte level is just below the solenoids. Since deposit is laid down on one side of the strip only, any built-in stress will cause the anode to bend, covering one phototransistor more than the other. The output from each phototransistor is used in

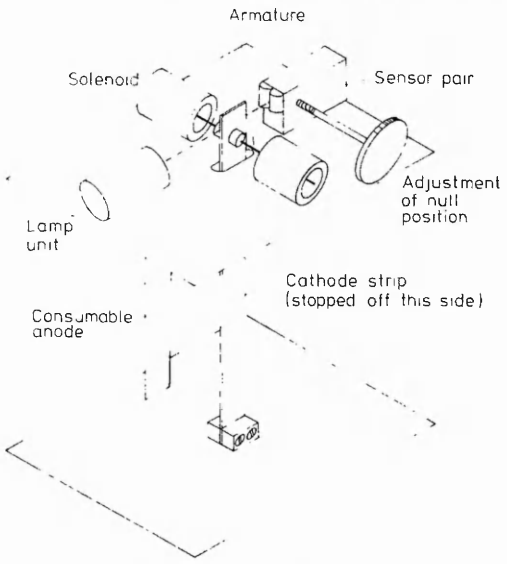


Figure 2 The modified apparatus. Note that the thin anode strip is held encastré in the base plate.

a bridge to control the ratio of currents in the solenoids (figure 3). Hence, any tendency of the strip to move from the null position results in a redistribution of the solenoid currents to correct the motion. The loop gain is determined by a variable, resistive feedback element since adding a capacitive term led to instability. The total current through the driver transistors, and hence the solenoid, is limited by a resistor in the common-emitter arrangement. To adjust the operating point, the potential on one base may be varied. A recorder output is taken, via a low-pass filter, from the

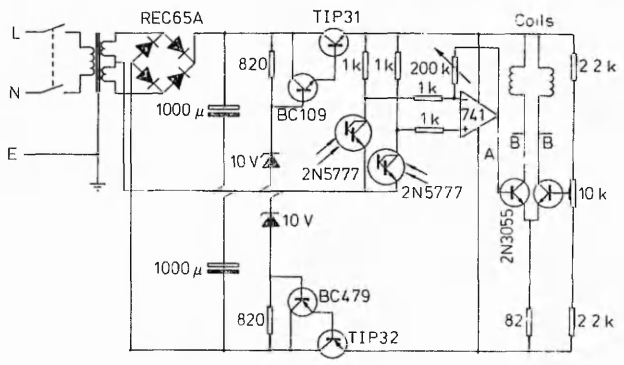


Figure 3 Circuit diagram of controller. A: disconnect for manual operation; B–B: recorder output.

difference of the collector voltages. The filter is necessary because, in practice, the strip oscillates, owing to the finite size of the semiconductor chips and their separation. A limit cycle is quickly established whose amplitude is partly controlled by the viscous damping of the bath: the amplitude is about 2 mm and provides enough agitation to reduce significantly the porosity of the plate.

Another small improvement is to fit a split armature which clamps across the strip, obviating the need to solder or glue the armature in place, and facilitating alignment of the strip.

0022-3735/79/030177+02 $01.00 © 1979 The Institute of Physics

3 Calibration

This was done, not by adding weights to the strip as commonly suggested in the literature, but by gradually tilting the apparatus over. Considering the bending load to consist of the distributed self-weight of the strip and the weight of the armature, the deflection due to these forces may be put equal to the deflection due to the restoring force alone:

$$F = g \sin \theta(\tfrac{3}{8} m_1 + m_2)$$

where m_1 is the mass of the strip and m_2 is the mass of the armature.

4 Conclusion

The apparatus is less tedious to use than a manually operated equivalent, and has the same accuracy. This is shown by disconnecting the bridge at point A (figure 3) and monitoring its output on a voltmeter. The base potential is manually adjusted with a potentiometer to maintain the same reading. The curve obtained is very similar to that obtained in an automatic run, but is smoother (figure 4). The output to the recorder is nearly linear within the working range, i.e. for $-550 < \sigma_{av} < 550$ (N mm^{-2}).

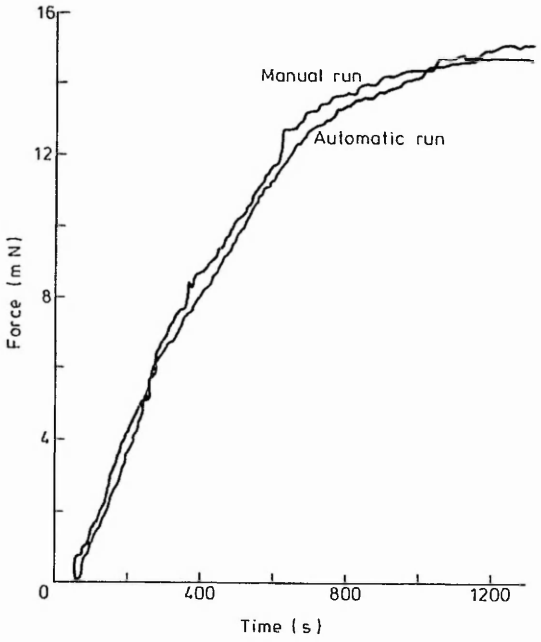


Figure 4 A comparison of the results obtained using the controller and by adjusting the solenoid current ratio manually.

Acknowledgments

The authors would like to express their thanks to Mr P J Thompson for the provision of laboratory facilities. Thanks are also due to Mr B Patterson for technical assistance.

References

Brenner A and Senderoff S J 1949 A spiral contractometer for measuring stress in electrodeposits
J. Res. NBS **42** 89–104

Hoar T P and Arrowsmith D J 1957 An instrument for the continuous measurement of stress in electrodeposits
Trans. Inst. Metal Finish. **34** 354–63

Hoar T P and Arrowsmith D J 1958–9 Stress in nickel electrodeposits
Trans. Inst. Metal Finish. **36** 1–6

Koch F B, Maher R A, Simms D L and Sard R 1976 An electronic plating stress monitor
Plating Surf. Finish. January 46–51

Perakh M 1974 Calculation of macrostress in electrodeposits
Proc. Symp. Electrostress Soc. of New York, 14–17 October pp 328–52

Sykes J M, Ives A G and Rothwell G P 1970 An apparatus for recording internal stresses in electrodeposits during plating
J. Phys. E: Sci. Instrum. **3** 941–2

THE PHYSICAL INFLUENCE OF SURFACE TREATMENTS ON WEAR

D. A Hills and D. W. Ashelby

Department of Mechanical and Production Engineering
Trent Polytechnic, Nottingham; England

R. B. Waterhouse

Department of Metallurgy and Materials Science
University of Nottingham
Nottingham, England

ABSTRACT

It is well known that surface treatments such as shot-peening, ball burnishing which produce hardened compressive surface layers effect improvements in wear resistance. The hardening mechanism is said to raise the yield pressure so that the contact stresses are below this value. Often it is assumed that the residual compressive stresses are beneficial because of their ability to hinder the propagation of surface fatigue cracks. This paper examines quantitatively the effect of pre-existing surface stresses on wear, and arrives at the conclusion that it may be a modification of the failure mode which is the important controlling influence; compressive stresses cause ductile behaviour whilst tensile stresses encourage cracking.

The effect of shakedown on pre-existing stresses, and the interdependence of measured hardness and stress are discussed. This indicates the difficulty of assessing the true yield stress of the material.

Experimental work using an electroplated layer where the locked in stresses can be controlled and measured is presented. The results tend to confirm the suggestion, made above, concerning failure mode.

NOMENCLATURE

σ_C	- built in stress in electrodeposit
$\sigma_z, \sigma_r, \sigma_\theta$	- contact stresses
a	- radius of contact
t	- instantaneous thickness of deposit
σ_{xx},&c τ_{xy},&c	- complete stresses under a roller
s_{xx},&c s_{xy},&c	- deviatoric stresses under a roller
J_{2A}	- 2nd. invariant stress deviator tensor for deposit stresses
$\bar{\sigma}_B$	- spherical component of contact stresses
q_o	- maximum contact pressure
σ_y	- yield stress
σ_{fl}	- fatigue limit
σ_{uts}	- ultimate tensile stress
A,B,k	- constants
Δ	- stress difference

INTRODUCTION

Surface treatments are popular in the impro of wear characteristics of surfaces. Because th thin they are usually not too expensive, and the interior properties do not have to be compromise tough component may be given a hard, though brit finish. Reviews of some possible treatments hav made by Hurricks (1) and Smart (2). The object o paper is to examine the effects of a built in st such as to be found after electroplating, shot- peening, burnishing, flame spraying or plasma spraying. Its affect on wear and its interdepen with hardness will be assessed.

First let us consider the influence of two processes which do not require the laying down o extra material, viz. shot-peening and ball-burni Both involve plastic working of the surface, whi therefore raises the yield stress, thereby permi higher subsequent loads to be carried under slid or rolling conditions without subsurface yieldin second and equally important effect is the gener of a residual compressive, biaxial stress. As w be shown, this residual stress alleviates the st experienced during contact loading, again postpo the onset of yield.

We assume that the presence of a subsurface region of plasticity is a key feature of wear, s its depth always plays a role in the detachment wear particles. Much work has been done, partic on bearings (for example see Ollerton (3)), and whilst it is still not completely resolved wheth cracks are surface or subsurface initiated under rolling conditions, they invariably pass through plastic zone, or zone of maximum shear. Disloca movement within a plastic zone expends much ener Also, if there are defects pre-existing in a mat this provides the opportunity for them to coales into an embryo crack.

Experimental work has shown the beneficial effects of shot-peening (4) and ball-burnishing We shall now examine the purely elastic stress f which might be expected to obtain between relati lightly loaded surfaces, eg. relay contacts or c followers, to quantify the effect.

ALLEVIATION OF CONTACT STRESSES

The exact form of the biaxial stress assume not critical, but we will use the Kushner model stress found in electroplates (6), to facilitate

comparison with experiment.

$$\sigma_c = A + B.(1 - k.t).e^{-kt} \qquad (1)$$

We now use the Hertz solution for contacting balls to model the solution in an elastic half space. In the coordinate system of Fig. 1;

$$\sigma_z = -q_o.a^2/(a^2 + z^2) \qquad (2)$$

$$\sigma_r = \sigma_\theta = -q_o.\frac{(1+\nu)}{a}.z\left\{\sin^{-1}\left[\frac{a}{\sqrt{(a^2+z^2)}}\right] - \frac{a}{z}\right\} - \sigma_z \qquad (3)$$

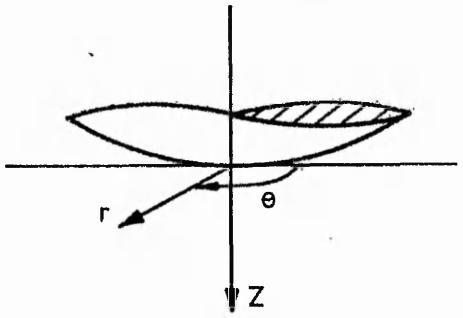


Fig. 1 Coordinate system used

Note that the stresses due to contact loading are all negative, and that the absolute value of σ_z is always greater than σ_r. For simplicity, we may temporarily assume Tresca's criterion, i.e.

$$|\sigma_z - \sigma_r| \leq \sigma_y \qquad (4)$$

It is clear, then, that to be beneficial the stress of eqn (1) must be compressive, as it is in burnishing and peening. Fig. 2 illustrates the two extreme cases of electrodeposit stress attainable (in this case for nickel), whilst Fig. 3 shows the stresses due to contact loading, with the highest compressive stress practically realised, superimposed. In Fig. 4 are plotted the yield loci, with and without superposition, and the hydrostatic component of stress. The contact stress system was chosen such that, in the absence of biaxial compression, yielding would just be attained. Note that, on the axis of symmetry, von Mises' and Tresca's criterion are equivalent. Also, for the particular case of superposing electrodeposit stresses, tensile stresses are always developed near the interface with the substrate. Whatever method is used to generate the biaxial stresses, there will always be a set of counterbalancing stresses further beneath the surface. Therefore the compressive stresses should persist to such a depth that the contact stresses have fallen substantially in this zone.

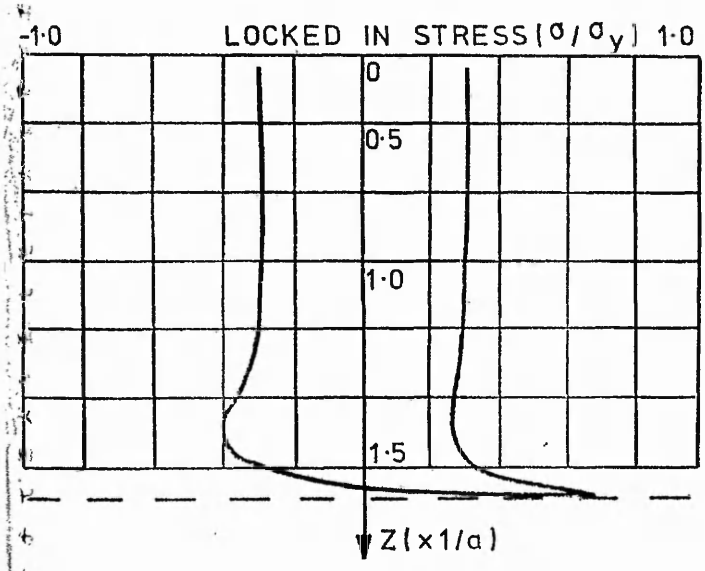


Fig. 2 Most tensile and most compressive stresses attainable in nickel plate.
Dotted line represents interface between substrate and electrodeposit.

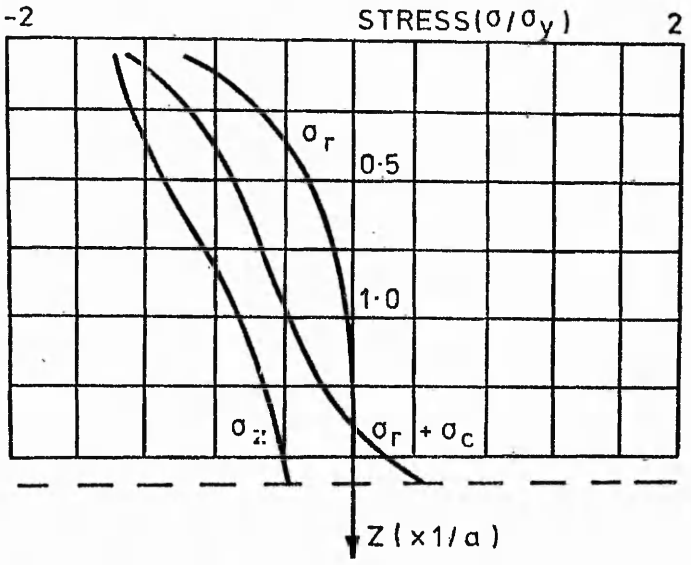


Fig. 3 Contact stresses and superimposed beneficial deposit stress

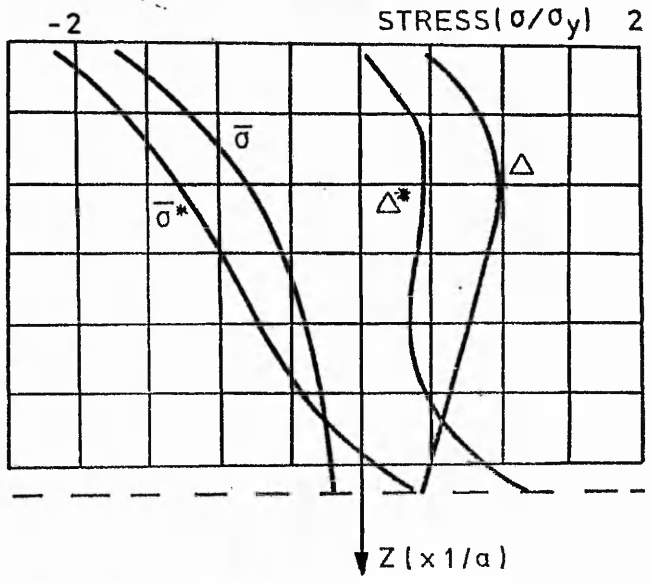


Fig. 4 Stress difference (Δ) and spherical stress components ($\bar{\sigma}$). *quantities indicate that the effect of the electrodeposit stress has been included.

The case of a more heavily loaded half-space is now considered, such that a zone of plasticity exists. To simplify our calculations we change our loading to that of a roller pressed onto the surface, and assume plane strain.

CONTROL OF A YIELDED ZONE

First the elastic stress field due to the applied load must be found. The solution used is that due to Beliaev, reported in Radzimovsky (7), but is too lengthy to repeat here. Von Mises' criterion is used to find the zone of plasticity, ie.

$$\sqrt{\frac{1}{6}\left[(\sigma_{yy}-\sigma_{xx})^2 + (\sigma_{xx}-\sigma_{zz})^2 + \sigma_{zz}-\sigma_{yy})^2\right] + \tau_{xy} + \tau_{yz} + \tau_{zx}} \leq \sigma_y \qquad (5)$$

This method is justified because the displacements just within the yielded zone must conform to the nearby elastic displacements, to achieve compatibility. Also, provided the elastic limit is not exceeded by too much, the strains produced will be very similar to those resulting from extended Hookean behaviour. The growth of the yielded zone is illustrated in Fig. 5. Again a stress distribution given by equation (1) was superimposed. Fig. 6 shows the result when a thick layer is used, so that the biaxial stress is substantially constant. The dramatic change in the size of the plastic zone can be seen, for a moderate change in biaxial stress. There are, though, pitfalls which are shown in Figs. 7, 8. Fig. 7 shows that if a very thin layer is applied, so that the interface lies just below the new plastic zone, the beneficial effects are removed at exactly the wrong time. The zone is extended slightly towards the surface but further below, it remains as before; the nett result is an extension of the zone of plasticity. By making the deposit a little thicker two plastic zones may be formed, separated by a thin elastic layer. This, too, occurs because the beneficial effects have been removed too soon, before the normal zone of plasticity has dwindled. A more insidious trap is shown in Fig. 8.

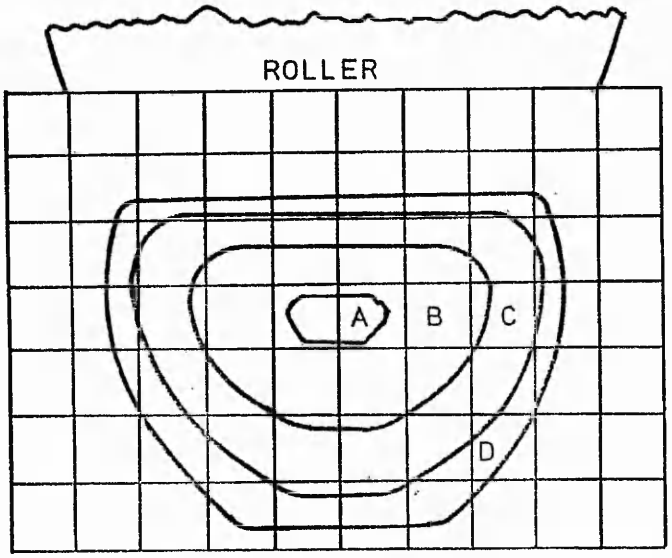


Fig. 5 Development of the yield zone beneath a roller. Line forces, normalized by yield stress are;
A : 0.246, B : 0.274, C : 0.309, D : 0.346
Zones are scaled to a constant contact width

Here, a more negative superimposed stress is shown As can be seen, the plastic zone has extended downwards, as yielding is now occurring in the opposite direction. The stress involved, 500 N/mm^2 is quit moderate and could easily be attained by the metho described earlier. Extreme compressive stresses, found in some ion-implanted layers (8) would not seem, by themselves, to be beneficial. The ideal compressive stress seems to be about a quarter of yield stress.

In order to assess the effect of these slidin systems on wear, sliding and rolling wear tests we carried out. Because of the integrity of the plat and long duration of rolling tests, results were o

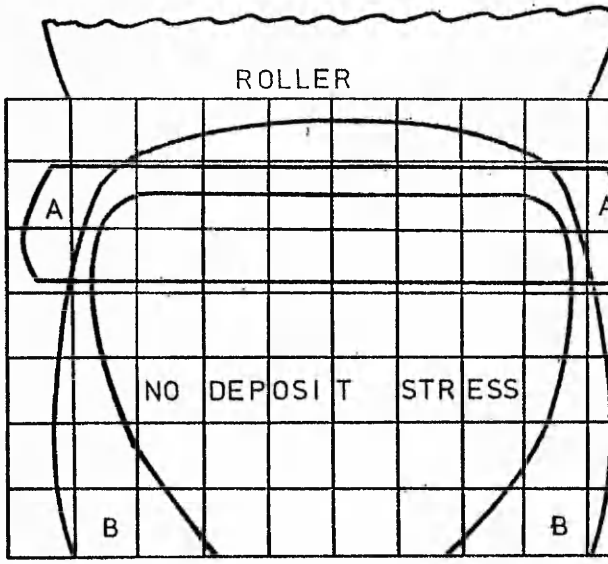


Fig. 6 The effect of superimposed stresses within thick layer.
Line force = 0.364 σ_y
Superimposed stresses; A = -0.364 σ_y
B = +0.454 σ_y

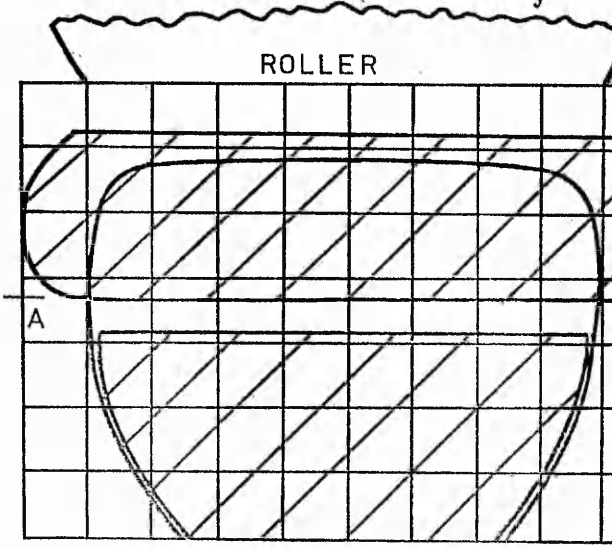


Fig. 7 The effect of using very thin layers.
Line force = 0.4 σ_y
Superimposed stress = -0.364 σ_y, interfac at A-A. Yielded zone shown hatched. Sin outline shows yielded zone in absence of deposit stress.

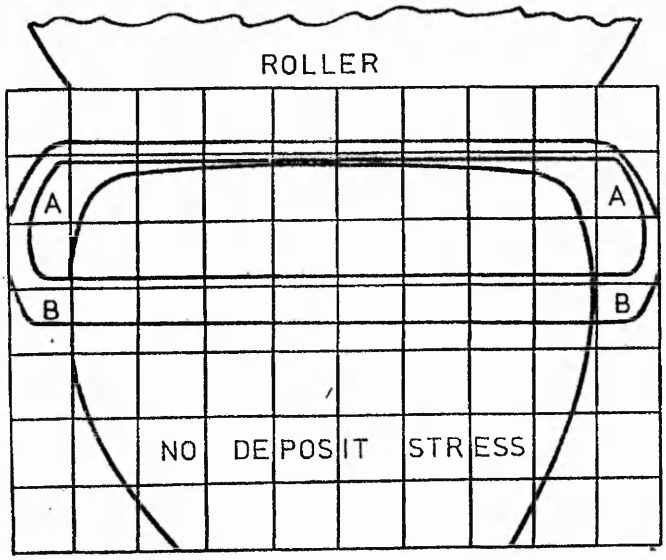


Fig. 8 Effect of excessively large compressive stress.
Line force = $0.364\ \sigma_y$
Deposit stress in zone A = $-0.364\ \sigma_y$
B = $-0.91\ \sigma_y$

qualitative. Delamination was found, though the surfaces containing compressive stresses did not show signs of serious degradation after 10^6 passes. Therefore, the main results were obtained from sliding wear tests.

SLIDING WEAR TESTS

Experiments were performed using a crossed-cylinder arrangement on a modified lathe. The samples consisted of nickel plated mild steel samples, 1 inch in diameter and 1 inch long. Plates between 1 and 10 μm thick were tried, and locked in stresses in the range -200 to +400 N/mm² used. Tensile stresses were easily obtained using cold all-chloride baths, and these were gradually reduced by warming the plating bath, and superimposing a 400 Hz square wave on the plating current. The latter idea is due to Kendrick (9), and proved very effective. Compressive stresses were created by adding suitable reagents, viz. toluene-4-sulphonic acid or thiourea. No reagents were found which did not contain sulphur although this would have been desirable because of its well known lubricating properties. However, no change in the coefficient of friction was noticed in continuous monitoring during wear tests. Stresses were found by using a bent strip method modified to provide a record of stress plated in throughout the depth. The conditions were then duplicated as nearly as possible using the cylindrical specimen.

No influence could be found of the change in thickness on the wear rate until very thin deposits were used (1-2 μm), when the varying geometry across the contact width probably accelerated wear. This conclusion is consistent with the results of Georges and Rabinowicz (10). The considerable effect of deposit stress on wear rate is shown in Fig. 9 which also shows the variation in measured hardness. Scanning electron micrographs were also taken of some of the wear surfaces and these are shown in Fig. 10.

It is clear at once that the simple stress theory presented so far is inadequate, particularly for the case of a locked in tensile stress. We must therefore amend our suggestions, and present three complicating effects to help explain the results;
1. Interdependence of hardness and locked in stress.
2. Effect of shakedown.
3. Effect of differing hydrostatic stress components.

HARDNESS

We have said that the presence and size of a plastic zone is important. Therefore, so is the hardness of the material, since this determines the elastic limit, and hence the size of the plastic zone. The yield stress is, of course, proportional to the hardness. However, the hardness measured in an indentation test is not necessarily the true hardness, because, if a set of biaxial stresses is present, it will supplement the stress field due to the indentor. Since gross plastic deformation occurs it is not possible to perform simple superposition, but since the vertical stress component is certainly larger than the radial component (in absolute magnitude), the superposition of a compressive stress will give an artificially high hardness reading, and vice versa. Thus, the true hardness of the electrodeposit containing a tensile stress is probably higher than that shown on the graph. To illustrate this, a supplementary experiment was done by fitting a tensometer onto the table of a Brinell hardness testing machine. A support was fitted under the specimen, which was indented at various applied tensile loads. The sizes of the indentations were measured with the same load applied so that the

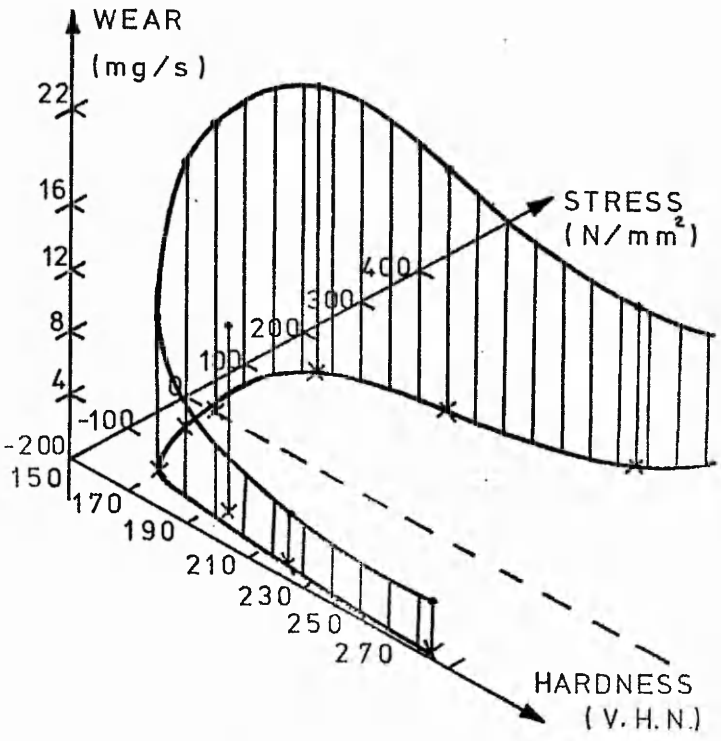
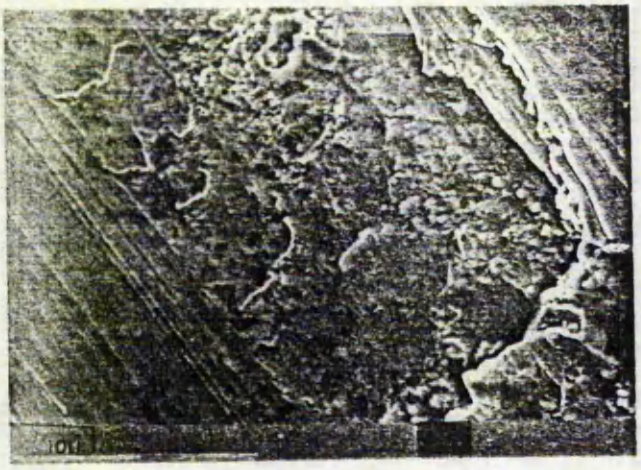


Fig. 9 Sliding tests wear v stress v hardness
Stress reliever used:
toluene-4-sulphonic acid



A Tensile electrodeposit stress (+400 N/mm^2)



B No electrodeposit stress



C Compressive electrodeposit stress (-250 N/mm^2)

Fig. 10 Scanning electron micrographs of wear tracks

relaxation of the indentation did not occur. Specimens chosen were an annealed aluminium and work hardened copper. The copper showed a monotonically decreasing hardness as the load was applied whilst the result for aluminium is shown in Fig. 11. It ca be seen that, for aluminium, the specimen shows an initial decrease in hardness, then work hardening occurs. When 90% of the yield had been attained the load was removed and the hardness again increased, this time to a higher value because of the work hardening. There is a permanent set, too, partly attributed to local yield around an indentation. Though the results are not directly applicable to th case considered above, the same trend should be followed, and with a biaxial stress the effect shoul be rather more marked.

So far it has been assumed that the only stress which persist are those locked into the plate as it is laid down. This may not be true if the elastic limit is exceeded, since additional residual stress may develop to confine the plastic zone. This is t concept of shakedown in a continuous medium.

SHAKEDOWN

The exact form of the residual stresses developed is known only for the case of two-dimensional rolling contact, though it is probable that similar stresses are developed in sliding contact. For rolling contact, Merwin and Johnson (11) found the value of residual stresses and worke out the subsequent yielding zone for an ideally elastoplastic material. It is very similar to that produced artificially in an electrodeposit. Why ar locked in stresses valuable at all then, if the system produces nearly ideal residual stresses on i own? From Melan's theorem we would expect the fina stress state to be independent of the initial conditions. In practice, the answers do not seem

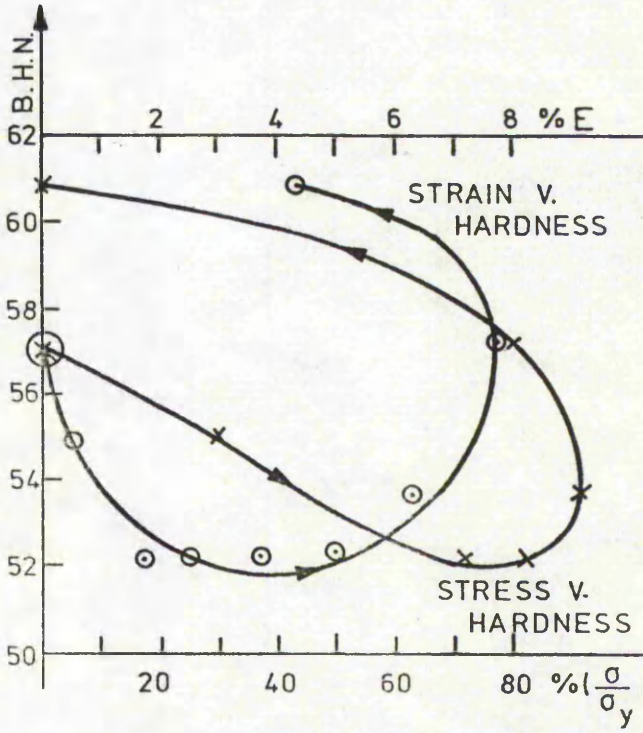


Fig. 11 The effect of a uniaxially applied load on measured hardness

nearly as clear cut. Fujita and Yoshida (12) have conducted some tests under rolling contact conditions and reversed the direction of rolling after a number of cycles. With some materials this affects their fatigue life. This is attributable to shakedown, but is not universal. Johnson does not consider the possibility of secondary plastic flow, and anyway we cannot be sure of the nature of shakedown stresses for a work hardening material.

EFFECT OF HYDROSTATIC STRESS COMPONENT

The last aspect to be discussed is the influence of the change in the spherical stress component due to an added stress system. All the effects discussed so far may be attributed to the deviatoric components of stress. This is most easily seen if we rewrite von Mises' citerion (5) in terms of deviatoric quantities;

$$\sqrt{3}\sqrt{\left\{\frac{1}{2}\left(s_{xx}^2+s_{yy}^2+s_{zz}^2\right)+s_{xy}^2+s_{yz}^2+s_{zx}^2\right\}} \leqslant \sigma_y \qquad (6)$$

It is now clear that what has been said so far is true whatever the spherical stress component. However, its value may well influence material behaviour.

When dealing with the failure criteria of metals we normally assume a plasticity criterion which takes no account of the spherical stress. Further, in wear we need to know not only about the onset of plasticity, but also the stress conditions under which actual cleavage occurs. If this occurs in a brittle manner then we cannot learn much about it from a traditional criterion. We do know, though, that under compressive conditions a material is more likely to flow, and that premature ultimate failure will be postponed. Observe the micrographs shown in Fig. 10. The samples containing the most negative spherical stress component all show extensive plastic flow, delaying the moment of particle separation. Samples containing a tensile stress, and therefore having a smaller spherical stress component show transverse cracking, which we may associate with the premature detachment of wear particles, and therefore higher wear rates.

Further, the hardness, and therefore the yield stress are determined with a particular intrinsic spherical stress, depending on the nature of the plastic field beneath the indentor, and the work hardening index of the material. It is unlikely that this will be the same as the spherical stress obtaining under wear conditions. We are assuming implicitly that the yield surface is a cylinder: it may well be a paraboloid.

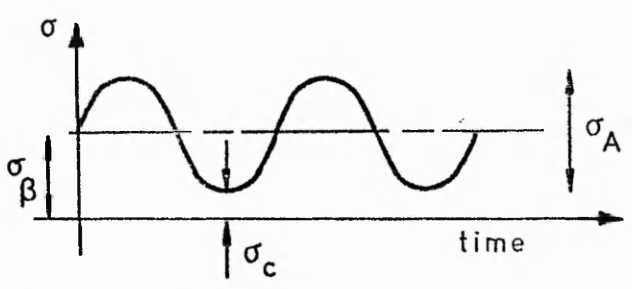


Fig. 12 Nomenclature used in equation (7)

We have treated wear as a continuum, bulk stress problem. Particle detachment must proceed by the propagation of subsurface cracks (13). The larger the confining pressure around the crack, the more likely the crack faces are to lock together and the more crack propagation will be hindered. It is not possible, however, to treat wear as a conventional fatigue process. This was tried by using a three-dimensional fatigue criterion due to Sines (14), which we may write in terms of stress invariants as

$$\sqrt{\frac{3.J_{2A}}{4}}+\frac{\sigma_{fl}}{\sigma_{uts}}\,\bar{\sigma}_B \leqslant \sigma_{fl} \qquad (7$$

where $\bar{\sigma}_B = \frac{1}{2}\,\bar{\sigma}_A + \sigma_C$ (see Fig. 12).

This relation in conjunction with the Hertzian solution used earlier (2, 3) predicts that no bearing surface should ever fail, Fig. 13. The beneficial effect of a compressive biaxial stress is nevertheless apparent. The main reason for the failure of a fatigue criterion would appear to be that the conditions for crack growth differ; in most fatigue cases propagation occurs under tensile conditions opening the crack, and possibly a superimposed shear. In wear, crack propagation occurs under compression normal to the crack face, and a significant component of shear. Because these mechanisms are so different the fatigue criterion, which is really only a justifiable 'curve-fit' under tensile/shear conditions, fails.

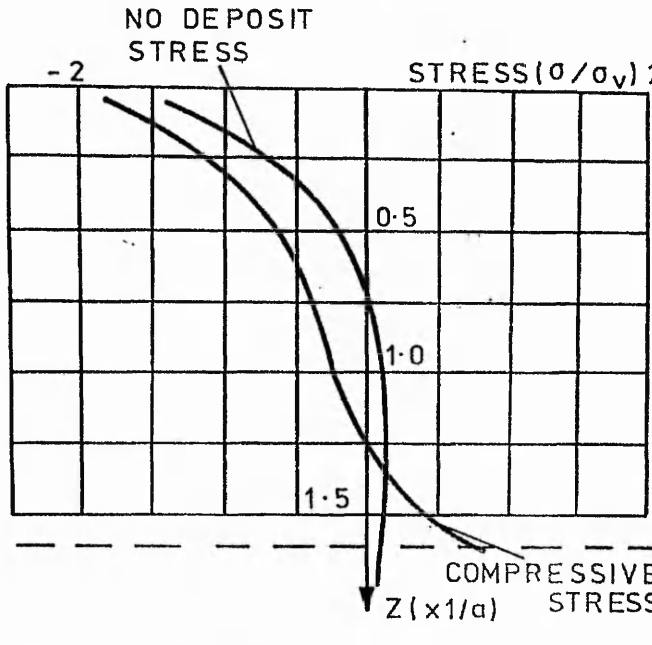


Fig. 13 Application of Sine's fatigue criterion

CONCLUSION

It is clear that we may modify both the wear rate and nature of particle detachment by adding stresses in the surface layers of a sliding pair. The resulting stress field from these locked in stresses and normal contact loading has been found. This, together with the changing material behaviour is offered as a reason for the modified material

response. Interaction of a locked in stress field with the material's hardness, and the possible establishment of additional near-surface stresses by the shaking down of the surface are presented as complicating factors which cannot be avoided. Until we can find an elastoplastic stress field for a sliding pair and determine the shakedown stresses for real materials under such conditions it is hoped that the purely normal contact model will prove adequate.

REFERENCES

1 Hurricks, P. L., "Review Paper: Some Aspects of the Metallurgy and Wear Resistance of Surface Coatings," Wear, Vol. 22, 1972, pp. 291-320.

2 Smart, R. F., "Selection of Surfacing Treatments," Tribology International, Vol. 11, No. 2, April 1978, pp. 97-104.

3 Ollerton, E., and Morey, J. W. W., "Fatigue Strength of Rail Steel in Rolling Contact," Symposium on Fatigue in Rolling Contact, Institute of Mechanical Engineers, 1964, pp. 11-22.

4 Hertzberg, R. W., "Deformation and Fracture Mechanics of Engineering Materials" John Wiley & Sons, N.Y., 1976, pp. 435-6.

5 Rajasekariah, R., and Vaidyanathan, S., "Increading the Wear Resistance of Steel Components by Ball Burnishing," Wear, Vol. 34, 1975, pp. 183-188.

6 Kushner, J. B., "Factors affecting Residual Stress in Electrodeposited Metals," Metal Finishing, April 1958, pp. 46-51.

7 Radzimovsky, E. I., "Stress Distribution and Strength Condition of Two Rolling Cylinders Pressed Together," University of Illinois Engineering Experiment Station Bulletin, No. 408.

8 Hartley, N. E. W., "The Tribology of Ion Implanted Metal Surfaces," Tribology International, Vol. 8, No. 2, April 1975, pp. 65-72.

9 Kendrick, R. J., "The Effect of Alternating Current on the Properties of Nickel Deposits from an All-Chloride Solution," Transactions of Institute of Metal Finishing, Vol. 44, 1966, pp. 78-83.

10 Georges, J. M., and Rabinowicz, E., "The Effect of Film Thickness on the Wear of Hard Electrodeposits," Wear, Vol. 14, 1969, pp. 171-180.

11 Merwin, J. E., and Johnson, K. L., "An Analysis of Plastic Deformation in Rolling Contact," Proceedings of Institution of Mechanical Engineers, Vol. 177, No. 25, 1963, pp. 676-685.

12 Fujita, K., and Yoshida, A., "The Effect of Changing the Rolling Direction on the Rolling Contact Fatigue Lives of Annealed and Case-hardened Steel Rollers," Wear, Vol. 43, 1977, pp. 315-327.

13 Suh, N. P., "An Overview of the Delamination Theory of Wear," Wear, Vol. 44, 1977, pp. 1-16.

14 Sines, G., "Failure of Materials Under Combined Repeated Stresses with Superimposed Static Stresses," NACA Technical Note 3495, 1955.

Wear, 54 (1979) 321 - 330

© Elsevier Sequoia S.A., Lausanne — Printed in the Netherlands

ON THE APPLICATION OF FRACTURE MECHANICS TO WEAR

D. A. HILLS and D. W. ASHELBY

Department of Mechanical and Production Engineering, Trent Polytechnic, Nottingham (Gt. Britain)

(Received November 8, 1978)

Summary

Theoretical considerations are presented which show that in general there may be two crack growth mechanisms proceeding simultaneously under wear conditions. Each pass of a rider over a particular subsurface flaw causes it to experience two distinct growth periods, separated by a period when there is no tendency for relative motion between the crack faces. Furthermore, one growth period, just before the rider arrives at the flaw, consists of mode II stress intensification with a light clamping force between the crack faces. The other growth period, following behind the rider, consists of both mode I and II openings. In the first growth period, because there will be some small relative motion between the crack faces under loading, a fretting type of degradation may occur.

1. Introduction

The application of fracture mechanics to wear is in its infancy. Hornbogen [1] used a dimensional analysis to show the importance of a material's fracture toughness to wear rate. More recently, Fleming and Suh [2] attempted to derive a more complete solution for the stress intensification factors (SIFs) from first principles. Their loci of equal SIF looked promising because they showed a maximum beneath the surface. Unfortunately, the crack propagation rates predicted were too small. Possible reasons are as follows.

(1) Because the SIFs are so small it is probable that growth occurs in stage 1 (see ref. 3). This means that the usual index in the Paris equation is too small:

$$\frac{dc}{dN} = C\Delta K^m \tag{1}$$

where c is the crack half-length, N is the number of cycles and K is the SIF. The data pertaining to this equation are normally obtained in stage 2.

(2) In Fleming and Suh's paper loads associated with an individual asperity are considered, *i.e.* the force distributed over the wearing surface is

$$F = 3\sigma_y s \tag{2}$$

where s is the cross section of an asperity. The effect of including the force contributions of many contacting asperities is not considered.

(3) Fleming and Suh made the assumption that all crack growth occurred in the region of tensile stress behind the point of load application where combined mode I and II growth occurs.

The present paper tries to overcome some of these drawbacks whilst using the same basic method to approximate the SIFs. It has been shown [4] that the lower bound solution of Fleming and Suh is a good approximation to finding the SIFs for mode II growth. This employs the pseudo-stress method, using a Green's function appropriate for a crack in an infinite solid. Since the solutions obtained by this technique are within 10% of the true solution, even at depths much closer to the surface than the turning point of the SIF function, it will be used here.

2. Method of solution

First the pseudo-stress field, *i.e.* the stress field in the absence of the crack, is found. The crack is then inserted at the desired location. It will then be found that the crack faces are not in general free of tractions. Equal opposite tractions are applied to the crack faces so that the boundary conditions there are again satisfied, and at the same time their contributions to the stress intensification are evaluated using the Green's weighting function. For pure mode II and a crack existing in an infinite solid, this gives

$$K_{II} = \frac{Q}{2(\pi c)^{1/2}} \left(\frac{c + b}{c - b} \right)^{1/2} \tag{3}$$

where Q is the element of shear force on the crack face and b is the distance from the crack centre line to that element. The application of stresses to the crack faces causes non-zero stresses to appear on the surface of the elastic half-space. For best accuracy, further surface tractions should be applied to give the correct boundary condition and the scheme outlined should be pursued iteratively, but sufficient accuracy has been attained already for the present calculation. Consider Fig. 1. For a distributed load, the region

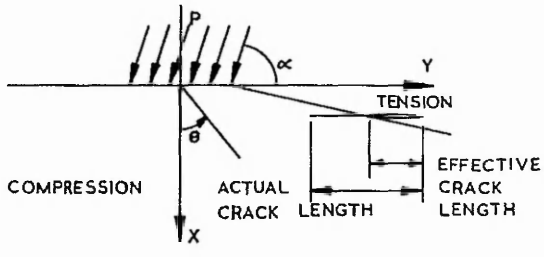


Fig. 1. The coordinate system used showing the region of tension behind the loading. Note that the crack is closed within the compression region.

behind the applied load is in tension, as in the Flamant solution for a point applied load. However, this is not the only region where crack growth may occur. The solution for just the central element P of the distributed load, in the coordinates of Fig. 1, is

$$\sigma_{xx} = -\frac{2P}{\pi d}\cos^3\theta\cos(\theta+\alpha)$$
$$\tau_{xy} = -\frac{2P}{\pi d}\sin\theta\cos^2\theta\cos(\theta+\alpha) \tag{4}$$

Although a horizontal crack is under compression, there is a significant component of shear present in front of the load. Naturally the vertical component σ_{xx} of stress, being negative, closes the crack and does not contribute to an SIF. However, letting the coefficient of friction be μ, the net shear across the crack which cannot be carried by friction forces and which therefore contributes to stress intensification is

$$\left.\begin{aligned}\tau_{\text{net}} &= \tau_{xy} + \mu\sigma_{xx} \qquad \tau_{xy} > 0\\ &= \tau_{xy} - \mu\sigma_{xx} \qquad \tau_{xy} < 0\end{aligned}\right\} \quad |\tau_{xy}| > |\mu\sigma_{xx}| \tag{5}$$

This quantity represents the residual pseudo-stress which appears on the crack boundary. Counterbalancing forces of equal magnitude are now applied to the crack faces, and their contributions to the stress intensification factor are found using the weighting function of eqn. (3).

3. Model of the wearing pair

In the present paper the surface load is assumed to be evenly distributed in order to facilitate calculations. The area over which the load is applied is divided into 20 equal strips, and a point load equal to the total load over the strip is applied at the centre of each. One can consider the contact width on one of two scales: first it can be assumed to be the load applied by a single plastically deformed asperity when the load applied is equal to the force given by eqn. (2); alternatively, the contact width can be assumed to approximate the contact loading when a cylinder is pressed into an elastic half-space or, equivalently, the load distribution found in a crossed-cylinder wear test. It is recognized that the envelope of pressure ordinates in such a case should be elliptical, but the difference in pseudo-stress fields is probably small at depths of interest as might be expected from St. Venant's theorem. Also from St. Venant's theorem, it might be expected that a continuously distributed load and one applied at discrete points would give similar pseudo-stress fields.

An example of the stress available to provide crack growth, with its derivation, is shown in Fig. 2. A selection of net shearing stresses for different surface and crack coefficients of friction is shown in Fig. 3. It is interesting to note that the type of crack extension under compression exists with a

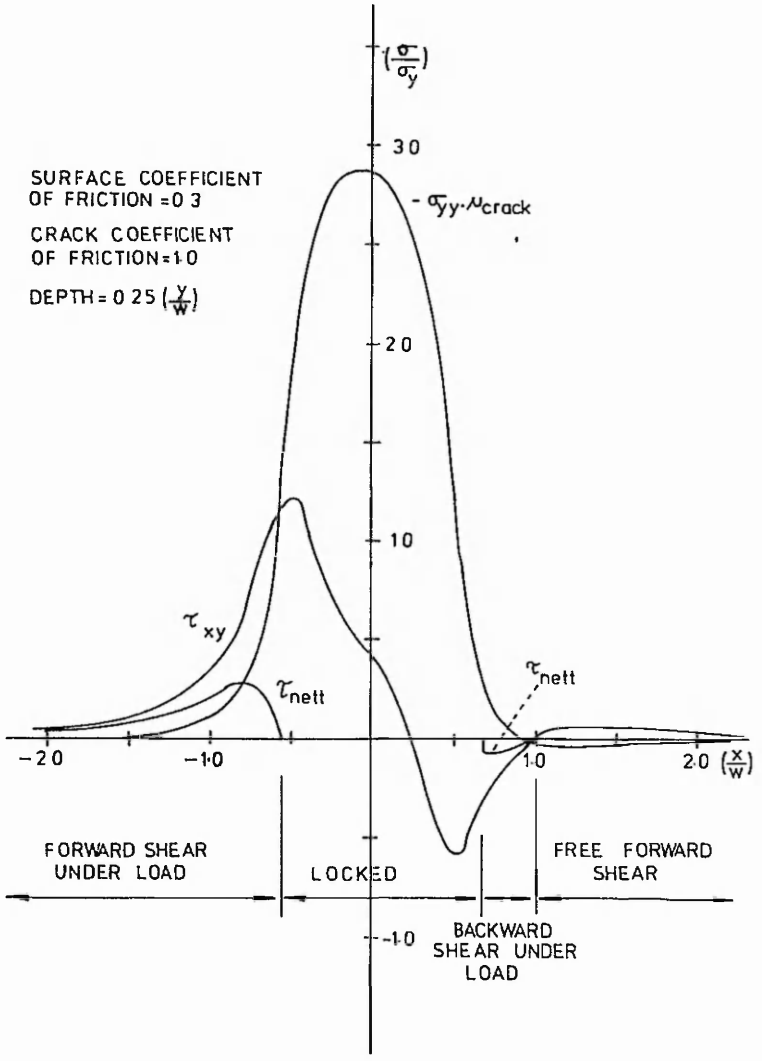


Fig. 2. The net shear stress available to propel a crack together with the stresses σ_{yy} and τ_{xy} from which it is derived.

purely normal load (Fig. 4). Although the contact loading is not identical to that under rolling contact, a similar result is anticipated. This illustrates a possible mode of crack propulsion under such conditions and has been investigated by McClintock [5]. Note that as the crack passes under the loaded region it experiences four possible regimes:

(1) forward shear under compression;

(2) "locking" (all load carried by frictional forces, no relative motion between crack faces);

(3) reversed shear under compression, which does not always occur, and the shear stress available to propel the crack is small; it is not expected to be very important under most wear conditions;

(4) free shear, which happens in the wake of the rider and is accompanied by a mode I opening.

The first regime raises interesting possibilities. It is apparent from the displacement fields given by the singular solutions that there should be a

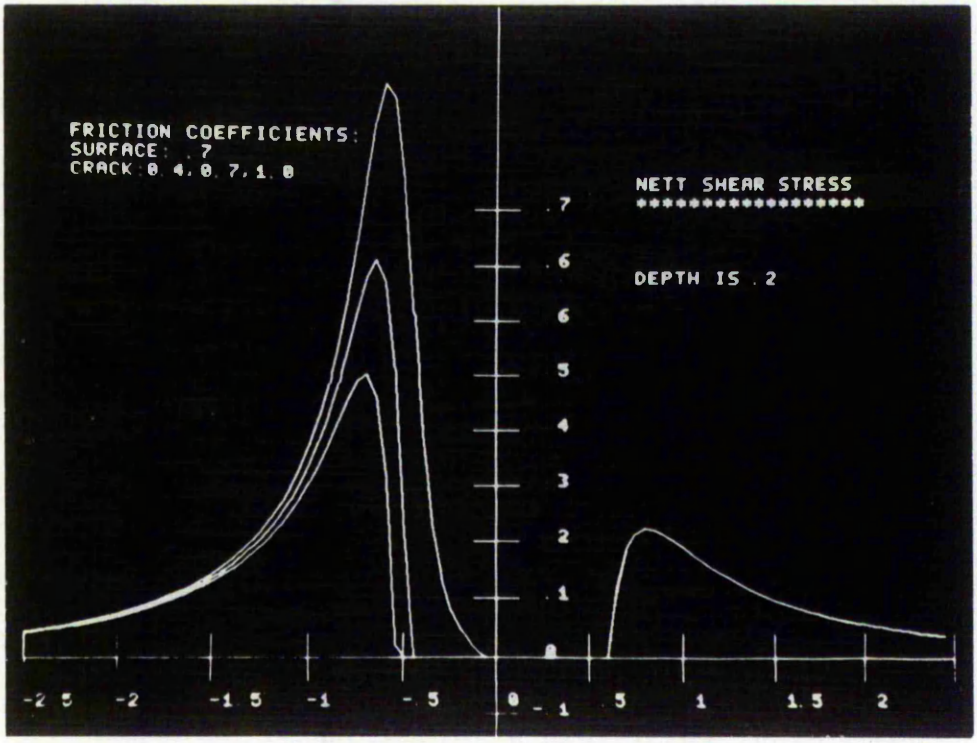

FRICTION COEFFICIENTS:
SURFACE: .7
CRACK: 0 4, 0 7, 1 0
NETT SHEAR STRESS
DEPTH IS .2
.7
.6
6
5
4
3
2
.1
-2 5
-2
-1 5
-1
- 5
0
- 1
5
1
1.5
2

Fig. 3 (a).

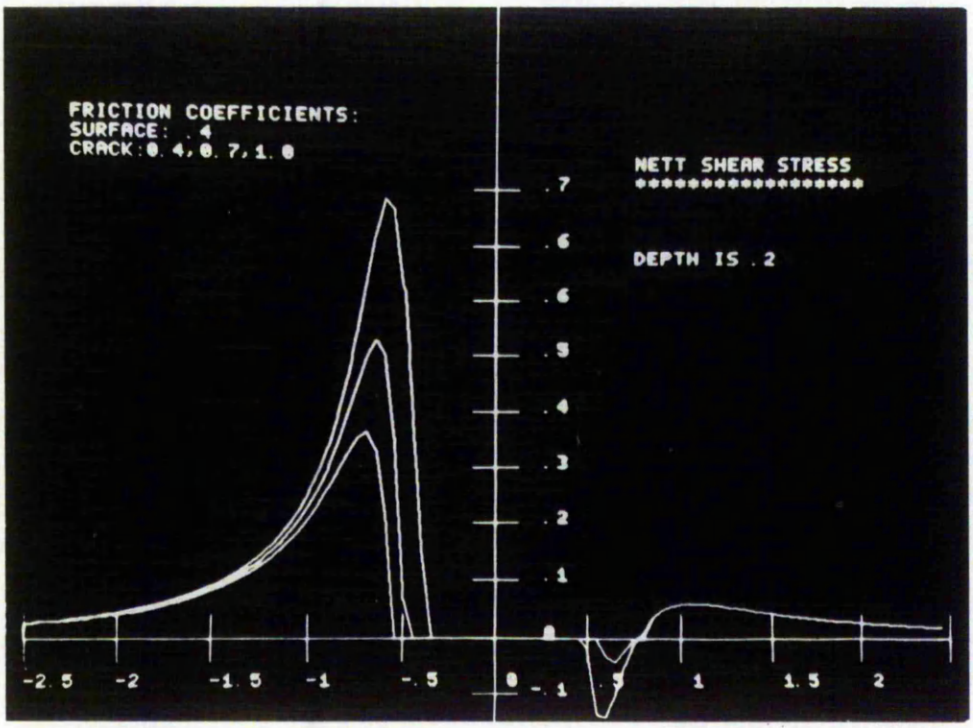
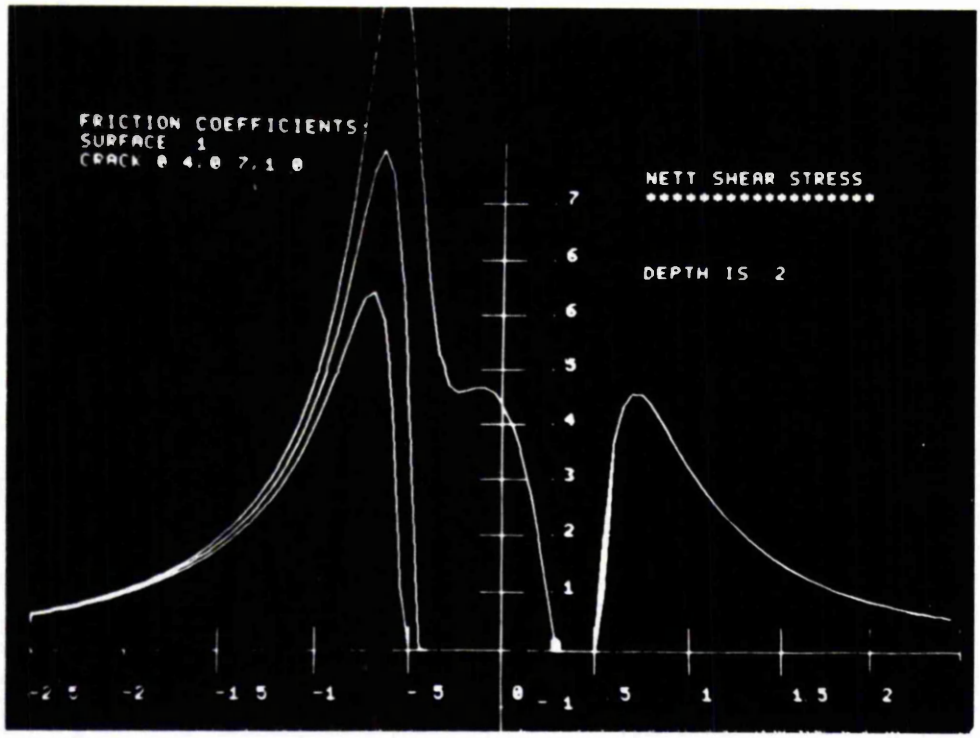

FRICTION COEFFICIENTS:
SURFACE: .4
CRACK: 0 4, 0 7, 1 0
NETT SHEAR STRESS
DEPTH IS .2
.7
.6
.6
.5
.4
.3
.2
.1
-2 5
-2
-1 5
-1
-.5
0
- 1
.5
1
1.5
2

Fig. 3 (b).



(c)

Fig. 3. Shear stress available to propel the crack under various conditions. Note that in each case the load was applied from the right acting towards the left. The highest peak corresponds to the lowest coefficient of friction between the crack faces and vice versa. The depth and distance from the centre line are normalized with respect to the width of loading and the stresses are normalized by the contact pressure.

small amount of relative motion between the crack faces; hence fretting should occur. This would degrade the surfaces of the crack and might accelerate wear, although the amplitude is smallest at the crack tip. The wear crack would experience some fretting and crack growth, followed by a rest period with a stress "set-in". After this rest period under load it would undergo combined mode extension. This would occur for each rider pass. The question of whether or not the same coefficient of friction should be used for the wear surface and for the crack face arises. If the nucleating crack were absolutely clean it would be welded back together again each time the crack passed through the locking (maximum compression) region, *i.e.* the propagating wear crack would continually heal! Since this is not so it must be assumed that a contaminant is present. This could be gases adsorbed from the atmosphere. The idea is consistent with the known experimental result that vacuum degassed components show a significant improvement in wear. The degree of adsorption may also play a role in deciding the thickness of the delaminating sheets. It is expected that friction coefficients between the crack faces will nevertheless be higher than at the surface because of the absence of contaminants.

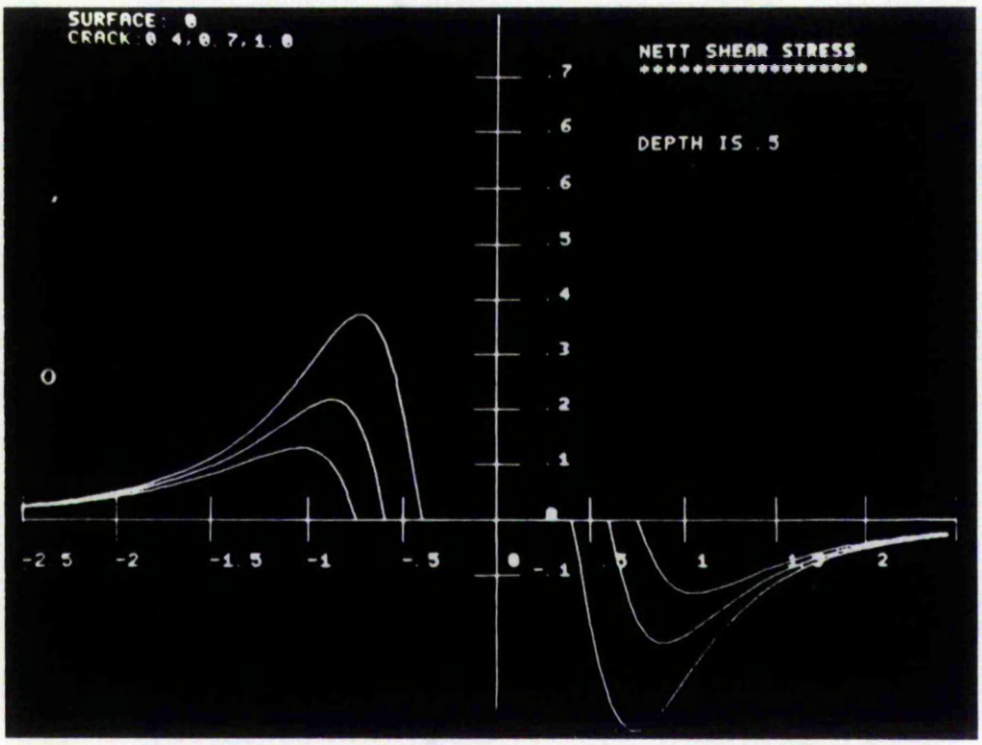


Fig. 4. The net shear available to propel a crack under normal loading (no tangential tractions). The graph is normalized in the same way as Fig. 3.

4. Generation of the SIF maps

Using the Green's function of eqn. (3) a computer program was written for mode II propagation in zones of both free shear and shear under compression. This enables the relative importance of the two regions to be assessed, and a typical result is shown in Fig. 5. It can be seen that the regions are approximately equal in their contribution to crack growth.

The program was then modified to perform a raster scan through the depth while remaining in the neighbourhood of the maximum SIF. This enabled the effect of crack length on SIF to be assessed conveniently, and at the same time shows the most likely propagation depth. The result is shown in Fig. 6.

To assess the feasibility of the model, consider a specific case. Let the wearing pair be a crossed-cylinder configuration, with an applied load of 50 N. Then, if the material hardness is 1 kN mm^{-2}, the contact diameter will be of the order of 0.25 mm. If the normal component of the contact pressure is the same as the hardness and the coefficients of friction are both unity, the SIFs will be

free shear: $K_{II} = 0.622$ kN mm$^{-3/2}$

$K_{I} = 0.434$ kN mm$^{-3/2}$

compression/shear: $K_{II} = 0.677$ kN mm$^{-3/2}$

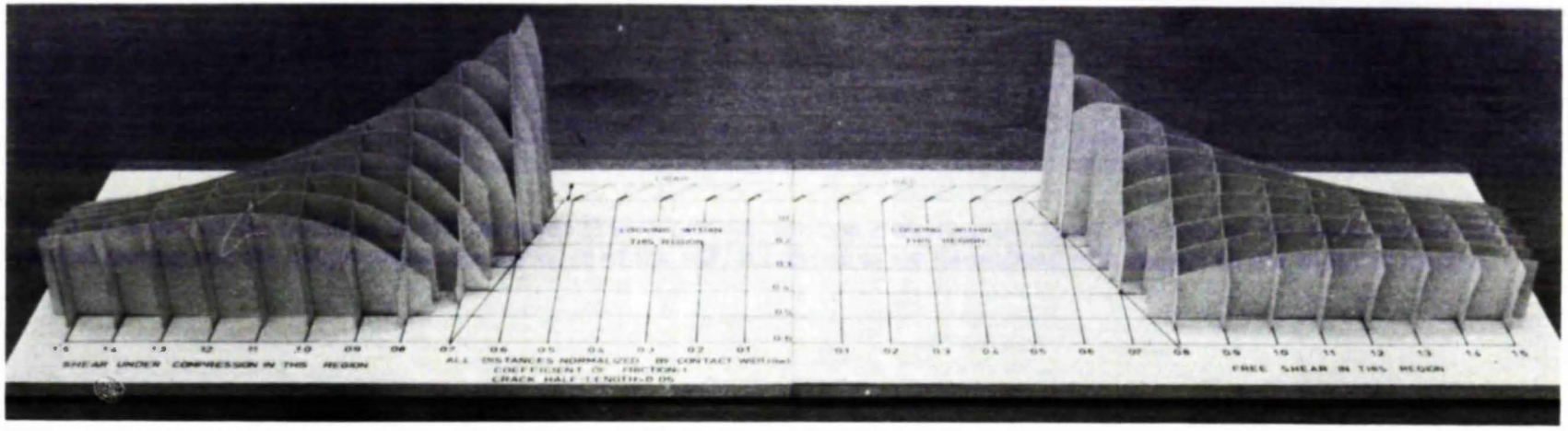


Fig. 5. A model of the variation of SIF for mode II with position beneath a wearing half-space. The base of the model represents a vertical section and the height represents the value of the SIF. All distances are normalized with respect to the width of loading.

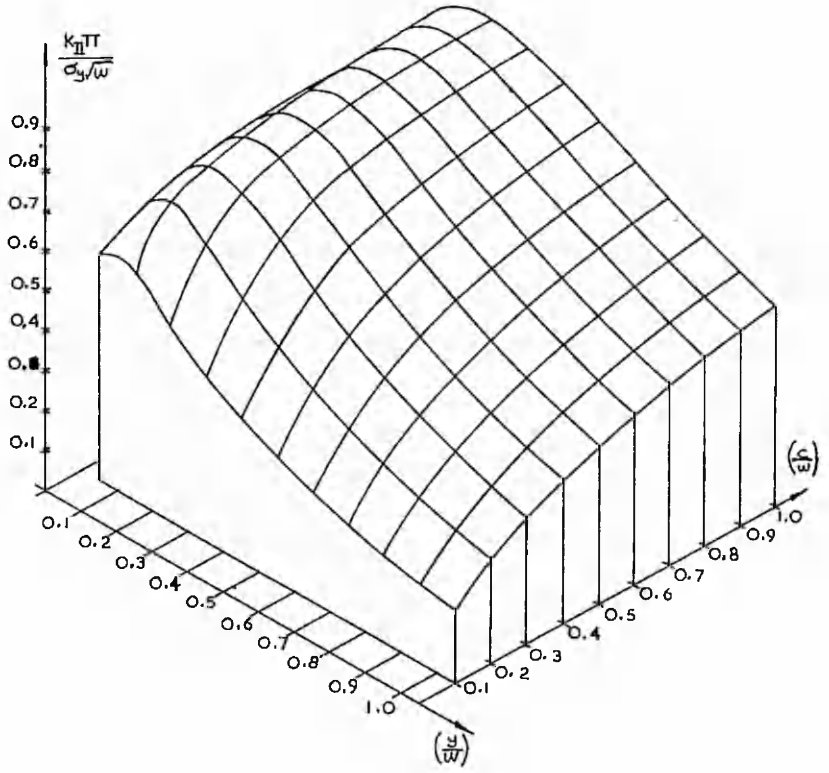


Fig. 6. The variation of the maximum mode II stress intensification factor with depth and crack length. The coefficient of friction is 0.8.

The combined mode crack growth rate can be determined using a method based on plastic zone sizes [6], giving the estimated rates shown in Table 1.

TABLE 1

	Stage 1	Stage 2
Free shear (nm cycle^{-1})	123	9
Compression/shear (nm cycle^{-1})	123	15

It is pure chance that the stage 1 values are equal, but it should be noted that these values are higher than those which would be predicted using the Paris equation. The results would seem to be more in keeping with the stage 1 part of the curve in which these very low SIFs occur, comparable with ΔK_{IC}. If the average size of a detaching plate is 12 μm then it would require about 50 passes to produce a wear particle. This is consistent with a particle being detached every 2 s at 1500 rev min^{-1}. At the moment this cannot be interpreted in terms of wear rate without making more assumptions: in particular, the number of cracks growing at any one time.

5. Conclusion

Fleming and Suh's model has been extended to cover all possible crack growths as the rider passes. Notwithstanding any acceleration of the wear process caused by fretting, which has been shown to occur, the crack propagation rates do not seem too remote from those obtained experimentally. The values of crack growth rate obtained have been significantly larger than those previously obtained for the following two reasons:

(1) It has been recognized that at such low SIFs it is probably true that most crack growth occurs in stage 1.

(2) The scale of the problem has been changed somewhat so that loads associated with the apparent area of contact have been used rather than those associated with a single asperity junction. The existence of two possible crack growth periods per rider pass has been shown, and the question of why subsurface cracks do not heal has been brought into the open. It is suggested that further progress will now be brought about by producing a model of wear rates deduced from crack propagation rates.

Acknowledgments

The authors would like to thank Dr. R. B. Waterhouse and Dr. P. Stanley of Nottingham University for their help and encouragement during this work. Thanks are also due to Mr P. J. Thompson, Head of the Department of Mechanical and Production Engineering, Trent Polytechnic, for providing computing facilities.

References

1 E. Hornbogen, Wear, 33 (1975) 251 - 259.
2 J. R. Fleming and N. P. Suh, Wear, 44 (1977) 39 - 56.
3 P. J. E. Forsyth, A two stage process of fatigue crack growth, Proc. Crack Symp., Cranfield, 1961.
4 D. A. Hills and D. W. Ashelby, Eng. Fract. Mech., to be published.
5 F. A. McClintock, Plastic flow around a crack under friction and combined stress, Fracture, 1977, ICF 4, Waterloo, Canada, June 1977, pp. 49 - 64, Pergamon, Oxford, 1978.
6 D. A. Hills and D. W. Ashelby, to be published.

A Fracture Mechanics Approach to Rolling Contact Fatigue

D.A.Hills and D.W.Ashelby*

Linear elastic fracture mechanics were used in the study of development of subsurface cracks in rolling contact fatigue. It is clear that such cracks are able to propagate by a shear mode, but it is suggested that the development of residual tensile stresses perpendicular to the wear surface may well result in a more important mode of growth which occurs when the load has passed over the crack

Nomenclature

a	contact half-width
J_{2c}	2nd invariant, stress deviator tensor, referred to completely reversed stresses
p_o	maximum contact pressure
σ_B	spherical component of static stresses
σ_{fl}	fatigue limit
σ_{uts}	ultimate tensile stress
μ	coefficient of friction between crack faces
L	life
Q	load
C_n	constant
ΔK_{IC}, ΔK_{IIC}	thresholds for modes I and II growth
c	crack half-length
n	number of load cycles
m	mass loss

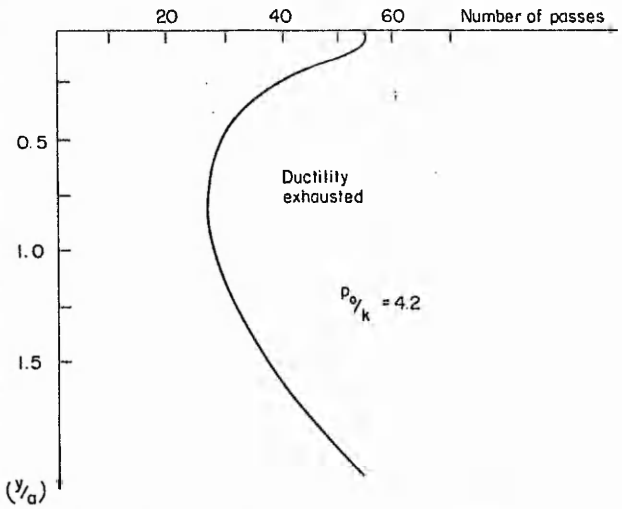


Fig 1 Number of passes required to initiate a crack in a single phase material, in this case nickel. P_o is the maximum contact pressure and k is the yield stress in pure shear

During the past twenty years many experiments have been performed to assess the growth of subsurface cracks during rolling contact fatigue. A review of such work was undertaken by Johnson[1]. Many questions have been answered, but two outstanding ones remain:

Do cracks initiate at or below the surface?
What governs the characteristic depth of propagation, and its rate?

The first question is still largely undecided, but it is generally accepted that in the presence of a lubricant any surface flaws will grow downwards by hydraulic action, and then turn and grow horizontally[2]. If the surfaces are dry and the surface finish good then it is possible that cracks will start at subsurface flaws. In fracture mechanics terms, the question could be recast as "What is the criterion for crack initiation?" Unfortunately, in relatively ductile materials, there are still no satisfactory universal criteria, although, if there are second phase particles present, it is often suggested that there is a critical strain beyond which plastic flow around the particles cannot accommodate the incompatibility. As the particle separates an embryo crack forms[3].

If there are no second-phase particles, initiation criteria become even more tentative but there is a natural assumption that cracks nucleate as ductility is exhausted. Such an assumption would be equivalent to saying that cracks form when the stored plastic energy of distortion reaches a critical value. To quantify this energy hysteresis loops found for nickel, and the corresponding energy dissipated by rolling contact fatigue plotted (Fig 1). Subsurface nucleation is predicted.

Crack propagation

Because crack initiation is so difficult to assess, most effort has been expended in examining the growth of pre-existing cracks. In the early experiments, two criteria used to judge the most likely crack growth depth were (Fig 2):

Depth at which τ_{45} is a maximum, ie where material experiences largest shear stress
Depth at which τ_{xy} is a maximum, ie where material experiences largest reversal of shear stress[4]

Of the two, the second seems to have been the more popular[5]. The use of continuum stress criteria, however, to assess the growth of a crack seems a little dubious. The next step would be to use a bulk, general fatigue criterion, eg that due to Sines[6]:

$$(\tfrac{1}{3}J_{2c})^{\frac{1}{2}} + 3\frac{\sigma_{fL}}{\sigma_{uts}}\ \bar{\sigma}_B \leqslant \sigma_{fl} \qquad (1)$$

*Department of Mechanical and Production Engineering, Trent Polytechnic, Burton Street, Nottingham NG1 4BU, UK

0301–679X/79/03115–05 $02.00 © 1979 IPC Business Press

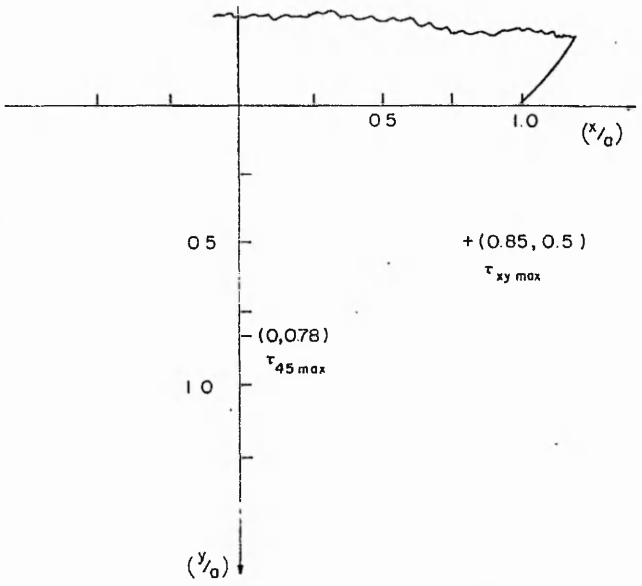


Fig 2 Coordinate system showing two most likely points at which cracks were thought to experience maximum growth

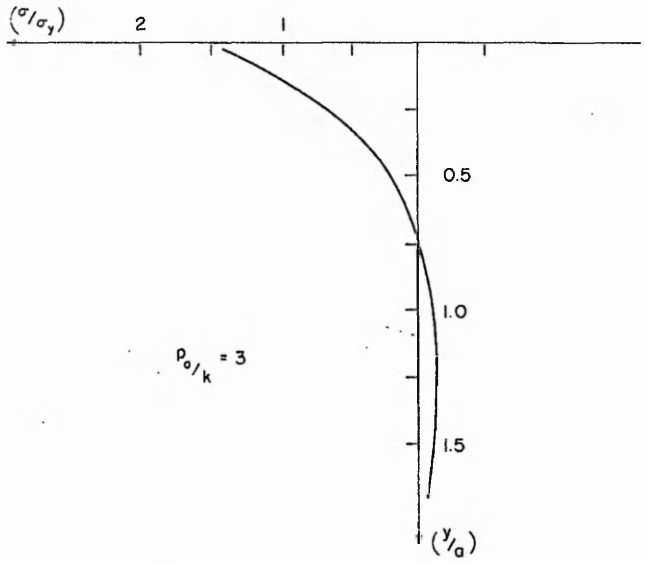


Fig 3 Sine's fatigue criterion. Failure is predicted to occur when the 'reduced' stress reaches a value +σfl.

Fatigue criteria seem to behave rather badly when the crack is in a high compressive environment, and indeed Sine's criterion shows that surfaces undergoing rolling contact should never fail (Fig 3). A fracture mechanics approach is needed. There has been little work in this area until recently, when McClintock[7] examined the behaviour of dislocations in the neighbourhood of a crack.

The present analysis uses the 'pseudo-stress' method previously used to find the stress intensification factors (SIF) beneath a wearing half-space[8]. Briefly, the method consists of finding the stresses within the wearing material due to the applied loads in the absence of a crack. A crack is inserted, and equilibrating forces applied to its faces. These will contribute to the SIF's, and at the same time will cause extra tractions to appear on the free surface. Further cancelling loads are applied, and these give rise to an extra pseudo-stress field. The method is repeated until convergence occurs. It should be noted that in the present case the normal compressive stress, σ_{yy}, tends to close the crack, so that the nett shear available to propel the crack is given by[9]:

$$\left.\begin{aligned} \tau_{\text{nett}} &= \tau_{xy} + \mu\,\sigma_{yy} \quad \tau_{xy} > 0 \\ &= \tau_{xy} - \mu\,\sigma_{yy} \quad \tau_{xy} < 0 \end{aligned}\right\} \left|\tau_{xy}\right| > \left|\mu\,\sigma_{yy}\right| \qquad (2)$$

The pseudo stress field used is that for two cylinders loaded together[4], and the resulting mode II SIF field is shown in Fig 4. It can be seen that the most favoured depth of propagation differs little from that predicted by a bulk criterion. Note, too, that directly beneath the roller, where the normal compressive stress is very large, the crack faces are locked together, and no growth can occur. Thus, each crack experiences two growth periods, punctuated by a 'rest' under sustained shear loading, per pass of the roller. Since the maximum SIF is known the crack growth rate can be found by use of a suitable fatigue law.

Evidence for a fracture model

Direct evidence is difficult to obtain, particularly in view of the ductile nature of most of the materials normally used. First, a dimensional argument will be used to show its feasibility. It was shown, many years ago, by Palmgren[10] that the fatigue life of a bearing followed a law:

$$L = \frac{C_1}{Q^3} \qquad (3)$$

If the Paris fatigue equation is adopted, but taking into account that the proportionality will be different because mode II growth is involved, the following relation between crack growth rate and applied load results:

$$\frac{dc}{dn} = C_2\,(\Delta K_{II})^m \qquad (4)$$

For bearing steel, $m = 3$, so that equations 3 and 4 give the same power law between load and life, if life is considered to be dependent on some critical crack length. The same conclusion is arrived at by using the IBM Zero Wear Model which states[11]:

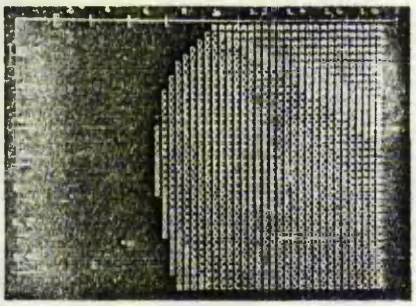
$$L = \frac{C_3}{\tau^9} \qquad (5)$$

In this relation, τ is any relevant stress, but under contact load conditions all stresses are related to the load by the usual Hertz relations[12]:

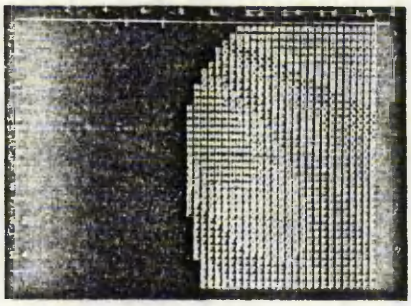
$$\tau_{ij} = C_{ij}\,p_o \;;\; p_o = C_5\sqrt[3]{Q} \qquad (6)$$

so that equations 5 and 6 also indicate a cubic relation between load and life. The results of sliding wear experiments using a variety of metals and alloys are shown in Fig 5. Correlation is not particularly good, but this is perhaps not surprising bearing in mind the variety of coefficients of friction and quantities of oxide formed.

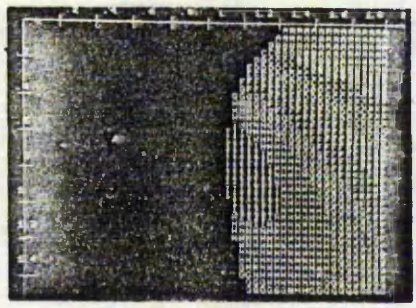
While comparing existing results, it might be valuable to draw an analogy between the IBM Zero Wear Model, and the Paris equation: below a certain load (corresponding to ΔK_{IIC}), both relations predict an extremely rapid fall off in wear. Taking values of ΔK_{IC} from Pook[13] one may obtain 'safe' design curves within which failure is most unlikely. Assuming that $\Delta K_{IIC} = 0.8\ \Delta K_{IC}$ the curves shown in Fig 6 are obtained. Also plotted is a line showing the shakedown limit[14], above which repeated plastic flow will occur. This is the limiting factor for small radii.



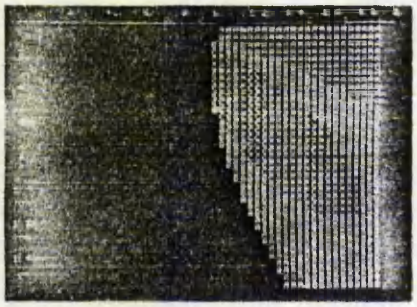
a) Crack coefficient of friction = 36
Crack half length = 1



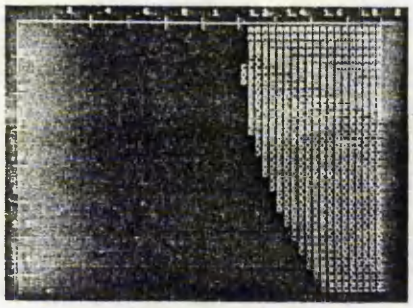
b) Crack coefficient of friction = 36
Crack half length = 3



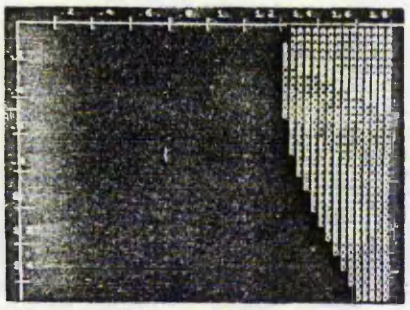
c) Crack coefficient of friction = 36
Crack half length = 5



d) Crack coefficient of friction = 72
Crack half length = 1



e) Crack coefficient of friction = 72
Crack half length = 3



f) Crack coefficient of friction = 72
Crack half length = 5

Fig 4 A vertical section through a quarter-space which is loaded by a heavy roller. Note the locking near the axis of symmetry. Key: $K_{II}/Qb^{-1/2} \times 10^{-3}$ – A 0 - 5, B 5 - 10, C 10 - 15, D 15 - 20, E 20 - 25, F 25 - 30, G 30 - 35, H 35 - 40, I 40 - 45

Experimental

Perspex was chosen as the material in which to perform contact loading experiments for the following reasons:

Being available in clear form, cracks are easily visible

Because of its low stiffness, large contact lengths are attainable with moderate contact loads

Above 25 °C the material shows a distinct yield point, and with large confining pressures, considerable ductility. Below – 40 °C it is totally brittle. Thus two material behaviours can easily be compared

It is optically active

It is amorphous, and so crystallographic effects are absent

120 ° segments of a 152 mm (6 in) diameter disc were cut from 9.5 mm (⅜ in) thick sheet, and were loaded against one another in an Instron test machine. Since the contact radii were equal, there should be negligible fretting, although a tiny amount was observed at the limits of the contact patch, and this was attributed to an anelastic effect. A polariscope was set up across the specimen, and an insulated box with viewing ports fitted around the specimens for low temperature work. To 'seed' cracks small holes (0.5 mm diameter) were drilled at various key points within the segments. It should be noted that, although the elastic contact stresses of rolling are correctly represented by this experiment, the residual 'shakedown' stresses associated with plastic behaviour will differ considerably.

It was anticipated that, within the 'locking' region, a crack would initiate along a 45 ° plane, where the shear stresses are largest, but would be unable to grow. This is not what

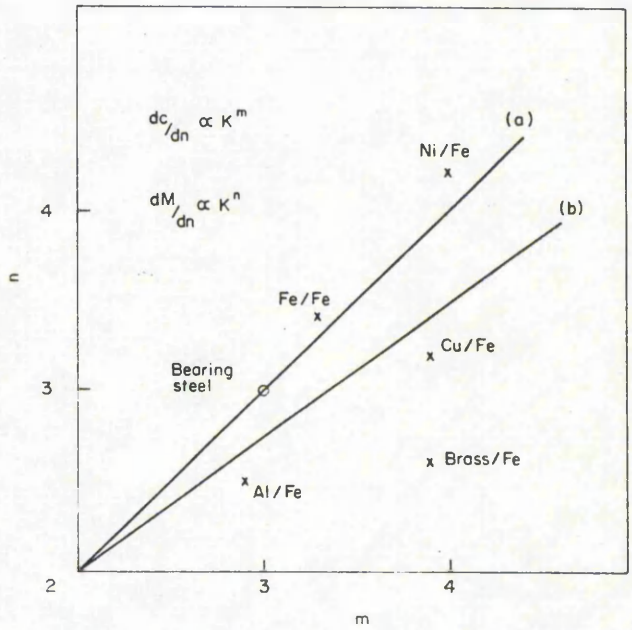


Fig 5 Wear rate sensitivity experiment for a selection of materials. The lines shown indicate a 1:1 correspondence (a), and an equivalent correspondence taking the varying contact widths in account (b)

happened at room temperature. By examining the specimen after the test, it was clear from the surface rippling that maximum shear had occurred on these planes, but the crack grew a short distance horizontally. Careful observation during a low-cycle fatigue test showed that the crack grew while the load was being removed. Therefore, a residual stress was causing the crack to grow[15]. The crack

grew beyond the stress-raising effect of the hole, but could not proceed very far because of the redistribution of residual stresses caused by the crack itself. Had it been possible to rotate the segment slightly, the crack should have continued to grow indefinitely.

In the very brittle regime, a short vertical crack grew from a hole drilled within the locking region. in neither case could a crack be grown from a hole drilled outside the locking region, where K_{II} is a maximum. The growth of a lateral crack is shown in Fig 7, while Fig 8 compares the strain distribution during and after loading of the specimens.

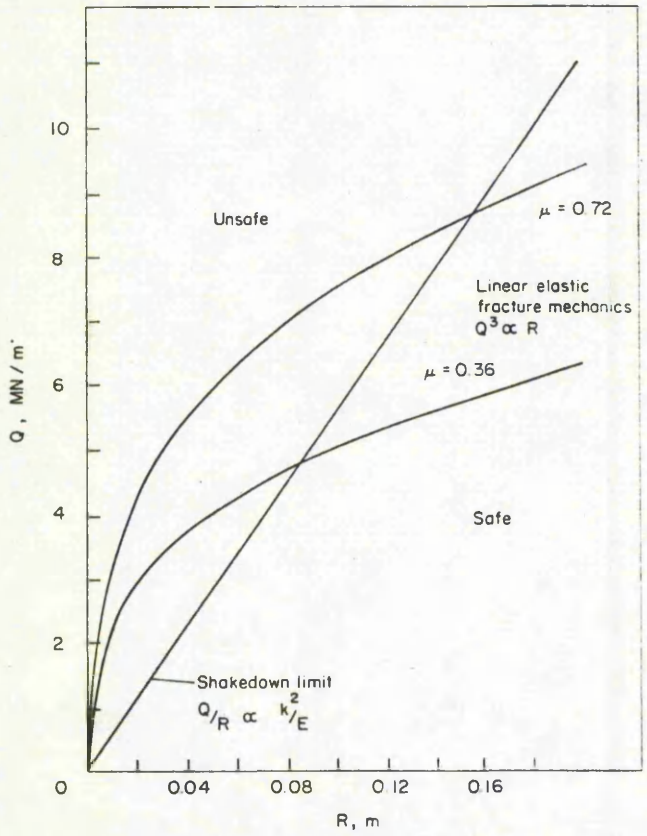


Fig 6 Design curves predicting the maximum safe loads which may be carried by a wheel moving over a flat surface, in this case for titanium. Note that for low loads it is continued plastic deformation which is the limiting factor. The crack is considered to be fully developed when c = 0.1 a. R is the roller radius

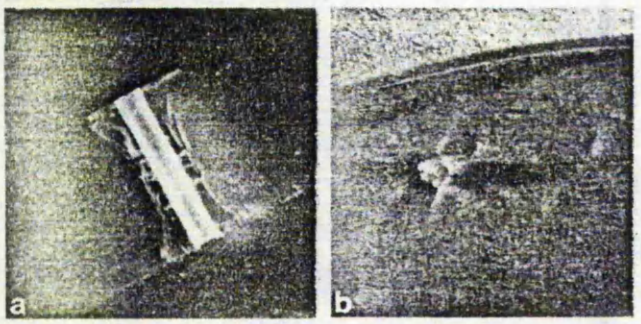


Fig 7 Growth of a lateral crack due to repeated contact loading (a) perpendicular to the crack and (b) the star-shaped rippling of the surface which represents the plane of maximum shear

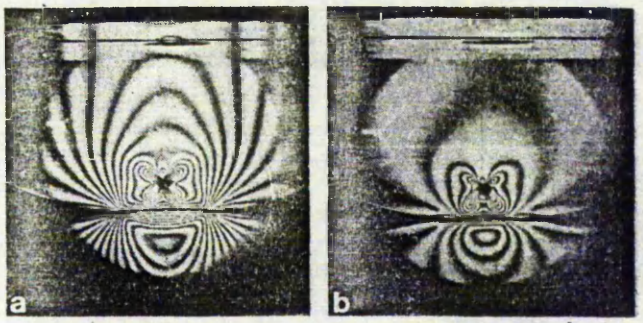


Fig 8 Photoelastic patterns showing (a) the applied and (b) residual stresses when loading two of the segments shown in Fig 7. Note the stress-raising effect of the holes, and the very considerable residual stresses, which propel the cracks

It is clear that a considerable tensile residual stress is present.

Conclusion

Analysis of the stress field beneath a roller indicates that a shear type growth should occur. It has not been possible to simulate this, but instead a tensile, mode I type extension occurred. It is possible that, because of their visco-elastic nature, this type of behaviour is greatly emphasised in plastics, with their ability to generate large residual stresses. Nevertheless, similar shakedown stresses might be expected to occur in real conditions either when a ball is rolled over an elasto-plastic half-space, or when two cylinders of differing widths are rolled together. An analysis of the former condition is currently being attempted. The important feature is that tensile stresses normal to the surface being rolled must be generated; the magnitude of such stresses will indicate whether or no. the mechanism is a feasible one. Under elastic-brittle conditions where a lower intrinsic toughness might be anticipated the material actually showed less tendency to crack. This may be explained in terms of the material's extended elastic behaviour, which prevented its accumulating any residual stress.

With a metal roller, it is often observed that cracks travel parallel to the surface for a considerable distance before tunring upwards. When a crack is subjected to pure shear loading it normally turns rapidly out of its own plane. This is not the case under rolling conditions, and there are two possible reasons. First, the crack is subjected to shears of (theoretically) equal magnitude but opposite sign each time it passes the load. Under this treatment one might expect the crack to weave up and down slightly and have an overall straight trajectory. However, owing to the rest period with a 'set-in' load it is probable that one shear will have a greater magnitude than the other, so that turning should result. Alternatively, the crack may be growing predominantly due to the action of residual stresses, in which case it would be stable growing in its own plane.

Arguments have been presented which show that contact fatigue might satisfactorily be represented by a fracture mechanics model, though the exact nature by which cracks grow is unresolved. Leaving aside questions of the applicability of lefm in a case where cracks are comparable in length to the grains in which they exist, the main problem is in deciding whether cracks are propelled by shakedown stresses. It is hoped to say something firmer about this when three-dimensional shakedown problems hav been solved, though they still present formidable problems.

Acknowledgements

The authors would like to thank Mr W.F.C. Fisher for his technical help with the experimental work.

References

1. Johnson K.L. Correlation of theory and experiment in research on fatigue in rolling contact. *Proc. I.M.E. 1963. Symposium on Rolling Contact Fatigue*
2. Cameron A. Surface fatigue in gears. Paper presented at the Institute of Physics Meeting *Contact stress problem in design, 11 May 1977*
3. Jahanmir S. and Suh N.P. Mechanics of subsurface void nucleation in delamination wear. *Wear*, 44 *(1977), 17-38*
4. Radzimovsky E.I. Stress distribution and strength condition of two rolling cylinders pressed together. *Univ. of Illinois Eng. Expt. station. Bulletin Series No. 408*
5. Ollerton E. and Morey J.W.W. Fatigue strength of rail steel in rolling contact *Proc. I.M.E. 1963. Symposium on Rolling Contact Fatigue.*
6. Sines G. Failure of materials under combined repeated stresses with superimposed static stresses, *NACA Tech. Note 3495, 1955*
7. McClintock F.A. Plastic flow around a crack under friction and combined stress *Fracture 1977, ICF4, Waterloo, Canada*, 4, *49-64*
8. Hills D.A. and Ashelby D.W. On the determination of stress intensification factors for a wearing half-space. *Submitted to Engineering Fracture Mechanics*
9. Hills D.A. and Ashelby D.W. On the application of fracture mechanics to wear. *To be published in Wear*
10. Palmgren A. Ball and roller bearing engineering. *Burbank Book Co..Inc. (1946)*
11. Bayer R.G., Clinton W.C., Ku T.C., Nelson C.W., Schumacher R.A., Sirico J.L. and Wayson A.R. Applying the wear model to design problems. *ASME Design Eng. Conf. Paper No. 66MD–12 (May 1966)*
12. Timoshenko S.P. and Goodier J.N. Theory of Elasticity *McGraw-Hill Ltd. 409-414*
13. Pook L. Analysis and application of fatigue crack growth data. *Strain Anal. (I.Mech.E.)* 10*(4) 242-250*
14. Merwin J.E. and Johnson K.L. An analysis of plastic deformation in rolling contact. *Proc. I.M.E. 1963. Symposium on Rolling Contact Fatigue.*
15. Bevan L. and Nugent H. Internal stress induced crazing of polymethylmethacrylate. Paper presented at the Institute of Physics Meeting *Residual stresses in plastics materials, 30 November 1978*